INAUGURAL - DISSERTATION

Zur
Erlangung der Doktorwürde
der
Naturwissenschaftlich-Mathematischen
Gesamtfakultät
der
Ruprecht-Karls-Universität
Heidelberg

vorgelegt von

Diplom-Chemikerin
Caroline Maria Magdolna Krauter

aus Karlsruhe

Tag der mündlichen Prüfung:
21.03.2014

Development, Benchmarking, and Applications of Efficient Theoretical Approaches for the Calculation of Excited States in Organic Systems

Gutachter:

PD Dr. rer. nat. Markus Pernpointner
Prof. Dr. rer. nat. Andreas Dreuw

Meinen Eltern in Dankbarkeit gewidmet

Kurzzusammenfassung

Durch Photoanregung induzierte Prozesse spielen eine große Rolle in zahlreichen biologischen Systemen wie auch technischen Anwendungen. Über die letzten Jahre ist eine große Bandbreite an quantenchemischen Methoden zur Behandlung solcher angeregter Zustände entwickelt worden. Allerdings sind viele dieser Methoden auf kleine bis mittelgroße Systeme beschränkt oder nur für bestimmte Arten von elektronisch angeregten Zuständen anwendbar. Daher stellt die Entwicklung effizienter quantenchemischer Methoden für angeregte Zustände einen zentralen Aspekt der modernen theoretischen Chemie dar.

In dieser Arbeit wurden verschiedene Verfahren zur Behandlung angeregter Zustände innerhalb der auf algebraischer diagrammatischer Konstruktion (ADC) basierenden Methoden hergeleitet und implementiert. Zunächst wurde die so genannte scaled-opposite spin Näherung verwendet um eine Variante der erweiterten ADC(2)-Methode zu erhalten. Diese ermöglicht eine verbesserte Beschreibung doppelt angeregter Zustände bei gleichzeitiger Reduzierung der Rechenzeit. Außerdem wurde die Berechnung von Spin-Bahn-Kopplungselementen basierend auf einem atomaren mean-field Ansatz für die gesamte Hierarchie von ADC-Methoden bis zur dritten Ordnung implementiert. Testrechnungen sowie Vergleich mit anderen bereits bestehenden Methoden ergaben sehr gute Resultate. Abschließend wurde eine Skalierungsmethode zur Identifizierung von Plasmonen in Molekülen von TDDFT auf ADC-Methoden übertragen. Solche Plasmonen spielen in der organischen Elektronik eine wichtige Rolle. Hier wurde gezeigt, dass dieser Ansatz für eine Reihe von linearen Polyenen zuverlässig funktioniert. Alle drei Methoden wurden in einer Entwicklerversion des `adcman` Moduls des Q-Chem Programmpakets implementiert, wodurch dessen Funktionalität weiter ausgebaut werden konnte. Schließlich wurden ADC-Methoden in Kombination mit experimentellen Resultaten verwendet um die photochemischen Relaxationsprozesse von Cumarinderivaten aufzuklären. Hierbei ergaben sich zwei parallele strahlungslose Relaxationsprozesse von Bedeutung.

Abstract

Processes initiated by photoexcitation play an important role in many biological systems as well as in technical applications. A whole variety of quantum chemical methods for the treatment of such excited states has been developed over the past years. However, many are either restricted to small or medium-sized systems or only applicable to certain types of electronic excitations. Therefore, the development of efficient quantum chemical excited states methods is one of the central aspects of modern theoretical chemistry.

In this work, different excited state approaches within the algebraic diagrammatic construction (ADC) family of methods were derived and implemented. First, the scaled-opposite spin approximation was used to develop a variant of the extended ADC(2) methods that allows for an improved treatment of doubly excited states at reduced computational cost. Additionally, the generation of spin-orbit coupling elements based on an atomic mean-field approach was implemented for the whole hierarchy of ADC methods up to third order. Test calculations and comparison with existing methods revealed very good results. Last but not least, a scaling approach for the identification of plasmons in molecules previously introduced for TDDFT has been adopted to the ADC methods. Such plasmons are of great importance in the field of organic electronics. Here, the scaling approach was shown to work efficiently for a series of linear polyenes. All three theoretical methods were implemented in a development version of the `adcman` module of the Q-Chem program package. Thereby, the functionality of this module has been further extended making it applicable to a wider range of molecular systems and photochemical problems. Finally, ADC methods were used in combination with experimental results to successfully unravel the photochemical relaxation network of coumarin derivatives which turned out to incorporate two parallel radiationless relaxation pathways.

Contents

1. Introduction

In nature and biological systems photoinitiated processes play an important role. Irradiation of molecules with visible or ultraviolet light can initiate the formation of electronically excited states and thereby trigger a whole variety of associated processes. Prominent examples are photosynthesis in plants, the process of vision or the photodamage of DNA together with mechanisms to revert or inhibit such photolesions.

However, excited states are of major importance for technical applications, too. The field of organic electronics has emerged during the past few years as a promising field of research and comprises, e. g., the development of organic photovoltaics or organic light-emitting diodes. In addition, light-induced processes can be used for chemical sensors, photoswitches, and many other functional molecules.

Upon interaction with light, molecules can absorb a photon and be transferred from the ground state into an optically allowed excited state. Usually, organic molecules as considered during this work have a ground state electronic structure with singlet spin symmetry, which is usually denoted as S_0. Because no spin-flip processes are allowed during optical excitation the initially populated states have a singlet spin symmetry, too. They are typically referred to as S_n, $n = 1, 2, \ldots$, depending on their energetic order.

As the motion of electrons is much faster than the one of the nuclei, the nuclear configuration does not change to a good approximation during the excitation process (Franck-Condon principle) leading to so-called vertical excitations (compare Figure 1.1). Once the excited state is reached, different processes can follow[1], the most important ones being illustrated in Figure 1.1. First of all, the molecules usually relax to the lowest vibrational level of the excited state surface. In the simplest case, the molecules can then decay back into a vibrationally excited level of the ground state by emitting a photon. This process is called fluorescence and occurs typically on time scales of 10^{-9} to 10^{-6} seconds [2]. Again, the Franck-Condon principle can be applied and the nuclear configuration stays almost constant during the emission. Because the minimum of the excited state is shifted with respect to the minimum of the ground state, the fluorescence energy is usually lower than the initial absorption energy. The difference between the two energies is called Stokes shift.

In the presence of other singlet excited states internal conversion procedures can occur. In this case the population is transferred from one electronic state to another. The intersections between two electronic states are called conical intersections [3, 4]. Such radiationless processes can compete with fluorescence and are often much faster. In some cases fluorescence is even completely quenched.

[1] For a general overview of the photochemistry of organic molecules see, e. g., [1, 2].

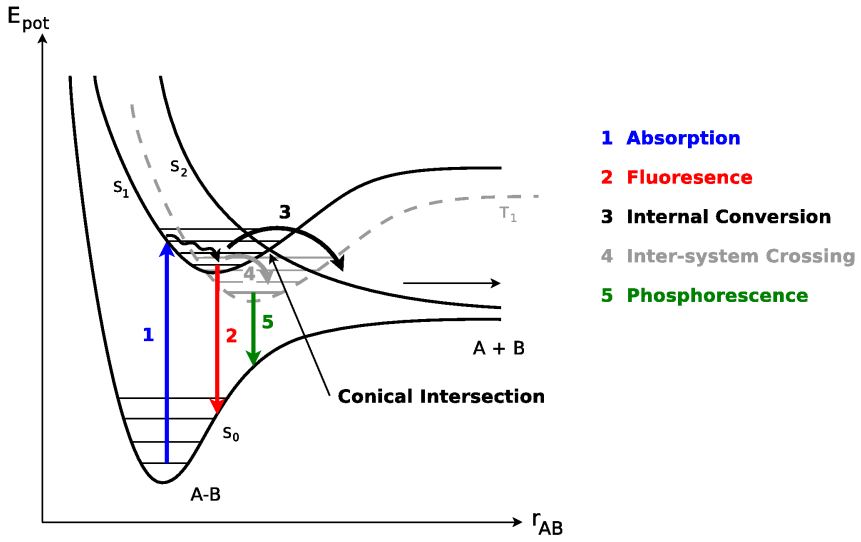

Figure 1.1.: Schematic representation of the potential energy surfaces and photophysical relaxation pathways occurring after initial absorption of a photon in a hypothetical molecule A-B. S_0 refers to the singlet electronic ground state and S_1 and S_2 to the first two excited singlet states. T_1 denotes the first triplet state. Singlet states are indicated by black solid lines while gray dashed lines were chosen for triplet states. Horizontal lines indicate vibrational sublevels of the respective electronic states.

Additionally, such internal conversion processes can mediate chemical transformations. In the example shown in Figure 1.1 the internal conversion would lead to a dissociation of the molecule.

So far, the spin symmetry was kept constant during all processes. When triplet states are close in energy, the molecules can undergo so-called inter-system crossing (ISC) and be transferred to a potential energy surface of different spin symmetry. States of different spin symmetry are coupled by interactions between the spin angular momenta and the spatial angular momenta of the electrons in the system (referred to as spin-orbit coupling). Such spin-orbit interactions gain strength with increasing nuclear charge. Additionally, the coupling is especially strong when the orbital types change during the transition (El-Sayed's rule) [5]. For example, between $\pi\pi^*$- and $n\pi^*$-states a stronger coupling is expected than between two $\pi\pi^*$-states[2]. Once in the triplet state, the molecules can relax again into the vibrational lowest level of this state. The radiative transition back into the singlet ground state of the molecule is called phosphorescence. Depending on the strengths of the spin-orbit interactions and other parameters as the energetic separation between the states and their shape, ISC processes occur on time scales of 10^{-11} to 10^{-6} seconds [2]. The time scale for phosphorescence lies typically in the region of 10^{-4} to 10^{2} seconds [2].

The electronically excited states themselves can be classified with respect to

[2] In the case of a $\pi\pi^*$-excitation, an electron is transferred from an occupied π-orbital into an unoccupied one. The symbol $n\pi^*$ denotes an excitation from a non-bonding orbital into an unoccupied π-orbital.

different characteristics. For example, one can differentiate between singly and doubly excited states. Another characteristic is the locality of the excitation. In local excitations only minor changes to the total electron density are induced. In the case of charge-transfer states this is not the case. Especially in systems that incorporate both, an electron donor as well as an electron acceptor, electronic density can be transferred from one part of the molecule to another. In the case of Rydberg states electron density is moved to larger radii and the electron density of the excited state is much more diffuse. Another differentiation, which is usually used in solid state physics, is between singly excited states and so-called plasmons. Plasmons are coherent oscillations of the electron density. As will be discussed in detail in Chapter 6 they can be characterized by certain linear combinations of single-particle excitations.

Depending on the symmetry and character of the excited states the direct optical excitation can be forbidden. However, such states can be reached by internal conversion processes. Their experimental detection is nevertheless complicated because they do not show fluorescence. Therefore, they are often referred to as dark states.

Prominent experimental methods to follow relaxation processes dynamically are transient absorption spectroscopy [6] or fluorescence upconversion [7, 8]. Here, time resolutions in the sub-picosecond range can be achieved. However, the resulting spectra can exhibit complex structures and time-dependencies. In these cases, quantum chemical calculations can be used to facilitate the evolution of the spectra and the assignment of states. Over the past years, combined theoretical and experimental studies have been successfully conducted for a vast variety of systems and photochemical problems.

To understand and predict the microscopic mechanisms that take place upon photoexcitation on a theoretical level, a thorough quantum chemical knowledge of the electronically excited states is necessary. This includes excitation energies as well as potential energy surfaces and properties of such states. Highly accurate excited state methods exist. However, they are only feasible for small molecular systems with only five to ten atoms from the second row of the periodic table. This is due to their steep scaling with molecular size. If larger systems are to be considered, more severe approximations have to be made. However, such approximations are usually not equally well suited for the different kinds of states. Often, even *a priori* knowledge of the excited states is necessary to find an appropriate method. Extensive comparisons with experimental results and other theoretical methods are indispensable in such cases. Especially, the consistent treatment of charge-transfer, Rydberg as well as doubly excited states is challenging [9–13].

The aim of the present work is twofold. On the one hand, new methods for the treatment and analysis of excited states are introduced within the framework of so-called algebraic diagrammatic construction scheme (ADC) methods. On the other hand, a combined theoretical and experimental photophysical study is presented. The chosen ADC approaches [14–18] are promising although largely overseen methods. Here, they were mainly used in second-order perturbation theory (ADC(2)). They have the advantage of including charge-transfer states

as well as Rydberg states in a physically correct way. Depending on the variant used, doubly excited states are as well properly accounted for. An efficient implementation of ADC methods up to third order including different properties like (transition) dipole moments or two-photon absorption cross sections is given by the `adcman` module as part of the Q-Chem program package [19]. An overview is given in [20]. The newly derived methods were all incorporated within this framework.

This thesis is organized as follows. First, Chapters 2 and 3 give an overview of existing quantum chemical methods for ground and excited state calculations including their strengths and deficiencies. In the subsequent chapter (Chapter 4) the so-called scaled-opposite spin approximation (SOS) [21] is discussed and applied to the extended version of ADC(2). The newly derived SOS-ADC(2)-x method aims at an improved inclusion of doubly excited states in second-order ADC methods and a simultaneous reduction of computational time.

In Chapter 5 an implementation of spin-orbit coupling elements with ADC methods up to third order in perturbation theory is introduced. For this purpose the atomic mean-field integral program `AMFI` of B. Schimmelpfennig [22] was incorporated into the `adcman` module of the Q-Chem program.

The final chapter of the theoretical part (Chapter 6) is concerned with the identification of plasmons by *ab initio* methods. A scaling approach that was previously established for the semi-empirical time-dependent density functional theory is transferred to the *ab initio* ADC methods. Additionally, the theory of plasmons from both, a classical as well as quantum theoretical point of view is reviewed. The discussion is based on the free electron gas as an illustrative example. Especially, characteristics are given for the classification of plasmons on a microscopic level.

The second part of this work is devoted to applications of the previously derived methods and to a joint theoretical and experimental investigation of the photoinitiated processes in coumarin derivatives. Chapters 7 and 8 present test calculations for the methods introduced in Chapters 5 and 6, respectively. For the spin-orbit coupling elements the molecules thiophene, dithiin and two coumarin derivatives were chosen. The approach for the identification of plasmons was applied to a series of linear polyenes. These molecules inhibit an electron system that is delocalized along the molecular chain and therefore allow for a comparison with the results of the homogeneous electron gas in Chapter 6.

Finally, Chapter 9 is concerned with the photochemical relaxation pathways in coumarin molecules. Mainly ADC methods have been used in combination with experimental results from the group of M. Motzkus [23]. This thesis closes with Chapter 10 where the achievements are summarized and an outlook on future work is given.

It should be mentioned at this point that parts of this work have already been published. Below, a list of publications related to this work is given:

1. **C. M. Krauter, M. Pernpointner, and A. Dreuw**
   Application of the scaled opposite-spin approximation to algebraic diagrammatic construction schemes of second order
   J. Chem. Phys. **138**, 044107 (2013).

2. **C. M. Krauter, J. Möhring, T. Buckup, M. Pernpointner, and M. Motzkus**
   Ultrafast branching in the excited state of coumarin and umbelliferone
   Phys. Chem. Chem. Phys. **15**, 17846 (2013).

3. **M. Wormit, D. R. Rehn, P. H. P. Harbach, J. Wenzel, C. M. Krauter, E. Epifanovsky, and A. Dreuw**
   Investigating Excited Electronic States using the Algebraic Diagrammatic Construction (ADC) Approach of the Polarisation Propagator
   Mol. Phys., accepted for publication.

4. **C. M. Krauter, M. Pernpointner, and A. Dreuw**
   Spin-orbit coupling elements using the atomic mean-field approximation with ADC(n) methods: implementation and test calculations
   to be submitted.

5. **C. M. Krauter, S. Bernadotte, M. Pernpointner, C. R. Jacob, and A. Dreuw**
   Identification of plasmons in molecules by ab initio methods
   to be submitted.

Part I.

Theoretical Methods

2. Basic Quantum Chemical Methods

The basic equation of quantum mechanics is the time-dependent Schrödinger equation

$$\hat{H}\Psi(\mathbf{x},t) = i\hbar\frac{\partial}{\partial t}\Psi(\mathbf{x},t). \tag{2.1}$$

The time-evolution of a system characterized by the Hamilton operator $\hat{H}$ is given by the wave function $\Psi(\mathbf{x},t)$ that depends on space $\mathbf{x}$ and time t. In the case of no explicit time-dependence of the Hamilton operator the wave function can be separated into a time-independent part $\psi(\mathbf{x})$ and a phase factor $\phi(t)$ describing the time-evolution:

$$\Psi(\mathbf{x},t) = \psi(\mathbf{x})\phi(t).$$

The time-independent, stationary wave functions $\psi(\mathbf{x})$ are eigenfunctions of the Hamilton operator with the energies E as eigenvalues:

$$\hat{H}\psi(\mathbf{x}) = E\psi(\mathbf{x}). \tag{2.2}$$

This eigenvalue equation is called the time-independent Schrödinger equation. Then, from the time-dependent Schrödinger equation one gets

$$\phi(t) = e^{-iEt/\hbar}.$$

For a molecular system composed of M nuclei with nuclear charges $\{Z_I\}$, masses $\{M_I\}$, and positions $\mathbf{R} = \{\mathbf{R}_I\}$ as well as N electrons located at positions $\mathbf{r} = \{\mathbf{r}_i\}$ the Hamilton operator in atomic units[1] reads as

$$\begin{aligned}\hat{H} = &\underbrace{-\frac{1}{2}\sum_{I=1}^{M}\frac{1}{M_I}\nabla_I^2}_{\hat{T}_N}\underbrace{-\frac{1}{2}\sum_{i=1}^{N}\nabla_i^2}_{\hat{T}_e} \\ &\underbrace{+\sum_{I=1}^{M}\sum_{J>I}^{M}\frac{Z_I Z_J}{|\mathbf{R}_I-\mathbf{R}_J|}}_{V_{NN}}\underbrace{-\sum_{i=1}^{N}\sum_{I=1}^{M}\frac{Z_I}{|\mathbf{r}_i-\mathbf{R}_I|}}_{V_{Ne}}\underbrace{+\sum_{i=1}^{N}\sum_{j>i}^{N}\frac{1}{|\mathbf{r}_i-\mathbf{r}_j|}}_{V_{ee}}.\end{aligned} \tag{2.3}$$

The first two terms represent the kinetic energy of the nuclei ($\hat{T}_N$) and the electrons ($\hat{T}_e$), respectively. The other three terms are the potentials of the repulsions between the nuclei (V_{NN}), the attractions between electrons and nuclei (V_{Ne}) and the repulsions of the electrons (V_{ee}).

[1] $m_e = e = \hbar = 4\pi\epsilon_0 = 1$

Unfortunately, the eigenvalue equation cannot be solved analytically for molecular systems with more than two particles, namely one-electron, hydrogen-like systems. Finding approximate solutions to the Schrödinger equation for many-electron systems is therefore the main goal of quantum chemistry. In the following sections some of the most important concepts and approximations will be introduced and discussed. While this chapter focuses primarily on the description of the electronic ground state, Chapter 3 deals with electronically excited states.

2.1. The Born-Oppenheimer Approximation

Usually, the first step to solve the molecular Schrödinger equation forms the separation into an electronic and a nuclear eigenvalue problem, called the adiabatic or Born-Oppenheimer approximation [24]. This is motivated by the fact that the light electrons move much faster than the heavy nuclei. Consequently, the electrons can be, to a good approximation, regarded to move in the field of fixed nuclei. The electronic Hamilton operator within this approximation is given by:

$$\hat{H}_{el} = \hat{T}_e + V_{Ne} + V_{ee}.$$

The corresponding purely electronic energies $E_{el}(\mathbf{R})$ and wave functions $\Psi_{el}(\mathbf{r}|\mathbf{R})$ are obtained by solving the electronic Schrödinger equation

$$\hat{H}_{el}\Psi_{el}(\mathbf{r}|\mathbf{R}) = E_{el}(\mathbf{R})\Psi_{el}(\mathbf{r}|\mathbf{R})$$

and depend parametrically on the coordinates of the nuclei $\mathbf{R}$. The total energy E_{tot} for the system with fixed nuclei can be retrieved by including the potential energy of the nuclear repulsions:

$$E_{tot}(\mathbf{R}) = E_{el}(\mathbf{R}) + V_{NN}(\mathbf{R}).$$

Finally, the nuclear Hamiltonian

$$\hat{H}_N = \hat{T}_N + E_{tot}(\mathbf{R})$$

describes the motion of the nuclei in the average field of electrons. By solving the respective nuclear Schrödinger equation information about vibrations, rotations and translations of the molecule can be obtained. Thus, within the Born-Oppenheimer approximation the total energy as a function of the nuclear coordinates provides a potential energy surface (PES) on which the nuclei are moving. It constitutes a good approximation as long as Ψ_{el} is a slowly varying function with respect to the nuclear coordinates which is usually the case as long as the PESs of the different electronic states under investigation are well separated. Consequently, the Born-Oppenheimer approximation breaks down close to avoided crossings and conical intersections.

Finally, the total wave function is given by the product of the electronic and nuclear wave function

$$\Psi(\mathbf{r}, \mathbf{R}) = \Psi_{el}(\mathbf{r}|\mathbf{R})\Psi_N(\mathbf{R}).$$

All methods introduced in the next sections will operate within the Born-Oppenheimer approximation and seek for solutions of the electronic Schrödinger equation only. Therefore, the subscript *el* will be omitted and all Hamiltonians and wave functions will be considered electronic unless stated otherwise.

2.2. The Electron Spin

In this work, the spin-free molecular Hamiltonian and non-relativistic quantum theory is considered. In this case, spin has to be postulated *a posteriori*. As spin is an intrinsic property of the electron and has no classical analogue, the correspondence principle cannot be used to derive the corresponding quantum mechanical operators. Instead, the spin angular momentum operators $\hat{\mathbf{S}}^2$, $\hat{S}_x$, $\hat{S}_y$, $\hat{S}_z$ are postulated in analogy to the orbital angular momentum operators as linear and Hermitian operators obeying the commutator relations [25, 26]

$$[\hat{S}_x, \hat{S}_y] = i\hbar\hat{S}_z, \qquad [\hat{S}_y, \hat{S}_z] = i\hbar\hat{S}_x, \qquad [\hat{S}_z, \hat{S}_x] = i\hbar\hat{S}_y.$$

The non-relativistic Hamiltonian of equation 2.3 commutes with the total spin $\hat{\mathbf{S}}^2$ and its z-component $\hat{S}_z$. Thus, its eigenfunctions are eigenfunctions to $\hat{S}^2$ and $\hat{S}_z$ with eigenvalues $S(S+1)\hbar^2$ ($S = 0, 1/2, 1, \dots$) and $M_s\hbar$ ($M_s = -S, -S+1, \dots, S-1, S$), respectively. Singlet states are characterized by $S = 0$ and triplet states by $S = 1$ ($M_s = 0, \pm 1$). Throughout this work capital letters will be used to denote spin eigenvalues of many-electron systems while lower case letters will be employed for one-electron systems.

For electrons ($s = \frac{1}{2}$) the two eigenfunctions to $\hat{S}_z$ with $m_s = +\frac{1}{2}$ and $m_s = -\frac{1}{2}$ are denoted as $\alpha(m_s)$ and $\beta(m_s)$, respectively. The discrete variable m_s represents a convenient choice for the spin coordinate and the form of the spin functions is determined by

$$\alpha(m_s) = \begin{cases} 1 & \text{for} \quad m_s = +\frac{1}{2} \\ 0 & \text{for} \quad m_s = -\frac{1}{2} \end{cases}$$
$$\beta(m_s) = \begin{cases} 0 & \text{for} \quad m_s = +\frac{1}{2} \\ 1 & \text{for} \quad m_s = -\frac{1}{2} \end{cases}$$

The spin functions $\alpha(m_s)$ and $\beta(m_s)$ form a complete basis of the spin space and are orthonormal to each other:

$$\langle\sigma|\tau\rangle = \sum_{m_s=-1/2}^{1/2} \sigma^*(m_s)\tau(m_s) = \delta_{\sigma,\tau}$$

where σ and τ refer to general spin functions ($\sigma, \tau \in \{\alpha, \beta\}$).

Finally, in non-relativistic theory one-electron functions (spin orbitals) χ are given by a product of a spatial function with the respective spin function. Given K spatial orbitals $\phi(\mathbf{r})$, $2K$ spin orbitals of the form

$$\chi_{2i-1}(\mathbf{x}) = \phi_i(\mathbf{r})\alpha(m_s)$$
$$\chi_{2i}(\mathbf{x}) = \phi_i(\mathbf{r})\beta(m_s)$$

with $i = 1, 2, \ldots K$ can be obtained. Here, $\mathbf{x}$ represents collectively spatial ($\mathbf{r}$) and spin coordinates (m_s). As long as the spatial orbitals are orthonormal, the spin orbitals are as well:

$$\langle \chi_i | \chi_j \rangle = \int \chi_i^*(\mathbf{x}) \chi_j(\mathbf{x}) d\mathbf{x} = \sum_{m_s} \int \chi_i^*(\mathbf{r}, m_s) \chi_j(\mathbf{r}, m_s) d\mathbf{r} = \delta_{ij}.$$

According to the spin-statistics theorem [25, 27] an N-electron wave function $\Psi(\mathbf{x}_1, \mathbf{x}_2, \ldots, \mathbf{x}_N)$ has to be antisymmetric with respect to interchange of any two electrons:

$$\hat{\mathcal{P}}_{ij} \Psi(\mathbf{x}_1, \mathbf{x}_2, \ldots, \mathbf{x}_N) = -\Psi(\mathbf{x}_1, \mathbf{x}_2, \ldots, \mathbf{x}_N),$$

where $\hat{\mathcal{P}}_{ij}$ denotes the permutation operator. In the simplest case of a system of N non-interacting electrons the total wave function is therefore given as the antisymmetrized product of spin orbitals. Such an antisymmetrized product is mathematically most easily expressed by a so-called Slater determinant (SD) $|\chi_1(\mathbf{x}_1)\chi_2(\mathbf{x}_2) \ldots \chi_N(\mathbf{x}_N)\rangle$ [25, 27]:

$$|\chi_1(\mathbf{x}_1)\chi_2(\mathbf{x}_2) \ldots \chi_N(\mathbf{x}_N)\rangle \equiv \frac{1}{\sqrt{N!}} \begin{vmatrix} \chi_1(\mathbf{x}_1) & \ldots & \chi_1(\mathbf{x}_n) \\ \vdots & \ddots & \vdots \\ \chi_n(\mathbf{x}_1) & \ldots & \chi_n(\mathbf{x}_n) \end{vmatrix}.$$

For later reference it will prove useful to define the ladder operators $\hat{S}_+$, $\hat{S}_-$, $\hat{S}_0$ as linear combinations of the Cartesian components $\hat{S}_x$, $\hat{S}_y$, $\hat{S}_z$ of the spin operator [26]:

$$\hat{S}_+ = \hat{S}_x + i\hat{S}_y \qquad \hat{S}_0 = \hat{S}_z \qquad \hat{S}_- = \hat{S}_x - i\hat{S}_y.$$

Their effect on the spin functions α and β is given by

$$\hat{S}_+\sigma = \begin{cases} 0 & \text{for} \quad \sigma = \alpha \\ \alpha & \text{for} \quad \sigma = \beta \end{cases}$$

$$\hat{S}_-\sigma = \begin{cases} \beta & \text{for} \quad \sigma = \alpha \\ 0 & \text{for} \quad \sigma = \beta \end{cases}$$

$$\hat{S}_0\sigma = \begin{cases} +1/2\hbar\alpha & \text{for} \quad \sigma = \alpha \\ -1/2\hbar\beta & \text{for} \quad \sigma = \beta \end{cases}.$$

Closely related are the tensor operators with the spherical components $\hat{S}_{+1}$, $\hat{S}_{-1}$, $\hat{S}_0$ defined by [26]

$$\hat{S}_{+1} = -\frac{1}{\sqrt{2}}(\hat{S}_x + i\hat{S}_y) \qquad \hat{S}_0 = \hat{S}_z \qquad \hat{S}_{-1} = \frac{1}{\sqrt{2}}(\hat{S}_x - i\hat{S}_y). \tag{2.4}$$

The cartesian components with respect to these operators are then given by

$$\hat{S}_x = \frac{1}{\sqrt{2}}(\hat{S}_{-1} - \hat{S}_{+1}) \qquad \hat{S}_z = \hat{S}_0 \qquad \hat{S}_y = \frac{i}{\sqrt{2}}(\hat{S}_{-1} + \hat{S}_{+1}). \tag{2.5}$$

A general irreducible tensor operator $\hat{\mathscr{T}}^{(k)}$ of rank k is an operator whose components transform among themselves under rotations. It has $2k+1$ components $\hat{\mathscr{T}}_q^{(k)}$ with $q = -k, -k+1, \ldots, k-1, k$ that form a basis of the three dimensional rotation group [26]. Tensor operators of rank zero are scalar operators that contain only one component and are invariant with respect to rotations. An example is the Hamilton operator (operator of the energy). The spin operators $\hat{S}_{\pm 1}$ and $\hat{S}_0$ are the components of the first-rank tensor or vector operator $\hat{\mathbf{S}}$. The relation between spherical and Cartesian components is specified by equations 2.4 and 2.5. The spatial angular momentum operator is of the same type. The notion of irreducible tensor operators will become important when discussing spin-orbit coupling elements in Chapter 5.

2.3. The Hartree-Fock Method

The Hartree-Fock method [25,27,28] is a fundamental approach to the approximate solution of the electronic Schrödinger equation given in Section 2.1 and its solutions will serve as the starting point for the methods introduced in the next section. Approximating the molecular N-electron wave function as a single SD $|\chi_1(\mathbf{x}_1)\chi_2(\mathbf{x}_2)\ldots\chi_N(\mathbf{x}_N)\rangle$ forms the basis of this method. Here, $\mathbf{x}$ represents again collectively spatial ($\mathbf{r}$) and spin (m_s) coordinates. By employing the variational theorem those orbitals are determined which minimize the expectation value of the energy under the restriction that $\langle\chi_i|\chi_j\rangle = \delta_{ij}$ (orthonormality of the orbitals). These are exactly those that satisfy the Fock equation (diagonalize the Fock operator)

$$\hat{F}\chi_i(\mathbf{x}) = \epsilon_i\chi_i(\mathbf{x})$$

with $\hat{F}$ being the Fock operator:

$$\hat{F} = -\frac{1}{2}\nabla^2 - \sum_{I=1}^{M}\frac{Z_I}{|r-R_I|} + v^{HF}.$$

Here, v^{HF} represents the average potential acting on electron i and is generated by the remaining $N-1$ electrons. Thus, the N-electron problem is replaced by a coupled set of N one-electron problems and the electron-electron interaction is averaged. The potential v^{HF} is given by

$$v^{HF} = \sum_j \int \chi_j^*(\mathbf{x}')\frac{1}{|\mathbf{r}-\mathbf{r}'|}(1-\mathcal{P}_{ij})\chi_j(\mathbf{x}')d\mathbf{x}' = \sum_j \hat{\mathscr{J}}_j - \hat{\mathscr{K}}_j.$$

The operators $\hat{\mathscr{J}}_j$ and $\hat{\mathscr{K}}_j$ are called Coulomb operator and exchange operator, respectively, and are defined as

$$\hat{\mathscr{J}}_j\chi_i(\mathbf{x}) = \left[\int \chi_j^*(\mathbf{x}')\frac{1}{|\mathbf{r}-\mathbf{r}'|}\chi_j(\mathbf{x}')d\mathbf{x}'\right]\chi_i(\mathbf{x})$$
$$\hat{\mathscr{K}}_j\chi_i(\mathbf{x}) = \left[\int \chi_j^*(\mathbf{x}')\frac{1}{|\mathbf{r}-\mathbf{r}'|}\chi_i(\mathbf{x}')d\mathbf{x}'\right]\chi_j(\mathbf{x}).$$

As v^{HF} depends on all (occupied) spin-orbitals, the Hartree-Fock equations are non-linear and need to be solved iteratively. Thus, this method is often called self-consistent field (SCF) method. Once the N occupied spin-orbitals have been determined, the Fock operator becomes a Hermitian operator with an – in principle – infinite number of solutions. In practical calculations, however, the spin-orbitals are represented in a finite set of K atomic basis functions. In this case, the SCF procedure yields a set of $2K$ spin orbitals $\{\chi_p\}$ with energies $\{\epsilon_p\}$. The ground state wave function within the Hartree-Fock approximation (within this work always referred to as Φ_0) is given by the SD over the N energetically lowest occupied spin orbitals:

$$\Phi_0 = |\chi_1 \chi_2 \dots \chi_N\rangle.$$

Consequently, the ground state energy is given by

$$E_0^{HF} = \sum_i \epsilon_i - \frac{1}{2}\sum_{ij}\langle ij||ij\rangle \tag{2.6}$$

with the orbital energies

$$\epsilon_p = \langle p|\hat{h}|p\rangle + \sum_j \langle pj||pj\rangle, \qquad \hat{h} = -\frac{1}{2}\nabla^2 - \sum_{I=1}^{M}\frac{Z_I}{|\mathbf{r}-\mathbf{R}_I|}.$$

Here and throughout the rest of this work $\{i, j, k, \dots\}$ denote occupied orbitals, $\{a, b, c, \dots\}$ are used for unoccupied orbitals and $\{p, q, r, \dots\}$ indicate general spin orbitals without a specific occupation. Moreover, the following convenient notation for two-electron integrals is employed:

$$\begin{aligned}&\langle pq||rs\rangle \equiv \langle pq|rs\rangle - \langle pq|sr\rangle \\ &\text{with} \qquad \langle pq|rs\rangle \equiv \int\int \chi_p^*(\mathbf{x})\chi_q^*(\mathbf{x}')\frac{1}{\mathbf{r}-\mathbf{r}'}\chi_r(\mathbf{x})\chi_s(\mathbf{x}')d\mathbf{x}d\mathbf{x}'.\end{aligned}$$

In the first term of the ground state energy expression 2.6 the orbital energy ϵ_i describes the energy of the electron occupying the spin orbital χ_i and includes the kinetic energies of this electron, its interactions with the nuclei and its Coulomb and exchange interactions with the remaining $N-1$ electrons. Here, the integrals $\langle ij|ij\rangle = \langle i|\hat{\mathscr{J}}_j|i\rangle$ are expectation values of the local Coulomb operator and describe the classical Coulomb interaction between the charge clouds $|\chi_i(\mathbf{x})|^2$ and $|\chi_j(\mathbf{x}')|^2$. Therefore, they are called Coulomb integrals. On the other hand, the exchange integrals $\langle ij|ji\rangle = \langle i|\hat{\mathscr{K}}_j|i\rangle$ are expectation values of the non-local exchange operator and arises due to the antisymmetric character of Slater determinants. They do not have any classical analogue.

Clearly, neither explicit interactions between the electrons nor dynamical effects are included in this method. Only the exchange correlation due to the antisymmetry restriction to the wave function is recovered. Consequently, the probability to find two electrons with same spin at the same position in space is zero while the respective probability for electrons with opposite spin is not.

The difference to the exact ground state energy $\mathcal{E}_0$ is called the correlation energy E_{corr}

$$E_{corr} = \mathcal{E}_0 - E_0^{HF}.$$

Some of the methods to recover at least parts of the correlation energy will be introduced during the next section. As they are based on a previous Hartree-Fock theory (HF) calculation, such methods are often referred to as *post*-HF methods. In most cases they make use of the fact that a HF calculation yields more spin orbitals than are needed to construct the N-electron HF ground state wave function. The remaining unoccupied or virtual orbitals are used to construct excited determinants which are then employed to derive an improved description of the ground state. This principle is used in most excited state methods, as well.

2.4. Electron Correlation

2.4.1. Second Quantization

Before proceeding to the description of electron correlation it will prove useful to introduce the concept of second quantization [28, 29]. Within this formalism not only observables are expressed as operators but also the wave functions. Specifically, the wave functions as well as the operators from first quantization are expressed in terms of creation and annilihation operators acting on the vacuum state. The antisymmetry of the wave functions follows directly from the anticommutation properties of these operators and the treatment of many-electron systems is greatly simplified.

Given a basis of K orthonormal spin orbitals $\{\chi_p(\mathbf{x})\}$, every SD can be associated with an occupation number (ON) vector $|\mathbf{k}\rangle = |k_1, k_2, \ldots, k_K\rangle$ with $k_p = 1$ if χ_i is occupied and $k_p = 0$ if χ_i is unoccupied. The ON vectors form a linear vector space called the Fock space and by

$$\langle \mathbf{k}|\mathbf{m}\rangle = \delta_{\mathbf{k},\mathbf{m}} = \prod_{p=1}^{K} \delta_{k_p,m_p}$$

an inner product between ON vectors $|\mathbf{k}\rangle$ and $|\mathbf{m}\rangle$ is defined. Thus, ON vectors with different numbers of electrons have a well defined overlap. This is one of the major advantages of this formalism and allows one to treat systems with different number of electrons in a consistent manner. The ON vector containing no electrons is called the vacuum state $|vac\rangle$ ($k_p = 0\ \forall p$).

The creation $c_p^\dagger$ and annihilation operators c_p change the number of electrons

when acting on ON vectors and are defined as follows:

$$c_p^\dagger|k_1,k_2,\ldots,k_p,\ldots,k_K\rangle = \begin{cases} \Gamma_p^{\mathbf{k}}|k_1,k_2,\ldots,1_p,\ldots,k_K\rangle & \text{for} \quad k_p=0 \\ 0 & \text{for} \quad k_p=1 \end{cases}$$

$$c_p|k_1,k_2,\ldots,k_p,\ldots,k_K\rangle = \begin{cases} \Gamma_p^{\mathbf{k}}|k_1,k_2,\ldots,0_p,\ldots,k_K\rangle & \text{for} \quad k_p=1 \\ 0 & \text{for} \quad k_p=0 \end{cases}$$

$$\text{with} \qquad \Gamma_p^{\mathbf{k}} = \prod_{q=1}^{p-1}(-1)^{k_q}.$$

Consequently, $c_a^\dagger$ increases the electron number by one and creates an electron in a virtual orbital a while c_i reduces the electron number by one and removes an electron from an occupied orbital i.

They fulfill the following anticommutation relations:

$$[c_p^\dagger, c_q^\dagger]_+ = 0, \qquad [c_p, c_q]_+ = 0, \qquad [c_p^\dagger, c_q]_+ = \delta_{pq}.$$

These relations determine all other algebraic properties of the wave functions and operators. Especially, the antisymmetry of the wave functions follows directly. Therefore, within the formalism of second quantization any antisymmetrized N-electron wave function represented as an ON vector can be generated by simply applying a chain of creation operators to the vacuum state:

$$|\mathbf{k}\rangle = \left[\prod_p (c_p^\dagger)^{k_p}\right]|vac\rangle.$$

Similarly, operators can be expressed in terms of creation and annihilation operators, too. Any one-electron operator $\hat{O}_1 = \sum_{i=1}^N \hat{o}(\mathbf{x}_i)$ acting on an N-electron system can be expressed within the basis of K orthonormal spin orbitals $\{\chi_p(\mathbf{x})\}$ as

$$\hat{O}_1 = \sum_{i=1}^N \sum_{pq} \underbrace{\langle\chi_p|\hat{o}|\chi_q\rangle}_{=O_{pq}} |\chi_p\rangle\langle\chi_q|.$$

With the restriction that the expectation values obtained within first or second quantization must be equal, i. e., that the matrix elements of the operators have to be the same, one-electron operators take on the following form in second quantization:

$$\hat{O}_1 = \sum_{pq} O_{pq} c_p^\dagger c_q.$$

Similarly, two-electron operators $\hat{O}_2 = \sum_{i,j=1,i\neq j}^N \hat{o}(\mathbf{x}_i,\mathbf{x}_j)$ are represented by

$$\hat{O}_2 = \sum_{pqrs} O_{pqrs} c_p^\dagger c_q^\dagger c_s c_r$$

$$\text{with} \qquad O_{pqrs} = \int\int \chi_p^*(\mathbf{x}_1)\chi_q^*(\mathbf{x}_2)\hat{o}(\mathbf{x}_1,\mathbf{x}_2)\chi_r(\mathbf{x}_1)\chi_s(\mathbf{x}_2)d\mathbf{x}_1 d\mathbf{x}_2.$$

Finally, the molecular Hamiltonian has the following form in second quantization:

$$\hat{H} = \sum_{pq} h_{pq} c_p^\dagger c_q + \frac{1}{2} \sum_{pqrs} \langle pq|rs\rangle c_p^\dagger c_q^\dagger c_s c_r,$$

where h_{pq} are the matrix elements of the one-particle terms of the electronic Hamiltonian according to:

$$h_{pq} = \langle p|\hat{h}|q\rangle \qquad \text{with} \qquad \hat{h} = -\frac{1}{2}\nabla^2 - \sum_{I=1}^{M} \frac{Z_I}{|\mathbf{r} - \mathbf{R}_I|}.$$

2.4.2. Møller-Plesset Perturbation Theory

Møller-Plesset perturbation theory [27,30] constitutes a special case of Rayleigh-Schrödinger perturbation theory [31]. Therefore the more general case will be presented before proceeding to Møller-Plesset perturbation theory itself.

Within perturbation theory (PT), the Hamiltonian is partitioned into two parts where the solutions to the first, dominating part $\hat{H}_0$ are known and the influence of the second part W is treated as a perturbation:

$$\hat{H} = \hat{H}_0 + W,$$

where the solutions to $\hat{H}_0|\Psi_i^{(0)}\rangle = E_i^{(0)}|\Psi_i^{(0)}\rangle$ are known. As long as the perturbation is small the eigenvalues and eigenfunctions of $\hat{H}_0$ should lie close to those of $\hat{H}$ (denoted as $\mathcal{E}_i$ and Ψ_i). PT seeks for a way to systematically improve $E_i^{(0)}$ and $\Psi_i^{(0)}$ to approach the exact solutions $\mathcal{E}_i$ and Ψ_i.

First, an ordering parameter λ (later, $\lambda = 1$ will be chosen) is introduced

$$\hat{H} = \hat{H}_0 + \lambda W$$

and the exact eigenfunctions and eigenvalues are expanded in a Taylor series in λ:

$$\mathcal{E}_i = E_i^{(0)} + \lambda E_i^{(1)} + \lambda^2 E_i^{(2)} + \dots \tag{2.7a}$$

$$\Psi_i = \Psi_i^{(0)} + \lambda \Psi_i^{(1)} + \lambda^2 \Psi_i^{(2)} + \dots \ . \tag{2.7b}$$

Additionally, the intermediate normalization $\langle \Psi_i^{(0)}|\Psi_i\rangle = 1$ is chosen leading to

$$\langle \Psi_i^{(0)}|\Psi_i^{(n)}\rangle = 0 \qquad \text{for} \quad n = 1, 2, 3, \dots \ .$$

By inserting the expansions 2.7 and equating coefficients of λ^n the eigenvalue equation $(\hat{H}_0 + W)\Psi_i = \mathcal{E}_i \Psi_i$ can be separated into multiple equations:

$$\hat{H}_0|\Psi_i^{(0)}\rangle = E_i^{(0)}|\Psi_i^{(0)}\rangle \tag{2.8a}$$

$$\hat{H}_0|\Psi_i^{(1)}\rangle + W|\Psi_i^{(0)}\rangle = E_i^{(0)}|\Psi_i^{(1)}\rangle + E_i^{(1)}|\Psi_i^{(0)}\rangle \tag{2.8b}$$

$$\hat{H}_0|\Psi_i^{(2)}\rangle + W|\Psi_i^{(1)}\rangle = E_i^{(0)}|\Psi_i^{(2)}\rangle + E_i^{(1)}|\Psi_i^{(1)}\rangle + E_i^{(3)}|\Psi_i^{(0)}\rangle \tag{2.8c}$$

$$\dots \qquad . \tag{2.8d}$$

Multiplication from left with $\langle\Psi_i^{(0)}|$ leads to the following expressions for the energy corrections up to second order:

$$\begin{aligned} E_i^{(0)} &= \langle\Psi_i^{(0)}|\hat{H}_0|\Psi_i^{(0)}\rangle \\ E_i^{(1)} &= \langle\Psi_i^{(0)}|W|\Psi_i^{(0)}\rangle \\ E_i^{(2)} &= \langle\Psi_i^{(0)}|W|\Psi_i^{(1)}\rangle. \end{aligned}$$

To obtain the first-order correction to the wave function, it is expanded in the complete orthonormal set of unperturbed eigenfunctions $\{\Psi_n^{(0)}\}$:

$$|\Psi_i^{(1)}\rangle = \sum_n a_n|\Psi_n^{(0)}\rangle \qquad \text{with} \quad a_n = \langle\Psi_n^{(0)}|\Psi_i^{(1)}\rangle. \tag{2.10}$$

Then the set of coefficients $\{a_n\}$ can be determined by multiplication of equation 2.8b with $\langle\Psi_n^{(0)}|$, $n \neq i$ from the left. This results in the following expression for the first-order correction to the wave function:

$$|\Psi_i^{(1)}\rangle = \sum_{n\neq i} \frac{\langle\Psi_n^{(0)}|\hat{H}_0|\Psi_i^{(0)}\rangle}{E_i^{(0)} - E_n^{(0)}}|\Psi_n^{(0)}\rangle.$$

The corrections for higher orders can be obtained similarly.

Finally, Møller-Plesset PT consists of a special choice of the unperturbed Hamiltonian, namely the Hartree-Fock operator [27, 30]:

$$\hat{H}_0 = \sum_p \epsilon_p c_p^\dagger c_p,$$

where $\{\epsilon_p\}$ are the Hartree-Fock orbital energies. The remaining part of the correlation energy is treated pertubatively:

$$W = -\sum_{pq}\sum_k \langle pk||qk\rangle c_p^\dagger c_q + \frac{1}{2}\sum_{pqrs}\langle pq|rs\rangle c_p^\dagger c_q^\dagger c_s c_r.$$

For convenience, the second quantized form of the operators was chosen.

Given this form of the Hamiltonian, the expressions for corrections to the ground state HF energy E_0 and wave function Φ_0 can be easily derived using equations 2.9 and 2.10:

$$\begin{aligned} E_0^{(0)} &= \sum_i \epsilon_i \\ E_0^{(1)} &= -\frac{1}{2}\sum_{ij}\langle ij||ij\rangle \\ E_0^{(2)} &= \sum_{i<j,a<b} t_{ijab}\langle ij||ab\rangle \\ \Psi_0^{(1)} &= \sum_{i<j,a<b} t_{ijab} c_a^\dagger c_b^\dagger c_i c_j|\Phi_0\rangle \end{aligned}$$

Here, t_{ijab} are the so-called T-amplitudes and are defined as

$$t_{ijab} = \frac{\langle ab||ij\rangle}{\epsilon_a + \epsilon_b - \epsilon_i - \epsilon_j}. \tag{2.11}$$

The sum $E_0^{(0)} + E_0^{(1)}$ just gives the Hartree-Fock energy. Therefore, the first improvement over HF is given by the second-order correction. The resulting MP2 method, whose computational effort scales with N^5 (N being the number of basis functions), offers a good compromise between cost and accuracy. As the MP perturbation series is not guaranteed to converge and due to the increasing computational cost, it is rarely employed in orders higher than third or fourth.

2.4.3. Configuration Interaction

In configuration interaction (CI) [27, 28], the wave function is expanded in a linear combination of N-electron excited Slater determinants:

$$|\Psi^{CI}\rangle = \left[c_0 + \sum_I c_I \hat{C}_I\right] |\Phi_0\rangle \tag{2.12}$$

$$\hat{C}_I \equiv \{c_a^\dagger c_i;\ c_a^\dagger c_b^\dagger c_i c_j, a<b, i<j;\ c_a^\dagger c_b^\dagger c_c^\dagger c_i c_j c_k, a<b<c, i<j<k;\ \dots\}.$$

The expansion coefficients c_I and c_0 are obtained by applying the variational principle. This is equivalent to representing the Hamilton operator within the basis of the excited Slater determinants $|\Phi_I\rangle = \hat{C}_I|\Phi_0\rangle$ and solving the eigenvalue equation

$$\mathbf{HC} = \mathbf{CE}^{CI}.$$

By diagonalization, the ground state energy as well as the excited state energies can be obtained. The matrix $\mathbf{C}$ contains the eigenvectors of $\mathbf{H}$ and therefore the coefficients c_I. The matrix $\mathbf{E}^{CI}$ is diagonal and gives the energies of the various excited states.

If all possible excitation classes are considered, the method is referred to as full-CI (FCI). It yields the exact results within the chosen basis. However, given an N-electron system and M basis functions, the dimension of the resulting eigenvalue problem amounts to $\begin{pmatrix} 2M \\ N \end{pmatrix}$. This is computationally not feasible for systems that comprise more than a few atoms.

By truncation after certain excitation classes approximate CI methods are obtained. Truncation after the single excitations leads to CIS, after doubles to CISD (or CID) and so on. Due to Brillouin's theorem [27] the ground state energy is not improved by singly excited determinants and the first corrections of the ground state are introduced by double excitations. Consequently, CIS is only an excited states method and will be discussed in detail in Section 3.1.

The major drawback of CI methods is that size-consistency is lost for all truncated methods apart from CIS. By contrast, the coupled-cluster ansatz presented in the next chapter allows for a truncation associated with excitation orders but conserves size-consistency. However, it is conceptually more demanding.

2.4.4. Coupled-Cluster Theory

The linear parametrization of the CI wave function is the cause for the loss of size-consistency when the CI expansion is truncated after a certain excitation class. In coupled-cluster (CC) a product form is chosen instead [28]:

$$|\Psi^{CC}\rangle = \left[\prod_I (1 + t_I \hat{C}_I)\right] |\Phi_0\rangle. \tag{2.13}$$

The expansion coefficients t_I are called coupled-cluster amplitudes. If all orders are included, the same result as with FCI is obtained and only the parametrization is changed. However, if this expansion is truncated after a certain class of excitations, the size-consistency is preserved.

In order to make algebraic manipulations more convenient, 2.13 is usually replaced by the following exponential ansatz ($1+\hat{C}_I = \exp(\hat{C}_I)$ due to $\hat{C}_I\hat{C}_I|\Phi_0\rangle = 0$):

$$|\Psi^{CC}\rangle = \exp(\hat{T})|\Phi_0\rangle,$$

where $\hat{T}$ is the cluster operator defined by

$$\begin{aligned}
&\exp(\hat{T}) = \sum_{k=0}^{\infty} \frac{\hat{T}^k}{k!} \\
&\hat{T} = \hat{T}_1 + \hat{T}_2 + \hat{T}_3 + \dots \\
&\hat{T}_1 = \sum_{ia} t_{ia} c_a^\dagger c_i, \qquad \hat{T}_2 = \sum_{a>b,i>j} t_{ijab} c_a^\dagger c_b^\dagger c_i c_j, \qquad \dots \ .
\end{aligned}$$

Unlike the previous methods, the solution is not obtained by a variational method, which would be cumbersome and applicable only for small systems, but by projection of

$$\hat{\bar{H}}|\Phi_0\rangle = E^{CC}|\Phi_0\rangle$$

to $\langle\Phi_0|$ and the excited Slater determinants $\langle\Phi_I| = \langle\Phi_0|\hat{C}_I^\dagger$. This yields the following set of coupled equations

$$\langle\Phi_0|\hat{\bar{H}}|\Phi_0\rangle = E^{CC} \tag{2.14a}$$

$$\langle\Phi_I|\hat{\bar{H}}|\Phi_0\rangle = 0. \tag{2.14b}$$

Here, $\hat{\bar{H}}$ denotes the similarity-transformed Hamilton operator

$$\hat{\bar{H}} = \exp(-\hat{T})\hat{H}\exp(\hat{T}).$$

As they are coupled, the CC equations 2.14 have to be solved iteratively. Apart from being size consistent at all truncation levels the hierarchy of CC methods converges faster with increasing truncation level than the respective CI methods because of the efficient parametrization. Therefore, CC methods are very popular methods and widely used. Nevertheless, the obtained energies are no longer an upper bound for the exact ground state energy due to the non-variational character. Because of the high accuracy, this does not, however, impose a serious restriction.

2.4.5. Complete Active Space Methods

The methods introduced so far are all so-called single-reference methods as they employ only one set of orbitals obtained during an initial HF calculation. The orbitals are, however, not well-suited for situations including strong correlation effects or when more than one SD is necessary for an adequate description. Thus, all these methods become problematic when the electronic states are not well separated. In such cases multi-configurational approaches are necessary in which the expansion coefficients of a full-CI expansion and the ones of the molecular orbitals are simultaneously optimized. However, this treatment has to be limited to a specific set of orbitals in order to guarantee numerical feasibility.

In complete active space self-consistent field (CASSCF) [11] a small subspace is selected from the Hartree-Fock orbitals in which a full-CI calculation is performed. This active space contains occupied as well as virtual orbitals. For all other orbitals the occupation numbers are left constant and only the orbital expansions with respect to the basis functions are re-optimized. To further save computational effort, the lowest occupied and maybe the highest unoccupied orbitals can be frozen as electron correlation is expected to have only little effect on them. In this case they are neither considered during the CI calculation nor are their expansion coefficients changed.

However, the choice of relevant orbitals for the active space is not a trivial task and usually requires *a priori* knowledge of the system under consideration. The fact that close lying orbitals may change their order when the molecular geometry is varied or even during the re-optimization of their coefficients hinders the selection furthermore. An additional limitation is given by the size of the active space. Usually not more than ten to twelve electrons in twelve to fourteen orbitals can be considered with reasonable computational effort.

Moreover, the state for which the optimal orbitals are determined is crucial. For instance, for excited state calculations it is recommended to use state-averaged orbitals which are optimized to simultaneously represent a certain number of excited states in addition to the ground state. With that approach one can avoid running a CASSCF calculation for every state of interest separately.

Despite the fact that it is definitely no black-box method and that the active space as well as the number of states during the state averaging have to be chosen with great care, CASSCF provides an efficient and reliable approach in cases where the multi-configurational character of the wave-function has to be considered as, e. g., close to conical intersections or at large bond distances.

In the CASSCF wave function only static correlation due to long-range effects is included. The effects due to dynamical correlation or, in other words, short-ranged and instantaneous electron-electron interaction are still not considered. One way to incorporate such effects is to use perturbation theory on top of the CASSCF wave function resulting in the popular complete active space second-order perturbation theory (CASPT2) [11] method. The multi-state CASPT2 approach offers an extension to conventional CASPT2 for situations in which more than one reference state is required for an appropriate assessment of the problem. Such calculations are usually performed on top of state-averaged

CASSCF and the coupling up to second order in dynamical correlation energy is considered. Apart from accounting appropriately for dynamical correlation effects, the obtained states are orthonormal to each other which is not guaranteed during single-state CASPT2 but highly desirable when the final states are to be used for further calculations like spin-orbit coupling effects.

2.5. Density Functional Theory

Density Functional Theory (DFT) [32] is a widely applied and efficient semi-empirical method. Its basic variable is given by the electron density. While the complexity of a wave-function based method increases exponentially with the number of electrons, the electron density of an N-electron system depends solely on the three spacial coordinates. This difference explains the efficiency of density functional methods.

Modern density functional theory is based on the Hohenberg-Kohn theorems [33]:

1. The electron density uniquely determines the Hamilton operator and all properties of the system.

2. Validity of the variational principle.

On the basis of these theorems the ground state energy E_0 can be written as a functional of the ground state density ρ_0:

$$E_0[\rho_0] = T[\rho_0] + E_{ee}[\rho_0] + E_{Ne}[\rho_0] = \int \rho_0(\mathbf{r}) V_{Ne} d\mathbf{r} + F_{HK}[\rho_0]$$

and

$$F_{HK}[\rho_0] = T[\rho_0] + E_{ee}[\rho_0]$$

is called the Hohenberg-Kohn functional. Here, $E_{Ne}[\rho_0]$ describes the interaction between nuclei and electrons and can be calculated. Unfortunately, neither the functional of the kinetic energy $T[\rho_0]$ nor the functional for the electron-electron interaction $E_{ee}[\rho_0]$ are known.

For the electron-electron interaction at least the classical Coulomb part $J[\rho_0]$ can be determined. The non-classical contribution $E_{ncl}[\rho_0]$ remains unknown and contains the correction for the self-interaction, exchange and Coulomb correlation.

$$E_{ee}[\rho_0] = J[\rho_0] + E_{ncl}[\rho_0] = \frac{1}{2} \int \int \frac{\rho_0(\mathbf{r}_1)\rho_0(\mathbf{r}_2)}{r_{12}} d\mathbf{r}_1 d\mathbf{r}_2 + E_{ncl}[\rho_0].$$

Although the functional in this form is generally valid, the fact that the form of the kinetic energy and the non-classical contributions to the electron-electron interaction are unknown prevents any application. The breakthrough was achieved 1965 by means of the Kohn-Sham ansatz [34] that uses the reintroduction of single-particle functions (orbitals) φ_i as a mathematical trick. Here,

φ_i is used instead of χ_i in order to distinguish them from Hartree-Fock spin orbitals and in order to stress their purely mathematical character.

First of all, a non-interacting reference system S consisting of N particles is defined and the ground state represented by a Slater determinant. The related density ρ_s is constructed to be equal to the exact density ρ. This trick makes the calculation of the exact kinetic energy of the non-interacting reference system $T_s[\rho]$ possible:

$$T_s = -\frac{1}{2}\sum_{i=1}^{N}\langle\varphi_i|\nabla^2|\varphi_i\rangle.$$

Even though this term does not give the whole kinetic energy the difference is small. The general density functional can be written as:

$$E_{DFT}[\rho] = E_{Ne}[\rho] + T_s[\rho] + J[\rho] + E_{XC}[\rho]. \tag{2.15}$$

The exchange-correlation functional $E_{XC}[\rho]$ contains the non-classical contributions to the electron-electron interaction E_{ncl} as well as that part of the kinetic energy $T_c[\rho]$ that is not included in $T_s[\rho]$:

$$E_{XC}[\rho] = (T[\rho] - T_s[\rho]) + (E_{ee}[\rho] - J[\rho]) = T_c[\rho] + E_{ncl}[\rho].$$

As in HF theory, the optimal orbitals are determined by employing the variational principle and minimizing the energy expression 2.15 under the constraint $\langle\varphi_i|\varphi_j\rangle = \delta_{ij}$. Finally, a set of equations is obtained that has to be solved iteratively:

$$\hat{F}^{KS}\varphi_i = \epsilon_i\varphi_i$$

with the Kohn-Sham operator

$$\hat{F}^{KS} = -\frac{1}{2}\nabla^2 + v_s(\mathbf{r}) = -\frac{1}{2}\nabla^2 + \int\frac{\rho(\mathbf{r}')}{|\mathbf{r}-\mathbf{r}'|}d\mathbf{r}' - \sum_I\frac{Z_I}{|\mathbf{r}-\mathbf{R}_I|} + v_{XC}[\rho](\mathbf{r}).$$

The external potential v_s contains the potential for the interaction between electrons and nuclei, a mean-field Coulomb interaction and the potential originating from the unknown exchange-correlation energy E_{XC} defined by

$$v_{XC}[\rho](\mathbf{r}) \equiv \frac{\delta E_{XC}[\rho]}{\delta\rho(\mathbf{r})}.$$

Then, the ground state density is given by

$$\rho_0(\mathbf{r}) = \rho_S(\mathbf{r}) = \sum_i\sum_{m_s}|\varphi_i(\mathbf{r}, m_s)|^2.$$

Evaluating the energy expression 2.15 by using this density yields the ground state energy.

If the exact form of the exchange-correlation functional E_{XC} was known, DFT would give an exact description of the system. The approximations start

by assuming an explicit form for E_{XC} and the search for better functionals is consequently an important field of research. However, it is not possible to improve the exchange and correlation functionals systematically. A whole variety of different exchange-correlation functionals have been developed, e. g., BLYP [35, 36], BP86 [35, 37], B3LYP [38], PBE0 [39], BHLYP [40]. Depending on the system under consideration they provide good approximations for the electronic ground state. It has to be stressed, however, that the obtained ground state energy is only an upper bound to the exact energy of the model Hamiltonian characterized by the chosen exchange-correlation functional but not to the exact ground state energy.

3. Quantum Chemical Methods for the Description of Electronic Excitations

One of the greatest challenges in computational chemistry is the accurate description of excited states of large molecular systems and their properties [9–13]. Widely used methods are, among others, time-dependent density functional theory (TDDFT) [10, 41, 42], configuration interaction (CI) methods as CI singles (CIS) [43] or CIS with a perturbation correction for connected double excitations (CIS(D)) [44], complete active space second-order perturbation theory (CASPT2) [45, 46], approximate linear response coupled-cluster (CC) theory of second order (ri-CC2) [47, 48], and a combination of density functional theory (DFT) with multi-reference configuration interaction methods (DFT/MRCI) [49]. If applied appropriately and with caution, they all can provide valuable insight, however, "black-box" methods applicable to a broad range of photochemical and -physical processes are still lacking and the description of charge-transfer and Rydberg states as well as of states with high double excitation character have proven to be especially challenging [9–13]. In this chapter, the most important excited state methods are presented.

A less known but nevertheless promising method for the calculation of excited states is the algebraic diagrammatic construction (ADC) scheme [14–18]. It constitutes a hermitian eigenvalue problem, like configuration interaction, and is size-consistent as coupled-cluster theory. The elements of the corresponding secular matrix are obtained by perturbation theory. Although originally obtained using propagator theory [14], an alternative derivation *via* the so-called intermediate state representation (ISR) has been introduced making the excited state wave function accessible and thereby enabling the calculation of excited state properties [15]. As this method will be extensively used throughout this work it will be introduced in Section 3.3.

3.1. Configuration Interaction Singles (CIS)

As mentioned in Section 2.4.3, CI singles (CIS) is a truncation of the full-CI expansion after the single excitations [11, 27]. It does not give an improved description of the HF ground state but can be used to calculate excited states. In addition, it is the only truncated CI method that is size-consistent. Both properties are consequences of Brillouin's theorem [27] which states that the HF ground state does not couple to singly excited SDs $|\Phi_i^a\rangle = c_a^\dagger c_i|\Phi_0\rangle$:

$$\langle\Phi_i^a|\hat{H}|\Phi_0\rangle = \langle\Phi_0|\hat{H}|\Phi_i^a\rangle = 0.$$

Within the CIS approximation the excitation energies are given by the eigenvalues of the shifted Hamiltonian $\hat{H} - E_0^{HF}$ represented in the basis of singly

excited SDs:

$$H_{ia,jb} = \langle \Phi_i^a | \hat{H} - E_0^{HF} | \Phi_j^b \rangle = (\epsilon_a - \epsilon_i)\delta_{ij}\delta_{ab} - \langle aj||bi \rangle$$

The shifted Hamiltonian is used in order to obtain directly excitation energies instead of absolute energies.

In dependence of the system and type of excited state that is considered, the quality of the results varies strongly. The resulting excitation energies can lie up to 2 eV too high in energy [10]. This is a consequence of the fact that the excitation energies are dominated by the orbital energy differences. The occupied and virtual orbital energies, however, correspond to ionization and electron attachment energies of the N-particle system, respectively. However, an excitation process is better described by ionization and subsequent electron attachment to the resulting $N-1$-particle system. The Coulomb-exchange integrals $-\langle aj||bi \rangle$ can only partially correct for this unbalanced treatment. Therefore, CIS is nowadays rarely used despite its high efficiency.

However, there are extensions using perturbation theory that yield more accurate and still size-consistent methods like CIS(D) [44] or CIS(D∞) [50].

3.2. The Approximate Coupled-Cluster Method CC2

The CC2 method [47] can be viewed as an approximation to CCSD in which the doubles amplitudes are included in first order only. It can be derived from the CC singles and doubles (CCSD) equations by neglecting all terms in which products of double excitation operators occur. Historically, however, CC2 has been introduced as a modification to MP2 in order to make the use of linear response and the calculation of excited states possible. For linear response being applicable corrections from single excitations have to be present. Therefore, the singles of CCSD were taken and added to MP2.

The final ground state CC2 amplitude equations are given by:

$$\langle \Phi_i^a | \hat{\bar{H}} + \left[\hat{\bar{H}}, \hat{T}_2 \right] | \Phi_0 \rangle = 0$$
$$\langle \Phi_{ij}^{ab} | \hat{\bar{H}} + \left[\hat{F}, \hat{T}_2 \right] | \Phi_0 \rangle = 0$$

where $\hat{\bar{H}}$ denotes the $\hat{T}_1$ similarity transformed Hamiltonian

$$\hat{\bar{H}} = \exp(-\hat{T}_1)\hat{H}\exp(\hat{T}_1)$$

and $|\Phi_i^a\rangle = c_a^\dagger c_i |\Phi_0\rangle$ and $|\Phi_{ij}^{ab}\rangle = c_a^\dagger c_b^\dagger c_i c_j |\Phi_0\rangle$ are singly and doubly excited SDs, respectively. The cluster operators $\hat{T}_1$ and $\hat{T}_2$ were already defined in Section 2.4.4. When the t_1-amplitudes are set to zero ($\hat{T}_1 = 0$), the MP2 results are recovered. However, due to the artificial introduction of singly excited configurations, some of the consistency of the MP2 method is lost and in general MP2 should be preferred for ground state calculations.

Starting from this coupled-cluster equations a method for excited states can be obtained by using linear response theory. Finally, the excitation energies are

obtained by determining the eigenvalues of the Jacobian (A-matrix):

$$\mathbf{A}^{CC2} = \left(\begin{array}{c|c} \langle \Phi_i^a | \left[(\hat{\tilde{H}} + \left[\hat{\tilde{H}}, \hat{T}_2 \right]), \hat{\tau}_j^b \right] | \Phi_0 \rangle & \langle \Phi_i^a | \left[\hat{\tilde{H}}, \hat{\tau}_{kl}^{cd} \right] | \Phi_0 \rangle \\ \hline \langle \Phi_{ij}^{ab} | \left[\hat{\tilde{H}}, \hat{\tau}_k^c \right] | \Phi_0 \rangle & \langle \Phi_{ij}^{ab} | \left[\hat{F}, \hat{\tau}_{kl}^{cd} \right] | \Phi_0 \rangle \end{array} \right) \tag{3.1}$$

$$\text{with} \qquad \hat{\tau}_i^a = c_a^\dagger c_i \qquad \text{and} \qquad \hat{\tau}_{ij}^{ab} = c_a^\dagger c_b^\dagger c_i c_j.$$

Here, $\hat{F}$ denotes the Fock operator. CC2 has the advantage that it scales only with fifth order and not like CCSD with sixth order with respect to the number of basis functions. However, it incorporates the same disadvantage as all coupled-cluster methods. The eigenvalue problem is not hermitian and in principle complex eigenvalues can occur. Close to the ground state minimum this is usually not a problem but at large distances or close to conical intersections it can become crucial.

When the t_1-amplitudes are set to zero, the eigenvalue equation of CIS with quasidegenerate second-order perturbation corrections (CIS(D_∞)) [50, 51] results:

$$\mathbf{A}^{CIS(D_\infty)} = \left(\begin{array}{c|c} \langle \Phi_i^a | \left[(\hat{H} + \left[\hat{H}, \hat{T}_2 \right]), \hat{\tau}_j^b \right] | \Phi_0 \rangle & \langle \Phi_i^a | \left[\hat{H}, \hat{\tau}_{kl}^{cd} \right] | \Phi_0 \rangle \\ \hline \langle \Phi_{ij}^{ab} | \left[\hat{H}, \hat{\tau}_k^c \right] | \Phi_0 \rangle & \langle \Phi_{ij}^{ab} | \left[\hat{F}, \hat{\tau}_{kl}^{cd} \right] | \Phi_0 \rangle \end{array} \right). \tag{3.2}$$

This secular matrix is closely related to the ADC(2)-s secular matrix introduced in the next section. Therefore, all three methods, CC2, CIS(D_∞) and ADC(2)-s, yield similar excitation energies in most cases and scale with N^5, N being the number of basis functions.

3.3. Algebraic Diagrammatic Construction

The algebraic diagrammatic construction (ADC) [14–18, 52] scheme has originally been derived within the framework of Green's function theory by employing diagrammatic perturbation theory to the polarization propagator and using the typical Møller-Plesset partitioned Hamilton operator [14]. Here, we present an alternative and conceptually less demanding route based on the intermediate state representation (ISR) approach [15].

Within the ISR, the exact excited states $|\Psi_J\rangle$ are expanded using a complete set of intermediate states $|\tilde{\Psi}_J\rangle$. These are constructed from the exact ground state $|\Psi_0\rangle$ by applying excitation operators $\hat{C}_I$ (compare equation 2.12) and subsequent Gram-Schmidt orthonormalization. Orthogonalization with respect to the ground state leads the so-called precursor states $|\Psi_I^\#\rangle$:

$$|\Psi_I^\#\rangle = \hat{C}_I|\Psi_0\rangle - |\Psi_0\rangle\langle\Psi_0|\hat{C}_I|\Psi_0\rangle$$

In a second step the precursor states are orthonormalized among each other according to

$$|\tilde{\Psi}_J\rangle = \sum_I |\Psi_I^\#\rangle (S^{-1/2})_{J,I}$$

where $S_{J,I}$ is the overlap between two precursor states:

$$S_{J,I} = \langle \Psi_I^{\#} | \Psi_J^{\#} \rangle = \langle \Psi_0 | \hat{C}_I^{\dagger} \hat{C}_J | \Psi_0 \rangle - \langle \Psi_0 | \hat{C}_I^{\dagger} | \Psi_0 \rangle \langle \Psi_0 | \hat{C}_J | \Psi_0 \rangle$$

Then, the excitation energies can be obtained by representing the subtracted Hamiltonian $\hat{H} - \mathcal{E}_0$ ($\mathcal{E}_0$ being the exact ground state energy) within the basis of these intermediate states

$$M_{IJ} = \langle \tilde{\Psi}_I | \hat{H} - \mathcal{E}_0 | \tilde{\Psi}_J \rangle.$$

and solving the corresponding eigenvalue problem

$$\mathbf{MX} = \mathbf{X\Omega}.$$

Here, $\mathbf{\Omega}$ denotes the eigenvalue matrix and $\mathbf{X}$ the matrix of eigenvectors.

Obviously, neither the exact ground state wave function nor the exact ground state energy are known. In the ADC class of models explicit expressions for the correlated excited states are derived by starting from the respective quantities in Møller-Plesset perturbation theory [30]. The resulting matrix $\mathbf{M}$ is called the ADC-Matrix and given as an explicit perturbation expansion:

$$\mathbf{M} = \mathbf{M}^{(0)} + \mathbf{M}^{(1)} + \mathbf{M}^{(2)} + \dots \ .$$

Truncation after the n-th order in perturbation theory yields ADC(n). Thus, if MP2 is used for the ground state, ADC(2) is obtained while MP3 leads to ADC(3). Figure 3.1 summarizes the structure of the ADC(n) secular matrix up to third order. In second order, which has been extensively used in this work, it spans the single (particle-hole, ph) and double excitation (2p2h) manifold. Singly excited states (ph/ph block) are treated through second order of perturbation theory and their coupling to doubly excited states (ph/2p2h and 2p2h/ph blocks) in first order. In its strict variant, denoted ADC(2)-s, doubly excited states are included in zeroth order and the 2p2h/2p2h block is diagonal containing only the orbital energy differences. Its computational cost scales as CC2 with N^5, N being the number of basis functions.

For further reference, the explicit expressions for the ADC(2)-s matrix elements are given below [53]:

$$\text{ph/ph block:} \qquad M_{ia,jb} = K_{ia,jb} + C^{(1)}_{ia,jb} + C^{(2)}_{ia,jb}$$

$$\begin{aligned}
\text{with} \qquad K_{ia,jb} &= (\epsilon_a - \epsilon_i)\delta_{ab}\delta_{ij} \\
C^{(1)}_{ia,jb} &= -\langle aj||bi\rangle \\
C^{(2)}_{ia,jb} &= C^{(2)A}_{ia,jb} + C^{(2)B}_{ia,jb} + C^{(2)C}_{ia,jb} \\
C^{(2)A}_{ia,jb} &= \frac{1}{4}\delta_{ij} \sum_{ckl} \left[t_{klac}\langle kl||bc\rangle + t^*_{klbc}\langle ac||kl\rangle \right] \\
C^{(2)B}_{ia,jb} &= \frac{1}{4}\delta_{ab} \sum_{cdk} \left[t_{ikcd}\langle jk||cd\rangle + t^*_{jkcd}\langle cd||ik\rangle \right] \\
C^{(2)C}_{ia,jb} &= -\frac{1}{2} \sum_{ck} \left[t_{ikac}\langle jk||bc\rangle + t^*_{jkbc}\langle ac||ik\rangle \right]
\end{aligned}$$

	ph	2p2h
ph	0,1,2,3	-,-,1,2
2p2h	-,-,1,2	-,-,0,1

Figure 3.1.: Structure of the ADC(n) matrix up to third order. The four numbers indicate in which order of perturbation theory the respective blocks are included in ADC(n) with n=0,1,2,3.

$$\text{Coupling blocks:} \qquad M_{ia,kcld} = C^{(1)}_{ia,kcld} \qquad \text{and} \qquad M_{iajb,kc} = C^{(1)}_{iajb,kc}$$

$$\text{with} \qquad C^{(1)}_{ia,kcld} = \langle kl||id\rangle\delta_{ac} - \langle kl||ic\rangle\delta_{ad} - \langle al||cd\rangle\delta_{ik} + \langle ak||cd\rangle\delta_{il}$$
$$C^{(1)}_{iajb,kc} = \langle kb||ij\rangle\delta_{ac} - \langle ka||ij\rangle\delta_{bc} - \langle ab||cj\rangle\delta_{ik} + \langle ab||ci\rangle\delta_{jk}$$

$$\text{2p2h/2p2h block:} \qquad M_{iajb,kcld} = K_{iajb,kcld}$$

$$\text{with} \qquad K_{iajb,kcld} = (\epsilon_a + \epsilon_b - \epsilon_i - \epsilon_j)\delta_{ac}\delta_{bd}\delta_{ik}\delta_{jl}$$

The same secular matrix results from symmetrizing the CIS(D_∞) Jacobian that is obtained from CC2 by setting the t_1-amplitudes to zero (compare equations 3.1 and 3.2), according to [51]

$$\mathbf{M} = \frac{1}{2}\left(\mathbf{A}^{CIS(D_\infty)} + \left(\mathbf{A}^{CIS(D_\infty)}\right)^\dagger\right).$$

This explains the close resemblance between the results from these three methods.

By adding the first-order correction terms from ADC(3) to the 2p2h/2p2h block, the so-called extended ADC(2) (ADC(2)-x) method is obtained. It incorporates doubly excited states in first-order perturbation theory and scales in sixth order with respect to the number of basis functions. However, the influence of doubly excited states is overestimated leading to excitation energies that are too low [54]. Nevertheless, it proofs useful for the determination of states with significant double excitation character as they are stronger shifted than singly excited states when switching from ADC(2)-s to ADC(2)-x.

The matrix elements of the 2p2h/2p2h block in ADC(2)-x are:

$$M_{iajb,kcld} = K_{iajb,kcld} + C^{(1)}_{iajb,kcld}$$

$$
\begin{aligned}
C^{(1)}_{iajb,kcld} = {} & \langle ab||cd\rangle\delta_{ik}\delta_{jl} + \langle kl||ij\rangle\delta_{ac}\delta_{bd} \\
& - [\langle ak||ci\rangle\delta_{bd}\delta_{jl} + \langle al||cj\rangle\delta_{bd}\delta_{ik} + \langle bk||di\rangle\delta_{ac}\delta_{jl} + \langle bl||dj\rangle\delta_{ac}\delta_{ik}] \\
& + [\langle al||ci\rangle\delta_{bd}\delta_{jk} + \langle ak||cj\rangle\delta_{bd}\delta_{il} + \langle bl||di\rangle\delta_{ac}\delta_{jk} + \langle bk||dj\rangle\delta_{ac}\delta_{il}] \\
& + [\langle ak||di\rangle\delta_{bc}\delta_{jl} + \langle al||dj\rangle\delta_{bc}\delta_{ik} + \langle bk||ci\rangle\delta_{ad}\delta_{jl} + \langle bl||cj\rangle\delta_{ad}\delta_{ik}] \\
& - [\langle al||di\rangle\delta_{bc}\delta_{jk} + \langle ak||dj\rangle\delta_{bc}\delta_{il} + \langle bl||ci\rangle\delta_{ad}\delta_{jk} + \langle bk||cj\rangle\delta_{ad}\delta_{il}]
\end{aligned}
$$

The ADC(n) hierarchy of methods comprises the advantages of both, configuration interaction and coupled-cluster, as containing an hermitian secular matrix as well as being size-consistent in all orders. For a detailed comparison between ADC, CI, and CC methods see, e. g., [18, 52, 55].

Once the eigenvectors $\mathbf{Y}_n$ have been determined, the excited state wave function is given by

$$|\Psi_n\rangle = \sum_I Y_{n,I}|\tilde{\Psi}_I\rangle.$$

Thus, the knowledge of the intermediate states allows the calculation of arbitrary one-particle properties O_n or one-particle transition properties O_{nm} where the respective one-particle operator $\hat{O}_1$ is given by $\hat{O}_1 = \sum_{pq} O_{pq} c_p^\dagger c_q$:

$$
\begin{aligned}
O_{nm} &= \langle\Psi_n|\hat{O}_1|\Psi_m\rangle = \sum_{pq} O_{pq}\rho^{n,m}_{pq} \qquad \text{with} \qquad \rho^{n,m}_{pq} = \langle\Psi_n|c_p^\dagger c_q|\Psi_m\rangle \\
O_n &= \langle\Psi_n|\hat{O}_1|\Psi_n\rangle = \sum_{pq} O_{pq}\rho^{n}_{pq} \qquad \text{with} \qquad \rho^{n}_{pq} = \rho^{n,n}_{pq}.
\end{aligned}
$$

The quantities $\rho^{n,m}_{pq}$ and ρ^{n}_{pq} are the one-particle reduced transition density matrix between states n and m and the one-particle reduced density matrix of state n, respectively. Examples for such one-particle properties are transition dipole moments, which allow the calculation of oscillator strengths, dipole moments or spin-orbit coupling elements.

Consequently, the determination of the transition density matrices is of great importance. The ADC one-particle reduced transition density between the ground and an excited state $|\Psi_n\rangle$ is given by

$$\rho^{n,0}_{pq} = \langle\Psi_n|c_p^\dagger c_q|\Psi_0\rangle = \sum_I Y_{n,I} \underbrace{\langle\tilde{\Psi}_I|c_p^\dagger c_q|\Psi_0\rangle}_{f_{pq,I}},$$

where $f_{pq,I}$ are the so-called spectroscopic amplitudes within the intermediate state basis. Like the ADC secular matrix the vector $\mathbf{f}_{pq}$ can be expressed as a perturbation series

$$\mathbf{f}_{pq} = \mathbf{f}^{(0)}_{pq} + \mathbf{f}^{(1)}_{pq} + \mathbf{f}^{(2)}_{pq} + \dots\ .$$

Depending on the truncation, corrections to the transition density of different order can be derived. Similarly, perturbation expansions can be deduced for the transition densities between excited states. Up to second order the following correction terms contribute to the transition densities:

$$
\begin{aligned}
\rho^{n,0}_{pq} &= \rho^{n,0(0)}_{pq} + \rho^{n,0(1)}_{pq} + \rho^{n,0(2)}_{pq} \\
\rho^{n,m}_{pq} &= \rho^{n,m(0)}_{pq} + \rho^{n,m(2)}_{pq}.
\end{aligned}
$$

The explicit expressions for obtaining transition densities can be found in [20]. Within the present ADC code, the same order of perturbation theory is used for the secular matrices as well as the transition density for ADC(1) and ADC(2) methods. However, in the case of ADC(3) the expansions are truncated after second order and the transition density matrices are calculated from the same expressions as in the case of ADC(2) but using the ADC(3) eigenvectors [56]. This approach is chosen for all properties and the calculation of oscillator strengths because the number of terms to consider increases immensely when going from ADC(2) to ADC(3). Nevertheless, it has been shown that this approach (usually referred to as ADC(3/2)) yields excellent results [15].

An efficient implementation of ADC methods up to third order including different properties like (transition) dipole moments or two-photon absorption cross sections is given by the `adcman` module as part of the Q-Chem program package. An overview is given in [20]. The methods developed within this work were implemented within this framework, as well.

3.4. Time-Dependent DFT

The time-dependent density functional theory (TDDFT) [10, 41, 42] is an extension of conventional density functional theory (DFT) to include the time-dependence of a system. It relies on the Runge-Gross theorem that establishes a one-to-one mapping between the time-dependent density $\rho(\mathbf{r}, t)$ and the time-dependent external potential $v_{ext}(\mathbf{r}, t)$. Thus, the time-dependent density determines all physical observables.

Instead of the total energy as in the case of DFT, the action integral $A[\rho]$ is introduced as an unique functional of the density. Its stationary points

$$\frac{\delta A[\rho]}{\delta \rho} = 0$$

$$\text{with} \qquad A[\rho] = \int_{t_0}^{t_1} \langle \Psi[\rho](t) | i\frac{\partial}{\partial t} - \hat{H}(t) | \Psi[\rho](t) \rangle dt.$$

yield the exact time-dependent density of the system.

Like in time-independent DFT (compare Section 2.5) a non-interacting Kohn-Sham system with the same density as the interacting system is introduced:

$$\rho(\mathbf{r}, t) = \rho_s(\mathbf{r}, t) = \sum_j |\varphi_j(\mathbf{r}, t)|^2.$$

The auxiliary single-particle functions $\varphi_j(\mathbf{r}, t)$ fulfill the time-dependent Kohn-Sham equations

$$i\hbar\frac{\partial}{\partial t}\varphi_j(\mathbf{r}, t) = \left(-\frac{1}{2}\nabla^2 + v_s(\mathbf{r}, t)\right)\varphi_j(\mathbf{r}, t)$$

$$\text{with} \qquad v_s(\mathbf{r}, t) = v_{ext}(\mathbf{r}, t) + \int \frac{\rho(\mathbf{r}', t)}{|\mathbf{r} - \mathbf{r}'|} d\mathbf{r}' + \frac{\delta A_{XC}[\rho]}{\delta \rho}.$$

Apart from the fact that the exact exchange-correlation action integral functional $A_{XC}[\rho]$ is not known and approximations have to be employed, it has been shown lately that the proofs of the Runge-Gross theorems are erroneous and that the action-integral is not suitable to construct equations of motion for the time evaluation of the system [57, 58]. Moreover, it is not a predictive method and the knowledge of the exact time-dependent exchange-correlation potential is necessary to reproduce the evaluation of the system.

However, within the framework of linear response theory, TDDFT can be considered as an *ad hoc* extension of DFT and used for the calculation of excited states. Usually, exchange correlation functionals from DFT are used.

Employing time-independent Kohn-Sham orbitals and energies from a ground state calculation, the excitation energies can be obtained from the following pseudo-eigenvalue problem:

$$\begin{pmatrix} \mathbf{A} & \mathbf{B} \\ \mathbf{B}^* & \mathbf{A}^* \end{pmatrix} \begin{pmatrix} \mathbf{X} \\ \mathbf{Y} \end{pmatrix} = \omega \begin{pmatrix} \mathbf{1} & \mathbf{0} \\ \mathbf{0} & -\mathbf{1} \end{pmatrix} \begin{pmatrix} \mathbf{X} \\ \mathbf{Y} \end{pmatrix}$$

$$\text{with} \qquad A_{ia,jb} = (\epsilon_a - \epsilon_i)\delta_{ij}\delta_{ab} + \langle aj|ib\rangle + f^{xc}_{ajib}$$

$$B_{ia,jb} = \langle ab|ij\rangle + f^{xc}_{abij}.$$

The exchange-correlation kernel f^{xc}_{ajib} is given by

$$f^{xc}_{ajib} = \langle aj|\delta v_{xc}|ib\rangle \qquad \text{with} \qquad \delta v_{xc}[\rho](\mathbf{r},\mathbf{r}') = \frac{\delta^2 E_{xc}[\rho]}{\delta\rho(\mathbf{r})\delta\rho(\mathbf{r}')}. \tag{3.3}$$

For locally excited states TDDFT usually leads to reasonable results with errors of 0.1-0.5 eV. However, for Rydberg states, charge-transfer states or states with a significant double excitation character TDDFT fails completely [10]. In the case of the former two, the respective states tend to lie far too low in energy. This can even lead to artificial minima on the potential energy surface [59]. Several approaches have been suggested to improve the description of CT-states (e. g., [60–70]). Nevertheless, this hinders the application to, e. g., donor-acceptor systems, systems with a largely delocalized electron system or transition metal complexes. Owing to its efficiency, TDDFT is still one of the most popular excited state methods for medium to large molecules.

4. Scaled-Opposite-Spin-(SOS)-ADC(2)-x

With the concept of scaled opposite-spin (SOS), a pragmatic semi-empirical approximation has been introduced to the ADC(2)-x method that leads to a significant saving in computational effort. The parameters included were fitted with respect to a benchmark set of electronically excited states in standard organic molecules that include some doubly excited states, as well. Like the original, unscaled ADC(2)-x scheme it can be used to identify electronically excited states with high double excitation character, however, at reduced computational cost. At the same time, it is possible to reduce the overestimation of doubly excited configurations that is inherent to ADC(2)-x (compare Section 3.3). Additionally, a scheme for the strict variant (ADC(2)-s) was derived directly from SOS-MP2 by application of the intermediate state formalism and compared to an existing version of SOS-ADC(2)-s.

4.1. Theoretical Background

In 2003, Grimme suggested an improved Møller-Plesset perturbation theory in second order (MP2) method, termed spin-component-scaled MP2 (SCS-MP2) [71], which is based upon the general observation that low-level methods as, e. g., MP2 underestimate those contributions to the correlation energy arising from electrons with opposite spin while those from electrons with same spin are overestimated. Introduction of two scaling parameters for the two contributions led to an improved description of the correlation energy

$$E^{(2)}_{SCS-MP2} = c^{os} E^{(2)os}_{MP2} + c^{ss} E^{(2)ss}_{MP2},$$

with $E^{(2)os}_{MP2}$ and $E^{(2)ss}_{MP2}$ being the contributions to the total correlation energy by opposite-spin (os) and same-spin (ss) terms:

$$E^{(2)os}_{MP2} = -\sum_{\overline{a}b\bar{i}j} t_{\bar{i}j\overline{a}b} \langle \bar{i}j|\overline{a}b\rangle$$

$$E^{(2)ss}_{MP2} = -\frac{1}{2}\sum_{abij} t_{ijab}(\langle ij|ab\rangle - \langle ij|ba\rangle) - \frac{1}{2}\sum_{\overline{abij}} t_{\overline{ijab}}(\langle \overline{ij}|\overline{ab}\rangle - \langle .\overline{ij}|\overline{ba}\rangle)$$

Parts of this chapter have already been published in
C. M. Krauter, M. Pernpointner, and A. Dreuw
Application of the scaled opposite-spin approximation to algebraic diagrammatic construction schemes of second order
J. Chem. Phys. **138**, 044107 (2013)

Here, spatial orbitals have been used and a bar indicates β-spin. The parameters c^{os} and c^{ss} were fitted to high-quality *ab initio* data leading to $c^{os} = 6/5$ and $c^{ss} = 1/3$ as optimal values. Later, Fink employed rigorous perturbation theory to derive a method that incorporates analogously defined scaling parameters and can be improved systematically [72].

The resulting SCS-MP2 method preserves two important properties: It is size-extensive and the correlation energy is invariant to unitary transformations among the occupied or virtual orbitals. By now, several variants of the original SCS-MP2 exist [73].

In principle, the size of the parameters was motivated from theoretical considerations: In two-electron systems (only one opposite-spin interaction) about 80-85 % of the correlation energy is recovered by MP2. From this $c_{os} = 6/5$ was chosen. Using the constraint that the total correlation energy of the unmodified MP2 should be recovered the following expression has to be fulfilled:

$$c^{ss} = 1 - \frac{E^{(2)os}_{MP2}}{E^{(2)ss}_{MP2}}(c^{os} - 1).$$

However, the ratio $E^{(2)os}_{MP2}/E^{(2)ss}_{MP2}$ varies in dependence of the importance of electron correlation (usually between 3 and 4). Therefore c^{ss} was obtained empirically.

The scaling mostly affects parallel-spin pair energies that are mainly due to electron pairs in distant orbitals [71]. Consequently, this term accounts mostly for long-range, non-dynamical correlation. The opposite is true for the opposite-spin part. Therefore, SCS-MP2 increases short-range, dynamical correlation ($c^{ss} > 1$) and reduces the influence of long-range, non-dynamical correlation ($c^{os} < 1$). It fails if electrons in spatially close lying orbitals have a large effect on the correlation energy [71].

It is worthwhile to mention at this point that the two parts of the correlation energy show a different behavior when convergence to full basis set limit is examined [21, 74]. While the same-spin correlation energy converges with X^{-5} the opposite-spin correlation energy shows a convergence of X^{-3} where X is the cardinal number of Dunnings cc-pVXZ basis sets [75]. Although the numerically larger part is given by $E^{(2)os}_{MP2}$, the main problems regarding an efficient implementation are caused by the same-spin part [21].

Jung et al. [21] further simplified the SCS approach by neglecting the same-spin contributions as a whole and scaling the opposite-spin part accordingly:

$$E_{SOS-MP2} = c^{os} E^{os}_{MP2}, \qquad c^{os} = 1.3.$$

It was implemented within a framework in which the computational cost has been reduced by one order [21] through the combined application of the resolution of the identity (ri) approach [76, 77] and Laplace-transformations [78] for the evaluation of energy denominators.

These basic ideas have been adopted to many methods, e. g., CIS(D) [79, 80] as well as to two variants of CIS with quasidegenerate second-order perturbation corrections (CIS(D_0) and CIS(D_1)) [50, 81–83]. Fourth-order scaling schemes of these methods were implemented into the Q-Chem program package [19].

The concept of SOS was applied to the ri-CC2 method [84], as well, and has been implemented into the TURBOMOLE program package [85]. Again, the scaling of the computational cost has been reduced from fifth to fourth order [86] by a combination of the ri-approximation and Laplace-transformations. Derived formulations of SOS-ADC(2)-s and single excitation configuration interaction with quasidegenerate second-order perturbation corrections (SOS-CIS(D_∞)) [50] have been included [86].

In the present work, the concept of scaled opposite-spin is applied to the extended version of ADC(2). For this purpose, we started by closely examining two different approaches for the derivation of SOS-ADC(2)-s. The first approach comprises the ISR in the SOS-MP2 framework, while the second one starts from SOS-CC2 similar to the variant previously implemented in TURBOMOLE [84–86]. It will be shown that only the latter one leads to a reduction of computational effort. The dependence of the results on the choice of scaling parameters is investigated. Based on SOS-ADC(2)-s a new SOS-ADC(2)-x method is suggested that reduces the computational cost significantly and, at the same time, reduces the overestimation of doubly excited configurations, which is inherent to the unscaled ADC(2)-x method.

4.2. Derivation of SOS-ADC(2)

Considering the derivation of ADC(2)-s from MP2 *via* ISR outlined in Section 3.3, the most intuitive way to apply the concept of scaled opposite-spin to ADC(2) is to use the ISR to derive SOS-ADC(2) from the SOS-MP2 wave function and energy. For this purpose, we will first examine the changes to MP2 introduced in SOS-MP2 a bit more closely.

Given the Møller-Plesset partitioning $H = H^0 + W$ of the Hamiltonian with H^0 being the Hartree-Fock Hamiltonian and W representing the electron correlation like in Section 2.4.2, the MP2 correlation energy is obtained as

$$E^{(2)}_{MP2} = \langle \Phi_0 | W | \Psi^{(1)}_0 \rangle = -\frac{1}{4} \sum_{ijab} t_{ijab} \langle ij||ab\rangle.$$

Accordingly, the following relation has to be fulfilled in the case of SOS-MP2 (using spatial orbitals):

$$E^{(2)}_{SOS-MP2} = c^{os} E^{(2)os}_{MP2} = -c^{os} \sum_{\bar{a}b\bar{i}j} t_{\bar{i}j\bar{a}b} \langle \bar{i}j|\bar{a}b\rangle \stackrel{!}{=} \langle \Phi_0 | W | \Psi_0^{(1)^{os}} \rangle.$$

It follows from comparison that the SOS-MP2 model is fully defined by replacing the original T-amplitudes in the first-order correction to the wave function by their scaled analogs (employing again spin orbitals):

$$t_{abij} \rightarrow t^{sos}_{ijab} = c^{os} t^{os}_{ijab} = c^{os} t_{ijab} (1 - \delta_{\sigma(i)\sigma(j)}). \tag{4.1}$$

Here, $\sigma(p)$ indicates the spin of the electron occupying orbital p.

Using this modified wave function in the ISR, a corresponding SOS-ADC(2)-s method can be deduced that is consistent with SOS-MP2. In order to avoid

confusion with the method introduced below this will be termed ISR-SOS-ADC(2)-s. As the only change in SOS-MP2 concerns the T-amplitudes, ISR-SOS-ADC(2)-s differs from the original ADC(2)-s only by replacing the T-amplitudes which occur in the second-order correction to elements of the ph/ph block.

This substitution leads to a systematic shift of the excitation energies by about 0.02–0.3 eV to lower but not improved values (compare Section 4.4.2). At the same time, no significant saving in computational effort can be achieved as no entries of the ADC(2)-matrix vanish.

Alternatively, SOS-ADC(2)-s can be obtained from SOS-CC2 using the relations between ADC(2)-s and CC2 introduced in Section 3.3 (compare as well [51]). The SOS-CC2 matrix is given by (the superscript *os* implies that only opposite-spin doubly excited configurations are considered and same-spin contributions are set to zero; compare t^{os}_{ijab} in equation 4.1)

$$\mathbf{A}^{SOS-CC2} = \left(\begin{array}{c|c} \langle \Phi_i^a | \left[(\hat{\bar{H}} + c^{os} \left[\hat{\bar{H}}, \hat{T}_2^{os} \right]), \hat{\tau}_j^b \right] | \Phi_0 \rangle & \langle \Phi_i^a | c^{os} \left[\hat{\bar{H}}, \tau_{kl}^{cd\,os} \right] | \Phi_0 \rangle \\ \hline \langle \Phi_{ij}^{ab\,os} | \left[\hat{\bar{H}}, \hat{\tau}_k^c \right] | \Phi_0 \rangle & \langle \Phi_{ij}^{ab\,os} | \left[\hat{F}, \tau_{kl}^{cd\,os} \right] | \Phi_0 \rangle \end{array} \right).$$

Putting the t_1-amplitudes to zero (yielding SOS-CIS(D_∞)), evaluation of the different blocks

$$\begin{aligned}
&\langle \Phi_i^a | \left[(\hat{H} + c^{os} \left[\hat{H}, \hat{T}_2^{os} \right]), \hat{\tau}_j^b \right] | \Phi_0 \rangle = (\epsilon_a - \epsilon_i)\delta_{ab}\delta_{ij} - \langle aj||bi \rangle \\
&\qquad + \frac{1}{2}\delta_{ij} \sum_{ckl} t^{sos}_{kalc} \langle kl||bc \rangle + \frac{1}{2}\delta_{ab} \sum_{cdk} t^{sos}_{ickd} \langle jk||cd \rangle - \sum_{ck} t^{sos}_{iakc} \langle jk||bc \rangle \\
&\langle \Phi_i^a | c^{os} \left[\hat{H}, \tau_{kl}^{cd\,os} \right] | \Phi_0 \rangle = \\
&\qquad c^{os} \left\{ \langle kl||id \rangle \delta_{ac} - \langle kl||ic \rangle \delta_{ad} - \langle al||cd \rangle \delta_{ik} + \langle ak||cd \rangle \delta_{il} \right\} (1 - \delta_{\sigma(k)\sigma(l)}) \\
&\langle \Phi_{ij}^{ab\,os} | \left[\hat{H}, \hat{\tau}_k^c \right] | \Phi_0 \rangle = \\
&\qquad \left\{ \langle kb||ij \rangle \delta_{ac} - \langle ka||ij \rangle \delta_{bc} - \langle ab||cj \rangle \delta_{ik} + \langle ab||ci \rangle \delta_{jk} \right\} (1 - \delta_{\sigma(i)\sigma(j)}) \\
&\langle \Phi_{ij}^{ab\,os} | \left[\hat{F}, \tau_{kl}^{cd\,os} \right] | \Phi_0 \rangle = \\
&\qquad \left\{ (\epsilon_a + \epsilon_b - \epsilon_i - \epsilon_j)\delta_{ac}\delta_{bd}\delta_{ik}\delta_{jl} \right\} (1 - \delta_{\sigma(i)\sigma(j)})(1 - \delta_{\sigma(k)\sigma(l)})
\end{aligned}$$

and symmetrization yields the following changes that have to be applied to arrive at SOS-ADC(2)-s (for a detailed derivation see appendix A):

- Replace all T-amplitudes by their scaled opposite-spin analogs as in SOS-MP2 (and ISR-SOS-ADC(2)-s).
- Delete all entries from same-spin contributions in the double excitation manifold meaning all configurations $(ijab)$ with $(\alpha\alpha\alpha\alpha)$ or $(\beta\beta\beta\beta)$ (compare Figure 4.1).
- Scale all remaining entries in the coupling (ph/2p2h and 2p2h/ph) blocks by a factor of

$$c^{os}_{coupling} = \frac{1 + c^{os}}{2} = 1.15.$$

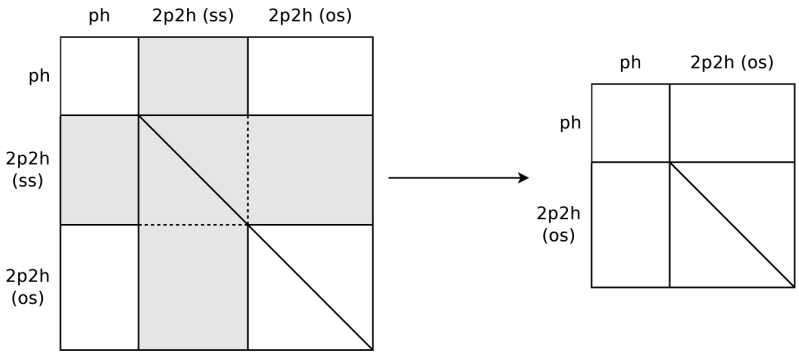

Figure 4.1.: Schematic representation of the effect of the SOS approximation on the dimensionality of the ADC(2)-s matrix.

This has been previously done by Hellweg et al. [84] and implemented into the `ricc2` [48] module of the TURBOMOLE program suite [85], however, without symmetrizing the full CIS(D_∞) matrix but only the ph/ph block. The non-hermiticity of the coupling blocks was retained and only the elements in the ph/2p2h block multiplied by a factor of $c^{os} = 1.3$ but not in the 2p2h/ph block. Nevertheless, this non-hermitian matrix can be similarity transformed to give a hermitian matrix with the same eigenvalues. This differs from our secular matrix in having $c^{os}_{coupling} = \sqrt{c^{os}} = 1.14$ instead of $c^{os}_{coupling} = {}^{1+c^{os}}/_{2} = 1.15$ as scaling parameter for the coupling blocks. The differences in the excitation energies are only small as c^{os} has a value close to unity. However, it should be borne in mind that to exactly reproduce excitation energies obtained by specifying a certain value for c^{os} in TURBOMOLE with our method it is necessary to choose $c^{os}_{coupling}$ in a different manner.

In contrast to ISR-SOS-ADC(2)-s, the deletion of same-spin components in the 2p2h configurations allows for a significant reduction of the dimensionality of the ADC matrix and a concomitant reduction of the computational cost. The scaling of the method itself is not affected but the prefactor is reduced. Compared to ISR-SOS-ADC(2)-s, this is an additional *ad hoc* approximation stemming from SOS-CC2. Both methods were implemented into a development version of the Q-Chem program package [19] and the results are discussed in Section 4.4.2. For the sake of clarity, the explicit expressions for the ADC matrices of the different approaches discussed so far are given in appendix A.

Finally, the concept of scaling with respect to spin components was applied to the ADC(2)-x method. For this purpose, the first-order correction terms have been added to the 2p2h/2p2h block and an additional scaling parameter has been introduced in order to reduce the overestimation of doubly excited configurations in ADC(2)-x. Because a reduction of computational cost is even more desirable here, this procedure was applied only to SOS-ADC(2)-s with already reduced dimensionality and not to the more "rigorous" ISR-SOS-ADC(2)-s. These results constitute the main achievement of this chapter and will be analyzed in detail in Section 4.4.2.

For correcting the overestimation of doubly excited configurations in the case of ADC(2)-x another method was tested additionally, namely the application

of a constant shift to the diagonal elements of the 2p2h/2p2h block. However, in first tests the definition of a constant shift parameter for a wide range of states and molecules does not seem not possible. Therefore, we concentrate on multiplicative scaling of certain matrix elements.

4.3. Implementation

The methods derived in Section 4.2 were implemented in a development version of Q-Chem [19]. In a first step, the same-spin blocks of the T-amplitudes are set to zero and the other ones scaled appropriately by the factor $c^{os} = 1.3$. These scaled T-amplitudes are then used for the subsequent MP2 and ADC(2) calculations.

In order to arrive at SOS-ADC(2)-s/x the coupling blocks of the ADC matrix have to be scaled. This is done by using scaled versions of the integrals of type $\langle oo|ov\rangle$ and $\langle ov|vv\rangle$ where o stands for occupied and v for virtual. Setting all $(\alpha\alpha\alpha\alpha)$ and $(\beta\beta\beta\beta)$ blocks to zero and scaling the others by $c^{os}_{coupling}$ leads to SOS-ADC(2)-s/x.

For SOS-ADC(2)-x, the first-order contributions to the satellite block have to be scaled additionally. This block includes integrals of the types $\langle oo|oo\rangle$, $\langle vv|vv\rangle$, as well as $\langle ov|ov\rangle$. For the correct scaling, the $(\alpha\alpha\alpha\alpha)$ and $(\beta\beta\beta\beta)$ blocks of the $\langle oo|oo\rangle$ and of the $\langle vv|vv\rangle$ integrals as well as the $(\alpha\beta\beta\alpha)$ and $(\beta\alpha\alpha\beta)$ blocks of the $\langle ov|ov\rangle$ integrals are set to zero. All other integrals are scaled by c^{os}_x.

The SOS-calculations can be controlled by the following input parameters:

ADC_SOS
Controls whether the SOS approximation is used.
TYPE:
LOGICAL
DEFAULT:
FALSE
OPTIONS:
TRUE Activate the SOS approximation.
FALSE Do not use the SOS approximation.
RECOMMENDATION:
None

ADC_C_T
Controls the scaling parameter for the T-amplitudes.
TYPE:
INTEGER
DEFAULT:
1300
OPTIONS:
n Equals the desired scaling parameter times 1000.
RECOMMENDATION:
Use default.

ADC_C_C
Controls the scaling parameter for the coupling blocks.
TYPE:
INTEGER
DEFAULT:
1170 in the case of ADC(2)-s
1000 in the case of ADC(2)-x
OPTIONS:
n Equals the desired scaling parameter times 1000.
RECOMMENDATION:
Use default.

ADC_C_X
Controls the scaling parameter for the satellite block in the case of an ADC(2)-x calculation.
TYPE:
INTEGER
DEFAULT:
900
OPTIONS:
n Equals the desired scaling parameter times 1000.
RECOMMENDATION:
Use default.

4.4. Parameter Fitting

4.4.1. Computational Methods

In all cases the resolution of the identity (ri) approximation for four-center integrals [76,77,87] was employed. For the parameter determination and evaluation of the numerical accuracy the benchmark set of organic molecules developed by Schreiber et al. [88] and Silva-Junior et al. [89] was used. The structures had been optimized at MP2/6-31G* level and were taken from the supporting information of [88]. The numbering scheme of the states was chosen in accordance with the original benchmark set which neglects Rydberg states.

As basis set the augmented correlation consistent double-ζ basis set aug-cc-pVDZ [75] was chosen and the resulting basis set error has been included in the fitting of the scaling parameters. We have chosen to use this basis set since diffuse functions are crucial for the determination of electronically excited states while the step from aug-cc-pVDZ to the corresponding triple-ζ basis aug-cc-pVTZ [75] introduces only minor changes (compare Table 4.1). As can be seen from comparison with values obtained from the non-augmented basis set cc-pVTZ [75], the reduction of basis set size by neglecting augmentation leads to significant deviations. Consequently, aug-cc-pVDZ offers a good compromise between accuracy and basis set size. In all cases the corresponding auxiliary basis sets according to [90] were used.

Altogether, three scaling parameters were introduced. One for the T-amplitudes (c^{os}), one for the coupling blocks ($c^{os}_{coupling}$) and one for the first-order contributions to the 2p2h/2p2h block (c^{os}_{x}) in the case of extended ADC(2). The first parameter was chosen in accordance with SOS-MP2 as $c^{os} = 1.3$ and was not subject to any changes. The other two parameters were fitted to theoretical best estimates (TBE-2) obtained by Silva-Junior et al. [89].

In the case of ADC(2)-s all states with significant double excitation character (more than 20% in CC3, compare [88]) were excluded from the fitting procedure. In the case of some states no clear assignment could be made. They were omitted, too.

Reference values with the aug-cc-pVDZ basis set using the implementation of SOS-ADC(2)-s by Hellweg et al. [84] were obtained with TURBOMOLE V6.3 [85].

4.4.2. Results and Discussion

As explained above, the ISR-SOS-ADC(2)-s method has been obtained *via* the ISR from SOS-MP2 while SOS-ADC(2)-s as derived from SOS-CC2 includes an additional *ad hoc* approximation by neglecting all same-spin contributions to the 2p2h configurations. As such an ISR-SOS-ADC(2)-s method has not been previously implemented, we first compare the performance of this scheme with our SOS-ADC(2)-s method derived from SOS-CC2. The scaling parameter for the T-amplitudes was kept as $c^{os} = 1.3$ and $c^{os}_{coupling} = \frac{c^{os}+1}{2} = 1.15$ was chosen in analogy. The results are shown in Tables B.2 (singlet excitations) and B.3 (triplet excitations) of the appendix. The statistical evaluation of the error with respect to the TBE-2 [89] is given in Table 4.1. The ADC(2)-s values are included for reference. Interestingly, in ISR-SOS-ADC(2)-s the excitation energies are systematically shifted to lower energies (by up to 0.36 eV) while in SOS-ADC(2)-s the opposite can be observed in most (but not all) cases. Nevertheless, the mean absolute errors (MAE) and standard deviations (std. dev.) are similar for the two methods, the one for ISR-SOS-ADC(2)-s being slightly smaller in the case of singlet states and *vice versa* for triplet states. However, compared to unscaled ADC(2)-s, no improvement can be observed and the MAE is raised by 0.07 eV and the std. dev. by 0.02–0.04 eV for singlet states. This effect is less pronounced for triplet states.

Although exhibiting a better predictable and systematic behavior the ISR-SOS-ADC(2)-s method does not have a significantly reduced computational cost which is the main motivation for applying the SOS approximation. Therefore, as standard method and basis for the development of SOS-ADC(2)-x we have adopted the SOS-ADC(2)-s scheme as derived from SOS-CC2 in Section 4.2. As discussed, this differs from the previous implementation in TURBOMOLE [84–86] and the values obtained by choosing $c^{os} = 1.3$ there are given for comparison in Tables B.2 and B.3. However, the results obtained with our method are in better agreement with the TBE-2.

Before proceeding to SOS-ADC(2)-x, we set out to investigate the dependency of the excitation energies in SOS-ADC(2)-s on the second scaling parameter $c^{os}_{coupling}$ and sought for an optimization of it. By increasing its value to $c^{os}_{coupling} = 1.17$ slightly improved values could be obtained and the MAE is

Table 4.1.: Maximum error, minimum error, mean error, mean absolute error, and standard deviation for the test sets of Tables B.2 and B.3 with respect to TBE-2. All values in eV. Unless stated otherwise aug-cc-pVDZ was employed. TBE-2 and CC3 values taken from [89]. For corresponding ADC values see supplementary material B. The numbers in brackets give the value of $c^{os}_{coupling}$.

Method	max. err.	min. err.	mean err.	mean abs. err.	std. dev.
	Singlet states (74)				
ADC(2)-s (aug-cc-pVTZ)	0.42	-0.28	0.01	0.11	0.08
ADC(2)-s (cc-pVTZ)	0.56	-0.12	0.14	0.18	0.15
ADC(2)-s (aug-cc-pVDZ)	0.46	-0.28	0.03	0.12	0.09
ISR-SOS-ADC(2)-s	0.19	-0.45	-0.17	0.19	0.11
SOS-ADC(2)-s (Turbomole)	0.72	-0.21	0.19	0.22	0.15
SOS-ADC(2)-s (1.15)	0.65	-0.26	0.13	0.19	0.13
SOS-ADC(2)-s (1.16)	0.59	-0.31	0.06	0.16	0.12
SOS-ADC(2)-s (1.17)	0.52	-0.39	0.00	0.15	0.12
SOS-ADC(2)-s (1.18)	0.45	-0.47	-0.07	0.16	0.13
SOS-ADC(2)-s (1.19)	0.38	-0.56	-0.14	0.19	0.15
CC3	0.36	-0.31	0.02	0.04	0.09
ADC(2)-x (only 66 states)	-0.21	-1.52	-0.82	0.82	0.23
	Triplet states (63)				
ADC(2)-s (aug-cc-pVTZ)	0.42	-0.26	0.11	0.17	0.10
ADC(2)-s (cc-pVTZ)	0.55	-0.15	0.17	0.20	0.10
ADC(2)-s (aug-cc-pVDZ)	0.45	-0.28	0.12	0.18	0.11
ISR-SOS-ADC(2)-s	0.19	-0.53	-0.19	0.20	0.11
SOS-ADC(2)-s (Turbomole)	0.61	-0.09	0.20	0.21	0.15
SOS-ADC(2)-s (1.15)	0.48	-0.14	0.15	0.17	0.12
SOS-ADC(2)-s (1.16)	0.45	-0.19	0.11	0.14	0.11
SOS-ADC(2)-s (1.17)	0.41	-0.24	0.06	0.12	0.10
SOS-ADC(2)-s (1.18)	0.38	-0.30	-0.30	0.11	0.09
SOS-ADC(2)-s (1.19)	0.34	-0.35	-0.04	0.11	0.09
CC3	0.31	-0.10	0.02	0.03	0.06
	All states (137)				
ADC(2)-s (aug-cc-pVTZ)	0.42	-0.28	0.06	0.14	0.09
ADC(2)-s (cc-pVTZ)	0.55	-0.15	0.16	0.19	0.14
ADC(2)-s (aug-cc-pVDZ)	0.46	-0.28	0.07	0.15	0.10
ISR-SOS-ADC(2)-s	0.39	-0.53	-0.17	0.20	0.11
SOS-ADC(2)-s (Turbomole)	0.72	-0.21	0.19	0.22	0.15
SOS-ADC(2)-s (1.15)	0.65	-0.26	0.14	0.18	0.13
SOS-ADC(2)-s (1.16)	0.59	-0.31	0.08	0.15	0.11
SOS-ADC(2)-s (1.17)	0.52	-0.39	0.02	0.14	0.11
SOS-ADC(2)-s (1.18)	0.45	-0.47	-0.03	0.13	0.12
SOS-ADC(2)-s (1.19)	0.38	-0.56	-0.09	0.15	0.13
CC3	0.36	-0.31	0.02	0.04	0.08

reduced by 0.04 eV (regarding singlet states). It is worthwhile to mention that the transition dipole moments and consequently the oscillator strengths were not severely affected by this approximation (see appendix B.2 for the corresponding values). This method was additionally benchmarked with respect to triplet states showing that in those cases even larger values (1.18-1.19) would be optimal. Interestingly, triplet states seem to be improved by applying the SOS approximation while singlet states are not.

Therefore, we chose $c^{os}_{coupling} = 1.17$ as the standard parameter and starting

point for SOS-ADC(2)-x although the improvement compared to $c^{os}_{coupling} = 1.15$ is only small. For the rest of this work, the term SOS-ADC(2)-s will refer to this method with $c^{os} = 1.3$ and $c^{os}_{coupling} = 1.17$ unless stated otherwise.

At this point it might prove useful to discuss the differences between CIS(D_∞), CIS(D_0), CIS(D_1) and ADC(2)-s in a bit more detail. The CIS(D_n) class of methods [50] is obtained from CIS(D_∞) through inversion of the diagonal 2p2h/2p2h block to eliminate the doubles from explicit consideration and binomial expansion up to order n. Solution of the corresponding (energy dependent) dressed singles response matrix follows. Considering the expansion up to infinite order is equivalent to diagonalizing the SOS-CIS(D_∞) matrix given in equation A.1 of the appendix. The advantage of such a partitioning is that the eigenvalue problem is solved in the single excitations space only. However, apart from CIS(D_0) a generalized, energy dependent eigenvalue problem has to be iteratively solved. While ADC(2)-s and CIS(D_∞) lead to very similar excitation energies, these differ more strongly for CIS(D_0) and CIS(D_1) due to the additional approximation (for some illustrative examples see [50, 51, 81]). Regarding the application of the SOS concept, extensive parameter optimizations were performed for SOS-CIS(D_0) and SOS-CIS(D_1) [81]. As in our case, different scaling parameters were allowed for the T-amplitudes in the main block and the elements of the coupling blocks. Interestingly, almost the same parameter as for our SOS-ADC(2)-s for the coupling blocks (in our notation: $c^{os}_{coupling} = \sqrt{1.38} = 1.175$) was obtained for SOS-CIS(D_1) [81].

As explained above, ADC(2)-x tends to overestimate contributions from doubly excited states leading to an exaggerated lowering of the energetic levels [54]. Singlet states are affected as well and lowered, however, to a smaller extent (compare Table 4.1). Consequently, ADC(2)-x serves as a valuable method to identify states with high double excitation character. We were therefore especially concerned about the performance of SOS-ADC(2)-x in the description of predominantly doubly excited states.

In a first test, the SOS-ADC(2)-s matrix was augmented with the corresponding first-order correlation elements in the 2p2h/2p2h block and the scaling parameters were kept constant. As a small test set the linear polyenes ethene, butadiene and octatetraene together with cyclopentadiene were chosen and only singlet states considered. The results are displayed in Table 4.2. Compared to unscaled ADC(2)-x the states are shifted even more strongly to lower energies.

It follows that the SOS-ADC(2)-x method in which no additional scaling parameters have been included can be used as efficiently as the unscaled version in order to distinguish between singly and doubly excited states. However, the question arises whether the strong overestimation of doubly excited states can be reduced. There are two possible remedies: On the one hand, the coupling of the doubly excited states to the singly excited states can be reduced (lowering the value of $c^{os}_{coupling}$) and, on the other hand, a new scaling parameter ($c^{os}_x < 1.0$) can be applied to the first-order correction terms in the 2p2h/2p2h block. In the latter case either diagonal, non-diagonal elements, or both can be scaled. Testing these two possibilities, the following observations were made:

Table 4.2.: Vertical excitation energies for a small test set of singlet excited states with either high single or double excitation character obtained with different SOS-ADC(2)-x schemes in eV. SOS-ADC(2)-s and ADC(2)-x values are given for comparison. TBE-2 from [89] and DFT/MRCI from [91]. The values in brackets give the net weight of doubly excited configurations in the expansion of the final states.

	state	TBE-2	DFT/ MRCI	SOS- ADC(2) -s	ADC(2) -x	SOS- ADC(2) -x	SOS- ADC(2) -x	SOS- ADC(2) -x
$c^{os}_{coupling}$				1.17	-	1.17	1.0	1.0
c^{os}_{x}				-	-	-	0.85	0.9
	singlet states with high double excitation character							
Butadiene	$2A_g$	6.55	6.18	7.17	5.12	4.71	6.39	6.19
				(0.08)	(0.55)	(0.50)	(0.40)	(0.47)
Hexatriene	$2A_g$	5.09	4.92	6.65	4.06	3.77	5.40	5.16
				(0.10)	(0.58)	(0.58)	(0.55)	(0.60)
Octatetraene	$2A_g$	4.47	4.01	6.04	3.36	3.12	4.69	4.45
				(0.12)	(0.61)	(0.61)	(0.60)	(0.66)
Cyclo-	$2A_1$	6.28	6.15	6.93	5.10	4.60	6.20	6.05
pentadiene				(0.10)	(0.49)	(0.43)	(0.37)	(0.42)
	singlet states with high single excitation character							
Butadiene	$1B_u$	6.18	6.02	6.16	5.56	5.26	6.21	6.19
				(0.06)	(0.10)	(0.12)	(0.09)	(0.09)
Hexatriene	$1B_u$	5.10	4.95	5.24	4.60	4.29	5.34	5.33
				(0.07)	(0.14)	(0.13)	(0.10)	(0.10)
Octatetraene	$1B_u$	4.66	4.25	4.62	3.96	3.65	4.77	4.75
				(0.08)	(0.12)	(0.14)	(0.11)	(0.11)
Cyclo-	$1B_2$	5.55	5.42	5.48	4.91	4.56	5.55	5.54
pentadiene				(0.06)	(0.09)	(0.09)	(0.08)	(0.10)

- Reducing $c^{os}_{coupling}$ influences both singly and doubly excited states to a similar extent. Therefore, once the doubly excited states have been adjusted to the right energy range the singly excited states lie far too high in energy.
- Scaling the first-order correction terms to the non-diagonal elements of the 2p2h/2p2h block leads to a strong influence on the doubly excited states but leaves the singly excited ones untouched. (Table 4.2).
- Scaling the first-order correction terms to the diagonal elements of the 2p2h/2p2h block influences both singly and doubly excited states strongly but in a less consistent and predictable way than scaling the off-diagonal terms.

Therefore, we decided to introduce only one additional scaling parameter for the off-diagonal elements of the 2p2h/2p2h block (termed c^{os}_{x}) and adjust it together with $c^{os}_{coupling}$. From a rough screening (modifying both parameters in steps of 0.1 and using only the small set of singlet states defined in Table 4.2) $c^{os}_{x} = 0.8$ and $c^{os}_{coupling} = 1.0$ were identified as promising starting values for a further refinement. In the course of this, $c^{os}_{coupling}$ can be used to adjust the singly excited states (using the full set of 74 singly excited singlet states) and then c^{os}_{x} has to be chosen in order to shift the doubly excited states to the right energy range leaving the singly excited states almost unchanged. By this procedure $c^{os}_{x} = 1.0$ (i. e., no scaling) was confirmed as a value that leads to similar errors as in SOS-ADC(2)-s (mean absolute errors of 0.15–0.17 eV if c^{os}_{x} is kept in the range of 0.85 to 0.90). Detailed statistical analysis is given in Table 4.3.

However, high quality reference data for doubly excited states is lacking. In the benchmark set used so far 17 states with high double excitation character are included. For seven of those TBE-2 and for twelve DFT/MRCI values exist. At the same time, we believe that TBE-2 are probably too high in energy while DFT/MRCI might be too low. Keeping $c^{os}_{coupling} = 1.0$ constant, fitting with respect to TBE-2 yields $c^{os}_{x} = 0.87$, to DFT/MRCI $c^{os}_{x} = 0.92$ as optimal values (Table 4.3). However, the number of states considered is very small making a proper statistical evaluation impossible for the time being.

Nevertheless, we suggest $c^{os}_{x} = 0.90$ and $c^{os}_{coupling} = 1.0$ (i. e., no scaling) as a preliminary parameter set which leads to a reasonable description of singly excited states (mean absolute error of 0.17 eV) and shifts the doubly excited states approximately into the correct energy region (with respect to both, TBE-2 and DFT/MRCI) at reduced computational cost. The values obtained for the full set of 74 singly and 17 doubly excited singlet states are displayed in Table B.1. When applied to the set of 63 triplet states of Table B.3, similar errors with respect to TBE-2 are obtained as with SOS-ADC(2)-s, i. e., an improvement compared to ADC(2)-s (Table 4.3 and appendix B.3). The oscillator strengths are not severely affected by the scaling as was already the case for SOS-ADC(2)-s (appendix B.3).

An important question regarding SOS-ADC(2)-s/-x is whether the spin symmetry of the final solutions is conserved. From the six primitive spin-configura-

Table 4.3.: Maximum error, minimum error, mean error, mean absolute error, and standard deviation for the test set of Table B.1 obtained with SOS-ADC(2)-x and different values for $c^{os}_{coupling}$ and c^{os}_{x}. Errors with respect to TBE-2 from [89] in the case of states with high single excitation character. In the case of states with high double excitation character comparison to either TBE-2 [89] or DFT/MRCI from [91]. For corresponding ADC values see supplementary material B. The numbers in the first column give the value of $c^{os}_{coupling}$ and c^{os}_{x}, respectively.

$c^{os}_{coupling}$, c^{os}_{x}	max. err.	min. err.	mean err.	mean abs. err.	std. dev.
	singlet states with high single excitation character (74) reference TBE-2				
1.0, 0.85	0.42	-0.63	-0.08	0.15	0.15
1.0, 0.90	0.38	-0.65	-0.11	0.17	0.16
	singlet states with high double excitation character (7) reference TBE-2				
1.0, 0.85	0.31	-0.46	0.01	0.23	0.15
1.0, 0.87	0.26	-0.48	-0.05	0.22	0.14
1.0, 0.89	0.20	-0.51	-0.11	0.21	0.16
1.0, 0.90	0.17	-0.52	-0.14	0.21	0.18
1.0, 0.92	0.10	-0.53	-0.21	0.23	0.20
1.0, 0.94	0.02	-0.56	-0.28	0.29	0.21
	singlet states with high double excitation character (12) reference DFT/MRCI				
1.0, 0.85	0.68	-0.18	0.16	0.22	0.19
1.0, 0.87	0.59	-0.25	0.11	0.19	0.17
1.0, 0.89	0.49	-0.32	0.06	0.18	0.13
1.0, 0.90	0.44	-0.36	0.04	0.17	0.12
1.0, 0.92	0.34	-0.44	-0.02	0.18	0.11
1.0, 0.94	0.22	-0.52	-0.08	0.18	0.13
	triplet states (63), reference TBE-2				
1.0, 0.90	0.31	-0.74	-0.04	0.11	0.12

tions (PSC) of (ijab) without spin-flips ($\Delta M_S = 0$) two singlet, three triplet and one quintet state can be constructed. When two (specifically ($\alpha\alpha\alpha\alpha$) and ($\beta\beta\beta\beta$)) of those PSCs are discarded in the SOS framework, only one of the two singlet states is retained and the other one has quintet admixtures. The triplet states remain orthogonal to the singlet/quintet states but one of them is lost. The contamination of singlet states with quintet ones was obtained for SOS-MP2, as well [72]. Therefore, some caution is recommended in cases where the double excitation contribution to the final wave function approaches unity.

4.5. Conclusion

The presented SOS-ADC(2)-x is a pragmatic semi-empirical approximation to ADC(2)-x that reduces its computational cost substantially. It can be used in order to identify excited states for which double excitations are important and in principle it is possible to tune the scaling parameters in a way that both singly and doubly excited states are in the correct energy range. However, appropriate reference data for doubly excited states is still lacking rendering a determination of the parameters for the doubly excited states problematic. Nevertheless, with the given parameter set singly excited states seem to be well described for standard organic molecules as incorporated in the benchmark set used and similar errors are obtained as with SOS-ADC(2)-s while doubly excited states are expected to lie approximately in the correct energy range.

As basis for the development of SOS-ADC(2)-x, also two variants of SOS-ADC(2)-s were implemented into Q-Chem and tested. On the one hand, ISR was used to "rigorously" derive a new SOS-ADC(2)-s method (termed ISR-SOS-ADC(2)-s) that is fully consistent with the approximations introduced in SOS-MP2. Although the changes obtained are more systematic, no significant saving in computational cost can be obtained. On the other hand, a SOS-ADC(2)-s scheme was derived from SOS-CC2 that is similar to the one implemented by Hellweg et al. in TURBOMOLE [84–86]. The mean absolute error and standard deviations obtained with the two implemented methods are similar. Reoptimization of the scaling parameter in the coupling blocks of our SOS-ADC(2)-s method led to slightly improved results.

Regardless of the desirable computational gain of the presented methods, larger deviations can occur in certain cases not well represented by this benchmark set of organic molecules and the applicability of the suggested methods for the given systems should be always carefully checked beforehand.

5. Spin-Orbit Coupling

It follows from special relativity [92] that all physical equations, including those of quantum mechanics, have to be invariant under Lorentz transformations. However, the time-dependent Schrödinger equation 2.1 does not fulfill this requirement as derivations with respect to time and space occur in different order.

A Lorentz invariant equation of motion for electrons is given by the Dirac equation [93, 94]. Within this fully relativistic description the electron spin arises naturally. The chemically most important effects introduced by a relativistic description are scalar relativistic effects (contraction of s-shells as well as expansion of d- and f-shells) and the energetic splitting of states with an orbital angular momentum $L > 0$ due to spin-orbit coupling (SOC).

Because of the coupling between them, the orbital angular momentum L as well as the spin angular momentum S are no good quantum numbers any more and only the total angular momentum J and its z-component are applicable [25, 95–97]. For organic molecules, which are composed of light elements, scalar relativistic effects do not play a significant role. Spin-orbit coupling effects, however, lead to an interaction between states of different spin symmetry (typically singlet and triplet states) and enable inter-system crossing processes (compare Section 1). Therefore, their consideration is of importance to fully grasp photochemical relaxation pathways.

While the Dirac equation offers a Lorentz invariant description for one-electron systems, a fully relativistic many-electron Hamiltonian is still missing and instead approximate ones have to be used [96,97]. One frequently employed example is the Dirac-Coulomb-Breit Hamiltonian which includes the Breit operator [98] in addition to the Coulomb operator. However, full-relativistic calculations are numerically very expensive. Consequently, methods have been derived that allow one to include spin-orbit coupling effects on top of a non-relativistic quantum chemical calculation (for an overview see, e. g., [26, 99])

The inclusion of spin-orbit coupling effects on the results of a non-relativistic calculation will be topic of this section. After discussing the used spin-orbit Hamiltonian, the Wigner-Eckart theorem [26, 100] will be introduced as it simplifies the respective calculations greatly. In Section 5.4 the implementation of SOC elements within the framework of Q-Chem and the ADC(n) family of methods will be presented. Finally, test calculations on the molecules thiophene, dithiin, and coumarin will be presented in Section 7.

5.1. Spin-Orbit Hamiltonians and the Atomic Mean-Field Approximation

Within the standard representation, the wave functions from the Dirac equation have four components [96, 97]

$$\Psi = \begin{pmatrix} \Psi_1 \\ \Psi_2 \\ \Psi_3 \\ \Psi_4 \end{pmatrix} = \begin{pmatrix} \Psi_L \\ \Psi_S \end{pmatrix}$$

that can be combined to give two two-component wave functions called the large Ψ_L and small component Ψ_S. Electronic solutions to the Dirac equation are dominated by the large component and within the non-relativistic limit ($E << mc^2$) they are even given by it. The opposite is true for positronic solutions. The two components of Ψ_L can be interpreted as the two spin components.

As we are interested in electronic solutions only, it would be desirable to split of the small component and restrict the calculation to the large component. A variety of methods has been developed for this goal [96, 97, 101].

In addition, spin-independent and spin-dependent terms can be separated. In this case the non-relativistic energies and wave functions are first obtained and then spin-orbit coupling effects are considered perturbatively [26, 97, 99, 101]:

$$\hat{H} = \hat{H}_{non-rel} + \hat{H}_{SO},$$

with $\hat{H}_{non-rel}$ corresponding to the non-relativistic molecular Hamiltonian of equation 2.3. A very popular spin-orbit Hamiltonian is given by the Breit-Pauli operator [102]:

$$\begin{aligned} \hat{H}_{SO}^{BP} = \frac{e^2}{2m_e^2c^2} \Bigg\{ & \sum_i \left(-\nabla_i \left(\sum_I \frac{Z_I}{|\mathbf{r}_i - \mathbf{R}_I|} \right) \times \hat{\mathbf{p}}_i \right) \hat{\mathbf{s}}_i \\ & + \sum_i \sum_{j \neq i} \left(\nabla_i \left(\frac{1}{|\mathbf{r}_i - \mathbf{r}_j|} \right) \times \hat{\mathbf{p}}_i \right) \hat{\mathbf{s}}_i \\ & + \sum_i \sum_{j \neq i} \left(\nabla_j \left(\frac{1}{|\mathbf{r}_i - \mathbf{r}_j|} \right) \times \hat{\mathbf{p}}_j \right) \hat{\mathbf{s}}_i \\ & + \sum_i \sum_{j \neq i} \left(\nabla_i \left(\frac{1}{|\mathbf{r}_i - \mathbf{r}_j|} \right) \times \hat{\mathbf{p}}_i \right) \hat{\mathbf{s}}_j \Bigg\}. \end{aligned}$$

Here, c is the speed of light, e is the electron charge, and m_e is the electron mass. The operators $\hat{\mathbf{p}}_i$ and $\hat{\mathbf{s}}_i$ denote the momentum and spin operator acting on electron i, respectively. This operator was originally derived by Pauli who considered an electron in an external electric and magnetic field. However, this spin-orbit operator can be obtained from the four-component Dirac-Coulomb-Breit Hamiltonian, as well [26, 97]. The first two terms describe spin-same-orbit interactions while the second two refer to spin-other-orbit interactions.

Specifically, the first term corresponds to the interaction of the spin-magnetic moment of electron i with the magnetic moment from rotating in the field of the nucleus I while the second term arises from the motion of electron i in the field of electron j. Finally, the last two terms give the coupling between the spin magnetic moment of electron i with the orbital magnetic moment of electron j and *vice versa*.

The Breit-Pauli operator can be recast in a more compact way [26]

$$\hat{H}_{SO}^{BP} = \frac{e^2}{2m_e^2c^2}\sum_i \left\{ \sum_I Z_I \left(\frac{\mathbf{r}_i - \mathbf{R}_I}{|\mathbf{r}_i - \mathbf{R}_I|^3} \times \hat{\mathbf{p}}_i \right) \hat{\mathbf{s}}_i - \sum_{i \neq j} \left(\frac{\mathbf{r}_i - \mathbf{r}_j}{|\mathbf{r}_i - \mathbf{r}_j|^3} \times \hat{\mathbf{p}}_i \right) (\hat{\mathbf{s}}_i + 2\hat{\mathbf{s}}_j) \right\}.$$

However, the Breit-Pauli operator has the problem of being unbound from below as it contains terms that couple the electronic solutions to the positronic ones. Consequently, it cannot be used safely beyond first-order perturbation theory. Although this is rarely a problem in practical examples including mainly light elements [101], it can be solved by the no-pair approximation where electron-positron pair creation is not allowed to occur [26, 96, 97]. The corresponding variationally stable no-pair Hamiltonian (also called Douglas-Kroll Hamiltonian) has the following form [26]:

$$\hat{H}_{SO}^{DK} = e^2\hbar c \sum_i \left\{ \sum_I Z_I \frac{\hat{A}_i}{\hat{E}_i + m_e c^2} \left(\frac{\mathbf{r}_i - \mathbf{R}_I}{|\mathbf{r}_i - \mathbf{R}_I|^3} \times \hat{\mathbf{p}}_i \right) \hat{\mathbf{s}}_i \frac{\hat{A}_i}{\hat{E}_i + m_e c^2} - \sum_{i \neq j} \frac{\hat{A}_i \hat{A}_j}{\hat{E}_i + m_e c^2} \left[\left(\frac{\mathbf{r}_i - \mathbf{r}_j}{|\mathbf{r}_i - \mathbf{r}_j|^3} \times \hat{\mathbf{p}}_i \right) (\hat{\mathbf{s}}_i + 2\hat{\mathbf{s}}_j) \right] \frac{\hat{A}_i \hat{A}_j}{\hat{E}_j + m_e c^2} \right\}$$

with the relativistic kinetic energy operator

$$\hat{E}_i = \sqrt{\hat{\mathbf{p}}_i c^2 + m_e^2 c^4}$$

and

$$\hat{A}_i = \sqrt{\frac{\hat{E}_i + m_e c^2}{2\hat{E}_i}}.$$

For both, the Breit-Pauli as well as the no-pair Hamiltonian, the computationally most cumbersome part is given by the two-electron terms. Moreover, in heavy elements the one-electron term is dominating and the two-electron terms contribute with only about 5-10 % [99, 101]. Therefore, it is advantageous to introduce effective one-electron operators that include the two-electron parts only in the form of screening effects and do not calculate them explicitly.

The mean-field approximation [103] is one of the most rigorous methods to obtain an effective one-electron spin-orbit Hamiltonian and can be applied with all molecular spin-orbit coupling Hamiltonians, including the Breit-Pauli as well

as the no-pair Hamiltonian introduced above. Denoting the one-electron part of the chosen Hamiltonian as $\hat{h}_{SO}(1)$ and the two-electron part as $\hat{H}_{SO}(1,2)$, a matrix element of the mean-field spin-orbit Hamiltonian within a certain orbital basis $\{i\}$ is given by

$$\langle i|\hat{H}_{SO}^{mf}|j\rangle = \langle i|\hat{h}_{SO}(1)|j\rangle + \frac{1}{2}\sum_k n_k \Big\{2\langle ik|\hat{H}_{SO}(1,2)|jk\rangle \tag{5.1}$$

$$- 3\langle ki|\hat{H}_{SO}(1,2)|jk\rangle - 3\langle ik|\hat{H}_{SO}(1,2)|kj\rangle\Big\} \tag{5.2}$$

The summation runs over all spatial molecular orbitals and n_k refers to the occupation number of these orbitals ($0 \leq n_k \leq 2$). By considering occupation numbers smaller than two, partially filled orbitals are considered, too, and their spin-orbit interactions are averaged over α and β spin orientations.

Benchmarks have revealed that this approximate Hamiltonian constitutes a good approximation and for heavy elements the error lies below 0.1 % [26, 103]. Even in lighter elements, where contributions from the two-electron terms can contribute up to 50 % of the total spin-orbit interaction, the errors introduced by the mean-field approximation did not exceed 1 % [99, 104].

The numerical effort can be further reduced if only an atomic mean-field is considered [103]. In this case all multicenter integrals are neglected. The mean-field summation now runs over a certain set of atom-centered orbitals which are usually either given by the atomic orbital basis or obtained *via* an atomic Hartree-Fock calculation [105]. The motivation for this approach is given by the $1/r^3$ dependence of the spin-orbit Hamiltonian. Moreover, the most significant contributions are due to molecular core orbitals which are usually very similar to atomic orbitals and mainly localized at one center. Finally, the full symmetry of the D_{2h} point group can now be used to further reduce the numerical cost.

The errors for the atomic mean-field approach are higher than for a molecular mean-field and can be up to 5 % in molecules composed of light elements [104, 106]. Nevertheless, this approach allows for a very efficient evaluation of spin-orbit coupling elements with reasonable accuracy.

5.2. Wigner-Eckart Theorem

Very useful for the evaluation of spin-orbit coupling elements is the Wigner-Eckart theorem (WET) [26, 100]. This theorem states that the matrix element $\langle AJ'M'|\hat{\mathscr{T}}_q^{(k)}|BJ''M''\rangle$ over the components $\hat{\mathscr{T}}_q^{(k)}$ of an irreducible tensor operator can be written as a product between a $3j$-symbol and the so-called Wigner-Eckart reduced matrix element $\langle AJ'||\hat{\mathscr{T}}^{(k)}||BJ''\rangle$:

$$\langle AJ'M'|\hat{\mathscr{T}}_q^{(k)}|BJ''M''\rangle = (-1)^{J'-M'} \underbrace{\begin{pmatrix} J' & k & J'' \\ -M' & q & M \end{pmatrix}}_{\text{3j-symbol}} \langle AJ'||\hat{\mathscr{T}}^{(k)}||BJ''\rangle$$

Here, J'(J") and M'(M") represent the angular momentum and its orientation associated with state A(B). The Wigner-Eckart reduced matrix element is independent of the orientation of the angular momenta M' and M''. Thus, by

knowing the Wigner-Eckart reduced matrix element all possible combinations of M' and M'' can be easily obtained. This can be used to greatly simplify the calculation of spin-orbit coupling elements.

The $3j$-symbols are obtained from the Clebsch-Gordon coefficients [107]

$$\begin{pmatrix} J' & k & J'' \\ -M' & q & M \end{pmatrix} = \frac{(-1)^{J'-k-M}}{\sqrt{2J+1}} \underbrace{\langle J'kM'q|j'kJM\rangle}_{\text{Clebsch-Gordon coefficient}} .$$

They impose some selection rules on the matrix elements. The elements are only nonzero if

$$M'' = M' + q \qquad \text{and} \qquad J' + J'' \geq k \geq |J'' - J'|.$$

Thus, for tensor operators of rank one, like the spin or spatial angular momentum operators, the matrix elements are zero unless the conditions

$$\Delta J = 0, \pm 1 \qquad \Delta M = 0, \pm 1 \qquad J'' + J' \geq 1$$

are fulfilled.

The phenomenological spin-orbit operator

$$\hat{H}_{SO} = A_{SO}(\mathbf{r})\hat{\mathbf{L}} \cdot \hat{\mathbf{S}} \tag{5.3a}$$

$$= A_{SO}(\mathbf{r}) \left(\hat{L}_0\hat{S}_0 - \hat{L}_{+1}\hat{S}_{-1} - \hat{L}_{-1}\hat{S}_{+1} \right) \tag{5.3b}$$

$$= A_{SO}(\mathbf{r}) \left(\hat{L}_x\hat{S}_x + \hat{L}_y\hat{S}_y + \hat{L}_z\hat{S}_z \right) \tag{5.3c}$$

is a compound tensor operator of rank zero while the two components $\hat{\mathbf{L}}$ and $\hat{\mathbf{S}}$ are first-rank tensors (compare Section 2.2). A_{SO} is the so-called spin-orbit parameter [26]. The phenomenological spin-orbit operator can easily be applied for the derivation of selection rules although it should not be used for actual computations of spin-orbit coupling elements [26]. It will prove useful to contract the spatial parts $A_{SO}(\mathbf{r})$ and $\hat{L}_p$, $p = x, y, z$, to give new operators defined by $\hat{l}_p = A_{SO}(\mathbf{r})\hat{L}_p$. The spin-orbit operator is then given by

$$\hat{H}_{SO} = \hat{l}_x\hat{S}_x + \hat{l}_y\hat{S}_y + \hat{l}_z\hat{S}_z.$$

In principle, the Wigner-Eckart theorem can be applied to calculate both, the spatial as well as the spin part of the matrix elements. However, due to the coupling the orbital angular momentum L is no good quantum number of the system anymore. Theoretically, this applies to the spin angular momentum, too, but in the usually used Russel-Saunders (LS) coupling scheme [25, 96], S is assumed to still be a good quantum number. Within this work, we therefore employ the usual procedure and apply the Wigner-Eckart theorem to the spin part of the matrix elements only (compare [26]).

In the Q-Chem program package, where the spin-orbit coupling elements were implemented as part of this thesis, only one of the three components of a triplet state is obtained as a result of an ADC(n) calculation, namely the $M = 0$ component. Due to the selection rules for non-zero $3j$-symbols one has

to choose the actual element from which the Wigner-Eckart reduced element is calculated with great care. To calculate the coupling between a singlet ($M' = 0$) state and the $M'' = 0$ component of a triplet state, only the $\hat{S}_0$ component of the spin operator can be used due to the restriction $M'' = M' + q$. To calculate couplings between triplet states, the $M = 0$ components cannot be used at all as

$$\begin{pmatrix} J' & k & J'' \\ -M' & q & M \end{pmatrix} = \begin{pmatrix} 1 & 1 & 1 \\ 0 & q & 0 \end{pmatrix} = 0 \qquad \forall q \in \{0, \pm 1\}.$$

Thus, for the implemented coupling elements between singlet and triplet states the elements $\langle A,0,0|\hat{l}_x\hat{S}_0|B,1,0\rangle$, $\langle A,0,0|\hat{l}_y\hat{S}_0|B,1,0\rangle$, and $\langle A,0,0|\hat{l}_z\hat{S}_0|B,1,0\rangle$ are calculated. Using the Wigner-Eckart theorem the spin-orbit coupling elements to the three triplet components are given by

$$\langle A,0,0|\hat{H}_{SO}|B,1,0\rangle = \langle A,0,0|\hat{l}_z\hat{S}_z|B,1,0\rangle = \langle A,0,0|\hat{l}_z\hat{S}_0|B,1,0\rangle \tag{5.4a}$$

$$\begin{aligned}\langle A,0,0|\hat{H}_{SO}|B,1,1\rangle &= \langle A,0,0|\hat{l}_x\hat{S}_x|B,1,1\rangle + \langle A,0,0|\hat{l}_y\hat{S}_y|B,1,1\rangle \\ &= \frac{1}{\sqrt{2}}\left(\langle A,0,0|\hat{l}_x\hat{S}_{-1}|B,1,1\rangle + \langle A,0,0|\hat{l}_y\hat{S}_{-1}|B,1,1\rangle\right) \\ &= \frac{1}{\sqrt{2}\sqrt{3}}\left(\langle A,0||\hat{l}_x\hat{\mathbf{S}}||B,1\rangle + i\langle A,0||\hat{l}_y\hat{\mathbf{S}}||B,1\rangle\right) \\ &= -\frac{1}{\sqrt{2}}\left(\langle A,0,0|\hat{l}_x\hat{S}_0|B,1,0\rangle + i\langle A,0,0|\hat{l}_y\hat{S}_0|B,1,0\rangle\right)\end{aligned} \tag{5.4b}$$

$$\begin{aligned}\langle A,0,0|\hat{H}_{SO}|B,1,-1\rangle &= \langle A,0,0|\hat{l}_x\hat{S}_x|B,1,-1\rangle + \langle A,0,0|\hat{l}_y\hat{S}_y|B,1,-1\rangle \\ &= \frac{1}{\sqrt{2}}\Big(-\langle A,0,0|\hat{l}_x\hat{S}_{+1}|B,1,-1\rangle \\ &\quad + i\langle A,0,0|\hat{l}_y\hat{S}_{+1}|B,1,-1\rangle\Big) \\ &= \frac{1}{\sqrt{2}}\left(\langle A,0,0|\hat{l}_x\hat{S}_0|B,1,0\rangle - i\langle A,0,0|\hat{l}_y\hat{S}_0|B,1,0\rangle\right).\end{aligned} \tag{5.4c}$$

In addition to the usually used spherical components of a triplet state with eigenvalues $M = 0, \pm 1$, Cartesian components can be formed according to equation 2.4. Because they can be helpful in deriving selection rules (compare next Section) the matrix elements with respect to these Cartesian triplet components are given here:

$$\begin{aligned}\langle A,0,0|\hat{H}_{SO}|B,1,X\rangle &= \langle A,0,0|\hat{l}_x\hat{S}_x|B,1,X\rangle = \langle A,0,0|\hat{l}_x\hat{S}_0|B,1,0\rangle \\ \langle A,0,0|\hat{H}_{SO}|B,1,Y\rangle &= \langle A,0,0|\hat{l}_y\hat{S}_y|B,1,Y\rangle = \langle A,0,0|\hat{l}_y\hat{S}_0|B,1,0\rangle \\ \langle A,0,0|\hat{H}_{SO}|B,1,Z\rangle &= \langle A,0,0|\hat{l}_z\hat{S}_z|B,1,Z\rangle = \langle A,0,0|\hat{l}_z\hat{S}_0|B,1,0\rangle.\end{aligned}$$

The effective one-electron operator within the atomic mean-field approximation can be written as well as a sum over Cartesian components which are given as products between a spatial part and a spin part as in the case of the

phenomenological operator 5.3:

$$\hat{H}_{SO}^{mf} = \sum_i \hat{\mathbf{l}}(i)\hat{\mathbf{S}}(i) = \sum_{p=x,y,z} \sum_i \hat{l_p}(i)\hat{S}_p(i) = \hat{H}_{SO,x}^{mf} + \hat{H}_{SO,y}^{mf} + \hat{H}_{SO,z}^{mf},$$

where $\hat{l_p}(i)$ denotes the spatial part of the operator acting on electron i and $\hat{S}_p(i)$ the respective spin part. Therefore, the spin-orbit coupling elements $\langle A, S', M'|\hat{H}_{SO,p}^{mf}|B, S'', M''\rangle$ can be written as products between a spatial and a spin integral [108]. The `AMFI` code of B. Schimmelpfennig [22], which was incorporated into the Q-Chem package to enable the calculation of spin-orbit coupling elements, yields these spatial components represented within the atomic basis. When multiplied by the spin part corresponding to $\hat{S}_0$, equations 5.4 can be used to calculate the final coupling elements as well in the case of the effective one-electron operator.

5.3. Selection Rules for Spin-Orbit Coupling Elements

In the previous section selection rules based on the Wigner-Eckart theorem and the $3j$-symbols were introduced. A second set of rules is imposed by molecular symmetry (for an introduction to molecular group theory see, e. g., [109]). As the spin-orbit operator transforms with respect to the totally symmetric irreducible representation (irrep) of a certain symmetry group, a matrix element

$$\langle A, S, M|\hat{H}_{SO}|B, S', M'\rangle$$

is non-zero if the direct product of the irreps of the two spatial ($\Gamma(A)$,$\Gamma(B)$) and the two spin parts ($\Gamma(S, M)$,$\Gamma(S', M')$) contains the totally symmetric irrep Γ_1, i. e.,

$$\Gamma_1 \in \Gamma(A) \otimes \Gamma(S, M) \otimes \Gamma(B) \otimes \Gamma(S', M').$$

Within this work, we only consider systems with an even number of electrons. In this case both, the spin and spatial part of the wave functions, transform according to boson irreps of the usual molecular point groups. In the case of an odd number of electrons the spin part transforms however with respect to fermion irreps and double groups need to be used. Further details can be found in, e. g., [26, 97].

In the case of an even number of electrons, the spin part of singlet wave functions transform like the totally symmetric irrep Γ_1 whereas the Cartesian components of the triplet spin functions transform according to rotations around the corresponding axis [26]. The irreps associated with such rotations can be determined from the respective character tables. For the point groups of the molecules used in the test calculations (Section 7) these tables are given in appendix C.

As an example, we will consider here a molecule with C_{2v} symmetry and analyze the coupling between a singlet state of B_1 symmetry and a triplet state whose spatial part transforms according to B_2 symmetry. The three spherical

components of the triplet state are given by linear combinations of the Cartesian components according to 2.4. Finally, the three Cartesian components x, y and z of the latter transform with respect to the irreps B_2, B_1 and A_2. Thus, a singlet $^1B_1$ state couples only to the $M = 0$ component of a $^3B_2$ state. According to the selection rules derived in the previous section, the only contribution to this element stems from the L_zS_z term of the spin-orbit operator. Similarly, a $^1A_1$ state couples to the x and, consequently, $M = \pm 1$ components of a $^3B_2$ state through the L_xS_x term of H_{SO}.

5.4. Implementation

The calculation of spin-orbit coupling elements was included into a development version of the program package Q-Chem. For this purpose the `AMFI` program of B. Schimmelpfennig [22] was incorporated. Based on the nuclear charge and the atomic basis functions it calculates the atomic mean-field integrals in D_{2h} symmetry and returns the Cartesian components of the spatial part (here denoted as l_p, $p = x, y, z$) of the spin-orbit coupling operator in the atomic basis. The basis functions are sorted according to the irreps to which the basis functions belong. In the mean-field summation the atomic orbitals are used. The occupation numbers are determined from an internally stored table which returns the ground state electron configurations for atoms with a nuclear charge of up to 103. The matrix representation of the spin-orbit coupling operator itself is then obtained by multiplying the spatial parts with the respective spin part (compare Section 5.2) and summation over the three resulting Cartesian components according to equation 5.4.

Like explained in Section 3.3, every matrix element of a general one-particle operator $\hat{O}$ with respect to two states A and B can be obtained by representing the operator in the atomic or molecular basis and summation over the elementwise products with the transition density matrix $\boldsymbol{\rho}^{A \leftarrow B}$ between states A and B:

$$\langle A|\hat{O}|B\rangle = \sum_{ij} O_{ij}\rho_{ij}^{A,B}.$$

This approach is used here to obtain the desired spin-orbit coupling elements, as well, and the respective transition density matrices and operators are represented within the atomic basis. The individual steps that have to be taken are explained in detail below.

The newly implemented interface to the `AMFI` program writes an input file with the relevant information which is then read by the `AMFI` code upon calling the master subroutine. Additionally, pointers to arrays of appropriate length are passed to the `AMFI` code in which the resulting matrix elements are given as lower triangular matrices. The `AMFI` code returns, as well, arrays containing the L and M values of the atomic basis function in the order used to express the matrix elements.

In the Q-Chem program package the atomic basis functions are, however, for each atom sorted by ascending L values. For a certain value of L the

basis functions are arranged with respect to M and according to the sequence $-L, -L+1, \ldots, L-1, L$. The groups of functions for each atom appear in the same order as given in the molecular structure. Special care has to be taken to the use of augmented basis functions. In these basis sets, a set of diffuse basis functions is added at the end of the basis set sorted in ascending order with respect to L and M.

In `adcman`, operators given within a certain atomic basis are stored as two-dimensional block tensors. This means that the matrix is divided into several smaller matrices in order to allow for an efficient shared memory parallelization [20]. Operations on the individual blocks can then be performed independently of each other and simultaneously. To save memory, only the blocks determining the triangular part of the matrix are stored. It should be stressed that all the blocks stored are given completely. More specifically, the blocks on the diagonal of the matrix are fully stored and not only their triangular elements.

When given the matrix elements of the angular momentum operator from the `AMFI` code, the interface rearranges the basis functions to the correct order in Q-Chem and inserts them into the respective block tensor at the correct position for the atom under consideration. Here, it has to be considered that the resulting matrix has to be antisymmetric. When the `AMFI` code has been executed for each atom of the molecule, three block tensors are obtained; one for each Cartesian component.

In the next step, the correct products with the $M = 0$ component of the spin operator (compare Section 5.2) have to be formed. It has to be considered that the `AMFI` code assumes the spin operators to be expressed in terms of the Pauli spin matrices σ_p ($p = 0, \pm$) which differ from our definitions by a factor of one half: $\hat{S}_p = 1/2\sigma_p$. Consequently, the operator products $\mathbf{l}_p\mathbf{S}_0$ for $p = x, y, z$ are given by matrices of the following structure:

$$\mathbf{l}_p\mathbf{S}_0 = \begin{array}{c} \\ \alpha \\ \beta \end{array} \begin{array}{c} \begin{array}{cc} \alpha & \beta \end{array} \\ \begin{pmatrix} \mathbf{P} & \mathbf{0} \\ \mathbf{0} & -\mathbf{P} \end{pmatrix} \end{array}$$

where $\mathbf{P}$ is the matrix of spatial integrals within the basis of atomic basis functions as given by the `AMFI` code for a certain p. These matrices are stored for further use by the `adcman` library that performs the actual ADC calculation.

During the ADC(n) calculation, transition density matrices between the ground state and the excited states $\boldsymbol{\rho}^{n\leftarrow 0}$ as well as among the excited states itself ($\boldsymbol{\rho}^{n\leftarrow m}$) are calculated, if requested. So far only between states of same spin symmetry transition densities were calculated. This has been changed within the current implementation to include those between singlet and triplet states in addition. After transformation from the molecular to the atomic basis, the spin-orbit coupling elements $\langle A, 0, 0|\hat{l}_p\hat{S}_0|B, 1, 0\rangle$ can be obtained by

$$\langle A, 0, 0|\hat{l}_p\hat{S}_0|B, 1, 0\rangle = \sum_{ij} (\mathbf{l}_p\mathbf{S}_0)_{ij}\rho_{ij}^{n,m} \qquad \text{with} \qquad p = x, y, z.$$

Finally, forming linear combinations according to equations 5.4 yields the desired spin-orbit coupling elements. In the output, in addition to the three

spin-orbit coupling elements their Euclidean norm is given as it constitutes a constant of the rotation and can be used to calculate further properties like inter-system crossing rates *via* Fermi's golden rule.

For the calculation of the spin-orbit coupling elements both, the Breit-Pauli as well as the Douglas-Kroll Hamiltonian, can be employed and are chosen by the following parameter:

ADC_AMFI_NOPAIR

Controls the spin-orbit operator used in the `AMFI` code

TYPE:

LOGICAL

DEFAULT:

TRUE

OPTIONS:

TRUE Use the no-pair (Douglas-Kroll) Hamiltonian.

FALSE Use the Breit-Pauli Hamiltonian.

RECOMMENDATION:

Use default.

The transition densities between the ground state and several excited states are given by default. However, if elements between excited states are desired, the parameter "ADC_PROP_ES2ES" has to be set to "TRUE" in order to guarantee the calculation of state to state transition density matrices.

6. Plasmons in Molecules

The term plasmons stems from solid state physics and originally refers to collective oscillations of the electron gas in metals [110]. They can occur as either volume or surface (Mie) plasmons and can be observed, e. g., by inelastic electron scattering on thin metal films or in photoionization spectra. Typically, the excitation energies lie in the region of 10 eV. Surface plasmons are accessible by optical excitation, as well, and exhibit very high absorption cross sections.

Plasmons have already been used for a very long time to color materials. For example, in medieval times, metallic nanoparticles (often gold or silver) were incorporated into church windows. Depending on their size and shape, the absorption wave lengths of the surface plasmons vary strongly thereby making a wide range of colors accessible. The phenomenon of ruby-red colloidal gold was also studied by Faraday [111].

Modern applications focus on the field of plasmonics. The high absorption cross sections and efficient energy and information transport make plasmons interesting targets for the field of electronics, e. g., as chemical or biological sensors [112–114], photovoltaic devices [115, 116], metamaterials [117–120] or high frequency computer chips [121–124]. The efficient energy or information transfer is due to the fact that after local excitation the plasmons propagate as electron waves along the material similar to wave propagation on a water surface initiated by a water droplet.

In solid state physics, electronic excitations in metals and metallic nanoclusters are often classified as single-particle excitations and plasmons (e. g., [110], [125], and [126]). In large extended systems the plasmon frequencies are well described by classical electrodynamics. Plasmons have, however, also been discussed for smaller clusters showing molecular-like electronic structures, e. g., for alkali metal, silver or gold clusters with dimensions of about 2 nm or even less [127]. Within this regime, quantum mechanical treatments become necessary for an appropriate description. The question arises how the macroscopic coherent density oscillations can be correlated with the discrete electronic excitations addressed in microscopic quantum theoretical treatments.

Many theoretical studies have been performed concerning the optical properties of small metal clusters, mainly employing TDDFT or random-phase approximation (RPA) methods [128–144]. Special attention has been given to the size dependence of the plasmon excitations in metal clusters. It should be noted that in small clusters the applicability of the plasmon concept is a matter of dispute. Bonačić-Koutecký et al. argued that there are no plasmon-type excitations in small clusters and molecules [129]. They used a similar approach as will be presented in this section to analyze plamons on a microscopic level but parts of their conclusions are questionable. By contrast, Kümmel et al. have used quantum fluid dynamics and TDDFT to show that microscopic electronic excitations

can indeed be correlated with density oscillations even in very small systems like Na_2 [134, 135]. Yasuike et al. used a so-called collectivity index [145, 146], corresponding to the effective number of single-particle replacements contributing to an excitation, to analyze plasmons in small sodium clusters [142]. They attribute the term plasmon only to such states for which the collectivity index is maximal and equal to the number of occupied orbitals.

With respect to molecular systems, plasmons have been mainly discussed for fullerenes. The occurrence of a plasmon resonance in the region of 20–30 eV was theoretically proposed by Bertsch et al. for C_{60} using a tight-binding model and linear response theory [147]. A plasmon excitation within the same energy range was experimentally observed by Hertel et al. using photoionization measurements shortly afterward [148]. This excitation lies well above the ionization limit of C_{60}. However, additional plasmonic states below the ionization limit at approximately 6 eV were proposed by electron energy loss spectroscopy [149–152] as well as theoretical studies using again a tight-binging model and linear response theory [153, 154]. Since then, many other experimental and theoretical studies of the (optical) absorption properties of fullerenes were performed, e. g., [155–166]. Although microscopic theories like the random-phase approximation or TDDFT were used in many of the theoretical studies, no clear definition of plasmons on a microscopical level was given. In some studies on the optical properties of fullerenes the notion of a plasmon is not even mentioned (e. g., [156, 161]). Moreover, Bauernschmitt et al. state that due to the restriction to single excitations the TDDFT approach is not able to detect plasmons.

Bernadotte et al. recently showed that the notion of a plasmon can indeed be transferred to molecular systems [167]. In the following section the main aspects of their analysis will be reviewed. Additionally, a thorough review of the quantum theoretical treatment of plasmons at the level of RPA will be given which allows for a clear characterization of plasmon excitations.

Based on their theoretical findings, Bernadotte et al. [167] suggested a scaling approach for the electron-electron correlation in TDDFT that allows for an efficient distinction between single-particle excitations and plasmons. This approach will be transferred to *ab initio*, Hartree-Fock based methods, namely CIS and ADC(2) in section 6.4. Due to the lack of electron correlation in the Hartree-Fock reference state the scaling has to be adapted to the present situation.

6.1. Classical Treatment

As mentioned above, plasmons are well described by classical electrodynamics in large and extended systems [29, 110, 167]. For this purpose one considers a uniform electron gas of particle density n_0 and a positive uniform background with the same density enclosed in volume V. An external electric field induces a shift in the electron density $\delta n(\mathbf{x}, t)$ and leads to the new density

$$n(\mathbf{x}, t) = n_0 + \delta n(\mathbf{x}, t).$$

This, on the other hand, induces an electric field $\mathcal{E}$ and the corresponding restoring force

$$F = -4\pi e^2 n_0 \delta n(\mathbf{x}, t),$$

where e is the electronic charge. Thus, the system behaves like a driven harmonic oscillator with the frequency

$$\omega_{pl}^2 = \frac{4\pi e^2 n_0}{m_e}, \tag{6.1}$$

where m_e the electron mass. This classical plasmon frequency agrees well to the observed frequency in metallic systems like, e. g., aluminum or manganese but fails for nanoclusters or molecular systems.

6.2. Quantum Chemical Treatment

In this section the collective modes of the electron gas will be described within the framework of quantum theory. As in the previous section we will be interested in the response of the electron gas to an external perturbation for which linear response theory and the RPA will be employed. Finally, the respective equations will be solved for a small model system that allows one to analyze the microscopic properties of plasmons as opposed to single-particle excitations of the free electron gas in more detail.

The homogeneous electron gas

Analogously to the previous section, we consider a homogeneous electron gas enclosed in volume V with periodic boundary conditions as a model for a metal and assume a uniform positively charged background. Neglecting any interaction between the electrons, the single-particle states (spin orbitals) are characterized by plane-waves

$$\chi_{\mathbf{k}\sigma}(\mathbf{x}, m_s) = \phi_{\mathbf{k}}(\mathbf{x})\sigma(m_s) = \frac{1}{\sqrt{V}} e^{i\mathbf{k}\mathbf{x}} \sigma(m_s), \qquad \sigma \in \{\alpha, \beta\}.$$

Here, $\mathbf{x}$ denotes the Cartesian coordinates and $\sigma(m_s)$ the spin function of the electron. Using the periodic boundary conditions, the components of the wave vector are given by:

$$k_i = \frac{2\pi n_i}{\sqrt[3]{V}} \qquad (i = x, y, z,\ n_i = 0, \pm 1, \pm 2, \dots).$$

The wave vectors are also referred to as momentum vectors. The single-particle (orbital) energies are

$$\epsilon(\mathbf{k}) = \frac{\hbar^2 |\mathbf{k}|^2}{2m_e}.$$

For $V \to \infty$ the wave vectors can be treated as being continuous.

In the ground state of a system containing N electrons, the N energetically lowest orbitals are occupied. The energy of the highest orbital is called Fermi energy ϵ_F. The corresponding Fermi wave number (also called Fermi momentum) k_F can be used to define occupation numbers $n_{\mathbf{k}}$:

$$n_{\mathbf{k}} = \Theta(k_F - |\mathbf{k}|) = \begin{cases} 0, & |\mathbf{k}| > k_f \\ 1, & |\mathbf{k}| \leq k_f \end{cases} .$$

As the free non-interacting electron gas will be used as a reference system within the RPA, it will be useful for the further discussion to analyze the two-electron integrals $V_{\mathbf{k}_1\sigma_1\mathbf{k}_2\sigma_2\mathbf{k}_3\sigma_3\mathbf{k}_4\sigma_4} = \langle\chi_{\mathbf{k}_1\sigma_1}\chi_{\mathbf{k}_2\sigma_2}|\chi_{\mathbf{k}_3\sigma_3}\chi_{\mathbf{k}_4\sigma_4}\rangle$ with respect to these single-particle states. In order to guarantee that all expressions are mathematically well defined an exponential convergence factor ($e^{-\mu|\mathbf{x}_i-\mathbf{x}_j|}$) has to be inserted into the interaction potential between electrons i and j. Taking the limit $\mu \to 0$ then recovers the original potential:

$$\begin{aligned} V_{\mathbf{k}_1\sigma_1\mathbf{k}_2\sigma_2\mathbf{k}_3\sigma_3\mathbf{k}_4\sigma_4} &= \langle\chi_{\mathbf{k}_1\sigma_1}\chi_{\mathbf{k}_2\sigma_2}|\chi_{\mathbf{k}_3\sigma_3}\chi_{\mathbf{k}_4\sigma_4}\rangle = \langle\phi_{\mathbf{k}_1}\phi_{\mathbf{k}_2}|\phi_{\mathbf{k}_3}\phi_{\mathbf{k}_4}\rangle\delta_{\sigma_1,\sigma_3}\delta_{\sigma_2,\sigma_4} \\ \langle\phi_{\mathbf{k}_1}\phi_{\mathbf{k}_2}|\phi_{\mathbf{k}_3}\phi_{\mathbf{k}_4}\rangle &= \frac{e^2}{V^2}\lim_{\mu\to 0}\int\int e^{-i\mathbf{k}_1\mathbf{x}_1}e^{-i\mathbf{k}_2\mathbf{x}_2}\frac{e^{-\mu|\mathbf{x}_1-\mathbf{x}_2|}}{|\mathbf{x}_1-\mathbf{x}_2|}e^{i\mathbf{k}_3\mathbf{x}_1}e^{i\mathbf{k}_4\mathbf{x}_2}d^3x_1d^3x_2 \\ &= \frac{e^2}{V^2}\lim_{\mu\to 0}\int\int e^{i(\mathbf{k}_3-\mathbf{k}_1)\mathbf{x}_1}\frac{e^{-\mu|\mathbf{x}_1-\mathbf{x}_2|}}{|\mathbf{x}_1-\mathbf{x}_2|}e^{-i(\mathbf{k}_2-\mathbf{k}_4)\mathbf{x}_2}d^3x_1d^3x_2. \end{aligned}$$

With the substitutions $\mathbf{x} = \mathbf{x}_1 - \mathbf{x}_2$ and $\mathbf{y} = \mathbf{x}_2$ this can be further evaluated:

$$\begin{aligned} \langle\phi_{\mathbf{k}_1}\phi_{\mathbf{k}_2}|\phi_{\mathbf{k}_3}\phi_{\mathbf{k}_4}\rangle &= \frac{e^2}{V^2}\lim_{\mu\to 0}\int e^{i(\mathbf{k}_3-\mathbf{k}_1)\mathbf{x}}\frac{e^{-\mu|\mathbf{x}|}}{|\mathbf{x}|}d^3x\int e^{-i(\mathbf{k}_1+\mathbf{k}_2-\mathbf{k}_3-\mathbf{k}_4)\mathbf{y}}d^3y \\ &= \frac{e^2}{V}\lim_{\mu\to 0}\delta_{\mathbf{k}_1+\mathbf{k}_2,\mathbf{k}_3+\mathbf{k}_4}\frac{4\pi}{(\mathbf{k}_1-\mathbf{k}_3)^2+\mu^2} \\ &= \frac{e^2}{V}\delta_{\mathbf{k}_1+\mathbf{k}_2,\mathbf{k}_3+\mathbf{k}_4}\frac{4\pi}{(\mathbf{k}_1-\mathbf{k}_3)^2}. \end{aligned}$$

The Kronecker delta reflects the fact that the momentum has to be conserved when two electrons interact. Finally, with inclusion of spin this yields:

$$V_{\mathbf{k}_1\sigma_1\mathbf{k}_2\sigma_2\mathbf{k}_3\sigma_3\mathbf{k}_4\sigma_4} = \frac{e^2}{V}\delta_{\mathbf{k}_1+\mathbf{k}_2,\mathbf{k}_3+\mathbf{k}_4}\delta_{\sigma_1,\sigma_3}\delta_{\sigma_2,\sigma_4}\frac{4\pi}{(\mathbf{k}_1-\mathbf{k}_3)^2}.$$

Linear response to an external perturbation and the polarization propagator

In linear response theory the density change $\delta\langle\hat{n}(\mathbf{x},t)\rangle$ induced by an external potential is described by the time-space integral over the product of the density correlation function or polarization propagator $\Pi(\mathbf{x}t,\mathbf{x}'t')$ and the external potential $\Phi_{ext}(\mathbf{x},t)$ [29, 167]. The poles of $\Pi(\mathbf{x}t,\mathbf{x}'t')$ determine the excitation energies of the states that are coupled to the ground state by the density operator. Fourier-transformation from the space domain into the momentum domain and from the time domain to the frequency domain as well as insertion of a complete set of eigenstates of $\hat{H}$ leads to the well-known spectral or

Lehmann representation of the polarization propagator [29]:

$$\Pi_{pr,p'r'}(\omega) = \underbrace{\sum_{m\neq 0} \frac{\langle\Psi_0|c_r^\dagger c_p|\Psi_m\rangle\langle\Psi_m|c_{p'}^\dagger c_{r'}|\Psi_0\rangle}{\omega-(E_m-E_0)+i\eta}}_{\Pi^+_{pr,p'r'}(\omega)} + \underbrace{\sum_{m\neq 0} \frac{\langle\Psi_0|c_{p'}^\dagger c_{r'}|\Psi_m\rangle\langle\Psi_m|c_r^\dagger c_p|\Psi_0\rangle}{\omega+(E_m-E_0)-i\eta}}_{\Pi^-_{pr,p'r'}(\omega)}.$$

Here, the indexes p and r denote spin-orbitals:

$$p \equiv \mathbf{j}\tau \qquad \text{and} \qquad r \equiv \mathbf{k}\sigma.$$

The factors $\pm i\eta$ guarantee convergence of the Fourier-transformations. The two terms of the matrix $\mathbf{\Pi}(\omega)$, denoted as $\mathbf{\Pi}^+(\omega)$ and $\mathbf{\Pi}^-(\omega)$, both contain the whole physical information. However, the poles of the first term $\mathbf{\Pi}^+(\omega)$ correspond to excitation energies (ph states) while those of $\mathbf{\Pi}^-(\omega)$ belong to deexcitations (hp states). They are connected by [14]

$$\mathbf{\Pi}^{+\dagger}(-\omega) = \mathbf{\Pi}^-(\omega).$$

To derive approximate expressions for the polarization propagator, we will use the homogeneous electron gas from above to define a non-interacting reference system and describe the electron-electron interaction approximately within the RPA.

Random-phase approximation (RPA)

Originally, the RPA has been derived by Pines and Bohm [168–171]. They used an effective screened Coulomb force, among other approximations, to separate collective modes (plasmons) from single-particle excitations. The resulting quantum mechanical description of plasmons constitutes one of the greatest successes of the RPA. Later, the RPA has been derived by other methods, as well. Among them is the ring-approximation which analyzes the interaction potential within diagrammatic perturbation theory and retains only certain (ring) diagrams [29].

Here, we refrain from deriving the RPA and just state that it is equivalent to describing the interaction approximately as the Coulomb-exchange integral over the single-particle states of the reference system [14]:

$$U^{RPA}_{pr,p'r'} = -V_{pr'[p'r]} = -\langle pr'||p'r\rangle.$$

At this point a word of caution is appropriate. The RPA as used in solid state physics differs slightly from this approach, which is more common in quantum chemistry. In solid state physics, the Coulomb part ($-\langle pr'|p'r\rangle$) of the antisymmetrized integral is neglected as an additional approximation [29, 167]. This will be discussed below in more detail.

Such two-electron integrals have already been evaluated above yielding (with $p \equiv \mathbf{j}\tau$ and $r \equiv \mathbf{k}\sigma$):

$$-V_{pr'[p'r]} = -V_{pr'p'r} + V_{pr'rp'} = -\frac{4\pi e^2}{V}\delta_{\mathbf{j}+\mathbf{k}',\mathbf{j}'+\mathbf{k}}\left(\frac{\delta_{\tau\tau'}\delta_{\sigma,\sigma'}}{(\mathbf{j}-\mathbf{j}')^2} - \frac{\delta_{\tau,\sigma}\delta_{\tau',\sigma'}}{(\mathbf{j}-\mathbf{k})^2}\right).$$

However, due to momentum conservation there are only three independent indexes. By defining the momentum transfer $\mathbf{q} \equiv \mathbf{j}-\mathbf{k} = \mathbf{j}'-\mathbf{k}'$ and subsequently writing $\mathbf{j} = \mathbf{k}+\mathbf{q}$ as well as $\mathbf{j}' = \mathbf{k}'+\mathbf{q}$ the following expressions are obtained:

$$\begin{aligned}-V_{r,r'}(\mathbf{q}) &\equiv -V_{(\mathbf{k}+\mathbf{q})\sigma\mathbf{k}'\sigma'[(\mathbf{k}'+\mathbf{q})\sigma'\mathbf{k}\sigma]} \\ &= -\underbrace{\frac{4\pi e^2}{V}\frac{1}{(\mathbf{k}-\mathbf{k}')^2}}_{V(\mathbf{k}-\mathbf{k}')}\delta_{\sigma,\sigma'} + \underbrace{\frac{4\pi e^2}{V}\frac{1}{\mathbf{q}^2}}_{V(\mathbf{q})} = -V(\mathbf{k}-\mathbf{k}')\delta_{\sigma,\sigma'} + V(\mathbf{q}).\end{aligned}$$

Consequently, the Coulomb-part of the antisymmetrized two-electron integral is only dependent on the momentum difference $\mathbf{k}-\mathbf{k}'$ while the exchange part is solely determined by the momentum transfer $\mathbf{q}$.

With this approximate electron-electron interaction the polarization propagator can be written as

$$\mathbf{\Pi}^{RPA}(\omega) = \mathbf{\Pi}^0(\omega) + \mathbf{\Pi}^0(\omega)\mathbf{U}^{RPA}\mathbf{\Pi}^{RPA}(\omega).$$

Alternatively, one can write for the individual matrix elements:

$$\Pi^{RPA}_{pr,p'r'}(\omega) = \Pi^0_{pr,p'r'}(\omega) + \Pi^0_{pr,pr}(\omega)\sum_{p''r''} U^{RPA}_{pr,p''r''}\Pi^{RPA}_{p''r'',p'r'}(\omega).$$

The matrix $\mathbf{\Pi}^0(\omega)$ is the zeroth order polarization propagator and with the non-interacting homogeneous electron gas as a reference its matrix elements are given by:

$$\Pi^0_{pr,p'r'}(\omega) = \left[\frac{(1-n_{\mathbf{j}})n_{\mathbf{k}}}{\omega+\epsilon_{\mathbf{k}}-\epsilon_{\mathbf{j}}+i\eta} - \frac{n_{\mathbf{j}}(1-n_{\mathbf{k}})}{\omega+\epsilon_{\mathbf{k}}-\epsilon_{\mathbf{j}}-i\eta}\right]\delta_{rr'}\delta_{pp'}.$$

The matrix elements of the polarization propagator are now given by

$$\begin{aligned}\Pi^{RPA}_{r,r'}(\mathbf{q},\omega) =& \Pi^0_{r,r'}(\mathbf{q},\omega) + \Pi^0_{r,r}(\mathbf{q},\omega)\sum_{r''}\left\{-V(\mathbf{k}-\mathbf{k}'')\delta_{\sigma,\sigma''} + V(\mathbf{q})\right\}\Pi^{RPA}_{r'',r'}(\mathbf{q},\omega) \\ =& \Pi^0_{r,r'}(\mathbf{q},\omega) - \underbrace{\Pi^0_{r,r}(\mathbf{q},\omega)\sum_{r''}V(\mathbf{k}-\mathbf{k}'')\delta_{\sigma,\sigma''}\Pi^{RPA}_{r'',r'}(\mathbf{q},\omega)}_{\text{direct term}} \\ &+ \Pi^0_{r,r}(\mathbf{q},\omega)V(\mathbf{q})\sum_{r''}\Pi^{RPA}_{r'',r'}(\mathbf{q},\omega).\end{aligned}$$

These equations can be largely simplified if the direct term is additionally neglected and only the exchange part of the interaction potential considered:

$$\Pi^{RPA}_{r,r'}(\mathbf{q},\omega) = \Pi^0_{r,r'}(\mathbf{q},\omega) + \Pi^0_{r,r}(\mathbf{q},\omega)V(\mathbf{q})\sum_{r''}\Pi^{RPA}_{r'',r'}(\mathbf{q},\omega).$$

This is the type of RPA that is usually used in solid state physics and that will be used in the further discussion, as well. This approximation is justified by the fact that $V(\mathbf{q})$ becomes the dominating term for small $\mathbf{q}$. It has to be emphasized, however, that in quantum chemical applications usually both terms are considered.

This RPA equations can be written in the form of a pseudo-eigenvalue equation, as well:

$$\begin{pmatrix} \mathbf{A} & \mathbf{B} \\ \mathbf{B}^* & \mathbf{A}^* \end{pmatrix} \begin{pmatrix} \mathbf{x} \\ \mathbf{y} \end{pmatrix} = \omega \begin{pmatrix} \mathbf{x} \\ -\mathbf{y} \end{pmatrix} \tag{6.2}$$

$$\text{with} \qquad \mathbf{A}_{pr,p'r'} = (\epsilon_{\mathbf{j}} - \epsilon_{\mathbf{k}})\delta_{p,p'}\delta_{r,r'} + V_{pr'rp'}$$
$$\mathbf{B}_{pr,r'p'} = V_{pp'rr'}.$$

As the resulting matrices are extremely large (if not even infinite) it is desirable to replace such matrix equations by analytical expressions. This can be achieved by summing over all matrix elements and defining $\Pi^{RPA}(\mathbf{q},\omega) \equiv \sum_{rr'} \Pi^{RPA}_{r,r'}(\mathbf{q},\omega)$. Analogously, we define $\Pi^0(\mathbf{q},\omega) \equiv \sum_{rr'} \Pi^0_{r,r'}(\mathbf{q},\omega)$ and get

$$\begin{aligned} \Pi^{RPA}(\mathbf{q},\omega) &= \Pi^0(\mathbf{q},\omega) + \Pi^0(\mathbf{q},\omega)V(\mathbf{q})\Pi^{RPA}(\mathbf{q},\omega) \\ &= \underbrace{(1 - \Pi^0(\mathbf{q},\omega)V(\mathbf{q}))}_{\epsilon^{RPA}(\mathbf{q},\omega)}{}^{-1}\Pi^0(\mathbf{q},\omega), \end{aligned}$$

where $\epsilon^{RPA}(\mathbf{q},\omega)$ is the dielectric function within the RPA. It describes the modification to the lowest order interaction by the polarization of the medium and can be used to determine several properties like the plasma oscillations or screening effects [29,110]. Determining the poles of the polarization propagator is equivalent to finding the roots of the dielectric function and the following dispersion relation has to be solved:

$$1 = \Pi^0(\mathbf{q},\omega)V(\mathbf{q}) \tag{6.3}$$

$$\text{with} \qquad \Pi^0(\mathbf{q},\omega) = \sum_{\mathbf{k}\sigma} \left[\frac{(1 - n_{\mathbf{k+q}})n_{\mathbf{k}}}{\omega + \epsilon_{\mathbf{k}} - \epsilon_{\mathbf{q+k}} + i\eta} - \frac{n_{\mathbf{k+q}}(1 - n_{\mathbf{k}})}{\omega + \epsilon_{\mathbf{k}} - \epsilon_{\mathbf{k+q}} - i\eta} \right].$$

The solutions to equation 6.3 in the complex ω plane determine the frequencies and live times of the collective modes. If the damping of the plasmon oscillations is small (given at long wave lengths), the real and imaginary parts can be approximately separated. The real part gives the frequencies and from the imaginary part an explicit formula for the damping constant can be deduced. When $Re\mathbf{\Pi}^0$ is expanded in a Taylor series for $q \to 0$ and terms up to fourth order in q are considered, the following expression for the plasmon frequency is obtained [29]:

$$\omega_{pl}^2 = \frac{4\pi e^2 n_0}{m_e} + \frac{3}{5}\left(\frac{\hbar k_F}{m} q\right)^2.$$

The first term is just the classical result from equation 6.1. The second can be seen as a quantum kinetic-energy correction. In the limit of $q \to 0$ and up

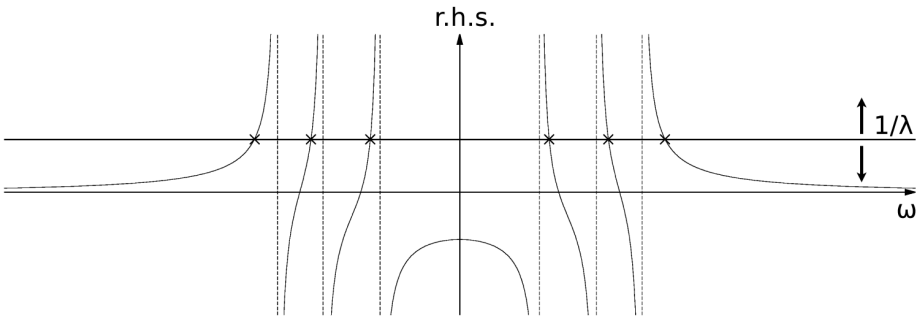

Figure 6.1.: Exemplary graphical solution of the dispersion relation 6.4. Based on [29, 172]

to this order of corrections the plasmon oscillations are undamped and completely decoupled from the single-particle states. For higher order corrections the plasma frequencies are damped at all wavelengths. For a more detailed discussion see, e. g., [29].

Graphical solution of the RPA equations

The dispersion relation 6.3 can be solved graphically by recasting it in the following form [29, 172]:

$$\begin{aligned} \frac{1}{V(\mathbf{q})} &= \sum_{\mathbf{k}\sigma} \left[\frac{(1-n_{\mathbf{k}+\mathbf{q}})n_{\mathbf{k}}}{\omega + \epsilon_{\mathbf{k}} - \epsilon_{\mathbf{q}+\mathbf{k}}} - \frac{n_{\mathbf{k}+\mathbf{q}}(1-n_{\mathbf{k}})}{\omega + \epsilon_{\mathbf{k}} - \epsilon_{\mathbf{k}+\mathbf{q}}} \right] \\ &= 2 \sum_{\mathbf{k}} \left[\frac{(1-n_{\mathbf{k}+\mathbf{q}})n_{\mathbf{k}}}{\omega + \epsilon_{\mathbf{k}} - \epsilon_{\mathbf{q}+\mathbf{k}}} - \frac{n_{\mathbf{k}+\mathbf{q}}(1-n_{\mathbf{k}})}{\omega + \epsilon_{\mathbf{k}} - \epsilon_{\mathbf{k}+\mathbf{q}}} \right]. \end{aligned} \tag{6.4}$$

The complex factors $\pm i\eta$ have been dropped because they are of no importance here. The excitation energies are given by the intersection points between the right hand side (r.h.s.) of equation 6.4 plotted in dependence of the frequency ω and the line given by the constant function $f(\omega) = \frac{1}{V(\mathbf{q})}$. This is shown schematically for an example where there are $n = 3$ single-particle replacements $\mathbf{k} \to \mathbf{k} + \mathbf{q}$ for a specific value of $\mathbf{q}$ and the interaction strength $V(\mathbf{q}) = \lambda$ in Figure 6.1.

As expected, to each positive excitation energy there is a negative counterpart that corresponds to a deexcitation with the same energy. Altogether, there are n excitation and deexcitation energies each. Here, we consider only excitations. From these n energies, $n-1$ correspond to ordinary single-particle energies while the nth and by absolute value highest one is the plasmon energy. The ordinary states are enclosed between two successive poles of the r.h.s. (corresponding to orbital energy differences) while the plasmon frequency is located above the highest pole and is strongly dependent on the interaction strength λ. Evaluation of the plasmon frequency ω_{pl} reveals that $\omega_{pl}^2 \propto \lambda$ [29, 167, 172].

Further simplification by the assumption that the orbital energies are equally distanced (with $\epsilon_{\mathbf{j}} - \epsilon_{\mathbf{k}} = \Delta\epsilon \quad \forall \mathbf{j}, \mathbf{k}$), allows one to analyze the eigenvectors

of the three possible excitations in more detail. Using the pseudo-eigenvalue equation 6.2, the eigenvector $\mathbf{v}_{pl}$ of the plasmon excitation is now given by (N being a normalization factor)

$$\mathbf{v}_{pl} = \begin{pmatrix} \mathbf{x}_{pl} \\ \mathbf{y}_{pl} \end{pmatrix}$$

$$\text{with} \qquad \mathbf{x}_{pl} = N \begin{pmatrix} 1 \\ 1 \\ \vdots \\ 1 \end{pmatrix} \qquad \text{and} \qquad \mathbf{y}_{pl} = -\frac{\omega_{pl} - \Delta\epsilon}{\omega_{pl} + \Delta\epsilon} N \begin{pmatrix} 1 \\ 1 \\ \vdots \\ 1 \end{pmatrix}$$

while the ones for the $(n-1)$ single-particle states are $(m = 1, \ldots, n-1)$

$$\mathbf{v}_m = \begin{pmatrix} \mathbf{x}_m \\ \mathbf{0} \end{pmatrix} \qquad \text{with} \qquad \mathbf{x}_m \perp \mathbf{x}_{pl} \quad \text{and} \quad |\mathbf{x}_m| = 1.$$

In contrast to the single-particle excitations, the plasmon is a linear combination of all n possible single-particle replacements with the momentum transfer $\mathbf{q}$. In other words, it is a coherent superposition of certain single-particle states [125]. This expresses the collective character of this state. Further evaluation of the dipole transition moments yields that only the plasmonic excitation shows some intensity [29, 172]. In a sense, the plasmon gathers the intensity of all the underlying single-particle replacements explaining the high absorption cross sections observed in experiments. These results finally explain how a plasmon differs microscopically from ordinary single-particle excitations. Moreover, this applies independent of the number of electrons present in the system.

The different behavior of the plasmon and single-particle frequencies on the interaction λ was also recognized by Bernadotte et al. using a slightly different approach [167]. They used it to establish a scaling approach for the identification of plasmon excitations which will be explained below.

These characteristics of a plasmon differ from the ones given by Bonačić-Koutecký et al. [129] and Yasuike et al. [142] with respect to the number of single-particle replacements present in the linear combinations because they did not recognize the separability with respect to the momentum transfer $\mathbf{q}$. While Yasuike et al. call only excitations with the maximum number of single-particle replacements a plasmon [142], Bonačić-Koutecký et al. even assume that a large if not infinite number of such transitions has to contribute independent of the size of the molecular system [129].

From the electron gas to molecular systems

Bernadotte et al. analyzed the behavior of the plasmon frequency as well as of the single-particle states with increasing $\mathbf{q}$ for different systems [167]. They compared a three dimensional electron gas with periodic boundary conditions, a one dimensional electron gas as well with periodic boundary conditions and finally a one dimensional electron gas of finite length. In all cases (including the finite model system) the plasmon energy is for small values of the momentum

transfer $\mathbf{q}$ well separated from the (continuous) band of single-particle excitations. Above a certain value of $\mathbf{q}$ the two types of states start to mix and the differentiation is no longer possible.

Finally, they compared the results of the one dimensional system with finite length with results obtained for a chain of twenty sodium atoms by using TDDFT. First, they assigned wave vectors to the frontier orbitals, which are mainly linear combinations of the 3s orbitals of the individual sodium atoms, based on their nodal structure. In a second step the excitation energies were plotted in dependence of the momentum transfer $\mathbf{q}$ associated with the dominating contribution. The results matched the ones obtained for a one dimensional model system of an electron gas with the same dimension and particle density almost perfectly. This shows that it is indeed possible to transfer the notion of a plasmon to at least some types of molecular systems.

During their analysis they encountered another interesting property that sets plasmons apart from single-particle excitations. The transition densities of the plasmons exhibit a distinct nodal structure. When the plasmon frequencies are enumerated with respect to ascending excitation energies, the number of nodes of the transition densities corresponds to the number of the plasmon. No such nodal structure can be observed for the single-particle transitions.

Plasmons within the CIS approximation

Within CIS the secular matrix is given by (compare Section 3.1)

$$M_{pr,p'r'} = (\epsilon_{\mathbf{j}} - \epsilon_{\mathbf{k}})\delta_{p,p'}\delta_{r,r'} - V_{pr'p'r} + V_{pr'rp'}$$

or with the neglect of the direct Coulomb type term by

$$M_{pr,p'r'} = (\epsilon_{\mathbf{j}} - \epsilon_{\mathbf{k}})\delta_{p,p'}\delta_{r,r'} + V_{pr'rp'}.$$

It corresponds to the submatrix $\mathbf{A}$ of the RPA secular matrix in equation 6.2. Considering only this reduced eigenvalue problem is also called Tamm-Dancoff approximation (TDA).

Carrying out a similar graphical analysis as above for RPA, reveals qualitatively the same results. The plasmon state is the highest in energy, gathers all the intensity and is a linear combination of all single-particle replacements with the correct value of $\mathbf{q}$. However, ω_{pl} is proportional to λ instead of ω_{pl}^2 as in the case of the RPA [29, 172].

6.3. Scaling Approach in TDDFT

As already mentioned above, Bernadotte et al. have used the different effect of electron correlation on single-particle and plasmon excitations to suggest a scaling parameter λ in the TDDFT pseudo-eigenvalue equation [167]

$$\begin{pmatrix} \mathbf{A} & \mathbf{B} \\ \mathbf{B}^* & \mathbf{A}^* \end{pmatrix} \begin{pmatrix} \mathbf{X} \\ \mathbf{Y} \end{pmatrix} = \omega \begin{pmatrix} \mathbf{1} & \mathbf{0} \\ \mathbf{0} & \mathbf{-1} \end{pmatrix} \begin{pmatrix} \mathbf{X} \\ \mathbf{Y} \end{pmatrix}$$

$$\text{with} \qquad A_{ia,jb} = (\epsilon_a - \epsilon_i)\delta_{ij}\delta_{ab} + \lambda\left(\langle aj|ib\rangle + f^{xc}_{ajib}\right)$$

$$B_{ia,jb} = \lambda\left(\langle ab|ij\rangle + f^{xc}_{abij}\right),$$

where f^{xc}_{ajib} as defined in equation 3.3. When varying the parameter λ from zero to one and analyzing the squared excitation energies in dependence of λ, some states remain almost constant in energy while others are shifted strongly. The latter type can be characterized as plasmons while the former type corresponds to single-particle states as long as the coupling between them is not too strong. This scheme has been applied to a variety of molecular systems (small metal clusters, a linear polyene and fullerene).

6.4. Scaling Approach Applied to ADC Methods

In this section, the scaling approach introduced above for TDDFT will be transferred to the *ab initio* ADC methods. The ground state orbitals and their energies obtained by Hartree-Fock (HF) differ significantly from the ones calculated with density functional theory (DFT). Firstly, electron-correlation effects are already included in the ground state of DFT which is not the case in HF. Moreover, the orbital energies in HF correspond, according to Koopman's theorem, to ionization potentials and electron affinities. Again, this is not the case in DFT. Consequently, the differences between HF orbital energies are much higher in energy than the final excitation energies. By contrast, the energetic separation between DFT orbitals resembles the excitation energies better. Consequently, when all the electron-correlation terms in *ab initio* based excited state methods are scaled (as was the case in TDDFT) all states drop strongly in energy and behave in the same way independent of the plasmonic character. Therefore, the scaling approach had to be adjusted for *ab initio* methods.

To derive an appropriate scaling scheme we will first consider the CIS (or ADC(1)) eigenvalue equations:

$$\begin{aligned} &\mathbf{A}x = \omega\mathbf{A} \\ \text{with} \qquad &A_{ia,jb} = (\epsilon_a - \epsilon_i)\delta_{ab}\delta_{ij} - \underbrace{\langle aj|bi\rangle}_{\text{Coulomb}} + \underbrace{\langle aj|ib\rangle}_{\text{exchange}} . \end{aligned}$$

The electron correlation has two contributions; the first term is of Coulomb type and can be seen as a correction to the orbital energies. The second term, however, is of exchange type and corresponds to the term included in the RPA approach as used in the graphical analysis in Section 6.2. This is the term that has to be scaled in order to arrive at a scaling approach analogous to the one suggested for TDDFT. Therefore, we suggest the following scaled CIS eigenvalue equations:

$$A_{ia,jb} = (\epsilon_a - \epsilon_i)\delta_{ab}\delta_{ij} - \langle aj|bi\rangle + \lambda\langle aj|ib\rangle.$$

While in the case of TDDFT the squared excitation energies have to be plotted in dependence of λ, the excitation energies themselves have to be considered due to $\omega_{pl} \propto \lambda$ in the case of CIS (compare Section 6.2). This approach has been successfully tested for a series of linear polyenes and the results are presented in Section 8.

In ADC(2), the ph/ph block of the secular matrix contains additionally the three second-order correction terms (compare Section 3.3). When analyzing the

diagrams corresponding to these terms, it can be seen that only one of them is of exchange type. However, the overall influence of the second-order terms is only small. Scaling only the exchange part of the first-order contribution did not yield significantly different results than scaling that exchange type second-order contribution additionally. Therefore, we refrain from scaling more than the exchange part of the first-order terms. The same approach can be chosen for ADC(3). However, because plasmons are important for extended systems and because ADC(3) is restricted to relatively small systems, we do not present any results at this level of theory within this work. As in the case of CIS, the ADC(2) approaches (strict and extended as well as with and without the SOS approximation) have been applied to polyenes and the results are shown in Section 8, too.

Part II.

Applications

7. Test Calculations for Spin-Orbit Coupling Elements

7.1. Introduction

In this section test calculations for the implementation of spin-orbit coupling elements as presented in Section 5.4 are discussed. Recently, M. Pabst has implemented a procedure [173] in which spin-orbit integrals generated with the ORCA program package [174] are used to calculate spin-orbit coupling elements between states obtained with the CC2 and ADC(2)-s methods in TURBOMOLE [85]. However, he has used a molecular and not an atomic mean-field as in this work. The method was tested with respect to the two molecules thiophene and 1,2-dithiin (compare Figure 7.1). In the case of thiophene the values were compared to results obtained with DFT/MRCI [49] in combination with the `AMFI` program [175]. Therefore, we chose these two molecules as test systems, too. To the best of our knowledge, ADC(2)-s is the only ADC method for which a previous implementation of spin-orbit coupling elements exists.

Additionally, we present results for coumarin in comparison to values from MS-CASPT2 (in combination with `AMFI`) as implemented in the MOLCAS program package [176]. These results will be of importance for the photochemical relaxation pathways of coumarin derivatives discussed in Chapter 9.

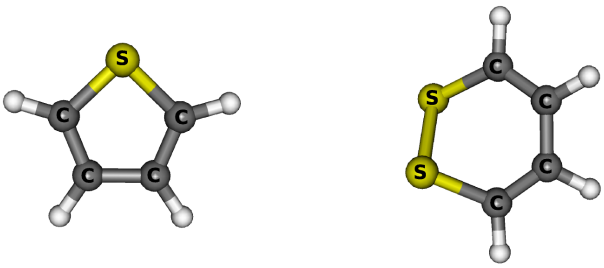

Figure 7.1.: Structures of thiophene (left) and 1,2-dithiin (right).

7.2. Results

7.2.1. Thiophene

In the case of thiophene the same experimental structure [177] was used as in [173,175]. The molecule is planar and has C_{2v} symmetry. The wave functions transform with respect to one of the four irreducible representations A_1, A_2, B_1, and B_2 (compare Table C.4). The Cartesian spin components of the triplet

states transform as B_2, B_1, and A_2. Therefore, the spin-orbit coupling elements between singlet states and triplet states of the same spatial symmetry are zero (compare Section 5.3).

In [173] CC2 was used in combination with the cc-pVDZ [75] basis set as well as the triple-ζ basis set TZVPP+R [178]. The latter basis set results from the TZVPP basis [179] by inclusion of three diffuse functions (1s1p1d) with the exponents 0.011253, 0.009988 and 0.014204 for the sulfur atom. This basis has also used in the DFT/MRCI calculations from which the reference values were taken [175]. ADC(2)-s values are, however, only given for the cc-pVDZ basis set. Therefore, we give first a detailed comparison of our different ADC(n) approaches in combination with the cc-pVDZ basis to ADC(2)-s and CC2 values from [173]. Then, we switch the basis set to TZVPP+R and compare with CC2 values from [173] and DFT/MRCI results from [175].

Table 7.1 shows spin-orbit coupling elements with ADC(2)-s obtained with both, the Breit-Pauli operator and the variationally stable no-pair (Douglas-Kroll) operator. They are compared to values from the ADC(2)-s approach in combination with a molecular mean-field and the Breit-Pauli operator from [173].

As expected for a molecule with no truly heavy atoms, the differences between the two operators are only marginal. When comparing to the results with the molecular mean-field, larger deviations occur. However, it has to be considered that in TURBOMOLE transition properties are only consistent in first-order perturbation theory [173]. To establish a better comparison with the values from [173] we have combined the second-order eigenvectors from ADC(2)-s with first-order transition densities instead of the full second-order quantities. In the case of transition densities between excited states the first-order contributions are zero and only contributions from zeroth or second order are relevant (compare Section 3.3 and [20]). Therefore, we give first-order values only for couplings to the electronic ground state. For the sake of completeness, values using the zeroth order transition densities are given, as well. These can be obtained for all transition densities. The resulting methods are referred to as ADC(2/1)-s or ADC(2/0)-s where the second number in brackets gives the order in which the transition densities have been calculated.

In all cases, the values with the first-order transition density matrices lie closer to the values from [173] than the ones with second-order transition matrices. The deviations are now in the expected region of about 5 % for using only an atomic mean-field (absolute errors of up to 5 %, [104,106]) instead of a molecular mean-field (absolute errors smaller than 1 %, [99, 104]). The only exception is given by the coupling element between 1^3B_1 and 1^1A_1 which is, however, very small. The influence of second-order terms in the transition density matrices on the couplings between excited singlet and triplet states is smaller than on the ones between the (singlet) ground state and the triplet manifold.

Table 7.1.: Excitation energies in eV and state-to-state spin-orbit coupling elements ($\langle H_{SO} \rangle = \sqrt{\sum_{M=0,\pm1} |\langle A,0,0|H_{SO}|B,1,M\rangle|^2}$) in cm^{-1} for thiophen. The methods ADC(2/1) and ADC(2/0) refer to a procedure were the second-order eigenvector is used in combination with first or zeroth order representations of the transition density matrices. The superscripts DK (for Douglas-Kroll) and BP (for Breit-Pauli) indicate the spin-orbit Hamiltonian used. Basis set: cc-pVDZ.

$T_n \rightarrow S_m$	ADC(2)-s ΔE	ADC(2)-s $\langle H_{SO}^{DK} \rangle$	ADC(2)-s $\langle H_{SO}^{BP} \rangle$	ADC(2/1) $\langle H_{SO}^{BP} \rangle$	ADC(2/0) $\langle H_{SO}^{BP} \rangle$	ADC(2)-s [173] $\langle H_{SO}^{BP} \rangle$	CC2 [173] $\langle H_{SO}^{BP} \rangle$
$1^3A_1 \rightarrow 1^1A_1$	5.01	-	-	-	-	-	-
$1^3A_1 \rightarrow 1^1A_2$	-2.10	37.40	37.86		39.00	40.32	44.94
$1^3A_1 \rightarrow 1^1B_1$	-1.44	0.70	0.71		0.76	0.61	0.75
$1^3A_1 \rightarrow 1^1B_2$	-2.16	0.04	0.06		0.09	0.07	0.08
$2^3A_1 \rightarrow 1^1A_1$	6.51	-	-	-	-	-	-
$2^3A_1 \rightarrow 1^1A_2$	-0.60	8.11	8.22		8.39	10.52	6.31
$2^3A_1 \rightarrow 1^1B_1$	0.06	0.71	0.72		0.82	0.45	0.42
$2^3A_1 \rightarrow 1^1B_2$	-0.65	7.25	7.28		7.45	5.42	7.28
$1^3A_2 \rightarrow 1^1A_1$	6.73	109.26	110.58	115.79	113.18	119.32	110.04
$1^3A_2 \rightarrow 2^1A_1$	0.76	48.26	48.85		48.94	51.23	56.26
$1^3A_2 \rightarrow 1^1B_1$	0.28	20.82	21.07		22.08	19.27	21.50
$1^3A_2 \rightarrow 1^1B_2$	-0.44	2.64	2.67		2.73	2.45	3.50
$2^3A_2 \rightarrow 1^1A_1$	7.93	5.54	5.55	5.14	5.69	5.01	5.48
$2^3A_2 \rightarrow 2^1A_1$	1.96	1.61	1.63		1.70	0.78	0.98
$2^3A_2 \rightarrow 1^1B_1$	1.48	4.18	4.26		4.46	7.53	9.00
$2^3A_2 \rightarrow 1^1B_2$	0.77	13.66	13.80		13.56	16.73	17.30
$1^3B_1 \rightarrow 1^1A_1$	4.18	0.20	0.21	0.22	0.35	0.33	0.30
$1^3B_1 \rightarrow 2^1A_1$	-1.79	0.43	0.44		0.46	0.19	0.45
$1^3B_1 \rightarrow 1^1A_2$	-2.93	2.12	2.15		2.19	2.08	2.93
$1^3B_1 \rightarrow 1^1B_2$	-2.98	42.51	43.03		44.85	42.54	54.72

$T_n \rightarrow S_m$	ADC(2)-s ΔE	ADC(2)-s $\langle H_{SO}^{DK} \rangle$	ADC(2)-s $\langle H_{SO}^{BP} \rangle$	ADC(2/1) $\langle H_{SO}^{BP} \rangle$	ADC(2/0) $\langle H_{SO}^{BP} \rangle$	ADC(2)-s [173] $\langle H_{SO}^{BP} \rangle$	CC2 [173] $\langle H_{SO}^{BP} \rangle$
$2^3B_1 \rightarrow 1^1A_1$	7.05	6.42	6.49	7.14	7.65	7.70	6.62
$2^3B_1 \rightarrow 2^1A_1$	1.08	0.26	0.26		0.22	0.42	0.25
$2^3B_1 \rightarrow 1^1A_2$	-0.06	15.29	15.41		15.95	13.42	15.22
$2^3B_1 \rightarrow 1^1B_2$	-0.11	4.68	4.74		4.85	5.53	4.11
$1^3B_2 \rightarrow 1^1A_1$	6.87	8.04	8.08	8.52	6.65	8.49	8.37
$1^3B_2 \rightarrow 2^1A_1$	0.90	3.28	3.35		3.15	4.20	3.02
$1^3B_2 \rightarrow 1^1A_2$	-0.24	2.27	2.29		2.11	2.35	2.34
$1^3B_2 \rightarrow 1^1B_1$	0.42	41.39	41.91		43.50	42.94	47.55
$2^3B_2 \rightarrow 1^1A_1$	7.84	99.06	100.10	102.81	97.32	108.70	111.42
$2^3B_2 \rightarrow 2^1A_1$	1.86	100.71	101.90		103.82	99.32	93.96
$2^3B_2 \rightarrow 1^1A_2$	0.73	1.78	1.80		1.78	1.78	1.87
$2^3B_2 \rightarrow 1^1B_1$	1.39	0.26	0.29		0.10	1.18	2.58

Table 7.2.: Excitation energies in eV and state-to-state spin-orbit coupling elements ($\langle H_{SO} \rangle = \sqrt{\sum_{M=0,\pm1} |\langle A,0,0|H_{SO}|B,1,M\rangle|^2}$) in cm^{-1} for thiophene. The Breit-Pauli operator was used in all cases. Basis set: cc-pVDZ.

$T_n \rightarrow S_m$	ADC(1)		ADC(2)-s		SOS-ADC(2)-s		ADC(2)-x		SOS-ADC(2)-x		ADC(3)	
	ΔE	$\langle H_{SO} \rangle$	ΔE	$\langle H_{SO} \rangle$	ΔE	$\langle H_{SO} \rangle$	ΔE	$\langle H_{SO} \rangle$	ΔE	$\langle H_{SO} \rangle$	ΔE	$\langle H_{SO} \rangle$
$1^3A_1 \rightarrow 1^1A_1$	4.64	-	5.01	-	4.83	-	4.38	-	4.75	-	4.72	-
$1^3A_1 \rightarrow 1^1A_2$	-2.71	32.18	-2.10	37.86	-2.19	35.98	-2.00	42.18	-2.09	37.59	-2.19	38.43
$1^3A_1 \rightarrow 1^1B_1$	-1.66	0.51	-1.44	0.71	-1.50	0.37	-1.42	0.69	-1.51	0.06	-1.47	0.58
$1^3A_1 \rightarrow 1^1B_2$	-3.16	2.26	-2.16	0.06	-2.48	1.38	-1.82	1.29	-2.12	0.44	-2.12	0.96
$2^3A_1 \rightarrow 1^1A_1$	6.17	-	6.51	-	6.44	-	5.89	-	6.37	-	6.17	-
$2^3A_1 \rightarrow 1^1A_2$	-1.18	21.14	-0.60	8.22	-0.58	10.59	-0.49	1.61	-0.48	8.43	-0.74	5.53
$2^3A_1 \rightarrow 1^1B_1$	-0.13	0.82	0.06	0.72	0.12	0.51	0.09	0.48	0.11	0.39	-0.02	0.48
$2^3A_1 \rightarrow 1^1B_2$	-1.62	5.30	-0.65	7.28	-0.87	5.29	-0.31	8.57	-0.50	5.06	-0.67	8.07

$T_n \rightarrow S_m$	ADC(1)		ADC(2)-s		SOS-ADC(2)-s		ADC(2)-x		SOS-ADC(2)-x		ADC(3)	
	ΔE	$\langle H_{SO} \rangle$	ΔE	$\langle H_{SO} \rangle$	ΔE	$\langle H_{SO} \rangle$	ΔE	$\langle H_{SO} \rangle$	ΔE	$\langle H_{SO} \rangle$	ΔE	$\langle H_{SO} \rangle$
$1^3A_2 \rightarrow 1^1A_1$	6.71	119.58	6.73	110.58	6.71	111.71	6.10	107.61	6.58	108.29	6.56	110.65
$1^3A_2 \rightarrow 2^1A_1$	-0.22	56.08	0.76	48.85	0.94	44.06	1.14	44.22	1.15	39.39	0.71	49.73
$1^3A_2 \rightarrow 1^1B_1$	0.42	21.67	0.28	21.07	0.38	17.77	0.30	21.03	0.32	18.38	0.37	20.94
$1^3A_2 \rightarrow 1^1B_2$	-1.08	2.57	-0.44	2.67	-0.61	2.72	-0.10	4.26	-0.29	3.86	-0.28	5.08
$2^3A_2 \rightarrow 1^1A_1$	8.11	8.85	7.93	5.55	8.03	4.23	7.32	1.91	7.86	1.70	7.74	2.61
$2^3A_2 \rightarrow 2^1A_1$	1.18	2.68	1.96	1.63	2.26	1.35	2.36	1.84	2.43	0.86	1.89	1.58
$2^3A_2 \rightarrow 1^1B_1$	1.81	2.52	1.48	4.26	1.70	2.62	1.52	7.39	1.60	4.31	1.56	7.26
$2^3A_2 \rightarrow 1^1B_2$	0.32	10.40	0.77	13.80	0.72	10.36	1.12	16.31	0.99	11.96	0.90	15.95
$1^3B_1 \rightarrow 1^1A_1$	3.23	0.16	4.18	0.21	4.01	1.40	3.59	0.09	3.89	1.27	3.75	0.12
$1^3B_1 \rightarrow 2^1A_1$	-3.70	0.10	-1.79	0.44	-1.75	0.32	-1.37	0.09	-1.54	0.32	-2.10	0.07
$1^3B_1 \rightarrow 1^1A_2$	-4.12	2.06	-2.93	2.15	-3.01	9.00	-2.79	3.23	-2.96	11.66	-3.16	4.50
$1^3B_1 \rightarrow 1^1B_2$	-4.56	34.00	-2.98	43.03	-3.30	36.91	-2.61	55.82	-2.98	37.83	-3.09	52.64
$2^3B_1 \rightarrow 1^1A_1$	7.46	16.54	7.05	6.49	7.02	7.89	6.10	3.15	6.58	4.25	6.59	3.84
$2^3B_1 \rightarrow 2^1A_1$	0.53	1.22	1.08	0.26	1.26	0.51	1.14	0.22	1.15	0.07	0.74	0.51
$2^3B_1 \rightarrow 1^1A_2$	0.11	23.21	-0.06	15.41	0.00	14.93	-0.28	12.85	-0.27	10.37	-0.31	12.11
$2^3B_1 \rightarrow 1^1B_2$	-0.33	8.07	0.11	4.74	-0.29	4.51	-0.10	3.30	-0.29	2.19	-0.25	0.69
$1^3B_2 \rightarrow 1^1A_1$	7.32	8.89	6.87	8.08	7.06	6.64	5.97	9.55	6.65	9.38	6.54	10.21
$1^3B_2 \rightarrow 2^1A_1$	0.39	5.06	0.90	3.35	1.30	2.84	1.01	1.96	1.23	0.33	0.69	0.15
$1^3B_2 \rightarrow 1^1A_2$	-0.03	1.45	-0.24	2.29	0.04	2.26	-0.41	2.96	-0.19	3.89	-0.37	4.17
$1^3B_2 \rightarrow 1^1B_1$	1.02	35.99	0.42	41.91	0.73	33.69	0.17	43.90	0.39	31.80	0.35	40.84
$2^3B_2 \rightarrow 1^1A_1$	8.28	106.67	7.84	100.10	7.96	105.50	7.09	95.55	7.83	101.94	7.73	100.81
$2^3B_2 \rightarrow 2^1A_1$	1.35	99.99	1.86	101.90	2.19	84.56	2.12	88.34	2.40	72.52	1.88	92.76
$2^3B_2 \rightarrow 1^1A_2$	0.93	0.45	0.73	1.80	0.94	3.36	0.71	1.82	0.99	4.14	0.82	2.31
$2^3B_2 \rightarrow 1^1B_1$	1.98	1.47	1.39	0.29	1.63	1.96	1.29	5.09	1.57	5.90	1.54	4.19

Summarized, the results from all presented methods agree well. The deviations of the ADC(2)-s values from [173] are due to using the one-center approximation and to using consistent second-order perturbation theory for the transition densities instead of obtaining transition properties only in first order. However, no systematic deviation to higher or lower values can be observed.

In Table 7.2 results from ADC(1) (CIS), (SOS)-ADC(2)-s, (SOS)-ADC(2)-x, and ADC(3) are displayed. In some cases significant deviations occur which is not surprising given the differences in the eigenvectors obtained with the different approaches. Nevertheless, they all give qualitatively the same results and the coupling elements lie in the same order of magnitude for the different methods.

Of special interest is the effect of the SOS approximation on the results of ADC(2)-s/x. In the case of the strict variant only minor shifts in the excitation energies are introduced. However, the overestimation of doubly excited states is effectively reduced by the SOS approximation in the case of the extended method and the excitation energies lie in the same region as with ADC(3). The spin-orbit coupling elements themselves are for both versions affected in a similar way. While the coupling elements between the ground state and the triplet states are only slightly shifted, the couplings involving excited singlet states are often reduced significantly in size (e. g., $1^3B_1 \rightarrow 1^1B_2$, $1^3B_2 \rightarrow 1^1B_1$ or $2^3B_2 \rightarrow 2^1A_1$). Nevertheless, the order of magnitude does not change and large contributions are given by the same elements as without the SOS approximation. The use of quantitative conclusions with the SOS approach should, however, be carefully checked.

Last but not least, we compare the results of our method with DFT/MRCI. For this purpose we use the TZVPP+R basis set and additionally the frozen core approximation. The results for (SOS)-ADC(2)-s, SOS-ADC(2)-x and ADC(3) are shown in Table 7.3. Values for ADC(1) are not given because the characters of the states differ strongly making a comparison meaningless.

Like above, the values agree well. The only exception is given by the coupling elements with ADC(3) and SOS-ADC(2)-s/x involving the $^3A_2$ states. With respect to DFT/MRCI as well as the ADC(2)-s the order between the first and second state of this symmetry is reversed in ADC(3) and SOS-ADC(2)-s. Additionally, these two states mix to a certain extent. While the coupling elements for the 2^3A_2 (according to the energetic order in ADC(2)-s) are very close to the DFT/MRCI values, the ones for the 1^3A_2 differ significantly due to the different character of the state.

In all other cases, the values obtained with ADC(2)-s and ADC(3) are of the same order of magnitude and agree well with both, CC2 and DFT/MRCI values. However, in most cases the ADC(3) values lie closer to the ones obtained with DFT/MRCI than to the ones obtained with CC2 or ADC(2)-s. On the other hand, ADC(2)-s values are in better agreement with CC2 than with DFT/MRCI or ADC(3). This is not surprising when the close relationship between ADC(2)-s and CC2 as well as the usually higher accuracy of ADC(3) and DFT/MRCI calculations are considered.

Table 7.3.: Excitation energies in eV and state-to-state spin-orbit coupling elements ($\langle H_{SO}\rangle = \sqrt{\sum_{M=0,\pm1} |\langle A,0,0|H_{SO}|B,1,M\rangle|^2}$) in cm^{-1} for thiophene. The Breit-Pauli operator was used in all cases. Basis set: TZVPP+R.

$T_n \rightarrow S_m$	ADC(2)-s		SOS-ADC(2)-s		SOS-ADC(2)-x		ADC(3)		CC2 [173]		DFT/MRCI [175]
	ΔE	$\langle H_{SO}\rangle$	ΔE	$\langle H_{SO}\rangle$	ΔE	$\langle H_{SO}\rangle$	ΔE	$\langle H_{SO}\rangle$	|ΔE|	$\langle H_{SO}\rangle$	$\langle H_{SO}\rangle$
$1^3A_1 \rightarrow 1^1A_1$	4.88	-	4.70	-	4.70	-	4.56	-	-	-	-
$1^3A_1 \rightarrow 1^1A_2$	-1.26	0.54	-1.50	1.87	-1.42	2.29	-1.48	1.02	1.12	0.56	0.14
$1^3A_1 \rightarrow 1^1B_1$	-1.28	0.78	-1.31	0.35	-1.33	0.01	-1.32	0.64	1.22	0.20	0.57
$1^3A_1 \rightarrow 1^1B_2$	-1.50	0.28	-1.78	3.90	-1.58	0.64	-1.63	1.27	1.36	1.16	2.26
$2^3A_1 \rightarrow 1^1A_1$	6.30	-	6.23	-	6.22	-	5.92	-	-	-	-
$2^3A_1 \rightarrow 1^1A_2$	0.16	0.06	0.03	0.51	0.10	0.45	-0.11	0.05	0.27	0.29	0.03
$2^3A_1 \rightarrow 1^1B_1$	0.14	0.65	0.22	0.43	0.20	0.28	0.05	0.34	0.17	1.97	0.05
$2^3A_1 \rightarrow 1^1B_2$	-0.08	2.76	-0.25	2.31	-0.05	1.65	-0.26	3.57	0.03	6.48	5.71
$1^3A_2 \rightarrow 1^1A_1$	6.10	8.16	6.18	17.45	6.09	13.03	5.92	66.92	6.03	1.93	1.21
$1^3A_2 \rightarrow 2^1A_1$	0.32	3.45	0.61	6.41	0.76	4.59	0.35	28.94	0.21	1.74	1.23
$1^3A_2 \rightarrow 1^1B_1$	-0.06	5.58	0.14	0.25	0.06	0.94	0.11	9.09	0.14	4.39	5.66
$1^3A_2 \rightarrow 1^1B_2$	-0.28	4.56	-0.32	1.06	-0.19	3.84	-0.20	1.98	0.28	4.37	5.63
$2^3A_2 \rightarrow 1^1A_1$	6.19	112.70	6.15	113.28	6.10	109.10	5.97	92.91	6.29	114.15	94.71
$2^3A_2 \rightarrow 2^1A_1$	0.42	47.91	0.64	40.48	0.77	36.30	0.33	40.24	0.47	57.89	44.26
$2^3A_2 \rightarrow 1^1B_1$	0.03	19.86	0.17	16.49	0.07	16.89	0.10	19.41	0.12	21.58	18.25
$2^3A_2 \rightarrow 1^1B_2$	-0.19	1.80	-0.30	4.80	-0.18	3.23	-0.21	5.78	0.01	0.61	0.59
$1^3B_1 \rightarrow 1^1A_1$	4.14	0.21	3.97	1.54	3.91	1.45	3.68	0.11	4.13	0.17	0.07
$1^3B_1 \rightarrow 2^1A_1$	-1.64	0.38	-1.58	0.31	-1.42	0.37	-1.96	0.31	1.69	2.14	0.35
$1^3B_1 \rightarrow 1^1A_2$	-2.00	4.26	-2.24	3.48	-2.21	4.22	-2.35	5.04	1.93	4.18	6.14
$1^3B_1 \rightarrow 1^1B_2$	-2.24	33.49	-2.51	15.08	-2.37	30.99	-2.51	46.18	2.17	43.00	45.21
$2^3B_1 \rightarrow 1^1A_1$	6.71	9.53	6.67	11.02	6.39	6.95	6.31	6.45	6.75	9.11	3.29
$2^3B_1 \rightarrow 2^1A_1$	0.93	0.38	1.12	0.55	1.06	0.09	0.67	0.77	0.93	2.41	0.47
$2^3B_1 \rightarrow 1^1A_2$	0.57	0.77	0.46	1.37	0.27	1.17	0.28	0.54	0.69	0.32	0.42
$2^3B_1 \rightarrow 1^1B_2$	0.33	2.54	0.19	0.94	0.11	1.36	0.12	0.50	0.45	0.14	1.83

$T_n \rightarrow S_m$	ADC(2)-s		SOS-ADC(2)-s		SOS-ADC(2)-x		ADC(3)		CC2 [173]		DFT/MRCI [175]
	ΔE	$\langle H_{SO} \rangle$	ΔE	$\langle H_{SO} \rangle$	ΔE	$\langle H_{SO} \rangle$	ΔE	$\langle H_{SO} \rangle$	|ΔE|	$\langle H_{SO} \rangle$	$\langle H_{SO} \rangle$
$1^3B_2 \rightarrow 1^1A_1$	6.23	4.52	6.39	0.82	6.14	5.21	5.99	6.37	6.15	9.67	6.49
$1^3B_2 \rightarrow 2^1A_1$	0.45	2.60	0.85	1.12	0.81	0.48	0.35	1.12	0.33	1.35	3.13
$1^3B_2 \rightarrow 1^1A_2$	0.09	5.02	0.19	3.43	0.02	4.72	-0.04	5.47	0.09	4.99	5.90
$1^3B_2 \rightarrow 1^1B_1$	0.06	37.30	0.38	25.86	0.11	27.66	0.11	39.13	0.01	43.63	38.64
$2^3B_2 \rightarrow 1^1A_1$	6.44	11.96	6.47	13.29	6.40	13.42	6.33	13.24	6.43	15.35	13.37
$2^3B_2 \rightarrow 2^1A_1$	0.66	3.41	0.93	4.28	1.06	3.87	0.69	3.80	0.61	3.32	3.22
$2^3B_2 \rightarrow 1^1A_2$	0.30	0.37	0.27	1.59	0.28	1.13	0.30	0.80	0.37	1.54	1.24
$2^3B_2 \rightarrow 1^1B_1$	0.28	1.98	0.46	7.50	0.37	2.07	0.45	2.66	0.27	1.89	4.59

Table 7.4.: Excitation energies in eV and state-to-state spin-orbit coupling elements ($\langle H_{SO} \rangle = \sqrt{\sum_{M=0,\pm1} |\langle A,0,0|H_{SO}|B,1,M\rangle|^2}$) in cm^{-1} for 1,2-dithiin. The Breit-Pauli operator was used in all cases. When eigenvectors of the involved states are very different from the ones in ADC(2)-s, the respective values are displayed in gray. Basis set: cc-pVDZ.

$T_n \rightarrow S_m$	ADC(1)		ADC(2)-s		SOS-ADC(2)-s		SOS-ADC(2)-x		ADC(3)		CC2 [173]	
	ΔE	$\langle H_{SO} \rangle$	ΔE	$\langle H_{SO} \rangle$	ΔE	$\langle H_{SO} \rangle$	ΔE	$\langle H_{SO} \rangle$	ΔE	$\langle H_{SO} \rangle$	|ΔE|	$\langle H_{SO} \rangle$
$1^3A \rightarrow 1^1A$	3.69	53.38	4.00	96.35	4.03	85.50	3.92	88.55	3.86	91.14	4.01	100.05
$1^3A \rightarrow 2^1A$	-1.83	8.05	-0.66	2.27	-0.78	5.49	-0.60	12.23	-0.55	15.40	0.65	4.97
$1^3A \rightarrow 3^1A$	-3.14	1.52	-2.01	3.26	-2.15	0.26	-1.18	10.18	-0.74	9.67	1.97	6.58
$1^3A \rightarrow 1^1B$	0.21	17.45	1.15	46.60	0.96	33.07	0.93	33.53	0.99	41.52	1.18	44.84
$1^3A \rightarrow 2^1B$	-1.52	11.26	-0.96	34.24	-1.03	24.04	-1.05	24.47	-0.96	25.75	0.91	29.15
$2^3A \rightarrow 1^1A$	5.04	155.68	5.18	90.69	5.12	112.17	4.99	102.38	4.92	99.70	5.19	89.91
$2^3A \rightarrow 2^1A$	-0.48	9.20	0.52	14.30	0.30	13.10	0.47	9.65	0.32	13.61	0.53	18.35
$2^3A \rightarrow 3^1A$	-1.79	16.28	-0.82	8.44	-1.06	10.55	-0.11	10.69	0.51	6.66	0.79	9.09
$2^3A \rightarrow 1^1B$	1.56	59.33	2.33	55.14	2.05	50.70	2.01	45.87	2.06	56.01	2.36	54.18
$2^3A \rightarrow 2^1B$	-0.17	32.90	0.23	38.12	0.05	30.23	0.03	30.21	0.10	38.70	0.27	38.96
$3^3A \rightarrow 1^1A$	6.11	23.73	5.63	31.04	5.82	27.21	5.67	34.65	5.47	13.12	5.63	29.77
$3^3A \rightarrow 2^1A$	0.59	21.48	0.97	6.41	1.01	11.89	1.15	7.58	0.87	0.58	0.96	4.56
$3^3A \rightarrow 3^1A$	-0.72	6.14	-0.37	5.36	-0.36	4.76	0.57	8.13	1.06	22.03	0.36	5.01
$3^3A \rightarrow 1^1B$	2.63	46.21	2.79	50.03	2.75	45.16	2.69	46.75	2.60	23.48	2.79	51.02
$3^3A \rightarrow 2^1B$	0.90	44.50	0.68	26.77	0.75	32.70	0.71	21.23	0.65	4.90	0.70	22.63
$1^3B \rightarrow 1^1A$	2.00	24.96	2.22	40.39	2.41	40.58	2.32	39.40	2.09	37.43	2.21	42.59

$T_n \leftarrow S_m$	ADC(1)		ADC(2)-s		SOS-ADC(2)-s		SOS-ADC(2)-x		ADC(3)		CC2 [173]	
	ΔE	$\langle H_{SO} \rangle$	ΔE	$\langle H_{SO} \rangle$	ΔE	$\langle H_{SO} \rangle$	ΔE	$\langle H_{SO} \rangle$	ΔE	$\langle H_{SO} \rangle$	|ΔE|	$\langle H_{SO} \rangle$
$1^3B \rightarrow 2^1A$	-3.52	38.07	-2.44	58.88	-2.41	46.94	-2.21	38.08	-2.51	52.72	2.45	53.76
$1^3B \rightarrow 3^1A$	-4.83	33.46	-3.78	49.41	-3.78	44.52	-2.78	31.76	-2.32	30.96	3.77	56.90
$1^3B \rightarrow 1^1B$	-1.48	15.15	-0.63	5.84	-0.67	4.28	-0.67	2.64	-0.78	11.88	0.63	5.19
$1^3B \rightarrow 2^1B$	-3.21	41.84	-2.73	70.67	-2.66	57.15	-2.65	45.57	-2.73	54.49	2.72	56.19
$2^3B \rightarrow 1^1A$	3.40	73.72	3.60	56.28	3.63	57.17	3.51	55.25	3.36	59.08	3.59	56.48
$2^3B \rightarrow 2^1A$	-2.13	50.30	-1.06	31.08	-1.19	30.21	-1.01	24.90	-1.24	35.59	1.07	31.02
$2^3B \rightarrow 3^1A$	-3.44	48.72	-2.40	40.65	-2.55	38.99	-1.59	16.15	-1.05	9.09	2.39	41.38
$2^3B \rightarrow 1^1B$	-0.09	43.40	0.75	69.11	0.56	49.10	0.53	48.11	0.49	67.65	0.76	78.62
$2^3B \rightarrow 3^1B$	-1.82	58.76	-1.35	37.70	-1.44	46.65	-1.45	45.93	-1.46	51.43	1.33	38.39
$3^3B \rightarrow 1^1A$	5.39	72.44	4.75	3.09	5.05	12.57	4.81	9.47	4.77	15.96	4.71	3.15
$3^3B \rightarrow 2^1A$	-0.13	80.99	0.09	39.80	0.23	47.23	0.28	43.32	0.17	53.13	0.05	42.19
$3^3B \rightarrow 3^1A$	-1.44	30.21	-1.26	40.22	-1.13	33.43	-0.29	24.33	0.36	6.21	1.27	39.96
$3^3B \rightarrow 1^1B$	1.91	91.07	1.90	30.03	1.98	47.60	1.82	39.55	1.91	43.04	1.88	20.90
$3^3B \rightarrow 2^1B$	0.18	72.17	-0.21	8.77	-0.02	24.99	-0.16	25.44	-0.05	29.73	0.21	11.81

With respect to the SOS approximation some coupling elements involving excited singlet states are significantly reduced in size (e. g., $1^3B_1 \rightarrow 1^1B_2$ or $1^3B_2 \rightarrow 1^1B_1$). The coupling elements involving the singlet ground state are influenced to a lesser extent. The same trend was already observed above.

7.2.2. 1,2-Dithiin

The structure of 1,2-dithiin was obtained by ground state geometry optimization at the MP2/cc-pVDZ level of theory. The molecular point group is C_2, which includes two different irreducible representations A and B (compare Table C.3). The Cartesian components of the triplet states transform according to B (x,y) and A (z). Therefore, between all states non-vanishing coupling elements exist. If the two states have different spatial symmetries, they are coupled by the x and y components of the spin-orbit Hamiltonian, while the z component couples states of the same spatial symmetry.

The spin-orbit coupling elements obtained with ADC(1), ADC(2)-s as well as ADC(3) in combination with the cc-pVDZ basis set are shown in Table 7.4. For comparison the CC2 values from [173] are given, as well. In all cases the Breit-Pauli operator was used. In some cases, the order of the states within a symmetry is reversed from one method to the other. In such cases the states were labeled according to the energetic order in ADC(2)-s.

As was the case for thiophene, our ADC(2)-s values agree well with the CC2 values from [173]. Again, differences arise because in [173] a molecular mean-field was used and the transition properties were obtained in first-order perturbation theory only. Larger deviations occur between ADC(2)-s and ADC(1) and ADC(3). This is due to changes in the character of the excited states. When the main contributions to the eigenvectors of certain states are substantially different from the respective contributions in ADC(2)-s, the values are shown in gray in Table 7.4.

Additionally, SOS-ADC(2)-s and SOS-ADC(2)-x values are also included in Table 7.4. Again, relatively large changes are induced by the SOS approximation and the results should not be used beyond qualitative discussions.

7.2.3. Coumarin

In this section, we present spin-orbit coupling elements for coumarin and 7-hydroxycoumarin at different points of their potential energy surfaces (PES) in comparison with MS-CASPT2. When considering different points of the PES with methods like MS-CASPT2 it can be challenging to find consistent active spaces that describe all states at all structures equally well. This is especially true when the symmetry of the molecule is broken at certain points. The consideration of explicit solvent molecules can pose additional problems. Therefore, the applicability of the newly implemented spin-orbit coupling elements with ADC(2)-s for the molecules coumarin and 7-hydroxycoumarin, whose photochemical relaxation pathways will be investigated in Chapter 9, is analyzed in comparison with MS-CASPT2 calculations.

The methodologies with which the coumarin structures were obtained are

Table 7.5.: Excitation energies in eV and state-to-state spin-orbit coupling elements ($\langle H_{SO}\rangle = \sqrt{\sum_{M=0,\pm1} |\langle A,0,0|H_{SO}|B,1,M\rangle|^2}$) in cm^{-1} for coumarin. The Breit-Pauli operator was used in all cases. In the case of MS-CASPT2 only elements $> 1\,cm^{-1}$ were included. Basis set: aug-cc-pVDZ for ADC(2)-s and cc-pVDZ for MS-CASPT2.

minimum structure of state	$T_n \rightarrow S_m$	ADC(2)-s		MS-CASPT2	
		ΔE	$\langle H_{SO}\rangle$	ΔE	$\langle H_{SO}\rangle$
gr. state (Fig. 9.4)	$1^3A' \rightarrow 2^1A'$	-0.94	0.10	n.c.	
	$2^3A' \rightarrow 2^1A'$	-0.09	0.07	n.c.	
	$1^3A'' \rightarrow 2^1A'$	0.03	11.08	0.10	2.48
	$2^3A'' \rightarrow 2^1A'$	1.55	2.02	1.90	
$1^1A''$ (Fig. 9.11)	$1^3A' \rightarrow 1^1A''$	0.29	40.72	0.28	51.03
	$2^3A' \rightarrow 1^1A''$	2.06	7.33	2.03	5.13
	$1^3A'' \rightarrow 1^1A''$	-0.06	0.11	n.c.	
	$2^3A'' \rightarrow 1^1A''$	2.38	0.18	n.c.	
$2^1A'$ (Fig. 9.6)	$1^3A \rightarrow 2^1A$	-0.07	3.64	-0.10	8.09
	$2^3A \rightarrow 2^1A$	0.62	35.82	1.02	43.23

given in detail in Section 9.2. For coumarin and hydroxycoumarin each, three important points of the PES were chosen. Namely, the ground state minimum, the minimum of the $S_1(\pi\pi^*, 2^1A')$ state and the minimum of the $S_2(n\pi^*, 1^1A'')$ state. At the ground state and $S_2(n\pi^*)$ structures the molecule has C_s symmetry while the symmetry is broken at the minimum of the $S_1(\pi\pi^*)$ state.

At these structures spin-orbit coupling elements were calculated with the ADC(2)-s/aug-cc-pVDZ method in combination with the Breit-Pauli spin-orbit operator. The results are shown in Tables 7.5 and 7.6.

Spin-orbit coupling elements with the multi-state complete active space perturbation theory (MS-CASPT2) [46,180,181] calculated with the MOLCAS V7.2 program package [176] are taken for comparison. As active space 12 electrons in 11 orbitals were chosen. Among them four π, four π^*, one non-bonding orbital and one pair of σ and σ^* orbitals. To avoid problems with Rydberg states the non-augmented cc-pVDZ [75] basis set was used. In the state-averaged calculations two states were used per symmetry. For the spin-orbit coupling elements the Breit-Pauli operator was employed. In the case of the ground state structures a level shift of 0.1 had to be applied in order to guarantee a high reference weight during the CASPT2 calculations.

Although the absolute values of the spin-orbit coupling elements differ significantly, the two methods predict for each structure the same coupling element as the dominating one. Additionally, both approaches identify the coupling elements between the $1^3A'$ and $1^1A''$ at the minimum structure of the $1^1A''$ state as the largest one. Therefore, we conclude that the ADC(2)-s method is well suited for the discussion of relative spin-orbit coupling elements in coumarin derivatives as will be important in Chapter 9.

Table 7.6.: Excitation energies in eV and state-to-state spin-orbit coupling elements ($\langle H_{SO} \rangle = \sqrt{\sum_{M=0,\pm1} |\langle A,0,0|H_{SO}|B,1,M\rangle|^2}$) in cm^{-1} for hydroxycoumarin. The Breit-Pauli operator was used in all cases. In the case of MS-CASPT2 only elements $> 1\,cm^{-1}$ were included. Basis set: aug-cc-pVDZ for ADC(2)-s and cc-pVDZ for MS-CASPT2.

minimum structure of state	$T_n \rightarrow S_m$	ADC(2)-s		MS-CASPT2	
		ΔE	$\langle H_{SO} \rangle$	ΔE	$\langle H_{SO} \rangle$
gr. state (Fig. 9.4)	$1^3A' \rightarrow 2^1A'$	-1.01	0.02	n.c.	
	$2^3A' \rightarrow 2^1A'$	0.08	0.04	n.c.	
	$1^3A'' \rightarrow 2^1A'$	0.12	14.32	0.11	7.48
	$2^3A'' \rightarrow 2^1A'$	1.16	0.65	1.89	4.41
$1^1A''$ (Fig. 9.11)	$1^3A' \rightarrow 1^1A''$	0.25	44.53	0.34	51.16
	$2^3A' \rightarrow 1^1A''$	2.05	13.52	1.68	19.87
	$1^3A'' \rightarrow 1^1A''$	-0.06	0.12	n.c.	
	$2^3A'' \rightarrow 1^1A''$	2.31	0.20	n.c.	
$2^1A'$ (Fig. 9.6)	$1^3A \rightarrow 2^1A$	-0.04	4.96	-0.05	20.40
	$2^3A \rightarrow 2^1A$	0.49	38.02	0.76	46.78

7.3. Summary

In this chapter test calculations for the implemented spin-orbit coupling elements with the whole hierarchy of ADC methods up to third order were presented and the implementation was shown to work reliably. For ADC(2)-s a procedure for the calculation of spin-orbit coupling elements had been presented before [173]. The newly implemented code reproduced those values nicely for the two test molecules thiophene and 1,2-dithiin. Deviations occurred because in the previous approach a molecular and not an atomic mean-field was used. Additionally, the transition density matrices were calculated only in first-order perturbation theory and not in full second order like in this work.

The calculation of coupling elements worked well for all other ADC methods, too. As long as the character of the states involved did not change significantly from one method to the other, similar values for the coupling elements were obtained at all orders of perturbation theory. The application of the SOS approximation worked well for coupling elements between the ground state and the triplet states. Between excited singlet states and triplet states larger deviations were obtained and the application of the SOS approach should be avoided when absolute values are needed. The values obtained with ADC(3) were in better agreement with DFT/MRCI values than the ADC(2)-s/x results in the case of thiophene. ADC(1) showed even larger differences. This might be an indication that the spin-orbit coupling elements are improved with increasing order of perturbation theory.

Finally, ADC(2)-s was tested for coumarin and 7-hydroxycoumarin in comparison to MS-CASPT2. Here, different points on the PES were chosen. The qualitative results agreed for all structures and both molecules. Both methods identified the same coupling elements as significant and yielded the same results regarding relative coupling elements. The advantage of the ADC ap-

proaches when applied to the investigation of relaxation pathways is that parameters like the active space, number of states used in the averaging process, etc., do not have to be adjusted for every point of the PES surface. Especially when the symmetry changes along certain pathways or states of very different character are important, it can be problematic to find consistent and reliable descriptions with complete active space methods like MS-CASPT2. On the other hand, single-reference methods like ADC can break down at points of the PES where the ground state has a strong multiconfigurational character or the Born-Oppenheimer approximation is not valid anymore.

In Chapter 4 the excitation energies were evaluated with respect to the benchmark set and theoretical best estimates for excited states developed by Schreiber et al. [88] and Silva-Junior et al. [89]. In the case of spin-orbit coupling elements no such benchmark sets exist. The molecules thiophene and 1,2-dithiin were chosen because the previously implemented ADC(2)-s approach had been evaluated for these two molecules giving valuable reference values for the present implementation. Therefore, the development of a benchmark set for which spin-orbit coupling elements at different levels of theory are available forms an important part of future work.

8. Plasmons in Linear Polyenes

8.1. Introduction

In this section test calculations for the scaling approach established in Section 6.4 are presented. First, the scaled versions of the ADC(1) (CIS) and the ADC(2) family of methods are applied to C_8H_{10} and shown to work reliably for the identification of plasmons. Additionally, results for the larger systems $C_{16}H_{18}$ and $C_{30}H_{32}$ are shown.

The scaling approach discussed in Section 6.4 was implemented into a development version of Q-Chem [19]. In all cases the resolution of the identity (ri) approximation for four-center integrals [76, 77, 87] was employed. All structures were obtained by geometry optimization at the level of Møller-Plesset perturbation theory of second order (MP2) [30]. As basis set the correlation consistent triple-ζ basis set aug-cc-pVTZ [75] was used. In the case of excited state calculations the cc-pVTZ or cc-pVDZ basis set was used. Finally, the excitation energies were determined in dependence of the scaling parameter λ which was varied from zero (no exchange correlation) to one (full exchange correlation) in steps of 0.05. In contrast to TDDFT, the excitation energies themselves (instead of the squared energies, compare Section 6.2) were plotted in dependence of λ to obtain the final plots.

The characteristics of plasmonic excitations have been discussed in detail for the electron gas in Section 6.2. Among them are a high intensity (when optically allowed) and a certain nodal structure of the transition density where the first plasmon has one node, the second two and so on. Additionally, the plasmon is a linear combination of all possible single-particle replacements with a certain momentum transfer. The scaling approach is based on the strong dependence of its energetic position on the amount of exchange correlation included while the other states are influenced to a smaller extend.

In linear polyenes the electrons occupying the π-orbitals can be viewed as forming an electron gas that is to a large extent delocalized along the molecule. Therefore, an analogy to the homogeneous one-dimensional electron gas can be established by associating wave vectors to the π-orbitals of the polyenes under consideration. Of course, the assignment of momentum vectors is not exact and only a means to classify the plasmons in the same way as in the homogeneous electron gas discussed in Section 6.2. In the one-dimensional case, the wave vectors have only one component. Therefore, a certain momentum transfer can be directly correlated with a certain change in quantum number (compare Figure 8.1).

The linear polyenes have C_{2h} symmetry and the π-orbitals transform according to the irreducible representations A_g or B_u. Therefore, the $\pi\pi^*$ excitations are, as well, either of A_g (even change in quantum number) or B_u (odd change

in quantum number) symmetry. While excitations of the latter type are optically allowed, the former ones are dark states and have no intensity. In this case the distinction between plasmons and single-particle excitations based on their oscillator strength is not possible and an alternative approach is of even greater importance.

8.2. Results

8.2.1. Octatetraene

The assignment of wave vectors to the relevant frontier orbitals is shown for octatetraene in Figure 8.1. As an example, the three possible single-particle replacements with a change in quantum number of $\Delta n = 3$ are shown.

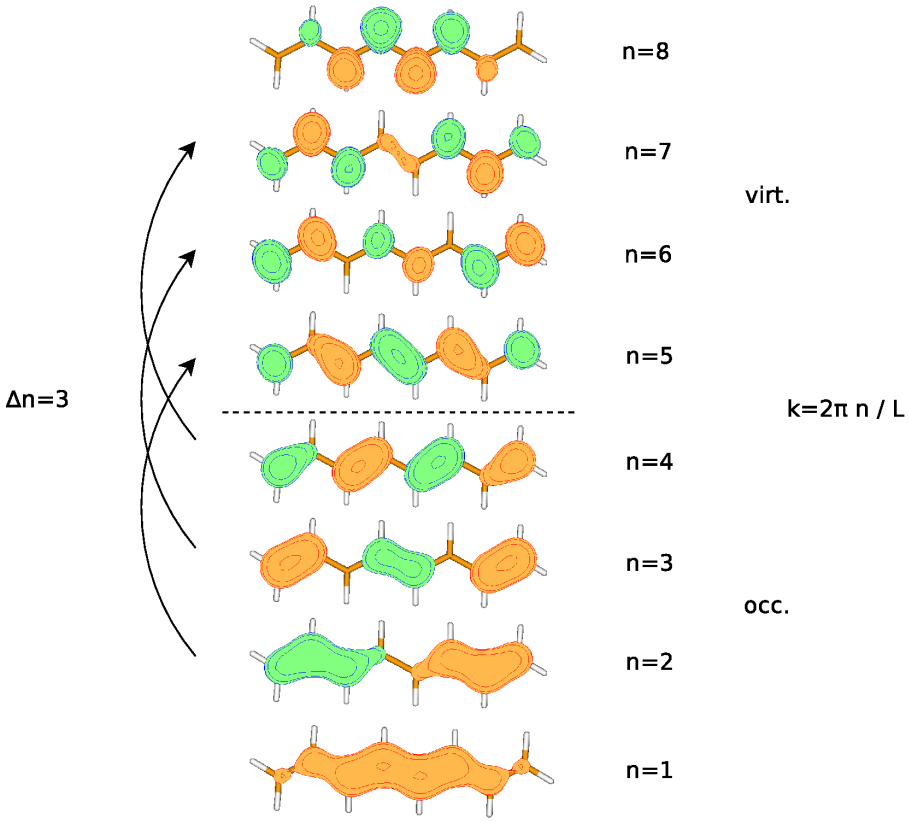

Figure 8.1.: Molecular orbitals of octatetraene and assignment of momentum vectors k. The symbol n denotes the quantum numbers of the orbitals. As an example, the three arrows indicate the three possible single-particle replacements with $\Delta n = 3$.

For most methods only the results for the optically allowed B_u states will be shown because the oscillator strength can be used as a further characteristic in this case. For selected methods the results obtained for A_g symmetry will be added. The B_u states are composed of single-particle replacements with an odd change in quantum number. Therefore, in B_u symmetry only odd-Δn plasmons can be observed while the even-Δn plasmons appear in A_g symmetry.

ADC(1)/CIS

Figure 8.2 shows the plot obtained with ADC(1) (CIS) for B_u symmetry. The first two states rise in energy while the other ones stay almost constant. When looking at the contributions to the excitation vector (Table 8.1), it can be seen that the first state is dominated by the HOMO to LUMO transition ($\Delta n = 1$) while the next three states are mainly composed of single-particle replacements with $\Delta n = 3$. While for the third and fourth state only one or two of the three possible single-particle replacements are important, all contribute significantly to the second excited state. In combination with the strong dependence on λ this indicates that the first two excited states correspond to the first and third plasmon of octatetraene.

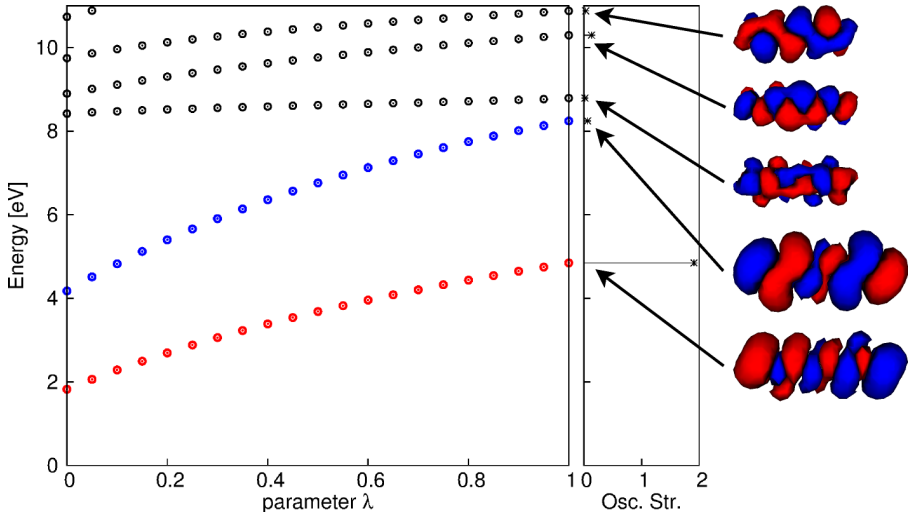

Figure 8.2.: Electronic excitation energies of states with B_u symmetry of the polyene C_8H_{10} as a function of the exchange correlation obtained with ADC(1)/cc-pVTZ (CIS). Included are the transition densities and the linear absorption spectrum.

Regarding the transition densities, these two states exhibit the expected nodal structure that distinguishes them from the other ones. This means one node for the first plasmon and three nodes for the third plasmon. The nodal structure will become even more apparent for the larger systems. It has to be mentioned, however, that in the case of $\Delta n = 3$ the plasmonic state is the lowest in energy within its group (it was the highest in the electron gas) and exhibits only the second largest intensity (largest in the electron gas). This is due to the fact that single-particle states and plasmons are not fully separated and that the electron density generated by the π-electrons is not at all homogeneous. Moreover, ADC(1) offers only a rough approximation to the excitation energies. Nevertheless, the combination of the dependence on λ, the nodal structure of the transition densities and the contributions of the eigenvector allow for a clear identification of the plasmons.

Table 8.1.: Excitation energies, important contributions to the eigenvectors and oscillator strengths for the first four excited states with B_u symmetry of octatetraene. The values for the first plasmon of this symmetry are given in red and the ones for the second in blue. Method: ADC(1)/cc-pVTZ.

State	Δ E[eV]	important contributions	[%]	Osc. Str.
1	4.85	**4** → **5**	92	1.91
2	8.25	**2** → **5**	16	0.07
		3 → **6**	17	
		4 → **7**	55	
3	8.79	**2** → **5**	63	0.02
		3 → **6**	2	
		4 → **7**	24	
4	10.30	**2** → **5**	9	0.13
		3 → **6**	56	
		4 → **7**	3	

(SOS)-ADC(2)-s/x

With the second-order methods (SOS)-ADC(2)-s/x qualitatively the same results are obtained (see Figures 8.3, 8.4 and 8.5 as well as Tables D.1,D.2 and D.3). For B_u symmetry, two states rise in energy and by analysis of their orbital contributions they can be identified as plasmons one and three. The transition densities suggest the same results. Again, the intensity of the first plasmon is very high while the intensity of the second one is not the highest within its group. A difference to the CIS results is given by the order of the states. Now, the plasmon with $\Delta n = 3$ is the second highest state that is dominated by this change in quantum number.

Interestingly, the energy of the plasmons are not strongly affected by the introduction of additional correction terms from second-order perturbation theory. By contrast, the single-particle states are shifted to lower energies thereby changing the order of states within the group of states with $\Delta n = 3$. Consequently, the plasmons seem to be mostly affected by long-range, non-dynamical correlation effects while the dynamical correlation accounted for by higher orders of perturbation theory seems to influence the single-particle states to a larger extent. This is in accordance with studies in which plasmons are considered to be due to long-range correlation effects (compare [168–171, 182]).

Because of the lower energies of the ordinary states, crossings between different states occur along the scans. Depending on the interaction strength between plasmons and single-particle states, there arise avoided crossings. The coloring scheme of the plasmons has been chosen based on the dominating contributions of the respective states.

The results with SOS-ADC(2)-s and ADC(2)-s are almost identical and only small shifts in the final energies occur (compare Tables D.1 and D.2). The same is true for all other properties like oscillator strengths and transition densities.

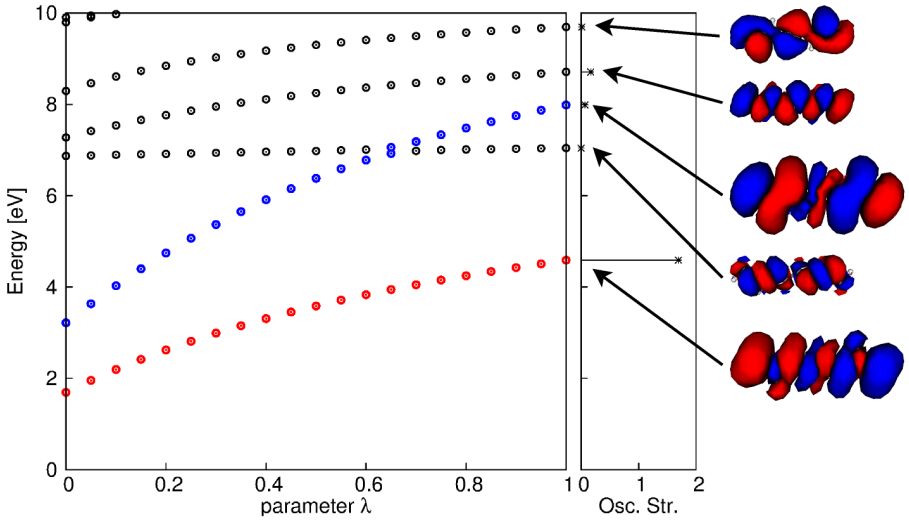

Figure 8.3.: Electronic excitation energies of states with B_u symmetry of the polyene C_8H_{10} as a function of the exchange correlation obtained with ADC(2)-s/cc-pVTZ. Included are the transition densities and the linear absorption spectrum.

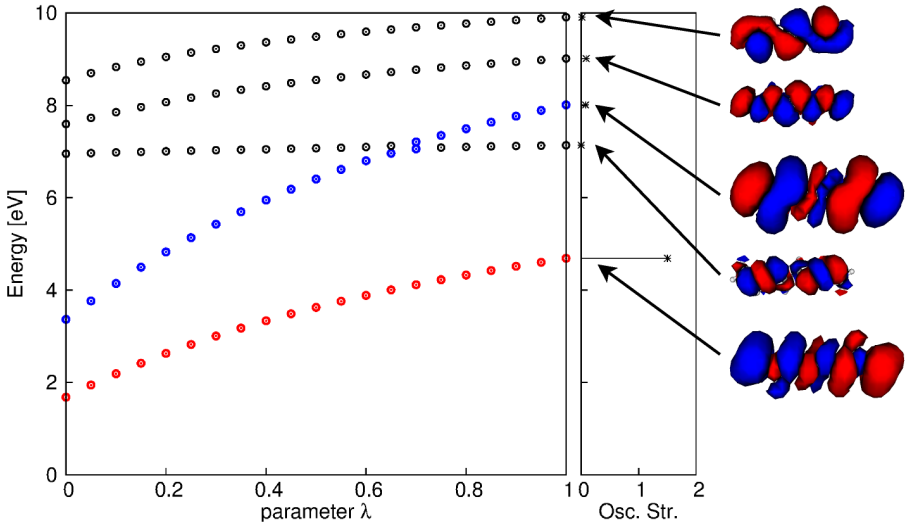

Figure 8.4.: Electronic excitation energies of states with B_u symmetry of the polyene C_8H_{10} as a function of the exchange correlation obtained with SOS-ADC(2)-s/cc-pVTZ. Included are the transition densities and the linear absorption spectrum.

Thus, the SOS approximation introduced in Section 4 works reliably in this case, too.

In the case of extended ADC(2) calculations, only those results are shown that were obtained with the SOS approximation because the overestimation of doubly excited configurations in ADC(2)-x is compensated in SOS-ADC(2)-x. As in the case of the transition from CIS to ADC(2)-s, the plasmon states are only slightly shifted in energy in SOS-ADC(2)-x. However, the other states are strongly shifted and some of them gain significant double excitation character (e. g., second state in B_u symmetry, compare Table D.3). Additionally, a state

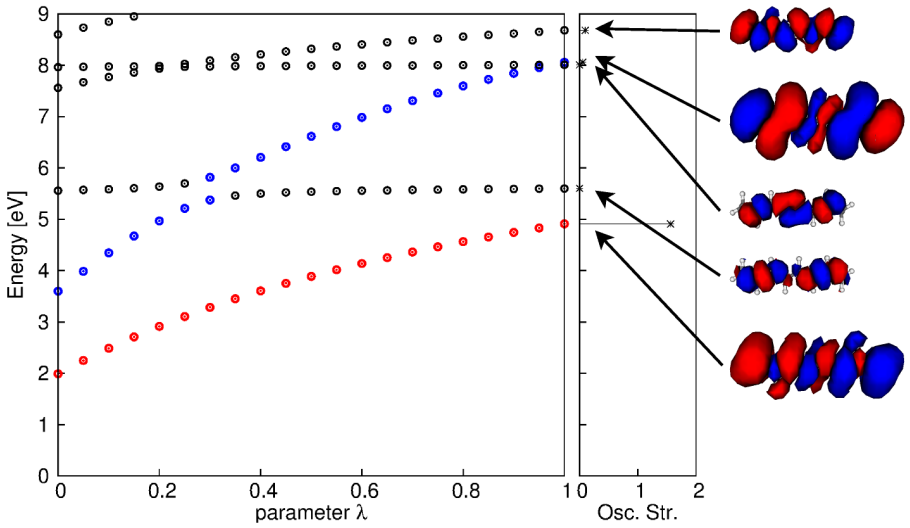

Figure 8.5.: Electronic excitation energies of states with B_u symmetry of the polyene C_8H_{10} as a function of the exchange correlation obtained with SOS-ADC(2)-x/cc-pVTZ. Included are the transition densities the plasmon transitions and the linear absorption spectrum.

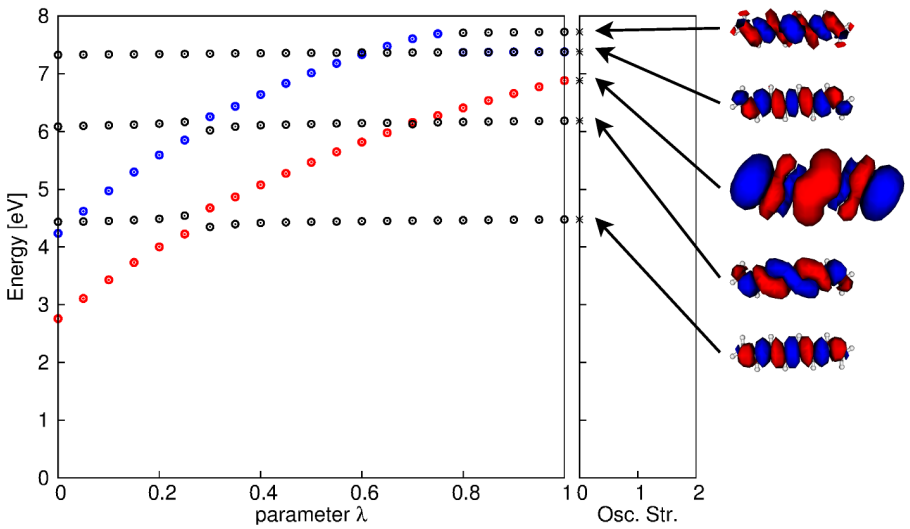

Figure 8.6.: Electronic excitation energies of states with A_g symmetry of the polyene C_8H_{10} as a function of the exchange correlation obtained with SOS-ADC(2)-x/cc-pVTZ. Included are the transition densities for the plasmon transitions.

that shows 80 % double excitation character is inserted below the second plasmon in B_u symmetry. Nevertheless, the general results are the same as with the previous methods and the same states are classified as plasmons.

With SOS-ADC(2)-x a second scan was performed for the states of A_g symmetry. The results are shown in Figure 8.6. Like in the case of B_u symmetry two states rise in energy which can be classified as plasmons two and four by inspection of the transition densities as well as of the contributions to the eigenvectors (compare Table D.4). Thus, the scaling approach works reliably for this

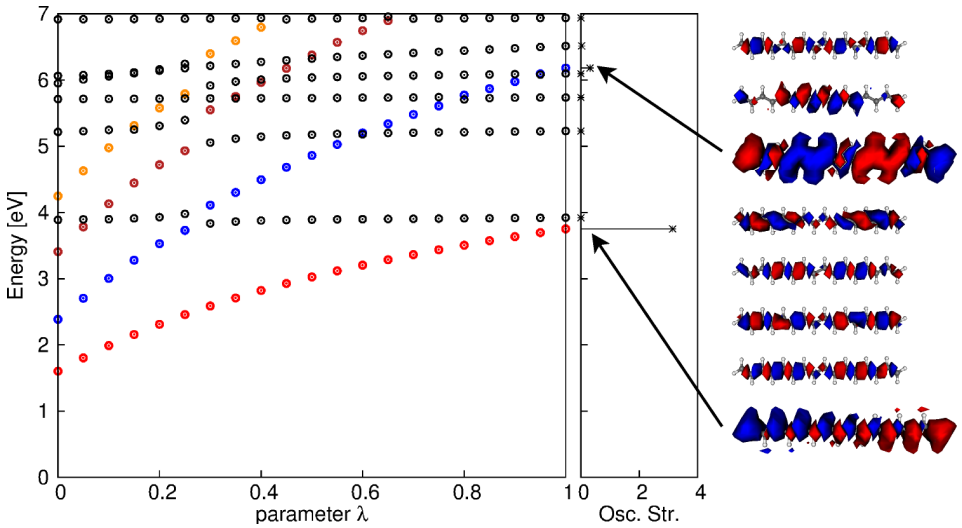

Figure 8.7.: Electronic excitation energies of states with B_u symmetry of the polyene $C_{16}H_{18}$ as a function of the exchange correlation obtained with SOS-ADC(2)-x/cc-pVDZ. Included are the transition densities and the linear absorption spectrum.

symmetry, too.

To summarize, with all ADC methods employed the scaling approach identifies plasmons in agreement with the analysis of transition densities or contributions to the eigenvector. Only the order of states within a group of excited states and their intensity is not always the same as in the homogenous electron gas. Nevertheless, the scaling approach works reliably for all methods considered. In the next two sections, the scaling approach will be applied to higher polyenes.

8.2.2. $C_{16}H_{18}$

To test the scaling approach for larger systems, it was applied to the $C_{16}H_{18}$ molecule. The results are shown in Figures 8.7 and 8.8. SOS-ADC(2)-x/cc-pVDZ was the method used because double excitations are known to be of great importance in extended linear polyenes.

Of the ten states included, four rise strongly in energy with increasing λ. When the full electron correlation is switched on, there are still two plasmon states within the manifold of the lowest ten states. The contributions to the eigenvectors are shown in Table D.5. Again, the states identified as plasmons show the characteristic composition of single-particle replacements. Finally, the transition densities of plasmons and single-particle excitations differ in the expected way with respect to their nodal structure. The transition density of the first plasmon shows one node while the one of the second within this symmetry (and the third overall) possess three nodes.

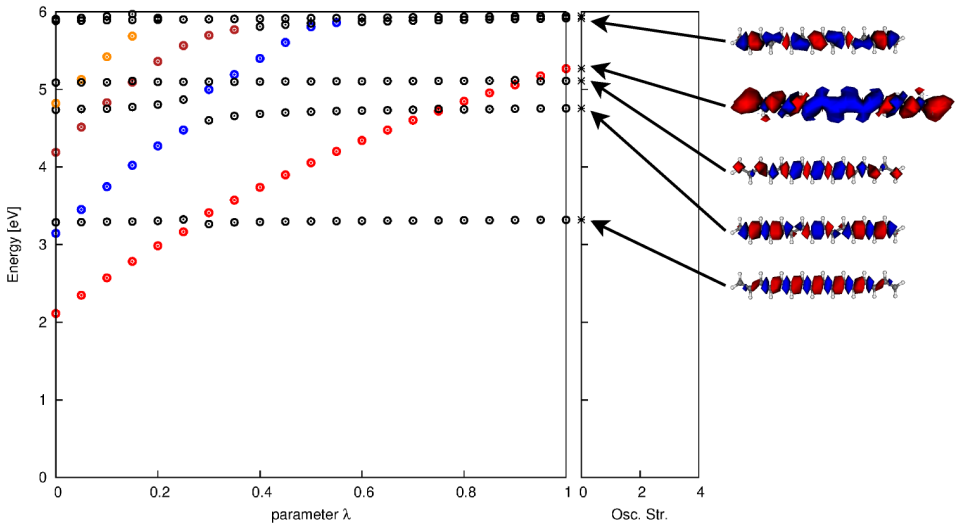

Figure 8.8.: Electronic excitation energies of states with A_g symmetry of the polyene $C_{16}H_{18}$ as a function of the exchange correlation obtained with SOS-ADC(2)-x/cc-pVDZ. Included are the transition densities and the linear absorption spectrum.

8.2.3. $C_{30}H_{32}$

In the original work by Bernadotte et al. [167] the polyene $C_{30}H_{32}$ was used as a test case. For comparison, we present some results on this molecule. Due to the large size of the molecule, however, only ADC(1) (CIS) computations have been performed for this case. The results are displayed in Figures 8.9 and 8.10.

At low energy, there are no ordinary states at all. This picture will change when a higher-order method is used. Like in the case of C_8H_{10} and $C_{16}H_{18}$ the plasmons can be expected to be only little affected while the ordinary states should be substantially lowered in energy. In addition, doubly excited states are expected to occur.

Due to the extended system size the characteristic nodal structure of the transition densities is easily recognizable. Regarding the intensities, the first plasmon exhibits by far the highest oscillator strength. The other plasmons have decreasingly lower intensities.

Compared to the TDDFT values [167], the ordinary states lie much higher in energy with ADC(1) (approximately 4 eV). The plasmons, on the other hand, are only about 1 eV higher in energy. This is another indication that the energies of the plasmons do not depend strongly on the method applied.

8.3. Summary

The scaling approach, as presented in a recent TDDFT study, was transferred to the hierarchy of ADC methods in Section 6.4 and applied to a series of linear polyenes. The plasmon states identified from the plots could be distinguished from ordinary states also by their transition density pattern and eigenvector characteristics. However, there are deviations from the picture associated with

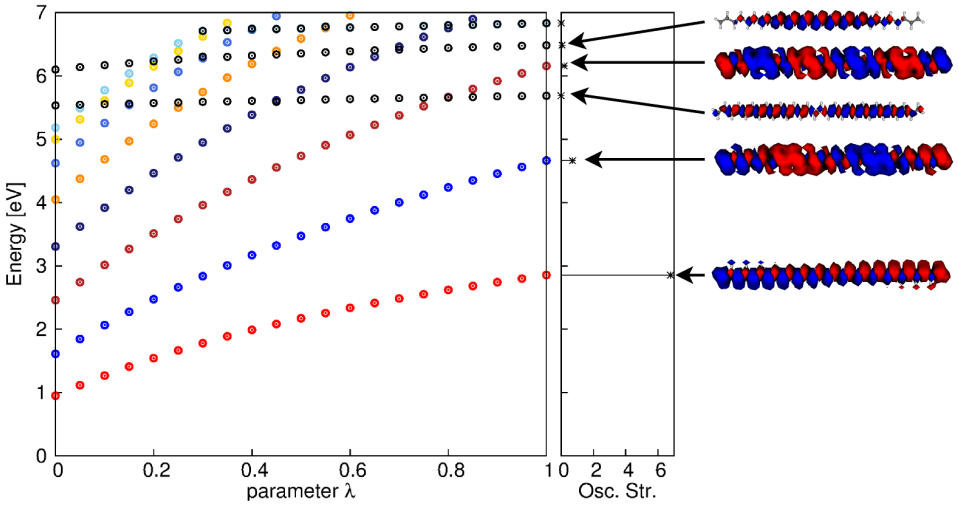

Figure 8.9.: Electronic excitation energies of states with B_u symmetry of the polyene $C_{30}H_{32}$ as a function of the exchange correlation obtained with ADC(1)/cc-pVDZ. Included are the transition densities and the linear absorption spectrum.

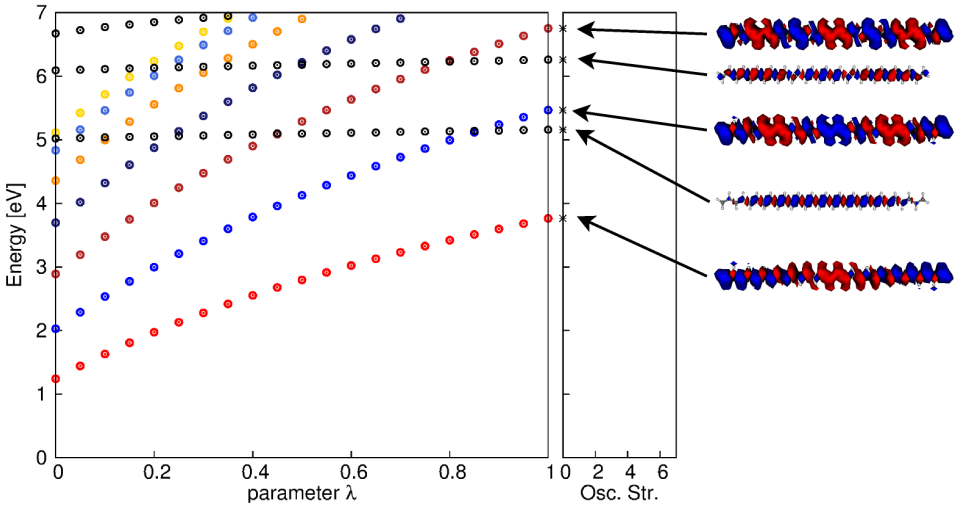

Figure 8.10.: Electronic excitation energies of states with A_g symmetry of the polyene $C_{30}H_{32}$ as a function of the exchange correlation obtained with ADC(1)/cc-pVDZ. Included are the transition densities and the linear absorption spectrum.

the free-electron model with respect to spectral intensities and the energetic order. This is not surprising because there is no clear separation between single-particle states and plasmons in these systems and because the electron densities of the linear polyenes are not perfectly homogeneous.

An interesting finding concerns the influence of correlation effects on the different type of states. While the single-particle states are strongly shifted in energy when the level of perturbation theory is changed, the energies of the plasmons are only slightly affected. This is in accordance with studies that attribute plasmons to long-range correlation effects (compare [168–171, 182]).

9. Relaxation Processes in Coumarin Derivatives

9.1. Introduction

Coumarins constitute an important class of molecules that are widely applied as laser dyes as well as in several bio-medical problems. They show many therapeutic effects and have been used, e. g., as lipid-lowering compounds, anti-carcinogenic agents, anti-coagulant agents and as HIV-inhibitors [183,184]. Another medical application is the photocontrolled drug-delivery for the treatment of cataract which is based on the weak toxicity and high stability of coumarins and their dimers [185–187]. Despite its importance, the ultrafast dynamics of coumarins particularly in the excited state is still not fully understood.

In this regard, one of the major aspects still lacking an appropriate account is the very weak fluorescence emission observed in the unsubstituted coumarin (1-benzopyran-2-one). At room temperature, coumarin in cyclohexane has a quantum yield of just 0.03 % [188]. This contrasts to fluorescence shown by substituted coumarins, like 4-methoxycoumarin derivatives and umbelliferone (7-hydroxycoumarin) in glycerol, which display quantum yields of about 60 % and 50 %, respectively [189]. Such a strong fluorescence emission in substituted coumarin is dependent on the polarity of the solvent. For example, while in methanol umbelliferone shows a quantum yield of merely 3.3 %, in aqueous solution it reaches about 51 % [189].

De Melo et al. have argued that the striking difference in quantum yields might be due to a different energetic ordering of the first singlet $n\pi^*$ and $\pi\pi^*$ states relative to each other [188]. Depending on the polarity of the solvent (and the substituents) the $n\pi^*$ state can be lower in energy and therefore mediate an efficient radiationless decay from the initially populated $\pi\pi^*$ state. This assumption was based on a strong change of the radiative lifetime from large values in non-polar systems (greater than 250 ns for coumarin in cyclohexane) to values typical for optically allowed processes in polar solvents (e. g., for 4-methyl-7-hydroxycoumarin 3 ns in dioxane:water 1:4). This indicated different characters of the fluorescent state, namely $n\pi^*$ in non-polar or $\pi\pi^*$ in polar

Parts of this chapter have already been published in
C. M. Krauter, J. Möhring, T. Buckup, M. Pernpointner, M. Motzkus
Ultrafast branching in the excited state of coumarin and umbelliferone
Phys. Chem. Chem. Phys. **15**, 17846 (2013).
http://pubs.rsc.org/en/content/articlelanding/2013/cp/c3cp52719k
Reproduced by permission of the PCCP Owner Societies.

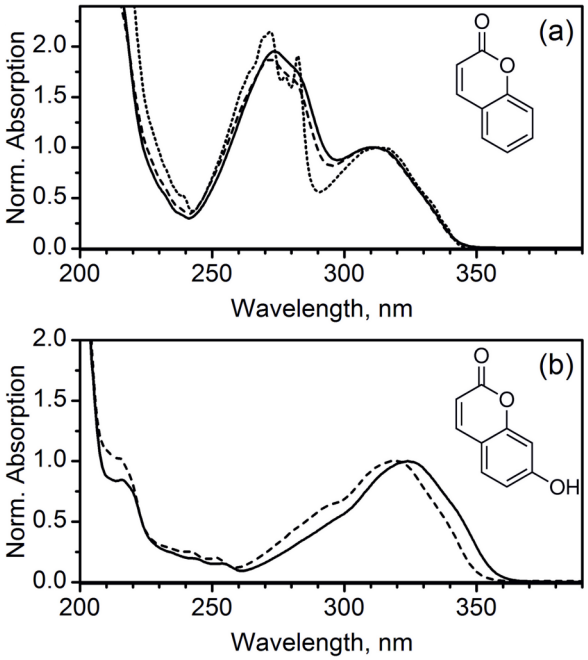

Figure 9.1.: (a) Absorption spectrum of coumarin in methanol (solid line), acetonitrile (dashed line) and cyclohexane (dotted line). (b) Absorption spectrum of umbelliferone in methanol (solid line) and acetonitrile (dashed line).

solvents. Two models for the radiationless transition in non-polar media were suggested: [190] 1) adiabatic relaxation from $\pi\pi^*$ *via* $n\pi^*$ back to S_0 or 2) *via* the so-called proximity effect [191, 192]. As $\pi\pi^*$ states are typically shifted to lower energies in polar media and $n\pi^*$ to higher ones, the energetic separation should increase with solvent polarity, the $n\pi^*$ now lying above the $\pi\pi^*$, and thereby hinder an efficient radiationless relaxation.

Within the framework of the proximity effect [191,192] the radiationless transition is explained by strong vibronic coupling (pseudo Jahn-Teller effect) between the close lying $n\pi^*$ and $\pi\pi^*$ states. The coupling (non-totally symmetric out-of-plane) modes leads to distortions of the PES thereby reducing the barrier width for the internal conversion process. The proximity effect was also used to explain the fluorescence quenching in psoralen [193] and, just recently, in benzo[g]chromen-2-ones [194]. Both are coumarin derivatives in which a third (hetero)aromatic ring has been annealed.

However, the fluorescence lifetime of coumarin has not been unambiguously verified. Measurements using time-correlated single-photon counting suggested an upper limit for the life constant of only around 100 ps [188]. This might be a hint for another ultrafast relaxation network than the one assumed so far.

An additional deactivation channel of coumarins is the formation of triplet states. Inter-system crossing (ISC) is an efficient process in the coumarin family and is very dependent on the solvent. The ISC quantum yield of coumarin in acetonitrile is just 1 %, but increases up to 30 % in trifluoroethanol [195]. Recently, the formation of dimers of coumarins has been explained in terms of

reactive triplet states, challenging the multiplicity selective formation of dimers isomers [195]. Absorption bands of the lowest excited triplet state have been identified at 400, 425 and 450 nm and it seems to decay within a timescale of 300-500 ns. The time scale of inter-system crossing and from which singlet electronic state it occurs are still not known for coumarins.

Many theoretical studies have been conducted regarding optical properties of coumarin derivatives, e. g., [196–217]. However, the main focus has been on vertical excitation energies, (excited state) dipole moments and fluorescence energies of strongly emitting compounds like aminocoumarins. Mostly semi-empirical or time-dependent density functional methods (TDDFT) were applied. For example, benchmarks of different TDDFT models for a wide range of coumarin derivatives have been provided [198, 199, 218]. However, coumarin molecules seem to be challenging systems for time-dependent DFT [198]. Nevertheless, the S_1 state was associated with a $\pi\pi^*$ excitation and S_2 (or higher) as $n\pi^*$ over a wide range of solvents and substituents although they can be close in energy (e. g., [196, 203, 206]).

The investigation of hydroxycoumarins is complicated by a possible proton transfer from the hydroxy to the carbonyl group [219]. Depending on the medium several tautomers or ionized forms can coexist. Moreover, the acidity of hydroxycoumarins is strongly increased in the excited state (e. g., for 7-hydroxy-4-methylcoumarin: $pK_a(S_0)\approx 7.7$ and $pK_a(S_1)\approx 0.45$) [204]. In aqueous systems intramolecular proton transfer (presumably *via* a bridge of water molecules) can play a significant role for fluorescence quenching and has been thoroughly investigated [204]. In neutral alcoholic, non-protic or non-polar solvents as used in this work these effects should, however, be of only little importance (for some illustrative spectra see, e. g., [220, 221]).

Tatchen et al. have investigated possible deactivation pathways for psoralen compounds [203]. They have located gas phase minima of several excited states among them S_2 ($n\pi^*$). At its minimum structure the order of $\pi\pi^*$ and $n\pi^*$ has been reversed, the latter one being more stable. However they did not investigate possible conical intersections or energy barriers for such a transition. Additionally, they suggested a ring opening of the pyrone ring at the lactone bond as a possible deactivation pathway in the S_1 ($\pi\pi^*$) state. Solvent effects were not examined. Such a ring opening reaction has, as well, been experimentally observed in matrix isolated coumarin [215]. To the best of our knowledge neither of these pathways has been applied to the basic coumarin unit or in solution, especially not in the context of the different fluorescence behavior of coumarin and its hydroxy derivatives.

Recently, transient absorption spectra where recorded in the group of M. Motzkus elucidating the difference between coumarin and umbelliferone in more detail [23]. As solvents methanol and acetonitrile were chosen and the relevant results are shown in Figures 9.2 and 9.3. In the case of coumarin the measurements were conducted in cyclohexane, additionally.

In transient absorption spectra the molecules are excited by a first pulse with a narrow band width, the so-called pump pulse (in this case centered around 330 nm). With certain time delays a broad band pulse, called the probe pulse, is applied. Finally, the development of the differences between the two

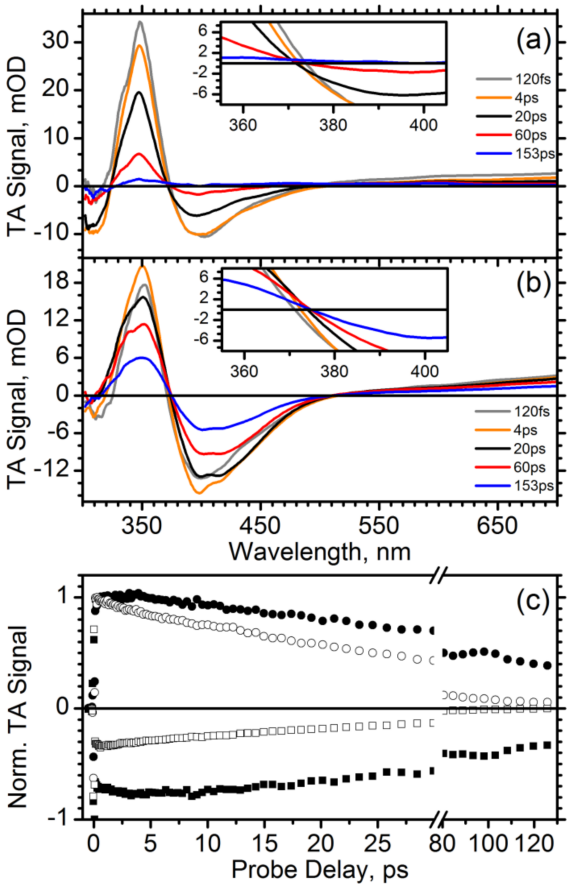

Figure 9.2.: (a) Selected transient spectra for umbelliferone in acetonitrile. (b) Selected transient spectra for umbelliferone in methanol. Insets show there is no isosbestic point in both solvents. (c) Transient absorption traces at the maximum of the ESA and the SE signals. For umbelliferone in acetonitrile at 350 nm (empty circle) and 400 nm (empty square). For methanol at 348 nm (filled circle) and 394 nm (filled square). For more details see [23].

spectra in dependence of the delay time is analyzed. Here, three types of bands are of importance. The excited state absorption (ESA) bands have a positive signal and arise when population is transferred from an excited state to even higher electronic levels. On the other hand, stimulated emission (SE) processes give rise to negative signals. The third type of bands, the ground state absorption, has a negative signal, as well. However, in the case of coumarin and umbelliferone the absorption from the ground state can not be observed as it is superposed by the ESA signal. The time constants with which the different signals arise and vanish give important information about the life times of the excited states and the relaxation network involved.

For the molecules in this work, the bands from ESA as well as SE decayed usually with two time constants indicating more than one relaxation pathway. However, strong differences occurred with respect to the solvent. For both molecules, the SE bands lived the longest in methanol although the one in coumarin being much weaker than in umbelliferone. In the case of coumarin

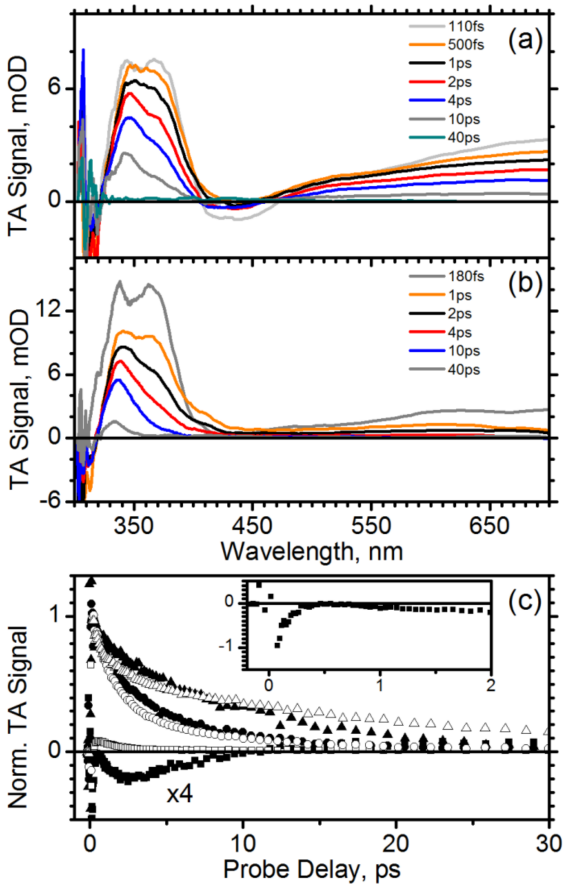

Figure 9.3.: (a) Selected transient spectra for coumarin in methanol. (b) Selected transient spectra for coumarin in acetonitrile. (c) Transient absorption traces at the maxima of the two contributions to the blue-shifted ESA signal, and at the maximum of SE signal. For coumarin in acetonitrile at 340 nm (empty triangle), 365 nm (empty circle) and 435 nm (empty square). For methanol at 343 nm (filled triangle), 373 nm (filled circle) and 435 nm (filled square). Inset shows the formation and relaxation of the initial ultrafast SE band of coumarin in methanol. For more details see [23].

in cyclohexane, the SE was even completely suppressed. The different time constants obtained experimentally are summarized in Table 9.1.

In this work, we investigate the electronic levels and the dynamics in the excited state of coumarin and umbelliferone (see insets of Figure 9.1) in polar and non-polar solvents using *ab initio* calculations. Our main goal is to explain the difference between the fluorescence intensity and the respective time-scales experimentally found in the relaxation of these two coumarins. This work is organized in the following way: In Section 9.2 we present briefly the numerical details. Results of quantum chemical calculations are presented in Sections 9.3-9.8. Results from global target analysis are summarized in Section 9.9. Finally, in Section 9.10 the experimental and numerical results are discussed and a relaxation model for coumarin and umbelliferone in dependence of the solvent polarity is described.

Table 9.1.: Decay time constants and amplitudes obtained at selected wavelengths λ (from [23]).

Molecule/ Solvent	λ/ nm	A1	t1 / ps	A2	t2 / ps	A3	t3 / ps
Umbelliferone							
Methanol	348	28(6)	16(2)	72(5)	>150	-	-
	394	30(5)	12(2)	70(5)	>150	-	-
Acetonitrile	350	98	35.3(4)	2	>300	-	-
	400	100	31.9(3)	-	-	-	-
Coumarin							
Methanol	343	16(3)	1.1(3)	84(3)	10.1(5)	-	-
	373	50(5)	1.5(2)	50(6)	6.5(7)	-	-
Acetonitrile	340	27(3)	1.4(2)	49(1)	19.7(7)	24(6)	0.2(5)
	365	69(2)	1.4(1)	31(2)	7.0(4)	-	-

9.2. Computational Details

Most calculations were carried out with the TURBOMOLE V6.3 program package [85]. Ground state stationary points were obtained by Møller-Plesset perturbation theory in second order (MP2) [30] within the resolution of the identity approximation (ri) and the `ricc2` module [48,222] of TURBOMOLE. If not stated otherwise, the correlation consistent polarized triple-ζ basis set cc-pVTZ [75] was employed together with the corresponding auxiliary basis set [90]. For orbital-relaxed first-order dipole moments the augmented cc-pVTZ (aug-cc-pVTZ) basis sets were used [75, 90]. In some cases the corresponding double-ζ basis sets (aug-)cc-pVDZ [75, 90] were employed. At all ground state minimum structures numerical frequency calculations were performed using the module `NumForce` in order to confirm that minima were obtained.

For the calculation of excited states, the second-order algebraic diagrammatic construction scheme [14–18] as implemented in the `ricc2` module [48, 51, 222, 223] of TURBOMOLE was employed. This largely overseen method comprises the advantages of both, coupled-cluster and configuration-interaction methods as it incorporates a hermitian eigenvalue problem and is, at the same time, size-consistent. Additionally, charge-transfer and, if the provided basis sets are large enough, Rydberg states are physically correctly described. The elements of the secular matrix are determined by perturbation theory and ADC(2) yields results that are of similar quality as those obtained with CC2 [47]. For all vertical excitation energies as well as excited state properties [223] (oscillator strengths and orbital-relaxed first-order dipole moments) the aug-cc-pVTZ basis set was chosen. If not stated otherwise, the cc-pVTZ basis set was used for excited state geometry optimizations. Due to the high numerical demand, only some of the obtained structures were characterized by harmonic analysis.

Solvent effects were considered by including explicit solvent molecules on the one hand and by application of the conductor-like screening model (COSMO) [224]. However, the COSMO model can only be applied on Hartree-Fock level but not in the ADC(2) (or CC2) calculations. Nevertheless, by considering the solvent perturbed molecular orbitals the largest part of the implicit solvent effect should be covered. To mimic methanol as solvent, a permittivity of 32.64

was chosen. For the radii based cavity construction the optimized atomic radii included in TURBOMOLE were used.

In some cases time-dependent density functional theory (TDDFT) [10,41,42] calculations were performed with the ESCF and EGRAD functionalities of TURBOMOLE. Two different hybrid functionals were used: B3LYP [38] and BH-LYP [40]. These two functionals differ with respect to the amount of exact Hartree-Fock (HF) exchange incorporated (20 % for B3LYP and 50 % for BH-LYP).

For some points of the PES multi-state complete active space perturbation theory (MS-CASPT2) calculations [46, 180, 181] were done. These were performed with the MOLCASV7.2 program package [176]. As active space 12 electrons in 11 orbitals was chosen. Among them were four π, four π^*, one non-bonding orbital and one pair of σ and σ^* orbitals. To avoid problems with Rydberg states the non-augmented cc-pVTZ [75] basis set was used. In the state-averaged calculations two states per symmetry were used.

9.3. Structure and Vertical Excitation Energies

In their electronic ground state, coumarin and its 7-hydroxyderivative are planar and have C_s symmetry. To decide on a basis set for the following geometry optimizations the four different correlation consistent polarized basis sets (aug-)cc-pVDZ and (aug-)cc-pVTZ were tested (Table 9.2). The value that changes most with basis set size is the C^3C^4 double bond (about 2pm, for numbering scheme see Figure 9.4). The largest change occurs between double-ζ and triple-ζ basis sets while the inclusion of diffuse functions in the augmented basis sets introduces hardly any changes. Therefore, we decided to use the cc-pVTZ basis set for ground state geometry optimizations throughout this work.

The obtained bond lengths are in good agreement with crystal structure

Table 9.2.: Basis set dependence of bond lengths in coumarin. All values in Å. Numbering scheme according to Figure 9.4. Method: MP2.

Bond	x-ray [225]	cc-pVDZ	aug-cc-pVDZ	cc-pVTZ	aug-cc-pVTZ
O^1C^2	1.374	1.397	1.399	1.381	1.380
$C^2{=}O^{11}$	1.213	1.211	1.218	1.203	1.205
C^2C^3	1.454	1.468	1.466	1.450	1.450
$C^3{=}C^4$	1.347	1.361	1.364	1.344	1.345
C^4C^{10}	1.438	1.447	1.446	1.428	1.428
$C^{10}C^9$	1.397	1.412	1.412	1.394	1.395
C^9O^1	1.378	1.369	1.376	1.358	1.359
C^8C^9	1.394	1.404	1.404	1.387	1.386
C^7C^8	1.383	1.399	1.401	1.383	1.383
C^6C^7	1.397	1.411	1.413	1.394	1.395
C^5C^6	1.380	1.396	1.398	1.380	1.380
$C^{10}C^5$	1.405	1.414	1.416	1.396	1.397

data [225]. The largest deviation occurs for the C=O double bond which is, however, strongly dependent on the environment. In Figure 9.4 the resulting MP2/cc-pVTZ structures for coumarin and umbelliferone are shown together with the numbering schemes used. In Figure 9.5 those molecular orbitals are depicted that will be important for the excitation process. The excitation energies, oscillator strengths and orbital-relaxed dipole moments of the three lowest excited singlet states are given in Table 9.3.

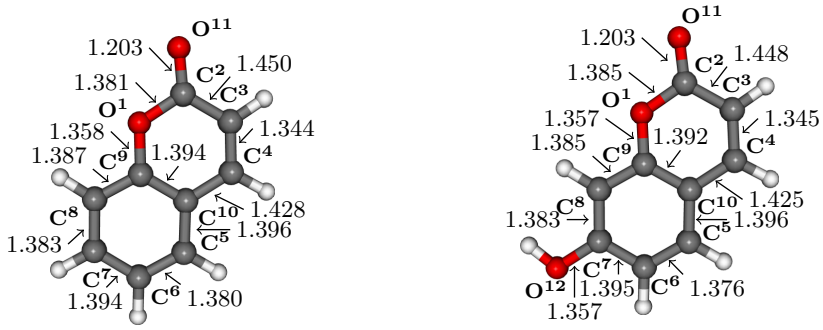

(a) coumarin **1** (b) umbelliferone **2**

Figure 9.4.: Ground state optimized structures of coumarin and umbelliferone. All bond lengths in Å. Method: MP2/cc-pVTZ

.

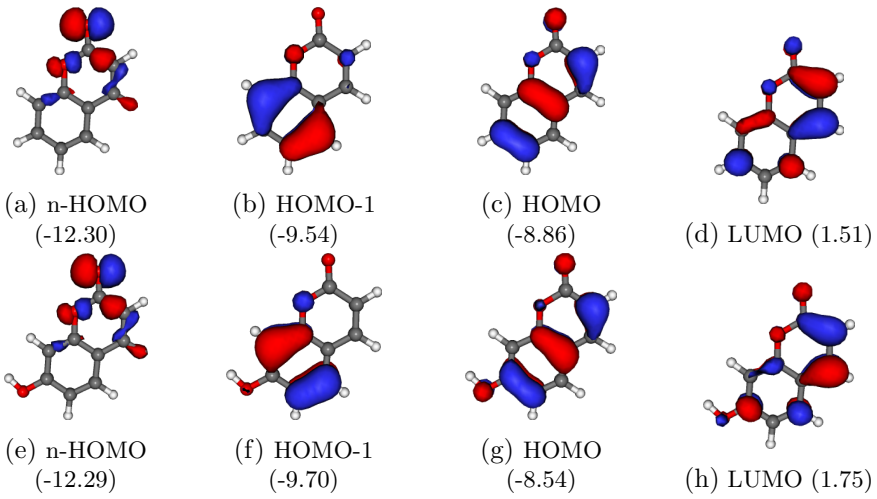

(a) n-HOMO (-12.30) (b) HOMO-1 (-9.54) (c) HOMO (-8.86) (d) LUMO (1.51)

(e) n-HOMO (-12.29) (f) HOMO-1 (-9.70) (g) HOMO (-8.54) (h) LUMO (1.75)

Figure 9.5.: Most relevant molecular orbitals of coumarin ((a)-(d)) and umbelliferone **2** ((e)-(h)) and their energies in eV. LUMO is the lowest unoccupied orbital when Rydberg orbitals are disregarded. n-HOMO denotes the highest occupied non-bonding orbital.

The obtained bond lengths are similar for both molecular structures. It should be mentioned that for umbelliferone another ground state minimum structure, denoted as **2a**, exists in which the hydroxy group has been rotated by 180 degrees around the C^7O^{12} bond. These two isomers have almost the

same bond lengths and the isomer shown in Figure 9.4 is only 0.3 kcal/mol lower in energy. However, they differ with respect to their dipole moments: The dipole moment of **2** amounts to 4.23 D and the one of its isomer **2a** is 6.80 D according to MP2/aug-cc-pVTZ. The dipole moment of unsubstituted coumarin itself is 4.49 D. As subtle differences in the electronic structure can lead to a significantly different photophysical and photochemical behavior, we considered both isomers in our calculations, especially with respect to solvent effects. However, no significant differences occurred although the excited state dipole moments differ, as well. Therefore, we omit this isomeric structure for the discussion here but mention that for an accurate determination of dipole moments both would have to be considered.

Table 9.3.: Vertical excitation energies (ΔE), oscillator strengths (f) and orbital-relaxed dipole moments (μ) of the three lowest electronically excited states in coumarin **1** and umbelliferone **2**. Ground state dipole moments are included for comparison. Method: MP2/cc-pVTZ//ADC(2)/aug-cc-pVTZ. Experimental values obtained in methanol solution (compare Figure 9.1).

State	ΔE		f	μ	exp.	
	(eV)	(nm)		(D)	(eV)	(nm)
Coumarin						
$1^1A'$				4.67		
$2^1A'$ ($\pi\pi^*$)	4.25	292	0.14	5.60	4.00	310
$3^1A'$ ($\pi\pi^*$)	4.98	249	0.22	6.46		
$1^1A''$ ($n\pi^*$)	4.50	275	-	0.31	-	-
Umbelliferone						
$1^1A'$				3.68		
$2^1A'$ ($\pi\pi^*$)	4.25	292	0.35	5.77	3.95	314
$3^1A'$ ($\pi\pi^*$)	4.71	263	0.08	5.17		
$1^1A''$ ($n\pi^*$)	4.60	270	-	0.75	-	

In all molecules the lowest excited singlet state ($2^1A'$) is of $\pi\pi^*$ character and dominated by a HOMO to LUMO transition (64 % and 72 % in **1** and **2**, respectively) although HOMO-1 to LUMO can play a significant role, as well (21 % and 10 % in **1** and **2**, respectively). The energetic position of this state with respect to the ground state is almost identical for all three molecules and a bit higher than experimentally measured in solution. However, the dipole moments increase slightly and a small energy stabilization by polar solvents can be expected. In the course of this excitation the electron density in the C^3C^4 double bond is reduced and an elongation of this bond is expected to take place after the photoexcitation into this state.

About 0.3 eV higher in energy a dark $n\pi^*$ state ($1^1A''$), corresponding to the excitation of the carbonyl lone pair into the ring system, is found. This excitation leads to a strong change of the dipole moment and therefore strong solvent effects are expected. Specifically, this state should be destabilized by polar solvents and shifted to higher energies which coincides with the general observation that $n\pi^*$ states are usually shifted to higher energies when the

solvent polarity is increased.

The next state ($3^1A'$) is again of $\pi\pi^*$ character and has significant multiconfigurational character. The largest contribution corresponds to a HOMO-1 to LUMO excitation but several others are included, as well. For umbelliferone this state is situated closer to the first excited state than for coumarin.

All in all, the gas phase vertical excitation calculations are able to represent the overall experimentally observed spectral features. As in the linear absorption spectra, the transition to the second optically-allowed excited singlet state is more pronounced than the one to the first in coumarin and *vice versa* in umbelliferone (compare oscillator strengths in Table 9.3). At the same time, the energies of these two electronic transitions are much closer in umbelliferone than in coumarin. Consequently, the second peak in the linear absorption spectrum of umbelliferone forms only a shoulder on the first peak.

9.4. Fluorescence and Relaxation Pathways

In this section, the position of energetic minima on the first $\pi\pi^*$ and $n\pi^*$ potential energy surfaces (PES) will be determined and two different radiationless relaxation pathways into the ground state will be suggested. The solvent effects on these pathways and the following implications for the different photophysical behavior of coumarin and umbelliferone will be discussed in Section 9.5.

9.4.1. Fluorescence and Ring cleavage

As mentioned above, the character of the $\pi\pi^*$ ($2^1A'$) state suggests an elongation of the C^3C^4 double bond upon electronic excitation. Surprisingly, geometry optimizations (without any symmetry restrictions and after a small distortion from planarity) on its surface led to structures shown in Figure 9.6. To exclude any basis set effects, the aug-cc-pVTZ basis set was used but with respect to numerically more demanding cases it is worthwhile to mention that similar structures were obtained with cc-pVTZ in all cases (not explicitly shown here).

The double bond is indeed longer than in the ground state (by about 4-5 pm). However, the lactone bond between O^1 and C^2 is broken in addition and the molecule is strongly distorted. The predicted fluorescence energy amounts to only 0.72 eV in coumarin (and 0.66 eV in **2**) which is far too low compared to experimental values of approximately 3 eV as well as the values for the SE presented above. Moreover, the oscillator strength is drastically reduced (to about 0.02) compared to the Franck-Condon region.

In several earlier studies, e. g., [196, 197], the obtained fluorescence energies matched the expected ones and no such distortion was observed. Consequently, we tested other methods for comparison to gain further insight into this phenomenon. First of all, ri-CC2 led to essentially the same results and ring-opened structures. However, TDDFT results varied strongly with the functional used. BHLYP (50 % exact Hartree-Fock exchange) gave a structure that is hardly distorted but with reduction of the amount of exact HF exchange the results became more and more similar to ADC(2). In Figure 9.7 the respective structures

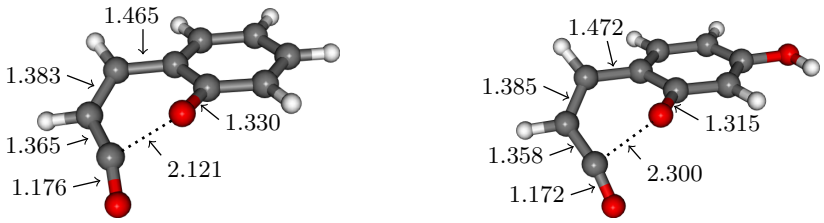

(a) coumarin **1** (b) umbelliferone **2**

Figure 9.6.: S_1 minimum geometries of coumarin and umbelliferone. All bond lengths in Å. Method: ADC(2)/aug-cc-pVTZ.

obtained for coumarin with the functionals B3LYP (20 % exact Hartree-Fock exchange) and BHLYP are displayed.

(a) TD-B3LYP (b) TD-BHLYP

Figure 9.7.: $1^1A'$ minimum geometries of coumarin obtained with TD-B3LYP and TD-BHLYP. All bond lengths in Å. Basis set: aug-cc-pVTZ.

In the next step we investigated the PES corresponding to this ring cleavage. For psoralen Tatchen et al. have previously suggested this pathway as a radiationless decay channel [203]. Here we focus on possible differences between coumarin and umbelliferone and seek for an explanation of this immense method discrepancy.

From the bond length of about 1.56 Å a relaxed PES scan was performed by elongating the C^2O^1 single bond of coumarin in small steps. This bond length was fixed and the rest of the molecule subjected to a geometry optimization on the S_1-surface. At smaller bond lengths constant root flipping with the dark $n\pi^*$ ($1^1A''$) state occurred so that no reasonable results could be obtained by constrained geometry optimizations. Up to this point a linear interpolation was performed by dividing the geometrical distortion into equal steps. This part of the PES is represented as dotted lines. At the point where the two methods are joined, a kink can be observed on the ground state surface. This is an artifact of the two different approaches. In the case of ground state optimizations a smooth surface without any intermediate minimum structures is obtained back from the distorted excited state structure to the ground state minimum presented above.

In all cases (regardless of the molecule or method used) the excited PES is quite flat (after an initial energy stabilization) and the oscillator strengths decrease continuously along the reaction coordinate. This flatness of the PES explains the large differences in the applied methods as small changes in the parameters can easily lead to extreme shifts of the shallow minima along the

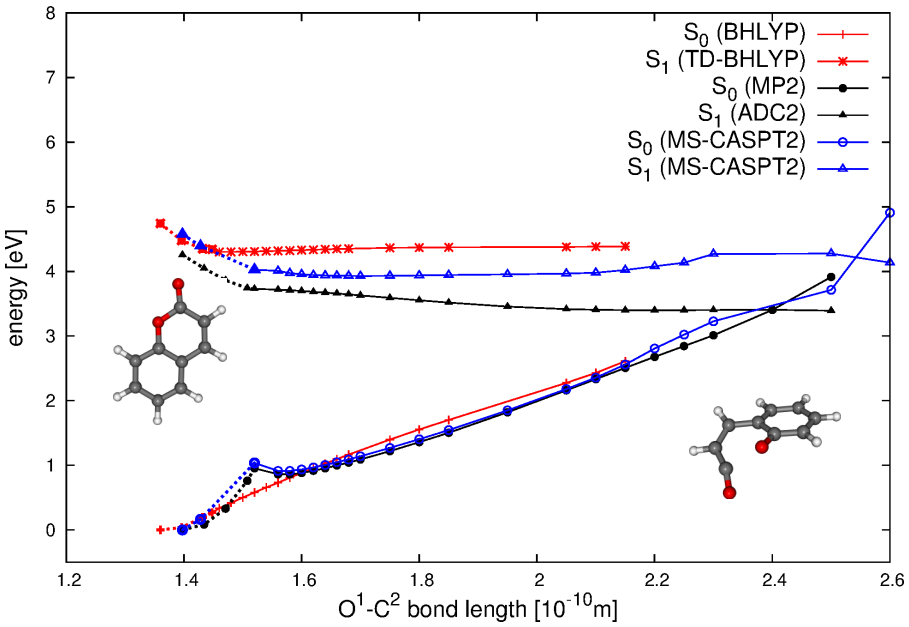

Figure 9.8.: Relaxed PES scan along the bond breaking path in coumarin obtained with ADC(2) and TD-BHLYP. Dotted lines obtained by linear interpolation. For structure optimization cc-pVDZ and for vertical excitation energies aug-cc-pVDZ as basis sets.

PES. In Figure 9.8 the analogous PES obtained by TD-BHLYP is included as an illustrative example. Although no significant energy barrier towards a ring opening exists either, the shallow minimum is shifted to the FC area of the potential energy surface.

The question arises whether the single-reference methods used so far are sufficient for the description of such a bond breaking. Therefore, MS-CASPT2 single point calculations were performed along the pathway obtained with ADC(2). The results are included in Figure 9.8. Here, as well, the excited state surface is very flat. Even the development of the ground state energies is almost identical to MP2. At large distortions stronger deviations between the two methods occur. However, this is not surprising because the structures were optimized with ADC(2). Geometry optimizations with MS-CASPT2, which we did not perform due to the high numerical effort, should lower the energy difference between the ground and first excited state and thereby reduce the slight reaction barrier towards the conical intersection observed here. Thus, we conclude that the flexibility of the configuration space included in ADC(2)-s is sufficient to describe the relaxation pathway. Moreover, Tatchen et al. obtained with the multi-reference method DFT/MRCI almost identical PESs for psoralen [203] as we for coumarin with ADC(2).

Additionally, this shows that such a ring cleavage might be a possible radiationless deactivation pathway not only in psoralen but other coumarin derivatives, as well. Once the molecules reach the ground state surface close to the intersection, the lactone ring closes yielding the original molecule and rendering the ring-opened structure an intermediate only. Similar ring opening reactions have also been observed in non-coumarinic systems, e. g., in benzospiropy-

ran [226], thiophene [178] or fluorinated indolylfulgides [227]. However, no significant differences between coumarin and 7-hydroxycoumarin can be observed in these gas phase calculations. The analogous PES for umbelliferone is depicted in Figure 9.9. Figures 9.9 and 9.10 show how higher excited singlet state and triplet states evolve along the PES of the bond breaking pathway in umbelliferone. In particular, it can be seen how the first excited singlet $n\pi^*$ state raises along this pathway rendering a transition as discussed in the next section less probable and supporting the assumption that the branching point between this and the second radiationless decay channel (see Section 9.4.2) lies close to the Franck-Condon point (compare as well Section 9.10). The same situation applies to coumarin, as well (not shown here).

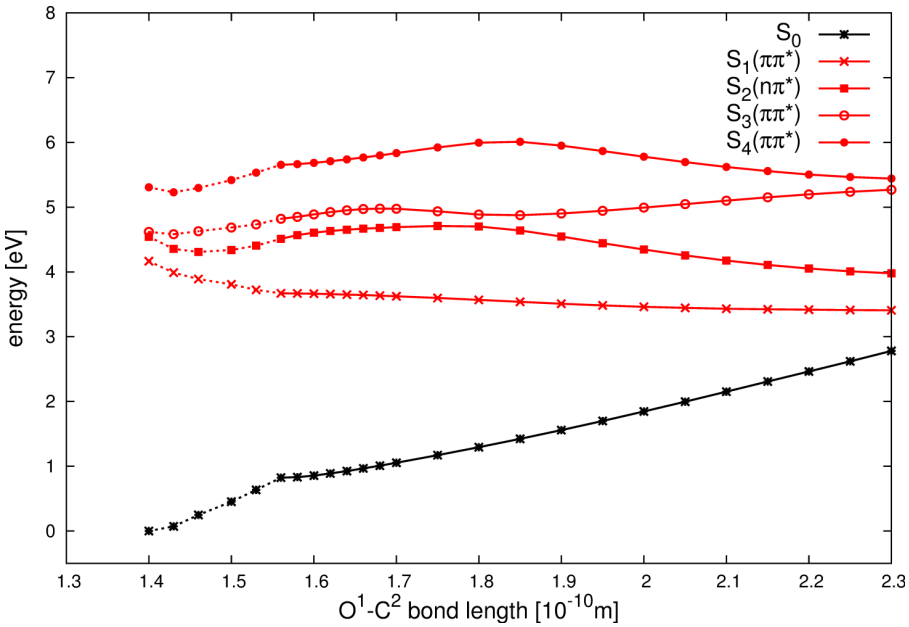

Figure 9.9.: Relaxed PES scan along the bond breaking path in umbelliferone in the gas phase. Red curves: Excited singlet states. Black curve: Ground state. Dotted lines obtained by linear interpolation. For structure optimization cc-pVDZ and for vertical excitation energies aug-cc-pVDZ were taken as basis sets. Character of the states ($n\pi^*$ or $\pi\pi^*$) with respect to Franck-Condon point (along the reaction pathway the states start to mix and intersections occur).

9.4.2. Carbonyl stretching mode

In order to find alternative reaction pathways, the potential energy surfaces of coumarin along the different vibrational normal modes were calculated and searched for hints to radiationless relaxation pathways. With this respect, the carbonyl stretching mode could be identified as a promising deactivation pathway. Figure 9.12 shows the obtained PES for coumarin and umbelliferone along the respective carbonyl stretching modes. As the $3^1A'(\pi\pi^*)$ state is not lowered in energy along this pathway and does not interact with the two energetically lower states it was omitted from the plots for the sake of clarity.

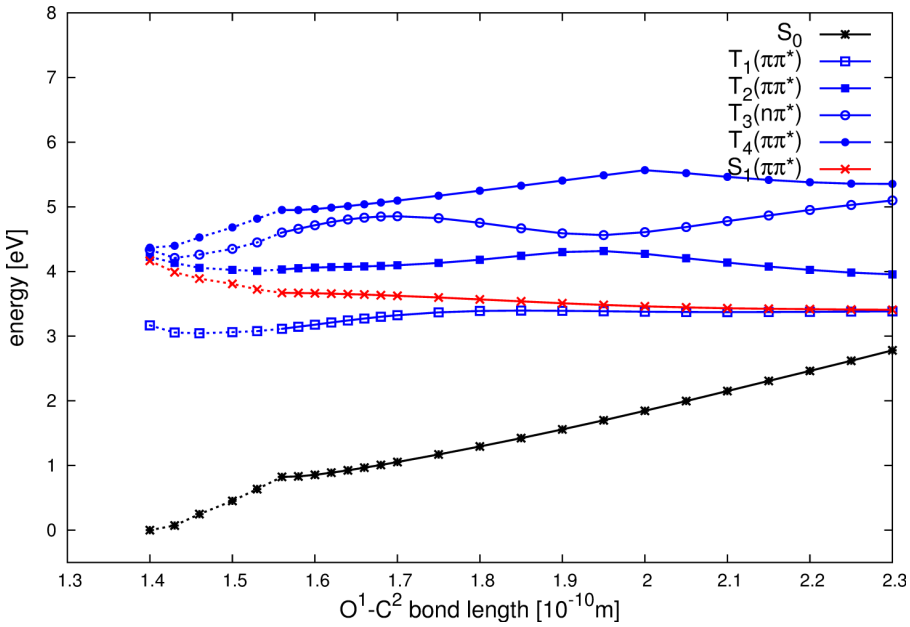

Figure 9.10.: Relaxed PES scan along the bond breaking path in umbelliferone in the gas phase. Red curves: Excited singlet states. Blue curves: Excited triplet states. Black curve: Ground state. Dotted lines obtained by linear interpolation. For structure optimization cc-pVDZ and for vertical excitation energies aug-cc-pVDZ were taken as basis sets. Character of the states ($n\pi^*$ or $\pi\pi^*$) with respect to Franck-Condon point (along the reaction pathway the states start to mix and intersections occur).

Along this normal mode, an intersection between $2^1A'(\pi\pi^*)$ and $1^1A''$ $(n\pi^*)$ is found. In principle, the two states belong to different irreducible representations rendering a transition forbidden, however strong vibrational coupling between the two states by non-totally-symmetric normal modes can be expected making this path accessible. After transition, a significant energy stabilization and a second intersection with the ground state occurs. This should lead to an efficient relaxation pathway back into the ground state. Indeed, a geometry optimization in the $1^1A''$ state shows that the minimum of the PES shown and the minimum of the $1^1A''$ surface lie close to each other (Figure 9.11). The motion along the carbonyl stretching mode can thus be used as a viable way to mimic the relaxation into the dark $n\pi^*$ state. These findings are in line with the observation by Tatchen et al. [203] that the energetic order of the two first excited states is reversed at the $1^1A''$ minimum geometry. Here we were able to identify roughly the position of the conical intersection between the two states. The activation energy for this pathway is negligible.

As far as the comparison of coumarin and umbelliferone is concerned no significant difference for the two molecules can be observed as was already the case for the relaxation pathway along the ring opening. The inclusion of solvent effects are of particular interest as significant shifts of the $n\pi^*$ state can be expected.

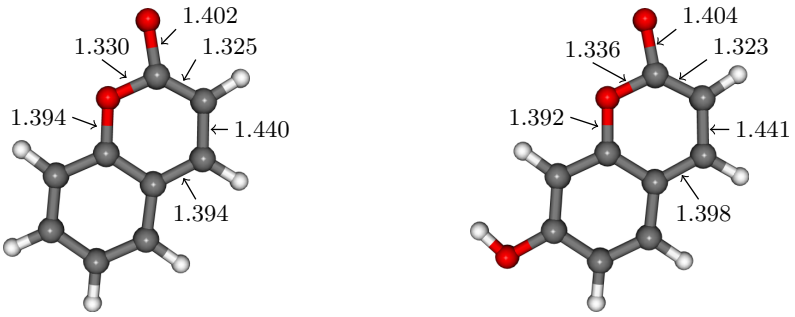

(a) coumarin (**1**) (b) umbelliferone (**2**)

Figure 9.11.: $1^1A''$ ($n\pi^*$) minimum geometries of coumarin and umbelliferone. All bond lengths in Å. Method: ADC(2)/cc-pVTZ.

9.5. Solvent Effects

As mentioned above, solvent effects play an important role for the photophysical behavior of coumarin derivatives. Therefore, we will focus in this part on their effect on coumarin and umbelliferone. Due to the low polarity of cyclohexane, the gas phase calculations are expected to be a good approximation and no big deviations from the results presented above should occur. Among the three solvents used in the experiments discussed in Section 9.1, methanol exhibits a high polarity and the largest effect on the photophysical behavior of coumarin. Consequently, we chose this solvent for our theoretical calculations to grasp the full solvent effect observed in the experiments.

9.5.1. Structures of solvated molecules and vertical excitation energies

As explicit interactions *via* H-bridges are significant in methanol, methanol molecules were explicitly included into the calculations. For coumarin two methanol molecules were included at the carbonyl group. In the case of the 7-hydroxycoumarin isomers two different arrangements of solvent molecules were tested. In the first one only two methanol molecules were incorporated in the same way as in coumarin. In the other one four methanol molecules were applied in order to mimic solvation effects at the hydroxy group. The ground state structures with inclusion of solvent molecules are shown in Figure 9.13. The frontier orbitals that are important for the first excited states are not significantly changed compared to the gas phase. Therefore we refrained from displaying them at this point.

The geometries are similar to the non-solvated structures. The bond lengths that are influenced most are the C^2O^{11} carbonyl double and the O^1C^2 lactone bond. This is not surprising as the coordination of solvent molecules leads to a shift of the electron density from the ring system (especially from O^1) towards O^{11}. Consequently, an elongation of the C^2O^{11} double bond and a contraction of the O^1C^2 lactone bond takes place.

Table 9.4 shows the vertical excitation energies at the optimized structures

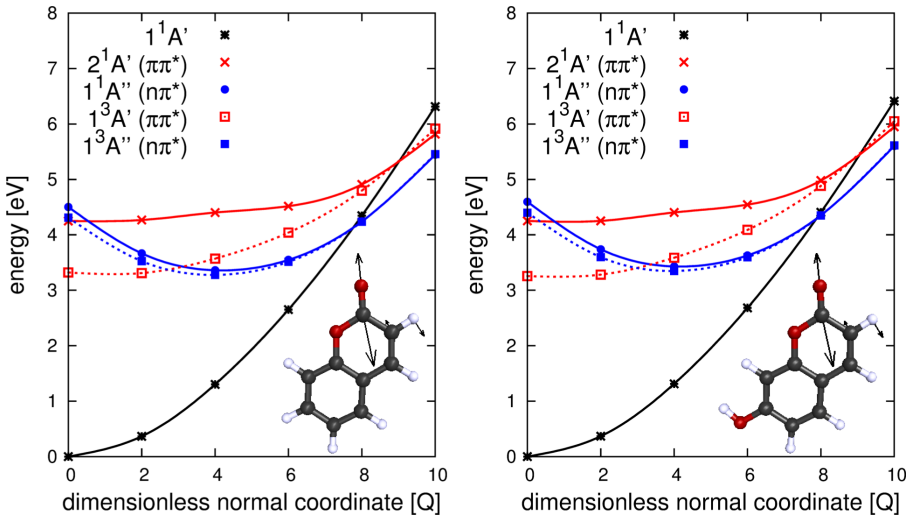

Figure 9.12.: Potential energy surfaces of the lowest excited singlet (continuous lines) and triplet (dotted lines) state of each symmetry along the carbonyl stretching mode of coumarin (left) and umbelliferone (right). Frequencies of the respective modes: 1822 cm^{-1} (coumarin) and 1824 cm^{-1} (umbelliferone). Distortion of 2Q leads to an elongation of the carbonyl double bond by about 0.1 Å in both molecules. Structures and frequencies obtained with MP2/cc-pVTZ and single point calculations with ADC(2)/aug-cc-pVTZ.

with and without application of the COSMO model. As expected, the $\pi\pi^*$ states are only slightly influenced while the $n\pi^*$ excitations are shifted to much higher energies and appear in most cases only as the third excited singlet states. These effects are more pronounced in umbelliferone and despite the large difference in the ground state dipole moments, the two umbelliferone molecules exhibit very similar excitation energies. Although the C_s symmetry of the gas phase structures is lifted, the lowest excited states still exhibit distinct $\pi\pi^*$ or $n\pi^*$ character.

As far as the validity of the different solvent models is concerned, it can be observed that explicit solvent interactions have a stronger effect on the energy of the first $\pi\pi^*$ excitation than implicit ones included *via* the COSMO model. However, the opposite is true for the first $n\pi^*$ state. Here, the excitation energies with or without explicit methanol molecules hardly differ as long as the COSMO model is applied additionally. Therefore it can be expected that explicit solvent interactions will mainly influence the pathway *via* ring opening while implicit interactions should be dominant for the relaxation into the dark $n\pi^*$ state along the carbonyl stretching mode.

The values obtained by a combination of the explicit solvent interactions and COSMO are in good agreement with the experimentally observed values (compare Table 9.3 and Figure 9.1). Concerning the oscillator strengths the same trends can be observed as in the gas phase calculations. While in coumarin the second transition has a higher intensity, the oscillator strength of the transition into the first excited singlet state is significantly larger in umbelliferone.

Table 9.4.: Vertical excitation energies (ΔE) and oscillator strengths (f) of the three lowest electronically excited states in coumarin **1** and umbelliferone **2** with inclusion of solvent molecules. Method: MP2/cc-pVTZ//ADC(2)/aug-cc-pVTZ.

State	ΔE	f	ΔE	f
	eV		eV	
Coumarin (**1**)			COSMO	
$2^1A'$ ($\pi\pi^*$)	4.25	0.14	4.30	0.14
$3^1A'$ ($\pi\pi^*$)	4.98	0.22	4.90	0.28
$1^1A''$ ($n\pi^*$)	4.50	-	5.02	-
Coumarin (**1**) + 2 MeOH			COSMO	
2^1A (mainly $\pi\pi^*$)	4.23	0.16	4.24	0.16
3^1A (mainly $\pi\pi^*$)	4.88	0.26	4.77	0.29
4^1A (mainly $n\pi^*$)	4.65	0.00	5.02	0.00
Umbelliferone (**2**)			COSMO	
$2^1A'$ ($\pi\pi^*$)	4.25	0.35	4.24	0.36
$3^1A'$ ($\pi\pi^*$)	4.71	0.08	4.68	0.06
$1^1A''$ ($n\pi^*$)	4.60	-	5.10	-
Umbelliferone (**2**) + 2 MeOH			COSMO	
2^1A (mainly $\pi\pi^*$)	4.16	0.37	4.11	0.40
3^1A (mainly $\pi\pi^*$)	4.66	0.05	4.60	0.04
4^1A (mainly $n\pi^*$)	4.73	0.00	5.10	0.00
Umbelliferone (**2**) + 4 MeOH			COSMO	
2^1A (mainly $\pi\pi^*$)	4.10	0.40	4.07	n.c.
3^1A (mainly $\pi\pi^*$)	4.61	0.05	4.57	n.c.
4^1A (mainly $n\pi^*$)	4.74	0.00	5.09	n.c.

9.5.2. Fluorescence and Ring cleavage

Geometry optimizations in the first excited $\pi\pi^*$-like state including methanol molecules were performed using the molecular ground state structures introduced above as starting points (Figure 9.13). While for coumarin with two methanol molecules only ring-opened structures were obtained, the S_1 minima of umbelliferone exhibit only small distortions and no broken bonds. The predicted fluorescence energies of umbelliferone are now in good agreement with the experiment where the broad fluorescence band is centered around approximately 3 eV (for respective values see Figure 9.13).

In order to determine the solvent effect on the energetic barrier for the relaxation *via* ring opening in umbelliferone, PES scans were performed. Up to the minimum structure a linear interpolation was used and from that point on a relaxed surface scan in which the O^1C^2 bond was gradually elongated. The results for umbelliferone are shown in Figure 9.14. It can be recognized that by inclusion of methanol molecules the minimum is clearly shifted towards the Franck-Condon zone. Additionally, a small energy barrier starts to form (about 0.9 and 1.4 kcal/mol for **2** + 2 MeOH and **2** + 4 MeOH, respectively). This barrier is not sufficiently high to efficiently suppress a relaxation along this pathway but it should be further enhanced by inclusion of more methanol molecules

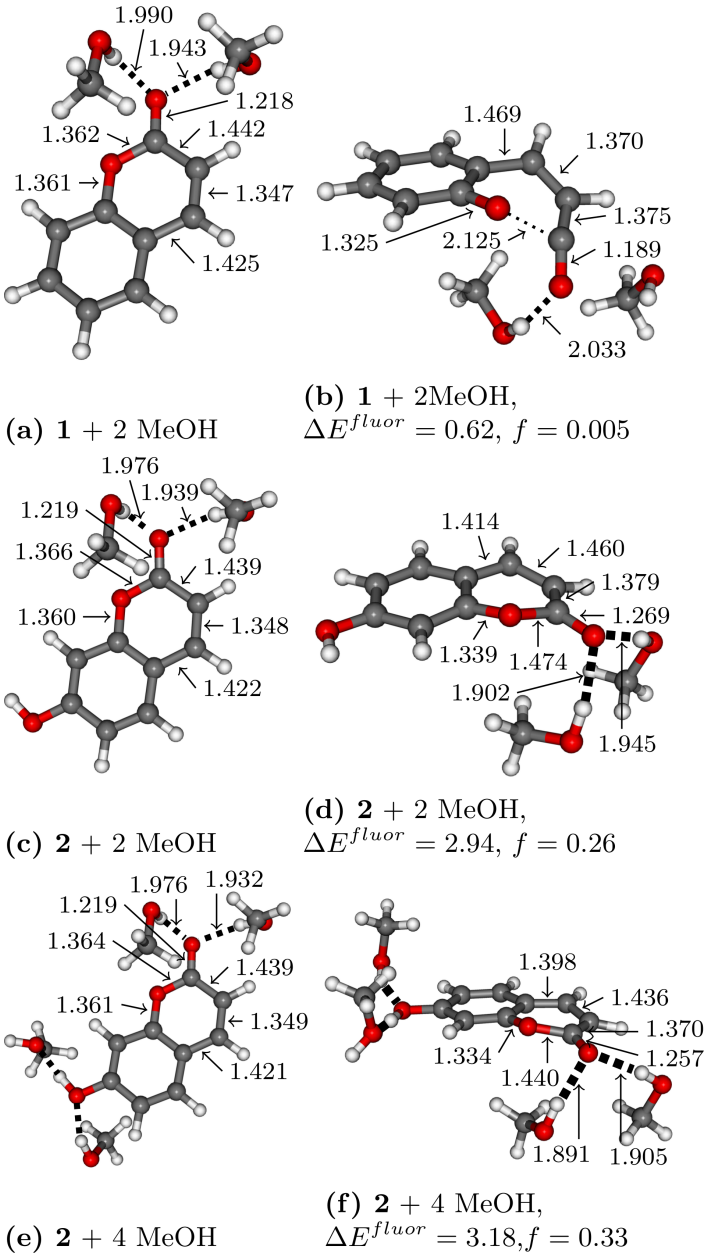

(a) 1 + 2 MeOH

(b) 1 + 2MeOH, $\Delta E^{fluor} = 0.62,\ f = 0.005$

(c) 2 + 2 MeOH

(d) 2 + 2 MeOH, $\Delta E^{fluor} = 2.94,\ f = 0.26$

(e) 2 + 4 MeOH

(f) 2 + 4 MeOH, $\Delta E^{fluor} = 3.18, f = 0.33$

Figure 9.13.: Optimized structures with inclusion of two or four methanol molecules at MP2/cc-pVTZ (ground state structures, left column) or ADC(2)/cc-pVTZ level (S_1 minimum structures, right column). All bond lengths in Å. Predicted fluorescence energies at these geometries in eV (ADC(2)/aug-cc-pVTZ) and oscillator strengths (length gauge) are given below the corresponding structure.

and by transition to more polar solvents like water. This is in accordance with the relatively low fluorescence quantum yields obtained for umbelliferone in methanol compared to the same molecule in water.

For coumarin several arrangements of methanol molecules were tested but in all cases ring-opened structures were obtained indicating that only the combined

effect of an electron donating group in the correct position and inclusion of solvent molecules can increase the electron density of the O^1C^2 bond sufficiently to avoid a ring opening.

All in all, it can be expected that with stronger electron donating substituents and with increasing solvent polarity the shift of electron density into the pyrone ring is enhanced and the relaxation *via* ring opening less pronounced. This might be a reason that in, e. g., 7-aminocoumarins with alkyl substituents at the nitrogen atom fluorescence quantum yields of approximately 1 can be achieved in polar solvents.

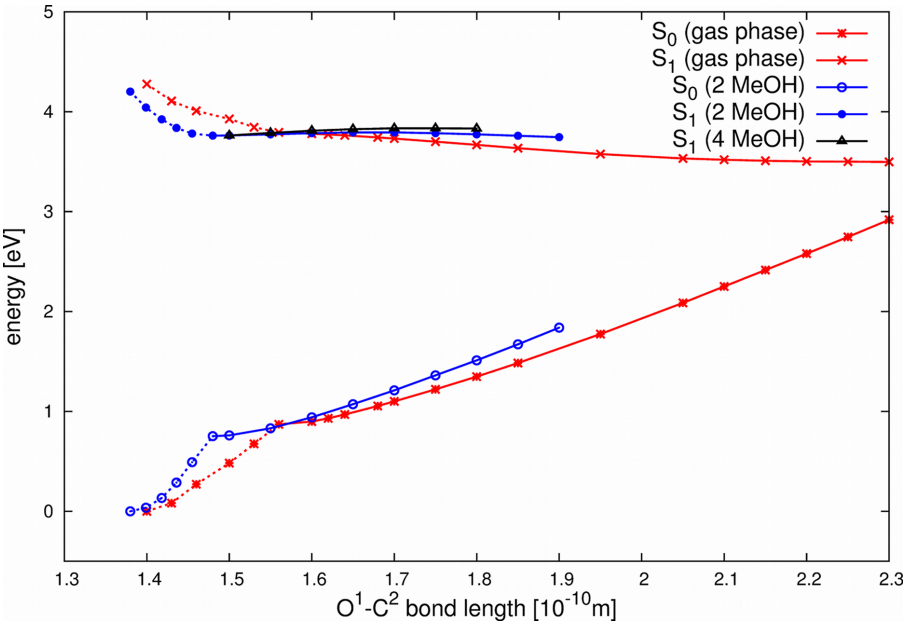

Figure 9.14.: Relaxed PES scan along the bond breaking path in umbelliferone in the gas phase, with inclusion of two methanol molecules and four methanol molecules. Dotted lines obtained by linear interpolation. For structure optimization cc-pVDZ and for vertical excitation energies aug-cc-pVDZ were taken as basis sets.

9.5.3. Carbonyl stretching mode

The PES for coumarin and umbelliferone along the carbonyl stretching mode with inclusion of solvent effects by the COSMO model in combination with explicit solvent molecules (two for **1** and four for **2**) are depicted in Figure 9.15. The C_s symmetry of the molecules is lifted by the methanol molecules and the former A' and A'' can principally interact leading to avoided crossings instead of the true crossings observed along the carbonyl stretching mode in the gas phase calculations. Therefore, additional single point calculations were performed close to such crossing points to estimate the splitting resulting from the reduced molecular symmetry. However, no significant splittings were observed. Therefore, we adopt the diabatic picture with true crossings of $\pi\pi^*$ and $n\pi^*$ states from the gas phase calculations for the plots of the PES with inclusion

of solvent molecules.

As was expected, the $n\pi^*$ state is strongly shifted upwards in energy for both molecules. This effect is stronger in umbelliferone and a relaxation into the dark $n\pi^*$ state seems to be quite disadvantageous as the crossing point lies about 0.32 eV (2581 cm^{-1}) above the FC point. For coumarin the intersection lies only approx. 0.04 eV (323 cm^{-1}) higher than the FC region. The corresponding radiationless relaxation should definitely be less efficient than in non-polar solvents such as cyclohexane but might be still well accessible. However, for a quantitative assessment more sophisticated solvent models would have to be applied and vibrational interactions between the states considered.

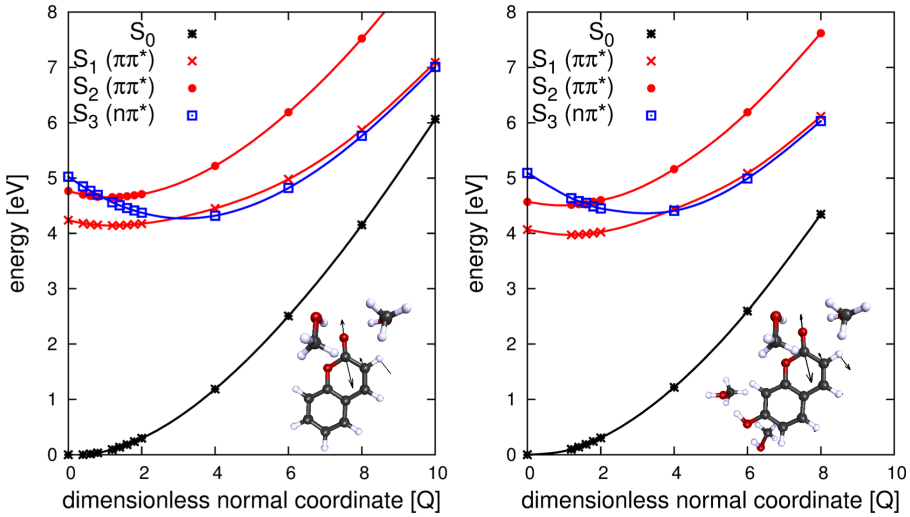

Figure 9.15.: Potential energy surfaces along carbonyl stretching mode of coumarin (left) and umbelliferone (right) with inclusion of two or four methanol molecules. Frequencies of the respective modes: 1773 cm^{-1} (coumarin) and 1770 cm^{-1} (umbelliferone). Distortion of 2Q leads to an elongation of the carbonyl double bond by about 0.1 Å in both molecules. Structures and frequencies are obtained with MP2/cc-pVTZ and single point calculations with ADC(2)/aug-cc-pVTZ.

9.6. Inter system crossing (ISC)

An interesting question remains concerning phosphorescence quantum yields. Coumarin in non-polar solvents can exhibit ISC which is reduced in more polar solvents. The question arises from which point of the PES the ISC occurs preferentially.

At the S_0 minimum structures a $^3n\pi^*$ state lies very close in energy to $^1\pi\pi^*$. According to El Sayed's rule [5], such a transition that is accompanied by a change in molecular symmetry should be enhanced. At the same time, a triplet state with $\pi\pi^*$ symmetry intersects with the $^1n\pi^*$ state close to its minimum (Figure 9.12).

To get an idea of the probability for transitions at these points the spin-orbit coupling matrix elements obtained with the newly implemented spin-orbit coupling code in Q-Chem (compare Section 5) and ADC(2)-s between $2^1A'$ and

$1^3A''$ at the S_0 geometry as well as between $1^1A''$ and $1^3A'$ at the $1^1A''$ minimum geometry were compared (Table 9.5). For comparison the respective values at the $2^1A'$ minimum geometry (ring-opened) were included although the lowest triplet state with $n\pi^*$ symmetry lies much higher in energy.

Table 9.5.: Singlet-triplet splittings (eV) and spin-orbit coupling matrix elements (cm^{-1}) at ADC(2)-s/aug-cc-pVDZ level at important points of the gas phase PES. Ψ_S and Ψ_T are the singlet and triplet wave functions used. $\langle \hat{H}_{SO} \rangle = \sqrt{\sum_{M=0,\pm1} |\langle A,0,0|H_{SO}|B,1,M\rangle|^2}$. $\Delta E = E(\Psi_T) - E(\Psi_S)$.

minimum structure of state	Ψ_S	Ψ_T	ΔE eV	$(\hat{H}_{SO})_{ST}$ cm^{-1}
Coumarin (1)				
gr. state (Fig. 9.4)	$2^1A'$ ($\pi\pi^*$)	$1^3A''$ ($n\pi^*$)	0.03	11.08
$1^1A''$ (Fig. 9.11)	$1^1A''$ ($n\pi^*$)	$1^3A'$ ($\pi\pi^*$)	0.29	40.72
$2^1A'$ (Fig. 9.6)	2^1A ($\pi\pi^*$-like)	2^3A ($n\pi^*$-like)	0.63	35.82
Umbelliferone (2)				
gr. state (Fig. 9.4)	$2^1A'$ ($\pi\pi^*$)	$1^3A''$ ($n\pi^*$)	0.12	14.32
$1^1A''$ (Fig. 9.11)	$1^1A''$ ($n\pi^*$)	$1^3A'$ ($\pi\pi^*$)	0.25	44.53
$2^1A'$ (Fig. 9.6)	2^1A ($\pi\pi^*$-like)	2^3A ($n\pi^*$-like)	0.49	38.02

While the values for **1** and **2** are similar, the coupling elements are significantly larger at the $1^1A''$ minimum structure than at the Franck-Condon point. This indicates that ISC from this state might be more efficient than from 2^1A‘ close to the vertical excitation. As the $n\pi^*$ state is less efficiently populated in polar solvents the ISC efficiency should decrease significantly. However, this assessment based on the energy splitting and spin-orbit coupling elements can only give a qualitative indication about the ISC efficiency and vibrational effects would have to be considered additionally for quantitative results.

9.7. Results for the Deprotonated, Anionic Form of Umbelliferone

Figure 9.16 shows the optimized structures for the anionic form of umbelliferone in the ground and first excited state. This molecule was only considered with inclusion of four methanol molecules as strong solvent effects can be expected and methanol is the only solvent used in this study in which it might be of importance (compare Section 9.10.5). The vertical excitation energies and strengths at the ground state minimum are given in Table 9.6 and the predicted fluorescence energy in Figure 9.16. Figure 9.17 shows the most important molecular orbitals for the first three excited states.

Both the predicted absorption and fluorescence energy are similar to values obtained for other umbelliferone derivatives [220, 228]. The minimum structure of the first excited state has a O^1C^2 bond length that is about 0.4 Å smaller than the one in umbelliferone itself (compare Figure 9.13) indicating an even larger reaction barrier for the ring opening. In order to estimate this barrier, a rough

relaxed PES scan was performed starting from the excited state minimum. The result is shown in Figure 9.19. The barrier is much larger than in umbelliferone and an efficient suppression of this radiationless decay channel can be expected. Due to the single-reference character of the ground state wave function used in our calculations we refrain from determining an explicit value for the activation energy.

Figure 9.18 shows the PES along the elongation of the $O^{12}C^7$ bond (former hydroxy group) as well as the carbonyl stretching mode. The shorter bond lengths, which the original carbonyl bond (C^1O^{11}) of umbelliferone has in the ground and excited state minima, indicate a higher carbonyl character in the C^1O^{11} bond than in the deprotonated hydroxy group. At the same time, the first $n\pi^*$ transition corresponds to an excitation of a non-bonding electron from the deprotonated hydroxy group. Therefore, we have chosen to perform scans along both bonds. However, no normal mode could be clearly attributed to the stretching of the $O^{12}C^7$ bond and this bond was manually distorted to obtain the respective PES. Along both pathways none of the higher states is sufficiently lowered in energy in order to allow for an interaction with the first excited state and the transition into a dark $n\pi^*$ state is not observable here.

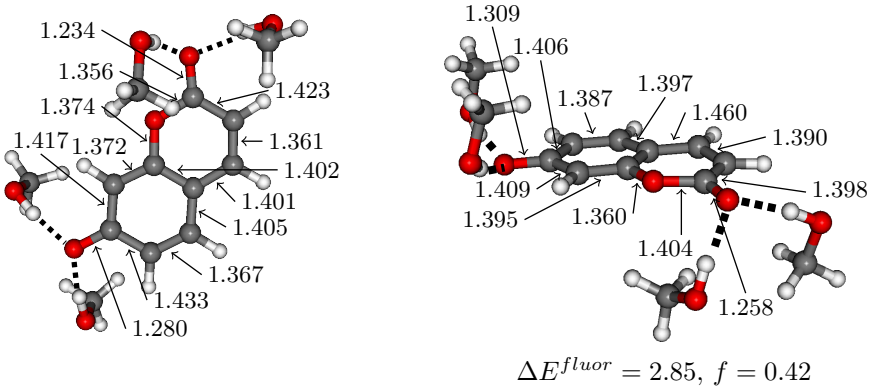

Figure 9.16.: Optimized structures of the deprotonated umbelliferone molecule with inclusion of four methanol molecules at MP2/cc-pVTZ (ground state structure, left column) or ADC(2)/cc-pVTZ level (S_1 minimum structure, right column). All bond lengths in Å. Predicted fluorescence energy in eV (ADC(2)/aug-cc-pVTZ, with COSMO) and oscillator strength (length gauge) are given below the corresponding structure.

9.8. Results for the Tautomerized Form of Umbelliferone

Figure 9.20 shows the optimized structures for the tautomerized form of umbelliferone in the ground state and first excited state. As in the case of the anionic system, no pure gas phase calculations were made. The obtained bond lengths clearly display that the C^7O^{12} bond of the former hydroxy group has double bond character. In the ground state, the tautomerized form is about 0.9 eV less stable than the original one. In the excited state, however, the energetic order is reversed and the tautomerized form is approx. 0.5 eV more stable

Table 9.6.: Vertical excitation energies (ΔE) and oscillator strengths (f) of the three lowest electronically excited states in the deprotonated umbelliferone with inclusion of four methanol molecules. Method: MP2/cc-pVTZ//COSMO-ADC(2)/aug-cc-pVDZ.

State	ΔE		f	dominant contribution
	(eV)	(nm)		
2^1A ($\pi\pi^*$)	3.32	374	0.48	HOMO→LUMO (57%)
3^1A ($\pi\pi^*$)	4.34	285	0.03	HOMO→LUMO+1 (22%)
				HOMO-1→LUMO(18%)
4^1A ($n\pi^*$)	4.40	282	0.00	n-HOMO→LUMO (53%)

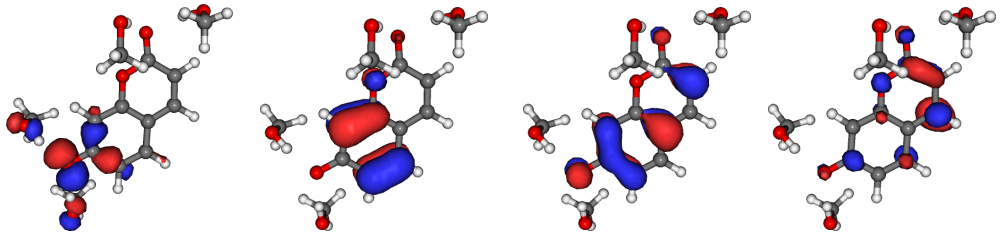

(a) n-HOMO (-12.53) (b) HOMO-1 (-9.21) (c) HOMO (-7.41) (d) LUMO (1.90)

Figure 9.17.: Most relevant molecular orbitals (HF/aug-cc-pVDZ) of the deprotonated form of umbelliferone and their energies in eV. LUMO is the lowest unoccupied orbital when Rydberg orbitals are disregarded. n-HOMO denotes the highest occupied non-bonding orbital.

(MP2/cc-pVTZ). The same result was obtained by Georgieva et al. [196, 204] who examined the tautomerization process along a chain of water molecules. They determined the excited state reaction barrier for such a tautomerization around 17.7 kcal/mol (0.8 eV) [204]. As methanol is slightly less basic than water this value can be seen as a lower bound for the activation barrier in methanol solution.

The vertical excitation energies and oscillator strengths at the ground state minimum are given in Table 9.7 and the predicted fluorescence energy in Figure 9.20. Figure 9.21 shows the most important molecular orbitals for the first three excited states. Again, the predicted absorption and fluorescence energies are similar to values obtained for other umbelliferone derivatives [220, 228].

In the minimum structure of the first excited state the O^1C^2 bond length is hardly elongated in this molecule. This indicates that the ring opening pathway is even less favored due to the substantial change in the electronic structure of the molecule. Concerning the relaxation *via* the carbonyl stretching mode (of the former hydroxy group) no normal mode could be identified that is largely decoupled from other bond and angle deformations. Therefore, the $O^{12}C^7$ bond was again manually distorted to obtain the respective PES (Figure 9.22). As was already the case for the anionic form of umbelliferone no efficient transition into the dark $n\pi^*$ state seems to be possible along this pathway.

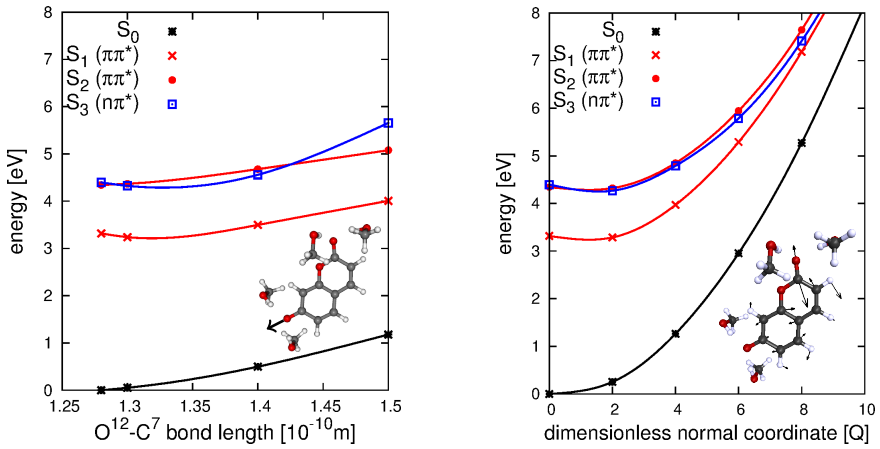

(a) (b)

Figure 9.18.: (a) PES along the elongation of the $O^{12}C^7$ bond (former hydroxy group) obtained by ADC(2)/aug-cc-pVDZ+COSMO. (b) PES of the lowest excited singlet states along the carbonyl stretching mode of the deprotonated umbelliferone molecule. Frequency of the respective mode: 1737 cm^{-1}. Distortion of 2Q leads to an elongation of the carbonyl double bond of about 0.08 Å. Structure and frequency obtained with MP2/cc-pVTZ and single point calculations with ADC(2)/aug-cc-pVDZ+COSMO.

Table 9.7.: Vertical excitation energies (ΔE) and oscillator strengths (f) of the three lowest electronically excited states in the tautomerized umbelliferone with inclusion of four methanol molecules. Method: MP2/cc-pVTZ//COSMO-ADC(2)/aug-cc-pVDZ.

State	ΔE		f	dominant contribution
	(eV)	(nm)		
2^1A ($\pi\pi^*$)	3.02	410	0.50	HOMO→LUMO (86%)
3^1A ($n\pi^*$)	3.76	330	0.00	n-HOMO→LUMO (80%)
4^1A ($\pi\pi^*$)	4.40	282	0.03	HOMO-1→LUMO (73%)

9.9. Global Target Analysis

Both the experimental as well as our theoretical results suggest a picture with two deactivation pathways back to the ground state. Therefore, a global target analysis (GTA) was performed in the group of M. Motzkus based on the model shown in Figure 9.23. Details can be found in [23].

A global target analysis allows one to interpret the experimental results with respect to a certain model. Among other characteristics, species associated spectra (SAS) can be obtained which show the spectral contribution to the signals arising from the different intermediate states in the model (here, A, B, and C). Additionally, the transient absorption traces based on the model assumed can be analyzed and compared with the experimental ones. The transient absorption traces show how the norm of a certain signal decays with time.

The agreement with the experimental results was very good and all main features of the relaxation dynamics were reproduced. Other models including

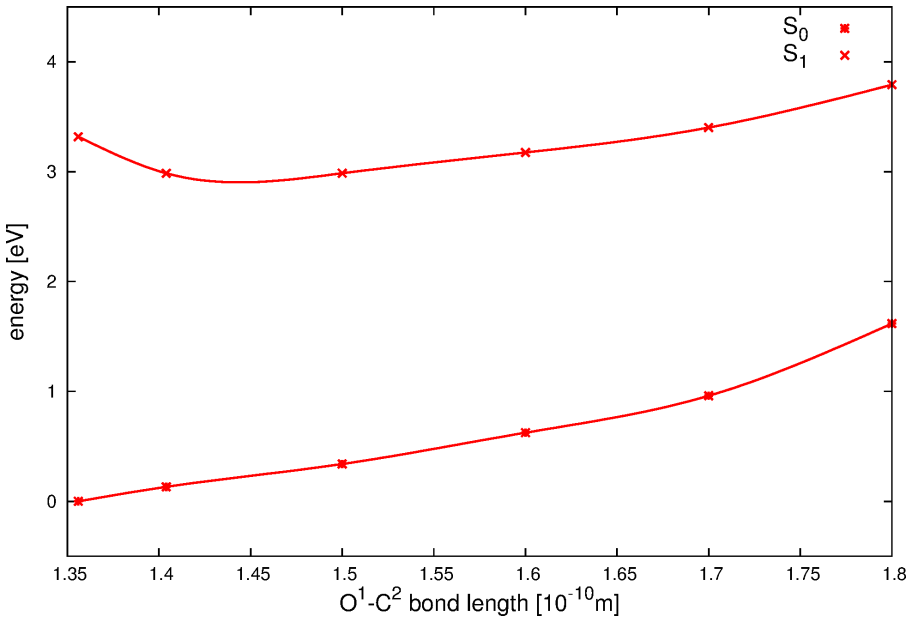

Figure 9.19.: Relaxed PES scan along the bond breaking path in deprotonated umbelliferone with inclusion of four methanol molecules. For structure optimization cc-pVDZ and for vertical excitation energies aug-cc-pVDZ (with COSMO) were taken as basis sets. The first point corresponds to the Franck-Condon point and the second one is the minimum of the S1 state as obtained by ADC(2)/cc-pVTZ (without COSMO).

a sequential relaxation matrix were tested, as well, but yielded a worse agreement with experiment. An important observation within the obtained transient spectra is that the simulated emission occurs mainly along only one of the two relaxation paths. This is in accordance with our theoretical results and the relaxation into a dark $n\pi^*$ state as one possibility. The rate constants obtained from the GTA for the two molecules in different solvents are shown in Table 9.8.

Table 9.8.: Time constants obtained by global target analysis using the model depicted in Figure 9.23.

Molecule/Solvent	t_1 / ps	t_2 / ps	t_3 / ps	t_4 / ps
Umbelliferone				
Methanol	0.9	1	7.1	>100
Acetonitrile	0.09	3.9	7.1	34
Coumarin				
Methanol	0.1	1.6	1.8	9.5
Acetonitrile	0.12	16	2	22
Cyclohexane	0.06	1.26	1.88	25

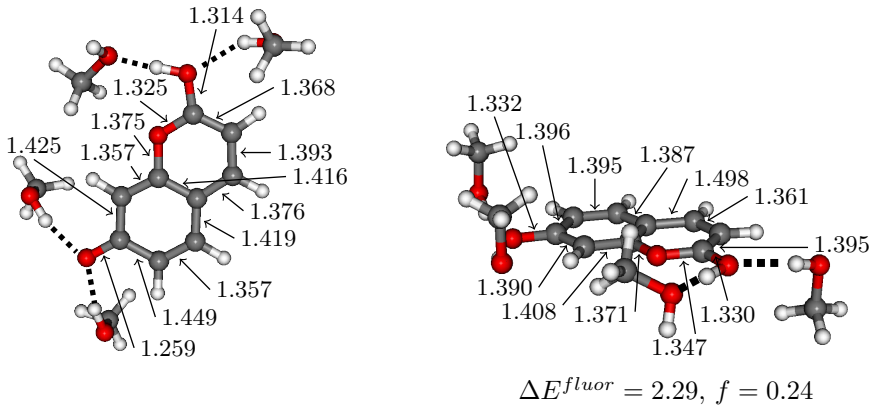

Figure 9.20.: Optimized structures of the tautomerized umbelliferone molecule with inclusion of four methanol molecules at MP2/cc-pVTZ (ground state structure, left column) or ADC(2)/cc-pVTZ level (S_1 minimum structure, right column). All bond lengths in Å. Predicted fluorescence energy in eV (ADC(2)/aug-cc-pVTZ, with COSMO) and oscillator strength (length gauge) are given below the corresponding structure.

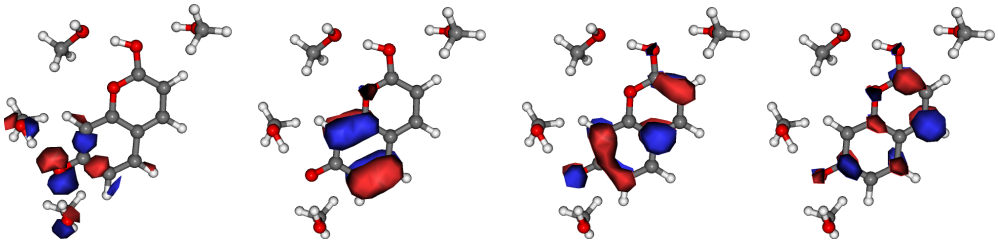

(a) n-HOMO (-11.38) (b) HOMO-1 (-9.81) (c) HOMO (-7.94) (d) LUMO (1.09)

Figure 9.21.: Most relevant molecular orbitals (HF/aug-cc-pVDZ) of the tautomerized form of umbelliferone and their energies in eV. LUMO is the lowest unoccupied orbital when Rydberg orbitals are disregarded. n-HOMO denotes the highest occupied non-bonding orbital.

9.10. Discussion

The results obtained by theoretical calculations and time-resolved spectroscopy will be compared and analyzed with respect to each other. In the first section, umbelliferone in methanol will be taken as an example and the experimentally and theoretically obtained relaxation pathways discussed and assigned to each other. In the next part, we will focus on the comparison between the two molecules, coumarin and umbelliferone. Then, solvent effects, inter-system crossing and, finally deprotonation and tautomerization of umbelliferone will be discussed. Figure 9.24 summarizes the main results obtained during this study.

9.10.1. Electronic State Assignment

The theoretically determined possibility of a branching of the photochemical relaxation pathways is strongly supported by the almost perfect agreement be-

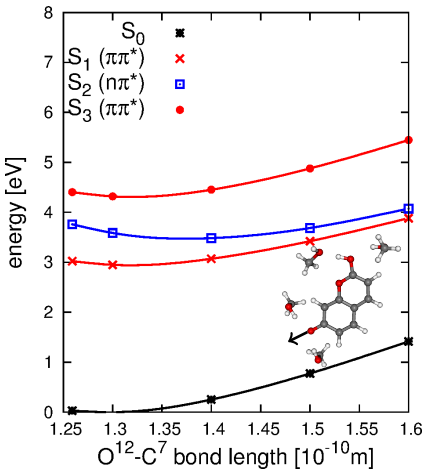

Figure 9.22.: PES along the elongation of the $O^{12}C^7$ bond (former hydroxy group) obtained by ADC(2)/aug-cc-pVDZ+COSMO.

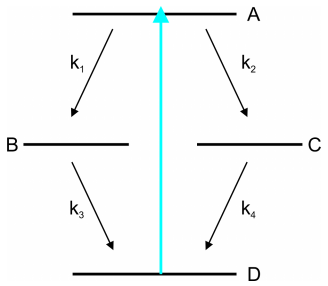

Figure 9.23.: Relaxation model used in the global target analysis. k_1-k_4 are rate constants for the respective decays.

tween the global target analysis and the experimental results. In the suggested model (compare Figure 9.23) state A is populated after an initial vertical excitation. From here, two parallel relaxation pathways start leading to components B and C. Based in the species associated spectra obtained from the global target analysis, no emission occurs from species B while component C shows strong stimulated emission.

During the theoretical calculations the two different relaxation pathways were identified as relaxation along the carbonyl stretching mode into the dark $n\pi^*$ and along the bright $\pi\pi^*$ state into the S_1 minimum. From the S_1 minimum either further relaxation *via* opening of the lactone ring or fluorescence is possible.

Based on these combined results, we assign state B to the minimum of the dark S_2 ($n\pi^*$) in which the carbonyl bond has been elongated and state C with the bright S_1 ($\pi\pi^*$) minimum (compare Figure 9.24). Consequently, the decay rates of component A into B and C reflect the whole decay time from the Franck-Condon region down to the minima of the S_2 and S_1 states, respectively.

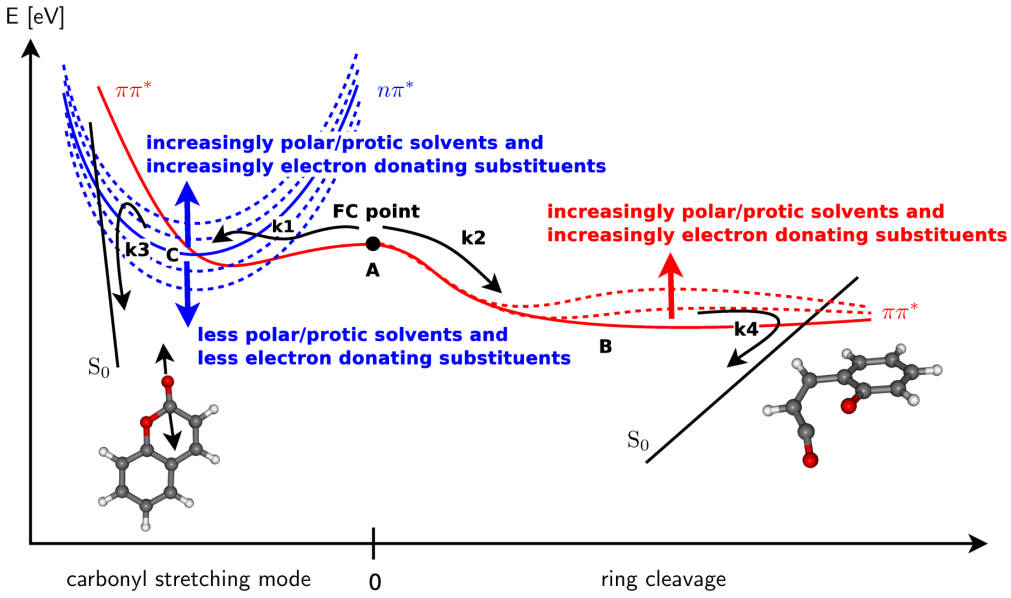

Figure 9.24.: Schematic representation of the relaxation pathways in coumarin and its derivatives. The solid lines correspond approximately to the situation of coumarin in methanol solution. Dotted lines indicate the effect of other solvents and substituents. The states A, B and C as well as the rate constants k1-4 correspond to the relaxation model of Figure 9.23 and Table 9.8.

9.10.2. Coumarin and Umbelliferone

The low barriers along the two relaxation pathways obtained theoretically may explain the ultrafast time scales obtained for the internal conversion from the FC region into the S_1 and S_2 minima of the PES.

However, calculations involving solvent effects *via* a combination of explicit methanol molecules and the COSMO model (Figure 9.15) show that for coumarin the position of the intersection with the dark S_2 state is closer to the FC point and lower in energy than for umbelliferone. At the same time, the relaxation process *via* ring opening in the $\pi\pi^*$ state exhibits only minor differences for the two molecules under consideration. The minimum on the $\pi\pi^*$ state of umbelliferone in methanol lies closer to the FC region than the one for coumarin but the reaction barrier along this branch seems to be negligible in both cases (compare Figure 9.14).

Thus, with the assumption of a similar evolution on the PESs of $n\pi^*$ and $\pi\pi^*$ states for both molecules, the shifting of the intersection with the dark $n\pi^*$ state must determine the different branching ratio between the S_2 and S_1 states (compare Figure 9.24). Such a variation of the branching ratio with the position of the intersection is nicely reproduced by the target analysis for coumarin and umbelliferone in methanol. The internal conversion between the FC region and the $n\pi^*$ state is much faster in coumarin than in umbelliferone. Additionally, the ratio between the decay rates favors relaxation into the dark state in the case of coumarin. This implies why coumarin shows much less fluorescence than other coumarin derivatives like, e. g., umbelliferone.

9.10.3. Solvent Effects

Although the evolution of the dynamics seems not to be coupled to any dynamic solvation effect, the static interaction of the electronic states with the solvent could be clearly observed for both coumarin derivatives in the theory as well as in the experiment.

In the gas phase calculations, both relaxation pathways observed during the computational analysis seem to be similarly well accessible. This changes when a solvent environment is taken into account. The influence on the $1^1\pi\pi^*$ PES is minor. However, the polarity of the solvent and its ability to form hydrogen bonds are significant for the energetic position of the $1^1n\pi^*$ state. In polar solvents, the $1^1n\pi^*$ state is strongly affected and is shifted up in energy for both derivatives, as expected, rendering a relaxation *via* this state and the carbonyl stretching mode less efficient. This effect is slightly more pronounced in umbelliferone. However, due to the curvatures of the PES of the first $\pi\pi^*$ and $n\pi^*$ states small differences in the relative energetic position lead to comparatively large shifts of the intersection (Figure 9.15, 9.24). The PES shown in Figure 9.15 was obtained by inclusion of both, interaction with explicit solvent molecules and a dielectric continuum *via* the COSMO model. When only the COSMO model is applied the PES is slightly shifted downwards in energy and the intersection lies much closer to the FC point. As the dielectric constant (the dominating parameter in continuum solvation models as COSMO) of acetonitrile is very similar to the one of methanol and given the unimportance of explicit solvent interactions in acetonitrile solution such a PES can serve as a good model for the situation in acetonitrile. This explains nicely the observed shift of the branching ratio favoring relaxation *via* the $n\pi^*$ state when using acetonitrile instead of methanol as solvent. Thus, the dielectric constant used in the COSMO model alone does not reproduce the strong differences observed in the polarity and the polarizability of methanol, acetonitrile and cyclohexane and explicit solvent interactions (or their absence) have to be considered.

9.10.4. Inter-system Crossing (ISC)

A long-living contribution to the signal of coumarin as well as umbelliferone [23] indicates the presence of a triplet absorption. The efficiency of the ISC is known to be extremely low for coumarins, leading to the very weak signal amplitudes observed in the experiment ($< 2\,\%$). In the theoretical calculations (Section 9.6) the ISC seems to be larger from the first $n\pi^*$ state than from the $\pi\pi^*$ state. Although it is not possible to determine experimentally from which singlet state the triplet manifold is populated, the relative amplitude of this long contribution in different solvents shows a similar trend like the one observed in the theoretical calculations: Less polar solvents like acetonitrile, which show a more efficient population of the $n\pi^*$ state, show slightly stronger ISC ($\sim 2\,\%$) than in the very polar methanol ($\sim 1\,\%$).

9.10.5. Deprotonation and Tautomerization of Umbelliferone

As mentioned in the introduction, the acidity of umbelliferone is strongly increased in the first excited state leading to a possible deprotonation of the hydroxy group. Alternatively, a tautomerization can occur, either *via* deprotonation and subsequent reprotonation at the former carbonyl functionality or *via* a proton transfer along a chain of solvent molecules. These species have been thoroughly studied [188, 190, 196–198, 202, 204, 209, 219, 220, 228–230]. Nevertheless, they play no role in neutral aprotic solvents (like acetonitrile or cyclohexane) and have only minor effects in neutral, non-aqueous alcoholic solutions (e. g., [220, 221]). A fluorescence spectrum in methanol that further supports this assumption can be found in the supporting information of [23].

For the sake of completeness we have investigated the influence of deprotonation on the presented relaxation pathways by theoretical methods. Within the experiment no clear contribution to the SE spectra of umbelliferone (in methanol expected to occur at wave lengths of approx. 450nm (deprotonated) and 500nm (tautomer) [220]) was observed. In summary, deprotonation as well as tautomerization leads to a significant reaction barrier along the ring opening pathway in accordance with the principles illustrated in Figure 9.24. Consequently, the fluorescence of these species is more efficient than of umbelliferone in its original form. If conditions are present that lead to an efficient formation of anionic or tautomerized species in the excited states, the fluorescence of umbelliferone itself is further quenched in favor of the stronger emitting forms. For the sake of simplicity we chose to use only pure solvents for this work. As the solubility in water is too low, we present no experimental results in water.

9.11. Conclusions

In the present chapter we have investigated the ultrafast relaxation network of coumarin derivatives using time-resolved femtosecond spectroscopy and quantum chemical calculations. The findings of this work finally clarify the long standing question about the low fluorescence quantum yields of coumarins and the related ultrafast relaxation deactivation of the excited state. On the basis of experimental and theoretical results, a model for the relaxation was suggested that comprises two parallel radiationless pathways after excitation into the first singlet $\pi\pi^*$ state. One leads along the PES of this bright $\pi\pi^*$ state *via* (intermediate) breaking of the lactone bond and the other one by transition into a dark $n\pi^*$ state along the carbonyl stretching mode. The fluorescence occurs from the initially excited $\pi\pi^*$ state close to the FC point. Especially, our results reveal that the radiationless relaxation *via* ring opening plays a crucial role for the photophysical behavior in the basic coumarin unit. To the best of our knowledge such a mechanism has only been previously observed in psoralen [203]. The branching ratio between the two pathways is determined by the position of the intersection that leads to a transition into the dark $n\pi^*$ state. Depending on the static interaction between solvent and coumarin derivative, this intersection can be shifted strongly affecting the branching ratio and, therefore, the fluorescence quantum yield. For example, for solutions in methanol, this intersection

lies much closer to the FC point in coumarin than in umbelliferone leading to a lower fluorescence quantum yield. Moreover, our results also clearly demonstrate the effect of an environment and the importance of taking into account the explicit interaction with solvent molecules.

10. Summary and Outlook

Within this work, methods for the description and analysis of electronically excited states of different type were implemented within the algebraic diagrammatic construction (ADC) family of methods and thoroughly tested. Additionally, ADC methods were employed in a photochemical study.

First, the scaled-opposite spin (SOS) approximation was applied to the extended ADC(2) method to provide a more efficient treatment of doubly excited states in extended systems. Secondly, the atomic mean-field integral program `AMFI` of B. Schimmelpfennig was used to implement the calculation of spin-orbit coupling elements for the whole hierarchy of ADC methods up to third order. These quantities play an important role for the understanding of photochemical relaxation pathways. First test calculations showed very good results. The third theoretical development was concerned with the differentiation between single-particle excitations and so-called plasmons, which are of great importance in the field of organic electronics. Here, an approach established by Bernadotte et al. for the semi-empirical time-dependent density functional theory (TDDFT) method [167] was transferred to the *ab initio* ADC models and shown to work reliably for the identification of plasmons in a series of linear polyenes. All three theoretical methods were implemented in a development version of the `adcman` module of the Q-Chem program package [19, 20]. Finally, ADC methods were used in combination with experimental results obtained in the group of M. Motzkus to successfully unravel the photochemical relaxation network of coumarin derivatives. In the following, the results from these four parts are discussed in more detail.

The newly derived extended SOS-ADC(2) approach was presented in Chapter 4. The SOS approximation [21] is based on the idea to neglect certain doubly excited configurations and to scale the remaining elements of the ADC secular matrix with an empirical parameter for compensation. Therefore, the dimensionality of the ADC secular matrix in second order can be reduced. The resulting strict and extended SOS-ADC(2) methods constitute pragmatic semi-empirical approaches. In the case of strict SOS-ADC(2) two empirical parameters are necessary while three were included in the extended version.

Previously, an SOS variant of strict ADC(2) had been implemented in the Turbomole program package. Here, we presented a similar implementation in the Q-chem program package where we have reoptimized one of the parameters to obtain slightly improved results. It was compared with a variant that we derived directly from SOS-MP2 using the intermediate state representation. Although the energetic shifts introduced by the latter variant behaved in a more systematic way, the computational cost could not be significantly reduced. Therefore, the original method was chosen as the standard procedure for strict

ADC(2) calculations. Finally, the main achievement was the establishment of an extended SOS-ADC(2) method that compensates for the overestimation of doubly excited configurations inherent to the original ADC(2)-x method at reduced computational cost.

However, appropriate reference data for doubly excited states is still lacking and only few states with considerable double excitation character were included into the benchmark set for electronically excited states by Schreiber et al. [88] and Silva-Junior et al. [89] which we used for our parameter optimizations. Nevertheless, the given parameter set yields a well-balanced description of singly excited states with similar errors as with SOS-ADC(2)-s and doubly excited states are shifted to the correct energy range. The development of reliable benchmark sets with a stronger focus on doubly excited states would be a desirable field of future research.

The implementation of spin-orbit coupling elements between singlet and triplet states using the atomic mean-field approximation and the `AMFI` program [22] of B. Schimmelpfennig was discussed in detail in Chapter 5. The corresponding test calculations for the molecules thiophene, dithiin, coumarin and umbelliferone were presented in Chapter 7. In an earlier work by M. Pabst, a combination of the Orca and Turbomole program packages was used to obtain spin-orbit coupling elements based on a molecular mean-field approximation for the methods CC2 and ADC(2)-s [173]. Therefore, we compared our results with their ones. The errors were in the expected range of about 5 % [104,106] for using an atomic instead of a molecular mean-field. Additional deviations occur because in Turbomole transition properties are evaluated only in first order and not like here in second order. Additionally, the results were compared to values from a combination of density functional theory (DFT) with multi-reference configuration interaction methods (DFT/MRCI) or multi-state CASPT2 (MS-CASPT2) calculations. A good correspondence was achieved.

Of special interest was the comparison between the different ADC methods up to third order. As long as the character of the excited states did not change significantly from one ADC method to the other, the spin-orbit coupling elements lay within the same region for all tested methods. The only exception was given by the SOS approximation where the coupling elements were often reduced in size. Therefore, the applicability of the SOS approximation should be carefully checked when employed for this kind of calculations.

Similar to the case of doubly excited states appropriate reference data for the calculation of spin-orbit coupling elements is rare. Among the most used methods are DFT/MRCI and (MS-)CASPT2. However, there is no benchmark set for which consistent values at different levels of accuracy are given. The establishment of such a benchmark set constitutes an important part of further efforts.

The last theoretical project was the identification of plasmons by *ab initio* methods. First, the theoretical background and description of plasmons in the context of the random-phase approximation was discussed in Chapter 6. The free electron gas provided an instructive example for the understanding of plasmons. Then the scaling approach introduced by S. Bernadotte et al. [167]

was transferred to the ADC methods. Because they have derived their approach for TDDFT, the scaling method had to be adjusted to the present situation. For the test of this newly established approach a series of linear polyenes (C_8H_{10}, $C_{16}H_{18}$, and $C_{30}H_{32}$) was chosen. The results were presented in Chapter 8. As their π-electrons are to a large extend delocalized along the molecular chain, an analogy to the one-dimensional electron gas could be drawn and the results analyzed with respect to the same characteristics as the electron gas in Chapter 6.

The scaling approach worked very well for all systems and methods chosen (including the SOS approximation for strict and extended ADC(2)). In all cases, this method identified the plasmons in agreement with the analysis of the eigenvectors as well as the transition densities. The only differences to the electron gas occurred regarding the order of the states and, in some cases, their intensity. However, it has to be considered that the analogy to the one-dimensional electron gas is by no means exact and that in molecular systems plasmons and single-particle states are always at least partly coupled. Accordingly, the difference in the character of these two types of states was more profound in the case of the higher polyenes than in octatetraene. Nevertheless, the scaling approach provides a reliable means for the identification of plasmons that can easily be transferred to other *ab initio* models and that can be applied to molecules where no such simple analogy to the free electron gas can be established.

A combined theoretical and experimental study of the relaxation pathways in coumarin molecules was presented in Chapter 9. The experimental results consisted of time-resolved measurements performed in the group of M. Motzkus. The aim was the elucidation of the fluorescence quenching observed in coumarin. Opposed to its derivatives, the fluorescence of coumarin is efficiently suppressed by ultrafast relaxation pathways throughout a wide range of solvents. Coumarin derivatives, e. g., 7-hydroxycoumarin which was analyzed here, show significant but strongly solvent dependent fluorescence quantum yields. These observations have never been fully understood although coumarin and its derivatives are important molecules for photochemical applications.

Here, the relaxation network of coumarin and 7-hydroxycoumarin were investigated by quantum chemical calculations. Based on these results, two parallel radiationless relaxation pathways were suggested. One involved an intermediate breaking of the lactone ring while the other one occurred along the stretching mode of the carbonyl group. The solvent effects were thoroughly investigated and were shown to influence the two pathways to different extent. The same is true for different substituents. Their combined effects explained the observed photophysical behavior of coumarin and its derivatives. Moreover, the resulting relaxation network was shown to be in perfect agreement with the experiments.

As part of this study the newly implemented code for the determination of spin-orbit coupling elements was applied. It was used to shed some new light onto inter-system crossing processes that were observed in certain solvents. Along one of the two relaxation pathways a point was identified where such a transition seems most probable. Depending on the combination of solvent and substituents this point is not reached, thereby explaining a lack of phosphores-

cence.

Summarized, with the implemented methods (SOS-ADC(2)-x, calculation of spin-orbit coupling elements, scaling approach for the identification of plasmons) the functionality of the `adcman` module as implemented in the Q-Chem program package was further extended. It is now applicable to a wider range of quantum chemical problems involving excited states, which play a significant role in many biological systems or technical applications. This work was complemented by a combined experimental and theoretical study that solved the long-standing question about the fluorescence quenching in coumarin.

Appendices

A. Explicit Expressions for (SOS)-ADC(2)-s/x

A.1. Explicit expressions for the ADC(2)-s/x and ISR-SOS-ADC(2)-s matrices

General structure of the ADC(2) matrix $\mathbf{M}$:

$$\begin{aligned}
&\text{ph/ph block:} && M_{ia,jb} = K_{ia,jb} + C^{(1)}_{ia,jb} + C^{(2)}_{ia,jb} \\
&\text{ph/2p2h block:} && M_{ia,kcld} = C^{(1)}_{ia,kcld} \\
&\text{2p2h/ph block:} && M_{iajb,kc} = C^{(1)}_{iajb,kc} \\
&\text{2p2h/2p2h block, strict:} && M_{iajb,kcld} = K_{iajb,kcld} \\
&\text{2p2h/2p2h block, extended:} && M_{iajb,kcld} = K_{iajb,kcld} + C^{(1)}_{iajb,kcld}
\end{aligned}$$

Explicit expressions in the unscaled ADC(2) schemes:

$$\begin{aligned}
K_{ia,jb} &= (\epsilon_a - \epsilon_i)\delta_{ab}\delta_{ij} \\
C^{(1)}_{ia,jb} &= -\langle aj||bi\rangle \\
C^{(2)}_{ia,jb} &= C^{(2)A}_{ia,jb} + C^{(2)B}_{ia,jb} + C^{(2)C}_{ia,jb} \\
C^{(2)A}_{ia,jb} &= \frac{1}{4}\delta_{ij}\sum_{ckl}\left[t_{kalc}\langle kl||bc\rangle + t^*_{kblc}\langle ac||kl\rangle\right] \\
C^{(2)B}_{ia,jb} &= \frac{1}{4}\delta_{ab}\sum_{cdk}\left[t_{ickd}\langle jk||cd\rangle + t^*_{jckd}\langle cd||ik\rangle\right] \\
C^{(2)C}_{ia,jb} &= -\frac{1}{2}\sum_{ck}\left[t_{iakc}\langle jk||bc\rangle + t^*_{jbkc}\langle ac||ik\rangle\right] \\
C^{(1)}_{ia,kcld} &= \langle kl||id\rangle\delta_{ac} - \langle kl||ic\rangle\delta_{ad} - \langle al||cd\rangle\delta_{ik} + \langle ak||cd\rangle\delta_{il} \\
C^{(1)}_{iajb,kc} &= \langle kb||ij\rangle\delta_{ac} - \langle ka||ij\rangle\delta_{bc} - \langle ab||cj\rangle\delta_{ik} + \langle ab||ci\rangle\delta_{jk} \\
K_{iajb,kcld} &= (\epsilon_a + \epsilon_b - \epsilon_i - \epsilon_j)\delta_{ac}\delta_{bd}\delta_{ik}\delta_{jl} \\
C^{(1)}_{iajb,kcld} &= \langle ab||cd\rangle\delta_{ik}\delta_{jl} + \langle kl||ij\rangle\delta_{ac}\delta_{bd} \\
&\quad - [\langle ak||ci\rangle\delta_{bd}\delta_{jl} + \langle al||cj\rangle\delta_{bd}\delta_{ik} + \langle bk||di\rangle\delta_{ac}\delta_{jl} + \langle bl||dj\rangle\delta_{ac}\delta_{ik}] \\
&\quad + [\langle al||ci\rangle\delta_{bd}\delta_{jk} + \langle ak||cj\rangle\delta_{bd}\delta_{il} + \langle bl||di\rangle\delta_{ac}\delta_{jk} + \langle bk||dj\rangle\delta_{ac}\delta_{il}] \\
&\quad + [\langle ak||di\rangle\delta_{bc}\delta_{jl} + \langle al||dj\rangle\delta_{bc}\delta_{ik} + \langle bk||ci\rangle\delta_{ad}\delta_{jl} + \langle bl||cj\rangle\delta_{ad}\delta_{ik}] \\
&\quad - [\langle al||di\rangle\delta_{bc}\delta_{jk} + \langle ak||dj\rangle\delta_{bc}\delta_{il} + \langle bl||ci\rangle\delta_{ad}\delta_{jk} + \langle bk||cj\rangle\delta_{ad}\delta_{il}]
\end{aligned}$$

Explicit expressions in the ISR-SOS-ADC(2)-s scheme (the remaining ele-

ments are unchanged, t^{sos}_{iajb} as defined in equation 4.1, $c_{os} = 1.3$):

$$C^{(2)A}_{ia,jb} = \frac{1}{4}\delta_{ij}\sum_{ckl}\left[t^{sos}_{kalc}\langle kl||bc\rangle + t^{sos^*}_{kblc}\langle ac||kl\rangle\right]$$
$$C^{(2)B}_{ia,jb} = \frac{1}{4}\delta_{ab}\sum_{cdk}\left[t^{sos}_{ickd}\langle jk||cd\rangle + t^{sos^*}_{jckd}\langle cd||ik\rangle\right]$$
$$C^{(2)C}_{ia,jb} = -\frac{1}{2}\sum_{ck}\left[t^{sos}_{iakc}\langle jk||bc\rangle + t^{sos^*}_{jbkc}\langle ac||ik\rangle\right]$$

A.2. Derivation of SOS-ADC(2)-s from SOS-CC2

In the following, the SOS-ADC(2)-s equations will be derived from SOS-CC2 *via* setting the t_1-amplitudes to zero (yielding SOS-CIS(D_∞)) and symmetrizing the result:

$$\mathbf{A}^{SOS-CC2} = \left(\begin{array}{c|c} \langle\Phi^a_i|\left[(\hat{\bar{H}} + c^{os}\left[\hat{\bar{H}}, \hat{T}^{os}_2\right]), \tau^b_j\right]|\Phi_0\rangle & \langle\Phi^a_i|c^{os}\left[\hat{\bar{H}}, \tau^{cd^{os}}_{kl}\right]|\Phi_0\rangle \\ \hline \langle\Phi^{ab^{os}}_{ij}|\left[\hat{\bar{H}}, \tau^c_k\right]|\Phi_0\rangle & \langle\Phi^{ab^{os}}_{ij}|\left[\hat{F}, \tau^{cd^{os}}_{kl}\right]|\Phi_0\rangle \end{array}\right)$$
$$\mathbf{A}^{SOS-CIS(D_\infty)} = \left(\begin{array}{c|c} \langle\Phi^a_i|\left[(\hat{H} + c^{os}\left[\hat{H}, \hat{T}^{os}_2\right]), \tau^b_j\right]|\Phi_0\rangle & \langle\Phi^a_i|c^{os}\left[\hat{H}, \tau^{cd^{os}}_{kl}\right]|\Phi_0\rangle \\ \hline \langle\Phi^{ab^{os}}_{ij}|\left[\hat{H}, \tau^c_k\right]|\Phi_0\rangle & \langle\Phi^{ab^{os}}_{ij}|\left[\hat{F}, \tau^{cd^{os}}_{kl}\right]|\Phi_0\rangle \end{array}\right)$$
$$\mathbf{A}^{SOS-ADC(2)-s} = \frac{1}{2}\left(\mathbf{A}^{SOS-CIS(D_\infty)} + \left(\mathbf{A}^{SOS-CIS(D_\infty)}\right)^\dagger\right) \tag{A.1}$$

Here, the same definitions are used as in Sections 2 and 3. $\hat{H}$ is the molecular Hamiltonian of the system

$$\begin{aligned}\hat{H} &= \sum_{pq} h_{pq}c^\dagger_p c_q + \frac{1}{2}\sum_{pqrs}\langle pq|rs\rangle c^\dagger_p c^\dagger_q c_s c_r \\ &= \sum_p \epsilon_p c^\dagger_p c_p - \sum_{pq}\sum_k \langle pk||qk\rangle c^\dagger_p c_q + \frac{1}{2}\sum_{pqrs}\langle pq|rs\rangle c^\dagger_p c^\dagger_q c_s c_r,\end{aligned}$$

$\hat{F}$ refers to the Fock operator

$$\hat{F} = \sum_p \epsilon_p c^\dagger_p c_p,$$

and $\hat{\bar{H}}$ the similarity transformed Hamilton operator

$$\hat{\bar{H}} = \exp(-\hat{T}_1)\hat{H}\exp(\hat{T}_1).$$

As usual, $|\Phi_0\rangle$ is the HF ground state wave function and $\{\epsilon_p\}$ are HF orbital energies. The excitation operators τ^a_i and τ^{ab}_{ij} are defined as

$$\tau^a_i = c^\dagger_a c_i \qquad \text{and} \qquad \tau^{ab}_{ij} = c^\dagger_a c^\dagger_b c_i c_j$$

and the cluster operators are defined accordingly as

$$\hat{T}_1 = \sum_{ai} t_{ia}\tau_i^a \qquad \text{and} \qquad \hat{T}_2 = \sum_{a>b,i>j} t_{ijab}\tau_{ij}^{ab}.$$

Finally, $|\Phi_i^a\rangle$ as well as $|\Phi_{ij}^{ab}\rangle$ specify excited SDs

$$|\Phi_i^a\rangle = \tau_i^a|\Phi_0\rangle \qquad \text{and} \qquad |\Phi_{ij}^{ab}\rangle = \tau_{ij}^{ab}|\Phi_0\rangle.$$

If no spin-flip processes are considered ($\Delta M_S = 0$), the indexes $(ijab)$ can be associated with six different spin configurations ($(\alpha\alpha\alpha\alpha)$, $(\beta\beta\beta\beta)$, $(\alpha\beta\alpha\beta)$, $(\beta\alpha\beta\alpha)$, $(\alpha\beta\beta\alpha)$ and $(\beta\alpha\alpha\beta)$). The superscript *os* implies that the two same-spin configurations $(\alpha\alpha\alpha\alpha)$ and $(\beta\beta\beta\beta)$ are neglected. When evaluating expressions as occurring for the matrix elements of $\mathbf{A}^{SOS-CIS(D_\infty)}$, the following commutator relations are helpful:

$$\left[c_p^\dagger, c_q^\dagger\right]_+ = 0, \qquad [c_p, c_q]_+ = 0$$
$$\left[c_p^\dagger, c_q\right]_+ = \delta_{pq} \qquad \Rightarrow \qquad c_p^\dagger c_q = \delta_{pq} - c_q c_p^\dagger$$

We start with the evaluation of the 2p2h/2p2h block:

$$\begin{aligned}
\langle\Phi_{ij}^{ab\,os}|\left[\hat{F}, \tau_{kl}^{cd\,os}\right]|\Phi_0\rangle &= \sum_p \epsilon_p \langle\Phi_0|c_j^\dagger c_i^\dagger c_b c_a \left[c_p^\dagger c_p, c_c^\dagger c_d^\dagger c_k c_l\right]|\Phi_0\rangle \\
&\cdot (1-\delta_{\sigma(i)\sigma(j)})(1-\delta_{\sigma(k)\sigma(l)}) \\
&= \sum_p \epsilon_p \Big\{\langle\Phi_0|c_j^\dagger c_i^\dagger c_b c_a c_p^\dagger c_p c_c^\dagger c_d^\dagger c_k c_l|\Phi_0\rangle \\
&- \Phi_0|c_j^\dagger c_i^\dagger c_b c_a c_c^\dagger c_d^\dagger c_k c_l c_p^\dagger c_p|\Phi_0\rangle\Big\}(1-\delta_{\sigma(i)\sigma(j)})(1-\delta_{\sigma(k)\sigma(l)})
\end{aligned}$$

The index p runs over all spin orbitals. If p is unoccupied, $c_p|\Phi_0\rangle$ vanishes. Similarily, $c_p|\Phi_{kl}^{cd}\rangle$ is only non-zero when p occupied and $p \neq k, l$ or $p = c, d$:

$$\begin{aligned}
\langle\Phi_{ij}^{ab\,os}|\left[\hat{F}, \tau_{kl}^{cd\,os}\right]|\Phi_0\rangle &= \left\{\sum_{m\neq k,l}\epsilon_m + \sum_{e=c,d}\epsilon_e - \sum_m \epsilon_m\right\} \\
&\cdot (1-\delta_{\sigma(i)\sigma(j)})(1-\delta_{\sigma(k)\sigma(l)})\langle\Phi_0|c_j^\dagger c_i^\dagger c_b c_a c_c^\dagger c_d^\dagger c_k c_l|\Phi_0\rangle \\
&= \left\{-\sum_{m=k,l}\epsilon_m + \sum_{e=c,d}\epsilon_e\right\} \\
&\cdot (1-\delta_{\sigma(i)\sigma(j)})(1-\delta_{\sigma(k)\sigma(l)})\langle\Phi_0|c_j^\dagger c_i^\dagger c_b c_a c_c^\dagger c_d^\dagger c_k c_l|\Phi_0\rangle
\end{aligned}$$

Now, the integral has to be evaluated. This can be done either by using Wick's theorem [29] or, as demonstrated below, by making use of the commutator relations above. In principle, the integral is zero if either a creation operator acting on an occupied orbital or an annihilation operator acting on a virtual

orbital is working on $|\Phi_0\rangle$. Therefore, we move such operators to the far right of the operator chain by a sequence of interchanges:

$$\begin{aligned}
\langle\Phi_0|c_j^\dagger c_i^\dagger c_b c_a c_c^\dagger c_d^\dagger c_k c_l|\Phi_0\rangle =& \langle\Phi_0|c_j^\dagger c_i^\dagger c_b c_d^\dagger c_k c_l|\Phi_0\rangle\delta_{ac} - \langle\Phi_0|c_j^\dagger c_i^\dagger c_b c_c^\dagger c_a c_d^\dagger c_k c_l|\Phi_0\rangle \\
=& \langle\Phi_0|c_j^\dagger c_i^\dagger c_k c_l|\Phi_0\rangle\delta_{ac}\delta_{bd} - \langle\Phi_0|c_j^\dagger c_i^\dagger c_d^\dagger c_b c_k c_l|\Phi_0\rangle\delta_{ac} \\
& - \langle\Phi_0|c_j^\dagger c_i^\dagger c_b c_c^\dagger c_k c_l|\Phi_0\rangle\delta_{ad} + \langle\Phi_0|c_j^\dagger c_i^\dagger c_b c_c^\dagger c_d^\dagger c_a c_k c_l|\Phi_0\rangle \\
=& \langle\Phi_0|c_j^\dagger c_l|\Phi_0\rangle\delta_{ac}\delta_{bd}\delta_{ik} - \langle\Phi_0|c_j^\dagger c_k c_i^\dagger c_l|\Phi_0\rangle\delta_{ac}\delta_{bd} \\
& - \underbrace{\langle\Phi_0|c_j^\dagger c_i^\dagger c_d^\dagger c_k c_l c_b|\Phi_0\rangle\delta_{ac}}_{=0} - \langle\Phi_0|c_j^\dagger c_i^\dagger c_k c_l|\Phi_0\rangle\delta_{ad}\delta_{cb} \\
& + \underbrace{\langle\Phi_0|c_j^\dagger c_i^\dagger c_c^\dagger c_b c_k c_l|\Phi_0\rangle\delta_{ad}}_{=0} + \underbrace{\langle\Phi_0|c_j^\dagger c_i^\dagger c_b c_c^\dagger c_d^\dagger c_k c_l c_a|\Phi_0\rangle}_{=0} \\
=& \delta_{ac}\delta_{bd}\delta_{ik}\delta_{jl} - \langle\Phi_0|c_j^\dagger c_k|\Phi_0\rangle\delta_{ac}\delta_{bd}\delta_{il} \\
& - \langle\Phi_0|c_j^\dagger c_i^\dagger c_k c_l|\Phi_0\rangle\delta_{ad}\delta_{cb} \\
=& \delta_{ac}\delta_{bd}\delta_{ik}\delta_{jl} - \delta_{ac}\delta_{bd}\delta_{il}\delta_{jk} - \delta_{ad}\delta_{cb}\delta_{ik}\delta_{jl} + \delta_{ad}\delta_{cb}\delta_{il}\delta_{jk}
\end{aligned}$$

From the restrictions $i > j$, $k > l$, $a > b$, and $c > d$ it follows that

$$\delta_{il}\delta_{jk} = 0 \qquad \text{and} \qquad \delta_{ad}\delta_{cb} = 0.$$

Finally, this yields

$$\begin{aligned}
&\langle\Phi_{ij}^{ab\,os}|\left[\hat{F}, \tau_{kl}^{cd\,os}\right]|\Phi_0\rangle = \\
&\qquad (\epsilon_a + \epsilon_b - \epsilon_i - \epsilon_j)\,\delta_{ac}\delta_{bd}\delta_{ik}\delta_{jl}(1 - \delta_{\sigma(i)\sigma(j)})(1 - \delta_{\sigma(k)\sigma(l)}).
\end{aligned}$$

The other matrix elements can be obtained using the same procedure. Below, the main steps are given.

$$
\begin{aligned}
&\langle \Phi_{ij}^{ab\,os}| \left[\hat{H}, \tau_k^c\right] |\Phi_0\rangle \\
=&\langle \Phi_{ij}^{ab\,os}| \left[\sum_p \epsilon_p c_p^\dagger c_p - \sum_{pq}\sum_m \langle pm||qm\rangle c_p^\dagger c_q + \frac{1}{2}\sum_{pqrs}\langle pq|rs\rangle c_p^\dagger c_q^\dagger c_s c_r, \tau_k^c\right] |\Phi_0\rangle \\
=&\sum_p \epsilon_p \underbrace{\langle \Phi_0| c_j^\dagger c_i^\dagger c_b c_a \left[c_p^\dagger c_p, c_c^\dagger c_k\right] |\Phi_0\rangle}_{=0} (1-\delta_{\sigma(i)\sigma(j)}) \\
&-\sum_{pq}\sum_m \langle pm||qm\rangle \langle \Phi_0| c_j^\dagger c_i^\dagger c_b c_a \left[c_p^\dagger c_q, c_c^\dagger c_k\right] |\Phi_0\rangle (1-\delta_{\sigma(i)\sigma(j)}) \\
&+\frac{1}{2}\sum_{pqrs}\langle pq|rs\rangle \langle \Phi_0| c_j^\dagger c_i^\dagger c_b c_a \left[c_p^\dagger c_q^\dagger c_s c_r, c_c^\dagger c_k\right] |\Phi_0\rangle (1-\delta_{\sigma(i)\sigma(j)}) \\
=&-\sum_{en}\sum_m \langle em||nm\rangle \langle \Phi_0| c_j^\dagger c_i^\dagger c_b c_a \left[c_e^\dagger c_n, c_c^\dagger c_k\right] |\Phi_0\rangle (1-\delta_{\sigma(i)\sigma(j)}) \\
&+\frac{1}{2}\Bigg\{\sum_{meon}\langle me|on\rangle \langle \Phi_0| c_j^\dagger c_i^\dagger c_b c_a \left[c_m^\dagger c_e^\dagger c_n c_o, c_c^\dagger c_k\right] |\Phi_0\rangle \\
&+\sum_{emon}\langle em|on\rangle \langle \Phi_0| c_j^\dagger c_i^\dagger c_b c_a \left[c_e^\dagger c_m^\dagger c_n c_o, c_c^\dagger c_k\right] |\Phi_0\rangle \\
&+\sum_{efgm}\langle ef|gm\rangle \langle \Phi_0| c_j^\dagger c_i^\dagger c_b c_a \left[c_e^\dagger c_f^\dagger c_m c_g, c_c^\dagger c_k\right] |\Phi_0\rangle \\
&+\sum_{efmg}\langle ef|mg\rangle \langle \Phi_0| c_j^\dagger c_i^\dagger c_b c_a \left[c_e^\dagger c_f^\dagger c_g c_m, c_c^\dagger c_k\right] |\Phi_0\rangle \Bigg\} (1-\delta_{\sigma(i)\sigma(j)}) \\
=&\frac{1}{2}\sum_{meon}\{\langle me|on\rangle(-\delta_{mk}\delta_{eb}\delta_{ca}\delta_{oj}\delta_{ni} + \delta_{mk}\delta_{cb}\delta_{ea}\delta_{oj}\delta_{ni} \\
&\qquad + \delta_{mk}\delta_{eb}\delta_{ca}\delta_{nj}\delta_{oi} - \delta_{mk}\delta_{cb}\delta_{ea}\delta_{nj}\delta_{oi}) \\
&+\langle em|on\rangle(-\delta_{mk}\delta_{cb}\delta_{ea}\delta_{oj}\delta_{ni} + \delta_{mk}\delta_{eb}\delta_{ca}\delta_{oj}\delta_{ni} \\
&\qquad + \delta_{mk}\delta_{cb}\delta_{ea}\delta_{nj}\delta_{oi} - \delta_{mk}\delta_{eb}\delta_{ca}\delta_{nj}\delta_{oi})\}(1-\delta_{\sigma(i)\sigma(j)}) \\
&+\frac{1}{2}\sum_{efgm}\{\langle ef|gm\rangle(\delta_{gc}\delta_{fb}\delta_{ea}\delta_{kj}\delta_{mi} - \delta_{gc}\delta_{eb}\delta_{fa}\delta_{kj}\delta_{mi} \\
&\qquad - \delta_{gc}\delta_{fb}\delta_{ea}\delta_{mj}\delta_{ki} + \delta_{gc}\delta_{eb}\delta_{fa}\delta_{mj}\delta_{ki}) \\
&+\langle ef|mg\rangle(\delta_{gc}\delta_{fb}\delta_{ea}\delta_{mj}\delta_{ki} - \delta_{gc}\delta_{eb}\delta_{fa}\delta_{mj}\delta_{ki} \\
&\qquad - \delta_{gc}\delta_{fb}\delta_{ea}\delta_{kj}\delta_{mi} + \delta_{gc}\delta_{eb}\delta_{fa}\delta_{kj}\delta_{mi})\}(1-\delta_{\sigma(i)\sigma(j)}) \\
=&\{\langle kb||ij\rangle\delta_{ac} - \langle ka||ij\rangle\delta_{bc} - \langle ab||cj\rangle\delta_{ki} + \langle ab||ci\rangle\delta_{kj}\}(1-\delta_{\sigma(i)\sigma(j)})
\end{aligned}
$$

$$
\begin{aligned}
&\langle\Phi_i^a|\left[H,\tau_{kl}^{cd\,os}\right]|\Phi_0\rangle \\
=&\langle\Phi_i^a|\left[\sum_p \epsilon_p c_p^\dagger c_p - \sum_{pq}\sum_m \langle pm||qm\rangle c_p^\dagger c_q + \frac{1}{2}\sum_{pqrs}\langle pq|rs\rangle c_p^\dagger c_q^\dagger c_s c_r, \tau_{kl}^{cd\,os}\right]|\Phi_0\rangle \\
=&-\sum_{pq}\sum_m \langle pm||qm\rangle\langle\Phi_0|c_i^\dagger c_a\left[c_p^\dagger c_q, c_c^\dagger c_d^\dagger c_k c_l\right]|\Phi_0\rangle(1-\delta_{\sigma(k)\sigma(l)}) \\
&+\frac{1}{2}\sum_{pqrs}\langle pq|rs\rangle\langle\Phi_0|c_i^\dagger c_a\left[c_p^\dagger c_q^\dagger c_s c_r, c_c^\dagger c_d^\dagger c_k c_l\right]|\Phi_0\rangle(1-\delta_{\sigma(k)\sigma(l)}) \\
=&-\sum_{ne}\sum_m \langle nm||em\rangle\langle\Phi_0|c_i^\dagger c_a\left[c_n^\dagger c_e, c_c^\dagger c_d^\dagger c_k c_l\right]|\Phi_0\rangle(1-\delta_{\sigma(k)\sigma(l)}) \\
&+\frac{1}{2}\Bigg\{\sum_{mnoe}\langle mn|eo\rangle\langle\Phi_0|c_i^\dagger c_a\left[c_m^\dagger c_n^\dagger c_o c_e, c_c^\dagger c_d^\dagger c_k c_l\right]|\Phi_0\rangle \\
&+\sum_{mneo}\langle mn|oe\rangle\langle\Phi_0|c_i^\dagger c_a\left[c_m^\dagger c_n^\dagger c_e c_o, c_c^\dagger c_d^\dagger c_k c_l\right]|\Phi_0\rangle \\
&+\sum_{mefg}\langle me|gf\rangle\langle\Phi_0|c_i^\dagger c_a\left[c_m^\dagger c_e^\dagger c_f c_g, c_c^\dagger c_d^\dagger c_k c_l\right]|\Phi_0\rangle \\
&+\sum_{emfg}\langle em|gf\rangle\langle\Phi_0|c_i^\dagger c_a\left[c_e^\dagger c_m^\dagger c_f c_g, c_c^\dagger c_d^\dagger c_k c_l\right]|\Phi_0\rangle\Bigg\}(1-\delta_{\sigma(k)\sigma(l)}) \\
=&-(1-\delta_{\sigma(k)\sigma(l)})\sum_{ne}\sum_m\langle nm||em\rangle\,(\\
&\quad+\delta_{ed}\delta_{ca}\delta_{li}\delta_{kn}-\delta_{ed}\delta_{ca}\delta_{ki}\delta_{ln}-\delta_{ec}\delta_{da}\delta_{li}\delta_{kn}+\delta_{ec}\delta_{da}\delta_{ki}\delta_{ln}) \\
&+\frac{1}{2}(1-\delta_{\sigma(k)\sigma(l)})\Bigg\{\sum_{mnoe}\langle mn|eo\rangle\,(\\
&\quad+\delta_{ed}\delta_{ca}\delta_{li}\delta_{km}\delta_{on}-\delta_{ed}\delta_{ca}\delta_{ki}\delta_{lm}\delta_{on}-\delta_{ed}\delta_{ca}\delta_{li}\delta_{om}\delta_{kn}+\delta_{ed}\delta_{ca}\delta_{oi}\delta_{lm}\delta_{kn} \\
&\quad+\delta_{ed}\delta_{ca}\delta_{ki}\delta_{om}\delta_{ln}-\delta_{ed}\delta_{ca}\delta_{oi}\delta_{km}\delta_{ln}-\delta_{ec}\delta_{da}\delta_{li}\delta_{km}\delta_{on}+\delta_{ec}\delta_{da}\delta_{ki}\delta_{lm}\delta_{on} \\
&\quad+\delta_{ec}\delta_{da}\delta_{li}\delta_{om}\delta_{kn}-\delta_{ec}\delta_{da}\delta_{oi}\delta_{lm}\delta_{kn}-\delta_{ec}\delta_{da}\delta_{ki}\delta_{om}\delta_{ln}+\delta_{ec}\delta_{da}\delta_{oi}\delta_{km}\delta_{ln}) \\
&+\sum_{mneo}\langle mn|oe\rangle\,(\\
&\quad-\delta_{ed}\delta_{ca}\delta_{oi}\delta_{lm}\delta_{kn}+\delta_{ed}\delta_{ca}\delta_{li}\delta_{om}\delta_{kn}+\delta_{ed}\delta_{ca}\delta_{oi}\delta_{km}\delta_{ln}-\delta_{ed}\delta_{ca}\delta_{ki}\delta_{om}\delta_{ln} \\
&\quad-\delta_{ed}\delta_{ca}\delta_{li}\delta_{km}\delta_{on}+\delta_{ed}\delta_{ca}\delta_{ki}\delta_{lm}\delta_{on}+\delta_{ec}\delta_{da}\delta_{oi}\delta_{lm}\delta_{kn}-\delta_{ec}\delta_{da}\delta_{li}\delta_{om}\delta_{kn} \\
&\quad-\delta_{ec}\delta_{da}\delta_{oi}\delta_{km}\delta_{ln}+\delta_{ec}\delta_{da}\delta_{ki}\delta_{om}\delta_{ln}+\delta_{ec}\delta_{da}\delta_{li}\delta_{km}\delta_{on}-\delta_{ec}\delta_{da}\delta_{ki}\delta_{lm}\delta_{on}) \\
&+\sum_{mefg}\langle me|gf\rangle\,(\\
&\quad+\delta_{gd}\delta_{ea}\delta_{cf}\delta_{li}\delta_{km}-\delta_{gd}\delta_{ea}\delta_{cf}\delta_{ki}\delta_{lm}-\delta_{gc}\delta_{ea}\delta_{df}\delta_{li}\delta_{km}+\delta_{gc}\delta_{ea}\delta_{df}\delta_{ki}\delta_{lm}) \\
&+\sum_{emfg}\langle em|gf\rangle\,(\\
&\quad-\delta_{gd}\delta_{ea}\delta_{cf}\delta_{li}\delta_{km}+\delta_{gd}\delta_{ea}\delta_{cf}\delta_{ki}\delta_{lm}+\delta_{gc}\delta_{ea}\delta_{df}\delta_{li}\delta_{km}-\delta_{gc}\delta_{ea}\delta_{df}\delta_{ki}\delta_{lm})\Bigg\} \\
=&\{-\langle kl||ic\rangle\delta_{ad}+\langle kl||id\rangle\delta_{ad}+\langle ak||cd\rangle\delta_{li}-\langle al||cd\rangle\delta_{ki}\}(1-\delta_{\sigma(k)\sigma(l)})
\end{aligned}
$$

$$
\begin{aligned}
&\langle\Phi_i^a|\left[c^{os}\left[\hat{H},\hat{T}_2^{os}\right],\tau_j^b\right]|\Phi_0\rangle \\
=&c^{os}\langle\Phi_0|c_i^\dagger c_a\left[\left[\sum_p \epsilon_p c_p^\dagger c_p - \sum_{pq}\sum_m \langle pm||qm\rangle c_p^\dagger c_q\right.\right. \\
&\left.\left.+\frac{1}{2}\sum_{pqrs}\langle pq|rs\rangle c_p^\dagger c_q^\dagger c_s c_r, \frac{1}{4}\sum_{ckdl} t_{klcd}^{os} c_c^\dagger c_d^\dagger c_k c_l\right], c_b^\dagger c_j\right]|\Phi_0\rangle \\
=&c^{os}\frac{1}{4}\sum_p\sum_{ckdl}\epsilon_p t_{klcd}^{os}\underbrace{\langle\Phi_0|c_i^\dagger c_a\left[\left[c_p^\dagger c_p, c_c^\dagger c_d^\dagger c_k c_l\right], c_b^\dagger c_j\right]|\Phi_0\rangle}_{=0} \\
&-c^{os}\frac{1}{4}\sum_{pq}\sum_m\sum_{ckdl} t_{klcd}^{os}\langle pm||qm\rangle\underbrace{\langle\Phi_0|c_i^\dagger c_a\left[\left[c_p^\dagger c_q, c_c^\dagger c_d^\dagger c_k c_l\right], c_b^\dagger c_j\right]|\Phi_0\rangle}_{=0} \\
&+c^{os}\frac{1}{8}\sum_{pqrs}\sum_{ckdl} t_{klcd}^{os}\langle pq|rs\rangle\langle\Phi_0|c_i^\dagger c_a\left[\left[c_p^\dagger c_q^\dagger c_s c_r, c_c^\dagger c_d^\dagger c_k c_l\right], c_b^\dagger c_j\right]|\Phi_0\rangle \\
=&\frac{1}{8}c^{os}\sum_{mnef}\sum_{ckdl} t_{klcd}^{os}\langle pq|rs\rangle\{ \\
&+\langle\Phi_0|c_i^\dagger c_a c_m^\dagger c_n^\dagger c_f c_e c_c^\dagger c_d^\dagger c_k c_l c_b^\dagger c_j|\Phi_0\rangle - \langle\Phi_0|c_i^\dagger c_a c_c^\dagger c_d^\dagger c_k c_l c_m^\dagger c_n^\dagger c_f c_e c_b^\dagger c_j|\Phi_0\rangle \\
&-\langle\Phi_0|c_i^\dagger c_a c_b^\dagger c_j c_m^\dagger c_n^\dagger c_f c_e c_c^\dagger c_d^\dagger c_k c_l|\Phi_0\rangle + \underbrace{\langle\Phi_0|c_i^\dagger c_a c_b^\dagger c_j c_c^\dagger c_d^\dagger c_k c_l c_m^\dagger c_n^\dagger c_f c_e|\Phi_0\rangle}_{=0}\} \\
=&\frac{1}{8}c^{os}\sum_{mnef}\sum_{ckdl} t_{klcd}^{os}\langle pq|rs\rangle\{ \\
&\quad-\delta_{ji}\delta_{da}\delta_{bf}\delta_{ce}\delta_{lm}\delta_{kn}+\delta_{ji}\delta_{ca}\delta_{bf}\delta_{de}\delta_{lm}\delta_{kn}+\delta_{ji}\delta_{da}\delta_{cf}\delta_{be}\delta_{lm}\delta_{kn} \\
&\quad-\delta_{ji}\delta_{ca}\delta_{df}\delta_{be}\delta_{lm}\delta_{kn}-\delta_{li}\delta_{ba}\delta_{df}\delta_{ce}\delta_{jm}\delta_{kn}+\delta_{li}\delta_{da}\delta_{bf}\delta_{ce}\delta_{jm}\delta_{kn} \\
&\quad+\delta_{li}\delta_{ba}\delta_{cf}\delta_{de}\delta_{jm}\delta_{kn}-\delta_{li}\delta_{ca}\delta_{bf}\delta_{de}\delta_{jm}\delta_{kn}-\delta_{li}\delta_{da}\delta_{cf}\delta_{be}\delta_{jm}\delta_{kn} \\
&\quad+\delta_{li}\delta_{ca}\delta_{df}\delta_{be}\delta_{jm}\delta_{kn}+\delta_{ji}\delta_{da}\delta_{bf}\delta_{ce}\delta_{km}\delta_{ln}-\delta_{ji}\delta_{ca}\delta_{bf}\delta_{de}\delta_{km}\delta_{ln} \\
&\quad-\delta_{ji}\delta_{da}\delta_{cf}\delta_{be}\delta_{km}\delta_{ln}+\delta_{ji}\delta_{ca}\delta_{df}\delta_{be}\delta_{km}\delta_{ln}+\delta_{ki}\delta_{ba}\delta_{df}\delta_{ce}\delta_{jm}\delta_{ln} \\
&\quad-\delta_{ki}\delta_{da}\delta_{bf}\delta_{ce}\delta_{jm}\delta_{ln}-\delta_{ki}\delta_{ba}\delta_{cf}\delta_{de}\delta_{jm}\delta_{ln}+\delta_{ki}\delta_{ca}\delta_{bf}\delta_{de}\delta_{jm}\delta_{ln} \\
&\quad+\delta_{ki}\delta_{da}\delta_{cf}\delta_{be}\delta_{jm}\delta_{ln}-\delta_{ki}\delta_{ca}\delta_{df}\delta_{be}\delta_{jm}\delta_{ln}+\delta_{li}\delta_{ba}\delta_{df}\delta_{ce}\delta_{km}\delta_{jn} \\
&\quad-\delta_{li}\delta_{da}\delta_{bf}\delta_{ce}\delta_{km}\delta_{jn}-\delta_{li}\delta_{ba}\delta_{cf}\delta_{de}\delta_{km}\delta_{jn}+\delta_{li}\delta_{ca}\delta_{bf}\delta_{de}\delta_{km}\delta_{jn} \\
&\quad+\delta_{li}\delta_{da}\delta_{cf}\delta_{be}\delta_{km}\delta_{jn}-\delta_{li}\delta_{ca}\delta_{df}\delta_{be}\delta_{km}\delta_{jn}-\delta_{ki}\delta_{ba}\delta_{df}\delta_{ce}\delta_{lm}\delta_{jn} \\
&\quad+\delta_{ki}\delta_{da}\delta_{bf}\delta_{ce}\delta_{lm}\delta_{jn}+\delta_{ki}\delta_{ba}\delta_{cf}\delta_{de}\delta_{lm}\delta_{jn}-\delta_{ki}\delta_{ca}\delta_{bf}\delta_{de}\delta_{lm}\delta_{jn} \\
&\quad-\delta_{ki}\delta_{da}\delta_{cf}\delta_{be}\delta_{lm}\delta_{jn}+\delta_{ki}\delta_{ca}\delta_{df}\delta_{be}\delta_{lm}\delta_{jn}\} \\
=&c^{os}\left\{\frac{1}{2}\delta_{ij}\sum_{ckl} t_{klac}^{os}\langle kl||bc\rangle+\frac{1}{2}\delta_{ab}\sum_{cdk} t_{ikcd}^{os}\langle jk||cd\rangle-\sum_{ck} t_{ikac}^{os}\langle jk||bc\rangle\right\} \\
=&\frac{1}{2}\delta_{ij}\sum_{ckl} t_{klac}^{sos}\langle kl||bc\rangle+\frac{1}{2}\delta_{ab}\sum_{cdk} t_{ikcd}^{sos}\langle jk||cd\rangle-\sum_{ck} t_{ikac}^{sos}\langle jk||bc\rangle
\end{aligned}
$$

$$
\begin{aligned}
&\langle\Phi_i^a|\left[\hat{H},\tau_j^b\right]|\Phi_0\rangle \\
=&\langle\Phi_0|c_i^\dagger c_a\left[\sum_p \epsilon_p c_p^\dagger c_p - \sum_{pq}\sum_m \langle pm||qm\rangle c_p^\dagger c_q + \frac{1}{2}\sum_{pqrs}\langle pq|rs\rangle c_p^\dagger c_q^\dagger c_s c_r, c_b^\dagger c_j\right]|\Phi_0\rangle \\
=&\sum_p \langle\Phi_0|c_i^\dagger c_a\left[c_p^\dagger c_p, c_b^\dagger c_j\right]|\Phi_0\rangle - \sum_{pq}\sum_m \langle pm||qm\rangle\langle\Phi_0|c_i^\dagger c_a\left[c_p^\dagger c_q, c_b^\dagger c_j\right]|\Phi_0\rangle \\
&+\frac{1}{2}\sum_{pqrs}\langle pq|rs\rangle\langle\Phi_0|c_i^\dagger c_a\left[c_p^\dagger c_q^\dagger c_s c_r, c_b^\dagger c_j\right]|\Phi_0\rangle \\
=&\sum_{m\neq j}\epsilon_m\delta_{ab}\delta_{ij} + \epsilon_b\delta_{ab}\delta_{ij} - \sum_m \epsilon_m\delta_{ab}\delta_{ij} \\
&-\sum_{no}\sum_m \langle nm||om\rangle\langle\Phi_0|c_i^\dagger c_a\left[c_n^\dagger c_o, c_b^\dagger c_j\right]|\Phi_0\rangle \\
&-\sum_{ef}\sum_m \langle em||fm\rangle\langle\Phi_0|c_i^\dagger c_a\left[c_e^\dagger c_f, c_b^\dagger c_j\right]|\Phi_0\rangle \\
&+\frac{1}{2}\sum_{klmn}\langle kl|mn\rangle\langle\Phi_0|c_i^\dagger c_a\left[c_k^\dagger c_l^\dagger c_n c_m, c_b^\dagger c_j\right]|\Phi_0\rangle \\
&+\frac{1}{2}\sum_{kdle}\langle kd|le\rangle\langle\Phi_0|c_i^\dagger c_a\left[c_k^\dagger c_d^\dagger c_e c_l, c_b^\dagger c_j\right]|\Phi_0\rangle \\
&+\frac{1}{2}\sum_{dkle}\langle dk|le\rangle\langle\Phi_0|c_i^\dagger c_a\left[c_d^\dagger c_k^\dagger c_e c_l, c_b^\dagger c_j\right]|\Phi_0\rangle \\
&+\frac{1}{2}\sum_{kdel}\langle kd|el\rangle\langle\Phi_0|c_i^\dagger c_a\left[c_k^\dagger c_d^\dagger c_l c_e, c_b^\dagger c_j\right]|\Phi_0\rangle \\
&+\frac{1}{2}\sum_{dkel}\langle dk|el\rangle\langle\Phi_0|c_i^\dagger c_a\left[c_d^\dagger c_k^\dagger c_l c_e, c_b^\dagger c_j\right]|\Phi_0\rangle \\
=&(\epsilon_a-\epsilon_i)\delta_{ab}\delta_{ij} \\
&-\sum_{no}\sum_m \langle nm||om\rangle\delta_{ab}\left\{\delta_{ij}\delta_{no}-\delta_{nj}\delta_{io}-\delta_{no}\delta_{ij}\right\} - \sum_{ef}\sum_m\langle em||fm\rangle\delta_{fb}\delta_{ae}\delta_{ij} \\
&+\frac{1}{2}\sum_{klmn}\langle kl|mn\rangle\left(-\delta_{mi}\delta_{ba}\delta_{jk}\delta_{nl}+\delta_{ni}\delta_{ba}\delta_{jk}\delta_{ml}+\delta_{mi}\delta_{ba}\delta_{nk}\delta_{jl}-\delta_{ni}\delta_{ba}\delta_{mk}\delta_{jl}\right) \\
&+\sum_{kdle}\langle kd||le\rangle\langle\Phi_0|c_i^\dagger c_a\left[c_k^\dagger c_d^\dagger c_e c_l, c_b^\dagger c_j\right]|\Phi_0\rangle \\
=&(\epsilon_a-\epsilon_i)\delta_{ab}\delta_{ij} + \sum_m\left\{\langle jm||im\rangle\delta_{ab}-\langle am||bm\rangle\delta_{ij}\right\} - \sum_m\langle jm||im\rangle\delta_{ab} \\
&+\sum_{kdle}\langle kd||le\rangle\delta_{ad}\delta_{eb}\left\{\delta_{kl}\delta_{ij}-\delta_{kj}\delta_{il}\right\} \\
=&(\epsilon_a-\epsilon_i)\delta_{ab}\delta_{ij} - \sum_m\langle am||bm\rangle\delta_{ij} + \sum_m\langle ma||mb\rangle\delta_{ij} - \langle ja||ib\rangle \\
=&(\epsilon_a-\epsilon_i)\delta_{ab}\delta_{ij} - \langle ja||ib\rangle
\end{aligned}
$$

This results in the following explicit expressions in the SOS-ADC(2)-s scheme derived from SOS-CC2 (the remaining elements are unchanged, t^{sos}_{iajb} as defined in Section 4.2, $c_{os} = 1.3$ and $c^{os}_{coupling} = 1.17$):

$$C^{(2)A}_{ia,jb} = \frac{1}{4}\delta_{ij} \sum_{ckl} \left[t^{sos}_{kalc} \langle kl||bc\rangle + t^{sos^*}_{kblc} \langle ac||kl\rangle \right]$$

$$C^{(2)B}_{ia,jb} = \frac{1}{4}\delta_{ab} \sum_{cdk} \left[t^{sos}_{ickd} \langle jk||cd\rangle + t^{sos^*}_{jckd} \langle cd||ik\rangle \right]$$

$$C^{(2)C}_{ia,jb} = -\frac{1}{2} \sum_{ck} \left[t^{sos}_{iakc} \langle jk||bc\rangle + t^{sos^*}_{jbkc} \langle ac||ik\rangle \right]$$

$$C^{(1)}_{ia,kcld} = c^{os}_{coupling} \left\{ \langle kl||id\rangle\delta_{ac} - \langle kl||ic\rangle\delta_{ad} - \langle al||cd\rangle\delta_{ik} + \langle ak||cd\rangle\delta_{il} \right\} (1 - \delta_{\sigma(k)\sigma(l)})$$

$$C^{(1)}_{iajb,kc} = c^{os}_{coupling} \left\{ \langle kb||ij\rangle\delta_{ac} - \langle ka||ij\rangle\delta_{bc} - \langle ab||cj\rangle\delta_{ik} + \langle ab||ci\rangle\delta_{jk} \right\} (1 - \delta_{\sigma(i)\sigma(j)})$$

$$K_{iajb,kcld} = (\epsilon_a + \epsilon_b - \epsilon_i - \epsilon_j)\delta_{ac}\delta_{bd}\delta_{ik}\delta_{jl}(1 - \delta_{\sigma(i)\sigma(j)})(1 - \delta_{\sigma(k)\sigma(l)})$$

B. Detailed Results SOS-ADC(2)-s/-x

B.1. Vertical excitation energies for the complete set of molecules

Table B.1.: Vertical excitation energies for singlet states in eV with SOS-ADC(2)-x and the final parameter set of $c^{os}_{coupling} = 1.0$ and $c^{os}_{x} = 0.9$. TBE-2 and CC3 values taken from [89] and DFT/MRCI from [91]. States with high double excitation character are in bold.

Molecule	State	TBE-2	CC3	DFT/MRCI	SOS-ADC(2)-x (1.0, 0.9)
Ethene	1^1B_{1u} ($\pi \rightarrow \pi^*$)	7.80	7.89	7.96	7.87
E-Butadiene	1^1B_u ($\pi \rightarrow \pi^*$)	6.18	6.21	6.02	6.19
	$2^1\mathbf{A_g}$ ($\pi \rightarrow \pi^*$)	**6.55**	**6.63**	**6.18**	**6.19**
E-Hexatriene	1^1B_u ($\pi \rightarrow \pi^*$)	5.10	5.32	4.95	5.33
	$2^1\mathbf{A_g}$ ($\pi \rightarrow \pi^*$)	**5.09**	**5.77**	**4.92**	**5.16**
E-Octatetraene	1^1B_u ($\pi \rightarrow \pi^*$)	4.66	4.84	4.25	4.75
	$2^1\mathbf{A_g}$ ($\pi \rightarrow \pi^*$)	**4.47**	**4.75**	**4.01**	**4.45**
Cyclopropene	1^1B_1 ($\sigma \rightarrow \pi^*$)	6.67	6.67	6.73	6.65
	1^1B_2 ($\pi \rightarrow \pi^*$)	6.68	6.68	6.74	6.80
Cyclopentadiene	1^1B_2 ($\pi \rightarrow \pi^*$)	5.55	5.49	6.15	5.54
	$2^1\mathbf{A_1}$ ($\pi \rightarrow \pi^*$)	**6.28**	**6.49**	**5.42**	**6.05**
Norbornadiene	1^1A_2 ($\pi \rightarrow \pi^*$)	5.37	5.37	5.30	5.53
	1^1B_2 ($\pi \rightarrow \pi^*$)	6.21	6.21	6.12	6.44
Benzene	1^1B_{2u} ($\pi \rightarrow \pi^*$)	5.08	5.03	5.04	4.57
	1^1B_{1u} ($\pi \rightarrow \pi^*$)	6.54	6.42	6.31	6.28
	1^1E_{1u} ($\pi \rightarrow \pi^*$)	7.13	7.14	7.19	7.06
	$1^1\mathbf{E_{2g}}$ ($\pi \rightarrow \pi^*$)	**8.15**	**8.31**	**7.51**	**7.63**
Naphthalene	1^1B_{3u} ($\pi \rightarrow \pi^*$)	4.25	4.25	4.10	3.92
	1^1B_{2u} ($\pi \rightarrow \pi^*$)	4.82	4.82	4.60	4.81
	2^1A_g ($\pi \rightarrow \pi^*$)	5.90	5.90	5.65	5.46
	$1^1\mathbf{B_{1g}}$ ($\pi \rightarrow \pi^*$)	**5.75**	**5.75**	**5.53**	**5.66**
	2^1B_{3u} ($\pi \rightarrow \pi^*$)	6.11	6.11	5.89	6.07
	2^1B_{2u} ($\pi \rightarrow \pi^*$)	6.36	6.36	6.21	6.29
	2^1B_{1g} ($\pi \rightarrow \pi^*$)	6.46	6.46	6.26	6.30
	$3^1\mathbf{B_{3u}}$ ($\pi \rightarrow \pi^*$)	**-**	**8.32**	**7.38**	**7.29**
Furan	1^1B_2 ($\pi \rightarrow \pi^*$)	6.32	6.26	6.33	6.33
	2^1A_1 ($\pi \rightarrow \pi^*$)	6.57	6.51	6.32	6.11
	3^1A_1 ($\pi \rightarrow \pi^*$)	8.13	8.13	8.21	8.08
Pyrrole	2^1A_1 ($\pi \rightarrow \pi^*$)	6.37	6.27	6.13	5.87
	3^1A_1 ($\pi \rightarrow \pi^*$)	7.91	7.60	7.88	7.59
Imidazole	$2^1A'$ ($\pi \rightarrow \pi^*$)	6.25	6.25	6.29	6.09
	$1^1A''$ ($n \rightarrow \pi^*$)	6.65	6.65	6.35	6.54
	$3^1A'$ ($\pi \rightarrow \pi^*$)	6.73	6.73	6.82	6.59
Pyridine	1^1B_2 ($\pi \rightarrow \pi^*$)	4.85	5.12	5.09	4.65
	1^1B_1 ($n \rightarrow \pi^*$)	4.59	4.95	4.75	4.97
	1^1A_2 ($n \rightarrow \pi^*$)	5.11	5.41	5.41	5.29
	2^1A_1 ($\pi \rightarrow \pi^*$)	6.26	6.60	6.47	6.44
	2^1B_2 ($\pi \rightarrow \pi^*$)	7.27	7.33	7.27	7.15
	3^1A_1 ($\pi \rightarrow \pi^*$)	7.18	7.39	7.43	7.32
	$3^1\mathbf{B_2}$ ($\pi \rightarrow \pi^*$)	**-**	**7.72**	**-**	**8.01**
	$4^1\mathbf{A_1}$ ($\pi \rightarrow \pi^*$)	**-**	**8.33**	**-**	**7.89**
Pyrazine	1^1B_{3u} ($n \rightarrow \pi^*$)	4.13	4.13	4.00	4.20
	1^1A_u ($n \rightarrow \pi^*$)	4.98	4.98	5.02	4.96

B. Detailed Results SOS-ADC(2)-s/-x

Molecule	State	TBE-2	CC3	DFT/MRCI	SOS-ADC(2)-x (1.0, 0.9)
	1^1B_{2u} ($\pi \rightarrow \pi^*$)	4.97	4.97	4.94	4.47
	1^1B_{2g} ($n \rightarrow \pi^*$)	5.65	5.65	5.26	5.52
	1^1B_{1g} ($n \rightarrow \pi^*$)	6.69	6.69	6.46	6.45
	1^1B_{1u} ($\pi \rightarrow \pi^*$)	6.83	6.83	6.71	6.75
	2^1B_{2u} ($\pi \rightarrow \pi^*$)	7.81	7.81	7.75	7.62
	2^1B_{1u} ($\pi \rightarrow \pi^*$)	7.86	7.86	7.82	7.83
	$1^1\mathbf{B_{3g}}$ ($\pi \rightarrow \pi^*$)	**-**	**8.69**	**-**	**7.94**
	$2^1\mathbf{A_g}$ ($\pi \rightarrow \pi^*$)	**-**	**8.78**	**-**	**7.74**
Pyrimidine	1^1B_1 ($n \rightarrow \pi^*$)	4.43	4.43	4.36	4.42
	1^1A_2 ($n \rightarrow \pi^*$)	4.85	4.85	4.82	4.77
	1^1B_2 ($\pi \rightarrow \pi^*$)	5.34	5.34	5.35	4.85
	2^1A_1 ($\pi \rightarrow \pi^*$)	6.82	6.82	6.69	6.64
Pyridazine	1^1B_1 ($n \rightarrow \pi^*$)	3.85	3.85	3.63	3.81
	1^1A_2 ($n \rightarrow \pi^*$)	4.44	4.44	4.25	4.30
	2^1A_1 ($\pi \rightarrow \pi^*$)	5.20	5.20	5.16	4.64
	2^1A_2 ($n \rightarrow \pi^*$)	5.66	5.66	5.29	5.53
s-Triazine	$1^1A"_1$ ($n \rightarrow \pi^*$)	4.70	4.70	4.69	4.53
	$1^1A"_2$ ($n \rightarrow \pi^*$)	4.71	4.71	4.56	4.78
	$1^1E"$ ($n \rightarrow \pi^*$)	4.75	4.75	4.77	4.71
	$1^1A'_2$ ($\pi \rightarrow \pi^*$)	5.71	5.71	5.70	5.17
	$2^1\mathbf{E'}$ ($\pi \rightarrow \pi^*$)	**-**	**9.44**	**-**	**8.78**
s-Tetrazine	1^1B_{3u} ($n \rightarrow \pi^*$)	2.46	2.46	2.35	2.45
	1^1A_u ($n \rightarrow \pi^*$)	3.78	3.78	3.70	3.70
	1^1B_{1g} ($n \rightarrow \pi^*$)	4.87	4.87	4.45	4.56
	1^1B_{2u} ($\pi \rightarrow \pi^*$)	5.08	5.08	5.07	4.43
	1^1B_{2g} ($n \rightarrow \pi^*$)	5.28	5.28	4.75	4.90
	2^1A_u ($n \rightarrow \pi^*$)	-	5.39	5.05	5.33
	$2^1\mathbf{B_{2g}}$ ($n \rightarrow \pi^*$)	**-**	**6.16**	**5.68**	**5.78**
	$3^1\mathbf{B_{1g}}$ ($n \rightarrow \pi^*$)	**-**	**7.12**	**6.49**	**6.70**
	$2^1\mathbf{B_{3g}}$ ($\pi \rightarrow \pi^*$)	**-**	**8.51**	**7.44**	**7.25**
Formaldehyde	1^1A_2 ($n \rightarrow \pi^*$)	3.88	3.88	3.71	3.74
	1^1B_1 ($\sigma \rightarrow \pi^*$)	9.04	9.05	8.76	9.01
	2^1A_1 ($\pi \rightarrow \pi^*$)	9.29	9.31	9.19	9.21
Acetone	1^1A_2 ($n \rightarrow \pi^*$)	4.38	4.38	4.23	4.23
	1^1B_1 ($\sigma \rightarrow \pi^*$)	9.04	9.04	8.56	9.09
p-Benzoquinone	1^1B_{1g} ($n \rightarrow \pi^*$)	2.74	2.74	2.22	2.75
	1^1A_u ($n \rightarrow \pi^*$)	2.86	2.86	2.29	2.83
	1^1B_{3g} ($\pi \rightarrow \pi^*$)	4.44	4.44	3.99	4.59
	1^1B_{1u} ($\pi \rightarrow \pi^*$)	5.47	5.47	5.07	5.54
	$1^1\mathbf{B_{3u}}$ ($n \rightarrow \pi^*$)	**5.55**	**5.71**	**5.81**	**5.72**
	2^1B_{3g} ($\pi \rightarrow \pi^*$)	7.16	7.16	6.71	7.08
	$2^1\mathbf{B_{1u}}$ ($\pi \rightarrow \pi^*$)	**-**	**7.62**	**7.60**	**7.24**
Formamide	$1^1A''$ ($n \rightarrow \pi^*$)	5.55	5.55	5.47	5.40
	$2^1A'$ ($\pi \rightarrow \pi^*$)	7.35	7.35	8.14	7.37
Acetamide	$1^1A''$ ($n \rightarrow \pi^*$)	5.62	5.62	5.48	5.45
	$2^1A'$ ($\pi \rightarrow \pi^*$)	7.14	7.14	7.51	7.00
Propanamide	$1^1A''$ ($n \rightarrow \pi^*$)	5.65	5.65	5.47	5.49
	$2^1A'$ ($\pi \rightarrow \pi^*$)	7.09	7.09	7.46	7.00

Table B.2.: Vertical excitation energies for singlet states in eV. TBE-2 and CC3 values taken from [89]. The numbers in brackets give the value of $c^{os}_{coupling}$.

Molecule	State	TBE-2	CC3	ADC(2)-s	SOS-ADC(2)-s (Turbomole)	ISR-SOS-ADC(2)-s	SOS-ADC(2)-s (1.15)	SOS-ADC(2)-s (1.17)
Ethene	1^1B_{1u} ($\pi \rightarrow \pi^*$)	7.80	7.89	7.87	7.95	7.85	7.92	7.85
E-Butadiene	1^1B_u ($\pi \rightarrow \pi^*$)	6.18	6.21	6.10	6.29	6.03	6.25	6.16
E-Hexatriene	1^1B_u ($\pi \rightarrow \pi^*$)	5.10	5.32	5.15	5.39	5.03	5.34	5.24
E-Octatetraene	1^1B_u ($\pi \rightarrow \pi^*$)	4.66	4.84	4.50	4.78	4.35	4.73	4.62
Cyclopropene	1^1B_1 ($\sigma \rightarrow \pi^*$)	6.67	6.67	6.77	6.92	6.70	6.88	6.80
	1^1B_2 ($\pi \rightarrow \pi^*$)	6.68	6.68	6.70	6.92	6.67	6.88	6.81
Cyclopentadiene	1^1B_2 ($\pi \rightarrow \pi^*$)	5.55	5.49	5.46	5.62	5.33	5.57	5.48
Norbornadiene	1^1A_2 ($\pi \rightarrow \pi^*$)	5.37	5.37	5.29	5.65	5.14	5.60	5.50
	1^1B_2 ($\pi \rightarrow \pi^*$)	6.21	6.21	6.10	6.61	5.95	6.56	6.45
Benzene	1^1B_{2u} ($\pi \rightarrow \pi^*$)	5.08	5.03	5.27	5.02	4.99	4.96	4.82
	1^1B_{1u} ($\pi \rightarrow \pi^*$)	6.54	6.42	6.46	6.33	6.19	6.28	6.19
	1^1E_{1u} ($\pi \rightarrow \pi^*$)	7.13	7.14	7.16	7.28	6.96	7.23	7.13
Naphthalene	1^1B_{3u} ($\pi \rightarrow \pi^*$)	4.25	4.25	4.43	4.31	4.07	4.24	4.10
	1^1B_{2u} ($\pi \rightarrow \pi^*$)	4.82	4.82	4.79	4.90	4.47	4.85	4.73
	2^1A_g ($\pi \rightarrow \pi^*$)	5.90	5.90	6.11	6.00	5.76	5.94	5.80
	2^1B_{3u} ($\pi \rightarrow \pi^*$)	6.11	6.11	6.04	6.23	5.73	6.17	6.05
	2^1B_{2u} ($\pi \rightarrow \pi^*$)	6.36	6.36	6.39	6.47	6.04	6.41	6.29
	2^1B_{1g} ($\pi \rightarrow \pi^*$)	6.46	6.46	6.51	6.63	6.22	6.57	6.45
Furan	1^1B_2 ($\pi \rightarrow \pi^*$)	6.32	6.26	6.40	6.47	6.22	6.43	6.33
	2^1A_1 ($\pi \rightarrow \pi^*$)	6.57	6.51	6.71	6.76	6.50	6.69	6.55
	3^1A_1 ($\pi \rightarrow \pi^*$)	8.13	8.13	8.17	8.31	8.03	8.26	8.17
Pyrrole	2^1A_1 ($\pi \rightarrow \pi^*$)	6.37	6.27	6.44	6.37	6.22	6.31	6.17
	3^1A_1 ($\pi \rightarrow \pi^*$)	7.91	7.60	7.74	7.84	7.54	7.80	7.71
Imidazole	$2^1A'$ ($\pi \rightarrow \pi^*$)	6.25	6.25	6.43	6.47	6.20	6.41	6.29
	$1^1A''$ ($n \rightarrow \pi^*$)	6.65	6.65	6.68	6.87	6.49	6.84	6.69
	$3^1A'$ ($\pi \rightarrow \pi^*$)	6.73	6.73	6.94	6.89	6.71	6.83	6.71
Pyridine	1^1B_2 ($\pi \rightarrow \pi^*$)	4.85	5.12	5.31	5.08	5.02	5.01	4.87
	1^1B_1 ($n \rightarrow \pi^*$)	4.59	4.95	4.99	5.31	4.78	5.24	5.11
	1^1A_2 ($n \rightarrow \pi^*$)	5.11	5.41	5.26	5.62	5.05	5.55	5.40
	2^1A_1 ($\pi \rightarrow \pi^*$)	6.26	6.60	6.64	6.54	6.37	6.49	6.39
	2^1B_2 ($\pi \rightarrow \pi^*$)	7.27	7.33	7.32	7.45	7.11	7.40	7.28
	3^1A_1 ($\pi \rightarrow \pi^*$)	7.18	7.39	7.42	7.66	7.24	7.60	7.49

Molecule	State	TBE-2	CC3	ADC(2)-s	SOS-ADC(2)-s (Turbomole)	ISR-SOS-ADC(2)-s	SOS-ADC(2)-s (1.15)	SOS-ADC(2)-s (1.17)
Pyrazine	1^1B_{3u} $(n \to \pi^*)$	4.13	4.13	4.19	4.48	3.96	4.41	4.28
	1^1A_u $(n \to \pi^*)$	4.98	4.98	4.88	5.29	4.66	5.22	5.06
	1^1B_{2u} $(\pi \to \pi^*)$	4.97	4.97	5.16	4.94	4.86	4.86	4.71
	1^1B_{2g} $(n \to \pi^*)$	5.65	5.65	5.86	6.10	5.65	6.03	5.89
	1^1B_{1g} $(n \to \pi^*)$	6.69	6.69	6.64	7.04	6.43	6.96	6.79
	1^1B_{1u} $(\pi \to \pi^*)$	6.83	6.83	6.85	6.79	6.60	6.73	6.63
	2^1B_{2u} $(\pi \to \pi^*)$	7.81	7.81	7.84	7.89	7.58	7.84	7.72
	2^1B_{1u} $(\pi \to \pi^*)$	7.86	7.86	7.94	8.07	7.74	8.01	7.89
Pyrimidine	1^1B_1 $(n \to \pi^*)$	4.43	4.43	4.37	4.71	4.13	4.64	4.50
	1^1A_2 $(n \to \pi^*)$	4.85	4.85	4.71	5.04	4.49	4.97	4.82
	1^1B_2 $(\pi \to \pi^*)$	5.34	5.34	5.49	5.26	5.19	5.18	5.03
	2^1A_1 $(\pi \to \pi^*)$	6.82	6.82	6.89	6.81	6.65	6.76	6.64
Pyridazine	1^1B_1 $(n \to \pi^*)$	3.85	3.85	3.83	4.16	3.60	4.09	3.95
	1^1A_2 $(n \to \pi^*)$	4.44	4.44	4.32	4.74	4.11	4.67	4.51
	2^1A_1 $(\pi \to \pi^*)$	5.20	5.20	5.38	5.14	5.07	5.06	4.91
	2^1A_2 $(n \to \pi^*)$	5.66	5.66	5.77	6.11	5.55	6.04	5.90
s-Triazine	$1^1A"_1$ $(n \to \pi^*)$	4.70	4.70	4.56	4.82	4.33	4.74	4.58
	$1^1A"_2$ $(n \to \pi^*)$	4.71	4.71	4.69	5.10	4.47	5.03	4.88
	$1^1E"$ $(n \to \pi^*)$	4.75	4.75	4.65	5.00	4.41	4.93	4.77
	$1^1A'_2$ $(\pi \to \pi^*)$	5.71	5.71	5.78	5.56	5.46	5.48	5.32
s-Tetrazine	1^1B_{3u} $(n \to \pi^*)$	2.46	2.46	2.48	2.79	2.21	2.72	2.56
	1^1A_u $(n \to \pi^*)$	3.78	3.78	3.67	4.13	3.43	4.05	3.89
	1^1B_{1g} $(n \to \pi^*)$	4.87	4.87	5.11	5.36	4.88	5.28	5.11
	1^1B_{2u} $(\pi \to \pi^*)$	5.08	5.08	5.24	4.97	4.90	4.89	4.72
	1^1B_{2g} $(n \to \pi^*)$	5.28	5.28	5.56	5.86	5.32	5.78	5.62
	2^1A_u $(n \to \pi^*)$	5.39	5.39	5.52	5.85	5.28	5.78	5.63
Formaldehyde	1^1A_2 $(n \to \pi^*)$	3.88	3.88	3.83	3.99	3.81	3.94	3.82
	1^1B_1 $(\sigma \to \pi^*)$	9.04	9.05	9.11	9.25	9.06	9.19	9.07
	2^1A_1 $(\pi \to \pi^*)$	9.29	9.31	9.41	9.51	9.34	9.46	9.36
Acetone	1^1A_2 $(n \to \pi^*)$	4.38	4.38	4.24	4.39	4.12	4.33	4.19
	1^1B_1 $(\sigma \to \pi^*)$	9.04	9.04	9.04	9.22	8.94	9.16	9.03
p-Benzoquinone	1^1B_{1g} $(n \to \pi^*)$	2.74	2.74	2.64	3.11	2.49	3.03	2.88
	1^1A_u $(n \to \pi^*)$	2.86	2.86	2.72	3.18	2.56	3.10	2.95
	1^1B_{3g} $(\pi \to \pi^*)$	4.44	4.44	4.69	5.03	4.52	4.97	4.84
	1^1B_{1u} $(\pi \to \pi^*)$	5.47	5.47	5.33	5.72	5.17	5.65	5.51
	2^1B_{3g} $(\pi \to \pi^*)$	7.16	7.16	7.10	7.49	6.49	7.43	7.29

Molecule	State	TBE-2	CC3	ADC(2)-s	SOS-ADC(2)-s (Turbomole)	ISR-SOS-ADC(2)-s	SOS-ADC(2)-s (1.15)	SOS-ADC(2)-s (1.17)
Formamide	$1^1A''$ $(n \rightarrow \pi^*)$	5.55	5.55	5.36	5.51	5.24	5.44	5.31
	$2^1A'$ $(\pi \rightarrow \pi^*)$	7.35	7.35	7.29	7.41	7.17	7.34	7.20
Acetamide	$1^1A''$ $(n \rightarrow \pi^*)$	5.62	5.62	5.36	5.53	5.20	5.47	5.33
	$2^1A'$ $(\pi \rightarrow \pi^*)$	7.14	7.14	7.04	7.04	6.89	6.97	6.84
Propanamide	$1^1A''$ $(n \rightarrow \pi^*)$	5.65	5.65	5.37	5.55	5.20	5.48	5.34
	$2^1A'$ $(\pi \rightarrow \pi^*)$	7.09	7.09	6.97	7.00	6.82	6.94	6.80

Table B.3.: Vertical excitation energies for triplet states in eV. TBE-2 and CC3 values taken from [89]. The numbers in brackets give the value of $c^{os}_{coupling}$.

Molecule	State	TBE-2	CC3	ADC(2)-s	SOS-ADC(2)-s (Turbomole)	ISR SOS-ADC(2)-s	SOS-ADC(2)-s (1.15)	SOS-ADC(2)-s (1.17)
Ethene	1^3B_{1u} ($\pi \rightarrow \pi^*$)	4.50	4.50	4.55	4.56	4.34	4.50	4.45
E-Butadiene	1^3B_u ($\pi \rightarrow \pi^*$)	3.20	3.34	3.43	3.51	3.21	3.45	3.39
	1^3A_g ($\pi \rightarrow \pi^*$)	5.08	5.15	5.22	5.18	4.95	5.12	5.07
E-Hexatriene	1^3B_u ($\pi \rightarrow \pi^*$)	2.40	2.71	2.81	2.94	2.59	2.88	2.81
	1^3A_g ($\pi \rightarrow \pi^*$)	4.15	4.33	4.40	4.38	4.11	4.33	4.27
E-Octatetraene	1^3B_u ($\pi \rightarrow \pi^*$)	2.20	2.32	2.44	2.60	2.20	2.54	2.46
	1^3A_g ($\pi \rightarrow \pi^*$)	3.55	3.69	3.77	3.78	3.47	3.73	3.66
Cyclopropene	1^3B_2 ($\pi \rightarrow \pi^*$)	4.28	4.28	4.37	4.43	4.13	4.36	4.30
	1^3B_1 ($\pi \rightarrow \pi^*$)	6.40	6.40	6.44	6.71	6.37	6.64	6.56
Cyclopentadiene	1^3B_2 ($\pi \rightarrow \pi^*$)	3.26	3.26	3.35	3.41	3.09	3.35	3.28
	1^3A_1 ($\pi \rightarrow \pi^*$)	5.09	5.09	5.18	5.07	4.82	5.01	4.95
Norbornadiene	1^3A_2 ($\pi \rightarrow \pi^*$)	3.68	3.68	3.68	3.85	3.44	3.78	3.71
	1^3B_2 ($\pi \rightarrow \pi^*$)	4.16	4.16	4.21	4.19	3.83	4.12	4.06
Benzene	1^3B_{1u} ($\pi \rightarrow \pi^*$)	4.15	4.12	4.34	4.29	4.03	4.24	4.17
	1^3E_{1u} ($\pi \rightarrow \pi^*$)	4.86	4.81	5.06	4.96	4.60	4.92	4.82
	1^3B_{2u} ($\pi \rightarrow \pi^*$)	5.88	5.78	5.87	5.93	5.59	5.91	5.82
	1^3E_{2g} ($\pi \rightarrow \pi^*$)	7.51	7.45	7.96	7.84	7.61	7.81	7.73
Naphthalene	1^3B_{2u} ($\pi \rightarrow \pi^*$)	3.09	3.09	3.27	3.29	2.89	3.24	3.16
	1^3B_{3u} ($\pi \rightarrow \pi^*$)	4.09	4.09	4.30	4.25	3.78	4.21	4.10
	1^3B_{1g} ($\pi \rightarrow \pi^*$)	4.42	4.42	4.59	4.55	4.20	4.51	4.42
	2^3B_{2u} ($\pi \rightarrow \pi^*$)	4.56	4.56	4.82	4.73	4.31	4.70	4.59
	2^3B_{3u} ($\pi \rightarrow \pi^*$)	4.92	4.92	4.94	5.06	4.58	5.04	4.94
	1^3A_g ($\pi \rightarrow \pi^*$)	5.42	5.42	5.67	5.52	5.16	5.48	5.39
	2^3B_{1g} ($\pi \rightarrow \pi^*$)	6.12	6.12	6.12	6.40	5.79	6.35	6.23
	2^3A_g ($\pi \rightarrow \pi^*$)	6.17	6.17	6.55	6.65	6.17	6.60	6.50
	3^3A_g ($\pi \rightarrow \pi^*$)	6.65	6.65	6.85	6.93	6.49	6.91	6.80
	3^3B_{1g} ($\pi \rightarrow \pi^*$)	6.67	6.67	6.92	7.18	6.62	7.02	6.94
Furan	1^3B_2 ($\pi \rightarrow \pi^*$)	4.11	4.11	4.33	4.29	4.01	4.26	4.19
	1^3A_1 ($\pi \rightarrow \pi^*$)	5.43	5.43	5.55	5.40	5.11	5.35	5.27
Pyrrole	1^3B_2 ($\pi \rightarrow \pi^*$)	4.44	4.44	4.65	4.59	4.32	4.55	4.48
	1^3A_1 ($\pi \rightarrow \pi^*$)	5.42	5.42	5.60	5.47	5.17	5.42	5.33
Imidazole	$1^3A'$ ($\pi \rightarrow \pi^*$)	4.65	4.65	4.85	4.80	4.50	4.77	4.69

Molecule	State	TBE-2	CC3	ADC(2)-s	SOS-ADC(2)-s (Turbomole)	ISR SOS-ADC(2)-s	SOS-ADC(2)-s (1.15)	SOS-ADC(2)-s (1.17)
Pyridine	$2^3A'$ $(\pi \rightarrow \pi^*)$	5.64	5.64	5.87	5.74	5.43	5.70	5.57
	$1^3A''$ $(n \rightarrow \pi^*)$	6.25	6.25	6.24	6.50	6.11	6.45	6.31
	$3^3A'$ $(\pi \rightarrow \pi^*)$	6.38	6.38	6.53	6.63	6.20	6.56	6.46
	1^3A_1 $(\pi \rightarrow \pi^*)$	4.06	4.28	4.48	4.44	4.16	4.39	4.32
	1^3B_1 $(n \rightarrow \pi^*)$	4.25	4.42	4.45	4.80	4.25	4.73	4.61
	1^3B_2 $(\pi \rightarrow \pi^*)$	4.64	4.72	4.97	4.88	4.52	4.86	4.76
	2^3A_1 $(\pi \rightarrow \pi^*)$	4.91	4.96	5.25	5.11	4.75	5.08	4.98
	1^3A_2 $(n \rightarrow \pi^*)$	5.28	5.35	5.22	5.65	5.01	5.55	5.40
	2^3B_2 $(\pi \rightarrow \pi^*)$	6.08	6.22	6.33	6.38	6.01	6.36	6.26
s-Tetrazine	1^3B_{3u} $(n \rightarrow \pi^*)$	1.87	1.87	1.88	2.23	1.62	2.15	2.01
	1^3A_u $(n \rightarrow \pi^*)$	3.49	3.49	3.43	3.94	3.19	3.82	3.68
	1^3B_{1g} $(n \rightarrow \pi^*)$	4.18	4.18	4.31	4.52	4.09	4.47	4.34
	1^3B_{1u} $(\pi \rightarrow \pi^*)$	4.36	4.36	4.66	4.49	4.21	4.44	4.36
	1^3B_{2u} $(\pi \rightarrow \pi^*)$	4.39	4.39	4.71	4.52	4.14	4.52	4.41
	1^3B_{2g} $(n \rightarrow \pi^*)$	4.89	4.89	5.04	5.33	4.82	5.29	5.16
	2^3A_u $(n \rightarrow \pi^*)$	4.96	4.96	5.06	5.41	4.83	5.37	5.23
	2^3B_{1u} $(\pi \rightarrow \pi^*)$	5.32	5.32	5.60	5.49	5.06	5.46	5.33
Formaldehyde	1^3A_2 $(\pi \rightarrow \pi^*)$	3.50	3.49	3.34	3.64	3.34	3.54	3.44
	1^3A_1 $(\pi \rightarrow \pi^*)$	5.87	5.86	6.01	5.91	5.63	5.86	5.80
Acetone	1^3A_2 $(n \rightarrow \pi^*)$	4.05	4.05	3.86	4.13	3.74	4.02	3.91
	1^3A_1 $(\pi \rightarrow \pi^*)$	6.07	6.07	6.18	6.14	5.78	6.08	6.01
p-Benzoquinone	1^3B_{1g} $(n \rightarrow \pi^*)$	2.50	2.50	2.32	2.87	2.19	2.76	2.62
	1^3A_u $(n \rightarrow \pi^*)$	2.61	2.61	2.41	2.96	2.27	2.84	2.70
	1^3B_{1u} $(\pi \rightarrow \pi^*)$	3.02	3.02	3.15	3.24	2.79	3.19	3.10
	1^3B_{3g} $(\pi \rightarrow \pi^*)$	3.37	3.37	3.51	3.66	3.26	3.62	3.54
Formamide	$1^3A''$ $(n \rightarrow \pi^*)$	5.28	5.28	5.04	5.29	4.94	5.21	5.09
	$1^3A'$ $(\pi \rightarrow \pi^*)$	5.69	5.69	5.75	5.85	5.41	5.77	5.67
Acetamide	$1^3A''$ $(n \rightarrow \pi^*)$	5.35	5.35	5.09	5.36	4.94	5.27	5.14
	$1^3A'$ $(\pi \rightarrow \pi^*)$	5.71	5.71	5.88	6.00	5.55	5.92	5.82
Propanamide	$1^3A''$ $(n \rightarrow \pi^*)$	5.38	5.38	5.10	5.38	4.95	5.29	5.16
	$1^3A'$ $(\pi \rightarrow \pi^*)$	6.08	6.08	5.89	6.02	5.55	5.94	5.84

B.2. Detailed results with strict ADC(2) methods

Excitation energies in eV (ΔE) and oscillator strangs for optically allowed transitions in legth gauge (f) obtained with ADC(2)-s, ISR-ADC(2)-s, our SOS-ADC(2)-s, and SOS-ADC(2)-s from TURBOMOLE [84–86]. If not stated otherwise, aug-cc-pVDZ [75] was used as basis set. Structures were taken from [88]. The numbers in brackets give the value of $c^{os}_{coupling}$.

Ethene

State	ADC(2)-s aug-cc-pVTZ	ADC(2)-s cc-pVTZ	ADC(2)-s aug-cc-pVDZ		SOS-ADC(2)-s Turbomole	ISR-SOS-ADC(2)-s		SOS-ADC(2)-s (1.15)		SOS-ADC(2)-s (1.16)		SOS-ADC(2)-s (1.17)		SOS-ADC(2)-s (1.18)	
	ΔE	ΔE	ΔE	f	ΔE	ΔE	f	ΔE	f	ΔE	f	ΔE	f	ΔE	f
Singlet states															
1^1B_{1u}	7.89	8.33	7.87	0.39	7.95	7.85	0.35	7.92	0.36	7.89	0.36	7.85	0.36	7.82	0.36
Triplet states															
1^3B_{1u}	4.56	4.58	4.55	-	4.52	4.34	4.50	-	4.48	-	4.45	-	4.43	-	

Butadiene

State	ADC(2)-s aug-cc-pVTZ	ADC(2)-s cc-pVTZ	ADC(2)-s aug-cc-pVDZ		SOS-ADC(2)-s Turbomole	ISR-SOS-ADC(2)-s		SOS-ADC(2)-s (1.15)		SOS-ADC(2)-s (1.16)		SOS-ADC(2)-s (1.17)		SOS-ADC(2)-s (1.18)	
	ΔE	ΔE	ΔE	f	ΔE	ΔE	f	ΔE	f	ΔE	f	ΔE	f	ΔE	f
Singlet states															
1^1B_u	6.10	6.35	6.10	0.75	6.29	6.03	0.64	6.25	0.70	6.20	0.70	6.16	0.69	6.12	0.69
Triplet states															
1^3B_u	3.43	3.44	3.43	-	3.48	3.21	-	3.45	-	3.42	-	3.39	-	3.36	-
1^3A_g	5.23	5.29	5.22	-	5.15	4.95	-	5.12	-	5.09	-	5.07	-	5.04	-

Hexatriene

State	ADC(2)-s aug-cc-pVTZ	ADC(2)-s cc-pVTZ	ADC(2)-s aug-cc-pVDZ		SOS-ADC(2)-s Turbomole	ISR-SOS-ADC(2)-s		SOS-ADC(2)-s (1.15)		SOS-ADC(2)-s (1.16)		SOS-ADC(2)-s (1.17)		SOS-ADC(2)-s (1.18)	
	ΔE	ΔE	ΔE	f	ΔE	ΔE	f	ΔE	f	ΔE	f	ΔE	f	ΔE	f
Singlet states															
1^1B_u	5.13	5.26	5.15	1.24	5.39	5.03	1.03	5.34	1.15	5.29	1.13	5.24	1.12	5.19	1.11
Triplet states															
1^3B_u	2.82	2.82	2.81	-	2.92	2.59	-	2.88	-	2.85	-	2.81	-	2.78	-
1^3A_g	4.40	4.42	4.40	-	4.36	4.11	-	4.33	-	4.30	-	4.27	-	4.24	-

Octatetraene

State	ADC(2)-s aug-cc-pVTZ	ADC(2)-s cc-pVTZ	ADC(2)-s aug-cc-pVDZ		SOS-ADC(2)-s Turbomole	ISR-SOS-ADC(2)-s		SOS-ADC(2)-s (1.15)		SOS-ADC(2)-s (1.16)		SOS-ADC(2)-s (1.17)		SOS-ADC(2)-s (1.18)	
	ΔE	ΔE	ΔE	f	ΔE	ΔE	f	ΔE	f	ΔE	f	ΔE	f	ΔE	f
Singlet states															
1^1B_u	4.48	4.56	4.50	1.71	4.78	4.35	1.36	4.73	1.56	4.67	1.54	4.62	1.52	4.57	1.51
Triplet states															
1^3B_u	2.44	2.44	2.44	-	2.58	2.20	-	2.54	-	2.50	-	2.46	-	2.42	-
1^3A_g	3.77	3.77	3.77	-	3.76	3.47	-	3.73	-	3.70	-	3.66	-	3.63	-

Cyclopropene

State	ADC(2)-s aug-cc-pVTZ	ADC(2)-s cc-pVTZ	ADC(2)-s aug-cc-pVDZ		SOS-ADC(2)-s Turbomole	ISR-SOS-ADC(2)-s		SOS-ADC(2)-s (1.15)		SOS-ADC(2)-s (1.16)		SOS-ADC(2)-s (1.17)		SOS-ADC(2)-s (1.18)	
	ΔE	ΔE	ΔE	f	ΔE	ΔE	f	ΔE	f	ΔE	f	ΔE	f	ΔE	f
Singlet states															
1^1B_1	6.75	6.93	6.77	0.01	6.92	6.70	0.01	6.88	0.00	6.84	0.00	6.80	0.00	6.75	0.00
1^1B_2	6.70	7.03	6.70	0.08	6.92	6.67	0.07	6.88	0.08	6.85	0.08	6.81	0.08	6.77	0.08
Triplet states															
1^3B_2	4.39	4.44	4.37	-	4.38	4.13	-	4.36	-	4.33	-	4.30	-	4.28	-
1^3B_1	6.45	6.60	6.44	-	6.68	6.37	-	6.64	-	6.60	-	6.56	-	6.51	-

Cyclopentadiene

State	ADC(2)-s aug-cc-pVTZ	ADC(2)-s cc-pVTZ	ADC(2)-s aug-cc-pVDZ		SOS-ADC(2)-s Turbomole	ISR-SOS-ADC(2)-s		SOS-ADC(2)-s (1.15)		SOS-ADC(2)-s (1.16)		SOS-ADC(2)-s (1.17)		SOS-ADC(2)-s (1.18)	
	ΔE	ΔE	ΔE	f	ΔE	ΔE	f	ΔE	f	ΔE	f	ΔE	f	ΔE	f
Singlet states															
1^1B_2	5.44	5.55	5.46	0.11	5.62	5.33	0.10	5.57	0.10	5.53	0.10	5.48	0.10	5.43	0.10
Triplet states															
1^3B_2	3.36	3.36	3.35	-	3.38	3.09	-	3.35	-	3.32	-	3.28	-	3.25	-
1^3A_1	5.19	5.21	5.18	-	5.04	4.82	-	5.01	-	4.98	-	4.95	-	4.92	-

Norbornadiene

State	ADC(2)-s aug-cc-pVTZ	ADC(2)-s cc-pVTZ	ADC(2)-s aug-cc-pVDZ		SOS-ADC(2)-s Turbomole	ISR-SOS-ADC(2)-s		SOS-ADC(2)-s (1.15)		SOS-ADC(2)-s (1.16)		SOS-ADC(2)-s (1.17)		SOS-ADC(2)-s (1.18)	
	ΔE	ΔE	ΔE	f	ΔE	ΔE	f	ΔE	f	ΔE	f	ΔE	f	ΔE	f
Singlet states															
1^1A_2	5.29	5.48	5.29	-	5.65	5.14	-	5.60	-	5.55	-	5.50	-	5.45	-
1^1B_2	6.12	6.30	6.10	0.02	6.61	5.95	0.02	6.56	0.04	6.51	0.03	6.45	0.03	6.40	0.03
Triplet states															
1^3A_2	3.71	3.74	3.68	-	3.81	3.44	-	3.78	-	3.74	-	3.71	-	3.68	-
1^3B_2	4.23	4.26	4.21	-	4.14	3.83	-	4.12	-	4.09	-	4.06	-	4.03	-

Benzene

State	ADC(2)-s aug-cc-pVTZ	ADC(2)-s cc-pVTZ	ADC(2)-s aug-cc-pVDZ		SOS-ADC(2)-s Turbomole	ISR-SOS-ADC(2)-s		SOS-ADC′(2)-s (1.15)		SOS-ADC′(2)-s (1.16)		SOS-ADC′(2)-s (1.17)		SOS-ADC′(2)-s (1.18)	
	ΔE	ΔE	ΔE	f	ΔE	ΔE	f	ΔE	f	ΔE	f	ΔE	f	ΔE	f
Singlet states															
1^1B_{2u}	5.23	5.28	5.27	-	5.02	4.99	-	4.96	-	4.89	-	4.82	-	4.75	-
1^1B_{1u}	6.42	6.55	6.46	-	6.33	6.19	-	6.28	-	6.24	-	6.19	-	6.14	-
1^1E_{1u}	7.13	7.37	7.16	0.73	7.28	6.96	0.74	7.23	0.79	7.18	0.79	7.13	0.78	7.07	0.78
Triplet states															
1^3B_{1u}	4.33	4.35	4.34	-	4.27	4.03	-	4.24	-	4.21	-	4.17	-	4.14	-
1^3E_{1u}	5.04	5.08	5.06	-	4.97	4.60	-	4.92	-	4.87	-	4.82	-	4.77	-
1^3B_{2u}	5.84	5.92	5.87	-	5.95	5.59	-	5.91	-	5.87	-	5.82	-	5.78	-
1^3E_{2g}	7.93	7.99	7.96	-	7.85	7.61	-	7.81	-	7.77	-	7.73	-	7.69	-

Naphthalene

State	ADC(2)-s aug-cc-pVTZ	ADC(2)-s cc-pVTZ	ADC(2)-s aug-cc-pVDZ		SOS-ADC(2)-s Turbomole	ISR-SOS-ADC(2)-s		SOS-ADC(2)-s (1.15)		SOS-ADC(2)-s (1.16)		SOS-ADC(2)-s (1.17)		SOS-ADC(2)-s (1.18)	
	ΔE	ΔE	ΔE	f	ΔE	ΔE	f	ΔE	f	ΔE	f	ΔE	f	ΔE	f
Singlet states															
1^1B_{3u}	4.39	4.43	4.43	0.00	4.31	4.07	0.00	4.24	0.00	4.17	0.00	4.10	0.00	4.03	0.00
1^1B_{2u}	4.74	4.81	4.79	0.09	4.90	4.47	0.07	4.85	0.07	4.79	0.06	4.73	0.06	4.67	0.06
2^1A_g	6.08	6.20	6.11	-	6.00	5.76	-	5.94	-	5.87	-	5.80	-	5.73	-
2^1B_{3u}	6.01	6.15	6.04	1.53	6.23	5.73	1.48	6.17	1.67	6.11	1.66	6.05	1.64	5.99	1.63
2^1B_{2u}	6.34	6.45	6.39	0.30	6.47	6.04	0.31	6.41	0.38	6.35	0.38	6.29	0.38	6.23	0.37
2^1B_{1g}	6.46	6.71	6.51	-	6.63	6.22	-	6.57	-	6.51	-	6.45	-	6.38	-
Triplet states															
1^3B_{2u}	3.26	3.26	3.27	-	3.28	2.89	-	3.24	-	3.20	-	3.16	-	3.11	-
1^3B_{3u}	4.27	4.30	4.30	-	4.26	3.78	-	4.21	-	4.16	-	4.10	-	4.05	-
1^3B_{1g}	4.58	4.63	4.59	-	4.55	4.20	-	4.51	-	4.47	-	4.42	-	4.38	-
2^3B_{2u}	4.79	4.82	4.82	-	4.75	4.31	-	4.70	-	4.64	-	4.59	-	4.54	-
2^3B_{3u}	4.90	4.96	4.94	-	5.09	4.58	-	5.04	-	4.99	-	4.94	-	4.89	-
1^3A_g	5.65	5.72	5.67	-	5.53	5.16	-	5.48	-	5.44	-	5.39	-	5.34	-
2^3B_{1g}	6.10	6.34	6.12	-	6.41	5.79	-	6.35	-	6.29	-	6.23	-	6.17	-
2^3A_g	6.53	6.72	6.55	-	6.64	6.17	-	6.60	-	6.55	-	6.50	-	6.45	-
3^3A_g	6.81	6.87	6.85	-	6.96	6.49	-	6.91	-	6.85	-	6.80	-	6.74	-
3^3B_{1g}	6.79	7.20	6.92	-	7.06	6.62	-	7.02	-	6.98	-	6.94	-	6.89	-

Furan

State	ADC(2)-s aug-cc-pVTZ	ADC(2)-s cc-pVTZ	ADC(2)-s aug-cc-pVDZ		SOS-ADC(2)-s Turbomole	ISR-SOS-ADC(2)-s		SOS-ADC(2)-s (1.15)		SOS-ADC(2)-s (1.16)		SOS-ADC(2)-s (1.17)		SOS-ADC(2)-s (1.18)	
	ΔE	ΔE	ΔE	f	ΔE	ΔE	f	ΔE	f	ΔE	f	ΔE	f	ΔE	f
Singlet states															
1^1B_2	6.40	6.69	6.40	0.19	6.47	6.22	0.18	6.43	0.18	6.38	0.18	6.33	0.18	6.29	0.17
2^1A_1	6.68	6.81	6.71	0.00	6.76	6.50	0.00	6.69	0.00	6.62	0.00	6.55	0.00	6.48	0.00
3^1A_1	8.23	8.69	8.17	0.40	8.31	8.03	0.37	8.26	0.43	8.22	0.43	8.17	0.44	8.13	0.44
Triplet states															
1^3B_2	4.31	4.36	4.33	-	4.29	4.01	-	4.26	-	4.22	-	4.19	-	4.15	-
1^3A_1	5.54	5.60	5.55	-	5.39	5.11	-	5.35	-	5.31	-	5.27	-	5.23	-

Pyrrole

State	ADC(2)-s aug-cc-pVTZ	ADC(2)-s cc-pVTZ	ADC(2)-s aug-cc-pVDZ		SOS-ADC(2)-s Turbomole	ISR-SOS-ADC(2)-s		SOS-ADC(2)-s (1.15)		SOS-ADC(2)-s (1.16)		SOS-ADC(2)-s (1.17)		SOS-ADC(2)-s (1.18)	
	ΔE	ΔE	ΔE	f	ΔE	ΔE	f	ΔE	f	ΔE	f	ΔE	f	ΔE	f
Singlet states															
2^1A_1	6.42	6.59	6.44	0.00	6.37	6.22	0.00	6.31	0.00	6.24	0.00	6.17	0.00	6.11	0.00
3^1A_1	7.84	8.41	7.74	0.37	7.84	7.54	0.33	7.80	0.41	7.75	0.42	7.71	0.42	7.66	0.42
Triplet states															
1^3B_2	4.63	4.69	4.65	-	4.59	4.32	-	4.55	-	4.52	-	4.48	-	4.45	-
1^3A_1	5.59	5.68	5.60	-	5.46	5.17	-	5.42	-	5.38	-	5.33	-	5.29	-

Imidazole

State	ADC(2)-s aug-cc-pVTZ	ADC(2)-s cc-pVTZ	ADC(2)-s aug-cc-pVDZ		SOS-ADC(2)-s Turbomole	ISR-SOS-ADC(2)-s		SOS-ADC(2)-s (1.15)		SOS-ADC(2)-s (1.16)		SOS-ADC(2)-s (1.17)		SOS-ADC(2)-s (1.18)	
	ΔE	ΔE	ΔE	f	ΔE	ΔE	f	ΔE	f	ΔE	f	ΔE	f	ΔE	f
Singlet states															
$2^1A'$	6.42	6.69	6.43	0.16	6.43	6.20	0.07	6.41	0.03	6.35	0.12	6.29	0.11	6.23	0.11
$1^1A''$	6.70	6.79	6.68	0.00	6.68	6.49	0.00	6.84	0.00	6.76	0.01	6.69	0.00	6.62	0.00
$3^1A'$	6.92	7.22	6.94	0.04	6.94	6.71	0.04	6.83	0.05	6.77	0.05	6.71	0.06	6.65	0.06
Triplet states															
$1^3A'$	4.82	4.87	4.85	-	4.80	4.50	-	4.77	-	4.73	-	4.69	-	4.66	-
$2^3A'$	5.84	5.96	5.87	-	5.74	5.43	-	5.70	-	5.66	-	5.57	-	5.57	-
$1^3A''$	6.27	6.38	6.24	-	6.51	6.11	-	6.45	-	6.39	-	6.31	-	6.27	-
$3^3A'$	6.54	6.67	6.53	-	6.60	6.20	-	6.56	-	6.51	-	6.46	-	6.42	-

Pyridine

State	ADC(2)-s aug-cc-pVTZ	ADC(2)-s cc-pVTZ	ADC(2)-s aug-cc-pVDZ		SOS-ADC(2)-s Turbomole	ISR-SOS-ADC(2)-s		SOS-ADC(2)-s (1.15)		SOS-ADC(2)-s (1.16)		SOS-ADC(2)-s (1.17)		SOS-ADC(2)-s (1.18)	
	ΔE	ΔE	ΔE	f	ΔE	ΔE	f	ΔE	f	ΔE	f	ΔE	f	ΔE	f
Singlet states															
1^1B_2	5.27	5.32	5.31	0.03	5.08	5.02	0.03	5.01	0.03	4.94	0.02	4.87	0.02	4.79	0.02
1^1B_1	4.96	5.03	4.99	0.00	5.31	4.78	0.00	5.24	0.01	5.18	0.00	5.11	0.00	5.04	0.00
1^1A_2	5.26	5.32	5.26	-	5.62	5.05	-	5.55	-	5.47	-	5.40	-	5.32	-
2^1A_1	6.60	6.72	6.64	0.01	6.54	6.37	0.01	6.49	0.01	6.44	0.01	6.39	0.01	6.33	0.01
2^1B_2	7.32	7.53	7.32	0.35	7.45	7.11	0.56	7.40	0.64	7.34	0.64	7.28	0.64	7.19	0.01
3^1A_1	7.43	7.60	7.42	0.37	7.66	7.24	0.51	7.60	0.46	7.55	0.47	7.49	0.48	7.43	0.48
Triplet states															
1^3A_1	4.48	4.49	4.48	-	4.42	4.16	-	4.39	-	4.36	-	4.32	-	4.29	-
1^3B_1	4.45	4.50	4.45	-	4.78	4.25	-	4.73	-	4.67	-	4.61	-	4.55	-
1^3B_2	4.93	4.98	4.97	-	4.91	4.52	-	4.86	-	4.81	-	4.76	-	4.70	-
2^3A_1	5.22	5.26	5.25	-	5.13	4.75	-	5.08	-	5.03	-	4.98	-	4.93	-
1^3A_2	5.23	5.29	5.22	-	5.62	5.01	-	5.55	-	5.48	-	5.40	-	5.33	-
2^3B_2	6.30	6.36	6.33	-	6.40	6.01	-	6.36	-	6.31	-	6.26	-	6.21	-

Pyrazine

State	ADC(2)-s aug-cc-pVTZ	ADC(2)-s cc-pVTZ	ADC(2)-s aug-cc-pVDZ		SOS-ADC(2)-s Turbomole	ISR-SOS-ADC(2)-s		SOS-ADC(2)-s (1.15)		SOS-ADC(2)-s (1.16)		SOS-ADC(2)-s (1.17)		SOS-ADC(2)-s (1.18)	
	ΔE	ΔE	ΔE	f	ΔE	ΔE	f	ΔE	f	ΔE	f	ΔE	f	ΔE	f
Singlet states															
1^1B_{3u}	4.15	4.22	4.19	0.01	4.48	3.96	0.01	4.41	0.01	4.34	0.01	4.28	0.01	4.21	0.01
1^1A_u	4.88	4.92	4.88	-	5.29	4.66	-	5.22	-	5.14	-	5.06	-	4.99	-
1^1B_{2u}	5.10	5.15	5.16	0.09	4.94	4.86	0.08	4.86	0.07	4.79	0.07	4.71	0.07	4.64	0.07
1^1B_{2g}	5.80	5.87	5.86	-	6.10	5.65	-	6.03	-	5.96	-	5.89	-	5.82	-
1^1B_{1g}	6.63	6.67	6.64	-	7.04	6.43	-	6.96	-	6.88	-	6.79	-	6.71	-
1^1B_{1u}	6.84	6.94	6.85	0.02	6.79	6.60	0.05	6.73	0.06	6.68	0.06	6.63	0.06	6.58	0.05
2^1B_{2u}	7.83	8.01	7.84	0.44	7.89	7.58	0.44	7.84	0.48	7.78	0.49	7.72	0.49	7.66	0.49
2^1B_{1u}	7.86	8.02	7.94	0.56	8.07	7.74	0.51	8.01	0.47	7.95	0.47	7.89	0.46	7.82	0.46

Pyrimidine

State	ADC(2)-s aug-cc-pVTZ	ADC(2)-s cc-pVTZ	ADC(2)-s aug-cc-pVDZ		SOS-ADC(2)-s Turbomole	ISR-SOS-ADC(2)-s		SOS-ADC(2)-s (1.15)		SOS-ADC(2)-s (1.16)		SOS-ADC(2)-s (1.17)		SOS-ADC(2)-s (1.18)	
	ΔE	ΔE	ΔE	f	ΔE	ΔE	f	ΔE	f	ΔE	f	ΔE	f	ΔE	f
Singlet states															
1^1B_1	4.34	4.40	4.37	0.01	4.71	4.13	0.00	4.64	0.01	4.57	0.01	4.50	0.01	4.42	0.01
1^1A_2	4.71	4.75	4.71	-	5.04	4.49	-	4.97	-	4.89	-	4.82	-	4.74	-
1^1B_2	5.44	5.49	5.49	0.03	5.26	5.19	0.03	5.18	0.02	5.11	0.02	5.03	0.02	4.96	0.02
2^1A_1	6.79	6.91	6.89	0.07	6.81	6.65	0.06	6.76	0.03	6.70	0.03	6.64	0.02	6.59	0.02

Pyridazine

State	ADC(2)-s aug-cc-pVTZ	ADC(2)-s cc-pVTZ	ADC(2)-s aug-cc-pVDZ		SOS-ADC(2)-s Turbomole	ISR-SOS-ADC(2)-s		SOS-ADC(2)-s (1.15)		SOS-ADC(2)-s (1.16)		SOS-ADC(2)-s (1.17)		SOS-ADC(2)-s (1.18)	
	ΔE	ΔE	ΔE	f	ΔE	ΔE	f	ΔE	f	ΔE	f	ΔE	f	ΔE	f
Singlet states															
1^1B_1	3.80	3.85	3.83	0.01	4.16	3.60	0.00	4.09	0.01	4.02	0.01	3.95	0.01	3.87	0.01
1^1A_2	4.32	4.37	4.32	-	4.74	4.11	-	4.67	-	4.59	-	4.51	-	4.43	-
2^1A_1	5.33	5.37	5.38	0.02	5.14	5.07	0.02	5.06	0.01	4.98	0.01	4.91	0.01	4.83	0.01
2^1A_2	5.71	5.76	5.77	-	6.11	5.55	-	6.04	-	5.97	-	5.90	-	5.83	-

Triazine

State	ADC(2)-s aug-cc-pVTZ	ADC(2)-s cc-pVTZ	ADC(2)-s aug-cc-pVDZ		SOS-ADC(2)-s Turbomole	ISR-SOS-ADC(2)-s		SOS-ADC(2)-s (1.15)		SOS-ADC(2)-s (1.16)		SOS-ADC(2)-s (1.17)		SOS-ADC(2)-s (1.18)	
	ΔE	ΔE	ΔE	f	ΔE	ΔE	f	ΔE	f	ΔE	f	ΔE	f	ΔE	f
Singlet states															
$1^1A_1''$	4.53	4.58	4.56	-	4.82	4.33	-	4.74	-	4.66	-	4.58	-	4.50	-
$1^1A_2''$	4.65	4.70	4.69	0.02	5.10	4.47	0.01	5.03	0.02	4.96	0.02	4.88	0.02	4.81	0.02
$1^1E''$	4.62	4.67	4.65	-	5.00	4.41	-	4.93	-	4.85	-	4.77	-	4.70	-
$1^1A_2'$	5.74	5.77	5.78	-	5.56	5.46	-	5.48	-	5.40	-	5.32	-	5.24	-

Tetrazine

State	ADC(2)-s aug-cc-pVTZ	ADC(2)-s cc-pVTZ	ADC(2)-s aug-cc-pVDZ		SOS-ADC(2)-s Turbomole	ISR-SOS-ADC(2)-s		SOS-ADC(2)-s (1.15)		SOS-ADC(2)-s (1.16)		SOS-ADC(2)-s (1.17)		SOS-ADC(2)-s (1.18)	
	ΔE	ΔE	ΔE	f	ΔE	ΔE	f	ΔE	f	ΔE	f	ΔE	f	ΔE	f
Singlet states															
1^1B_{3u}	2.44	2.46	2.48	0.01	2.79	2.21	0.01	2.72	0.01	2.64	0.01	2.56	0.01	2.48	0.01
1^1A_u	3.66	3.70	3.67	-	4.13	3.43	-	4.05	-	3.97	-	3.89	-	3.81	-
1^1B_{1g}	5.01	5.07	5.11	-	5.36	4.88	-	5.28	-	5.20	-	5.11	-	5.03	-
1^1B_{2u}	5.16	5.19	5.24	0.06	4.97	4.90	0.05	4.89	0.05	4.80	0.05	4.72	0.05	4.63	
1^1B_{2g}	5.48	5.51	5.56	-	5.86	5.32	-	5.78	-	5.70	-	5.62	-	5.54	-
2^1A_u	5.44	5.48	5.52	-	5.85	5.28	-	5.78	-	5.70	-	5.63	-	5.55	-
Triplet states															
1^3B_{3u}	1.87	1.88	1.88	-	2.21	1.62	-	2.15	-	2.08	-	2.01	-	1.94	-
1^3A_u	3.44	3.46	3.43	-	3.89	3.19	-	3.82	-	3.75	-	3.68	-	3.60	-
1^3B_{1g}	4.27	4.28	4.31	-	4.53	4.09	-	4.47	-	4.41	-	4.34	-	4.28	-
1^3B_{1u}	4.65	4.65	4.66	-	4.47	4.21	-	4.44	-	4.40	-	4.36	-	4.32	-
1^3B_{2u}	4.64	4.67	4.71	-	4.58	4.14	-	4.52	-	4.47	-	4.41	-	4.35	-
1^3B_{2g}	5.00	5.02	5.04	-	5.35	4.82	-	5.29	-	5.23	-	5.16	-	5.10	-
2^3A_u	5.01	5.04	5.06	-	5.44	4.83	-	5.37	-	5.30	-	5.23	-	5.16	-
2^3B_{1u}	5.56	5.59	5.60	-	5.52	5.06	-	5.46	-	5.40	-	5.33	-	5.27	-

Formaldehyde

State	ADC(2)-s aug-cc-pVTZ	ADC(2)-s cc-pVTZ	ADC(2)-s aug-cc-pVDZ		SOS-ADC(2)-s Turbomole	ISR-SOS-ADC(2)-s		SOS-ADC(2)-s (1.15)		SOS-ADC(2)-s (1.16)		SOS-ADC(2)-s (1.17)		SOS-ADC(2)-s (1.18)	
	ΔE	ΔE	ΔE	f	ΔE	ΔE	f	ΔE	f	ΔE	f	ΔE	f	ΔE	f
Singlet states															
1^1A_2	3.83	3.92	3.83	-	3.99	3.81	-	3.94	-	3.88	-	3.82	-	3.76	-
1^1B_1	9.03	9.14	9.11	0.00	9.25	9.06	0.00	9.19	0.00	9.13	0.00	9.07	0.00	9.01	0.00
2^1A_1	9.37	9.28	9.41	0.15	9.51	9.34	0.13	9.46	0.18	9.41	0.18	9.36	0.18	9.31	0.18
Triplet states															
1^3A_2	3.38	3.43	3.34	-	3.59	3.34	-	3.54	-	3.49	-	3.44	-	3.38	-
1^3A_1	6.01	6.02	6.01	-	5.89	5.63	-	5.86	-	5.83	-	5.80	-	5.77	-

Acetone

State	ADC(2)-s aug-cc-pVTZ	ADC(2)-s cc-pVTZ	ADC(2)-s aug-cc-pVDZ		SOS-ADC(2)-s Turbomole	ISR-SOS-ADC(2)-s		SOS-ADC(2)-s (1.15)		SOS-ADC(2)-s (1.16)		SOS-ADC(2)-s (1.17)		SOS-ADC(2)-s (1.18)	
	ΔE	ΔE	ΔE	f	ΔE	ΔE	f	ΔE	f	ΔE	f	ΔE	f	ΔE	f
Singlet states															
1^1A_2	4.25	4.31	4.24	-	4.39	4.12	-	4.33	-	4.26	-	4.19	-	4.13	-
1^1B_1	8.96	9.06	9.04	0.00	9.22	8.94	0.00	9.16	0.00	9.10	0.00	9.03	0.00	8.97	0.00
Triplet states															
1^3A_2	3.89	3.91	3.86	-	4.08	3.74	-	4.02	-	3.97	-	3.91	-	3.85	-
1^3A_1	6.17	6.17	6.18	-	6.12	5.78	-	6.08	-	6.05	-	6.01	-	5.97	-

Benzoquinone

State	ADC(2)-s aug-cc-pVTZ	ADC(2)-s cc-pVTZ	ADC(2)-s aug-cc-pVDZ		SOS-ADC(2)-s Turbomole	ISR-SOS-ADC(2)-s		SOS-ADC(2)-s (1.15)		SOS-ADC(2)-s (1.16)		SOS-ADC(2)-s (1.17)		SOS-ADC(2)-s (1.18)	
	ΔE	ΔE	ΔE	f	ΔE	ΔE	f	ΔE	f	ΔE	f	ΔE	f	ΔE	f
Singlet states															
1^1B_{1g}	2.65	2.67	2.64	-	3.11	2.49	-	3.03	-	2.95	-	2.88	-	2.80	-
1^1A_u	2.73	2.75	2.72	-	3.18	2.56	-	3.10	-	3.03	-	2.95	-	2.87	-
1^1B_{3g}	4.63	4.69	4.69	-	5.03	4.52	-	4.97	-	4.91	-	4.84	-	4.78	-
1^1B_{1u}	5.29	5.37	5.33	0.61	5.72	5.17	0.50	5.65	0.64	5.58	0.63	5.51	0.62	5.43	0.61
2^1B_{3g}	7.09	7.16	7.10	-	7.49	6.94	-	7.43	-	7.36	-	7.29	-	7.21	-
Triplet states															
1^3B_{1g}	2.35	2.36	2.32	-	3.11	2.19	-	2.76	-	2.69	-	2.62	-	2.54	-
1^3A_u	2.45	2.46	2.41	-	2.92	2.27	-	2.84	-	2.77	-	2.70	-	2.63	-
1^3B_{1u}	3.14	3.13	3.15	-	3.23	2.79	-	3.19	-	3.14	-	3.10	-	3.05	-
1^3B_{3g}	3.48	3.51	3.51	-	3.66	3.26	-	3.62	-	3.58	-	3.54	-	3.50	-

Formamide

State	ADC(2)-s aug-cc-pVTZ	ADC(2)-s cc-pVTZ	ADC(2)-s aug-cc-pVDZ		SOS-ADC(2)-s Turbomole	ISR-SOS-ADC(2)-s		SOS-ADC(2)-s (1.15)		SOS-ADC(2)-s (1.16)		SOS-ADC(2)-s (1.17)		SOS-ADC(2)-s (1.18)	
	ΔE	ΔE	ΔE	f	ΔE	ΔE	f	ΔE	f	ΔE	f	ΔE	f	ΔE	f
Singlet states															
$1^1A''$	5.34	5.50	5.36	0.00	5.51	5.24	0.00	5.44	0.00	5.37	0.00	5.31	0.00	5.24	0.00
$2^1A'$	7.25	7.83	7.29	0.33	7.41	7.17	0.31	7.34	0.29	7.27	0.29	7.20	0.28	7.14	0.28
Triplet states															
$1^3A''$	5.04	5.17	5.04	-	5.27	4.94	-	5.21	-	5.15	-	5.09	-	5.03	-
$1^3A'$	5.76	5.86	5.75	-	5.81	5.41	-	5.77	-	5.72	-	5.67	-	5.63	-

Acetamide

State	ADC(2)-s aug-cc-pVTZ	ADC(2)-s cc-pVTZ	ADC(2)-s aug-cc-pVDZ		SOS-ADC(2)-s Turbomole	ISR-SOS-ADC(2)-s		SOS-ADC(2)-s (1.15)		SOS-ADC(2)-s (1.16)		SOS-ADC(2)-s (1.17)		SOS-ADC(2)-s (1.18)	
	ΔE	ΔE	ΔE	f	ΔE	ΔE	f	ΔE	f	ΔE	f	ΔE	f	ΔE	f
Singlet states															
$1^1A''$	5.36	5.51	5.36	0.00	5.53	5.20	0.00	5.47	0.00	5.40	0.00	5.33	0.00	5.25	0.00
$2^1A'$	7.10	7.54	7.04	0.23	7.04	6.89	0.21	6.97	0.14	6.90	0.14	6.84	0.14	6.77	0.14
Triplet states															
$1^3A''$	5.10	5.21	5.09	-	5.33	4.94	-	5.27	-	5.20	-	5.14	-	5.08	-
$1^3A'$	5.83	5.96	5.88	-	5.97	5.55	-	5.92	-	5.87	-	5.82	-	5.77	-

Propanamide

State	ADC(2)-s aug-cc-pVTZ	ADC(2)-s cc-pVTZ	ADC(2)-s aug-cc-pVDZ		SOS-ADC(2)-s Turbomole	ISR-SOS-ADC(2)-s		SOS-ADC(2)-s (1.15)		SOS-ADC(2)-s (1.16)		SOS-ADC(2)-s (1.17)		SOS-ADC(2)-s (1.18)	
	ΔE	ΔE	ΔE	f	ΔE	ΔE	f	ΔE	f	ΔE	f	ΔE	f	ΔE	f
Singlet states															
$1^1A''$	5.37	5.53	5.37	0.00	5.55	5.20	0.00	5.48	0.00	5.41	0.00	5.34	0.00	5.27	0.00
$2^1A'$	7.04	7.47	6.97	0.20	7.00	6.82	0.19	6.94	0.11	6.87	0.10	6.80	0.10	6.73	0.10
Triplet states															
$1^3A''$	5.12	5.24	5.10	-	5.35	4.95	-	5.29	-	5.22	-	5.16	-	5.09	-
$1^3A'$	5.90	5.97	5.89	-	5.99	5.55	-	5.94	-	5.89	-	5.84	-	5.78	-

B.3. Detailed results with extended ADC(2) methods

Excitation energies in eV (ΔE) and oscillator strangs for optically allowed transitions in legth gauge (f) obtained with ADC(2)-x, and SOS-ADC(2)-x with different values for $c^{os}_{coupling}$ and c^{os}_{x}. In all cases aug-cc-pVDZ [75] was used as basis set. States with high double excitation character are in bold. Structures were taken from [88].

Ethene

State	ADC(2)-x		SOS-ADC(2)-x		SOS-ADC(2)-x	SOS-ADC(2)-x	SOS-ADC(2)-x		SOS-ADC(2)-x	SOS-ADC(2)-x
$c^{os}_{coupling}$			1.0		1.0	1.0	1.0		1.0	1.0
c^{os}_{x}			0.85		0.87	0.89	0.9		0.92	0.94
	ΔE	f	ΔE	f	ΔE	ΔE	ΔE	f	ΔE	ΔE
Singlet states										
1^1B_{1u}	7.45	0.37	7.88	0.36	7.87	7.87	7.87	0.35		
Triplet states										
1^3B_{1u}							4.42			

Butadiene

State	ADC(2)-x		SOS-ADC(2)-x		SOS-ADC(2)-x	SOS-ADC(2)-x	SOS-ADC(2)-x		SOS-ADC(2)-x	SOS-ADC(2)-x
$c^{os}_{coupling}$			1.0		1.0	1.0	1.0		1.0	1.0
c^{os}_{x}			0.85		0.87	0.89	0.9		0.92	0.94
	ΔE	f	ΔE	f	ΔE	ΔE	ΔE	f	ΔE	ΔE
Singlet states										
1^1B_u	5.56	0.66	6.21	0.68	6.20	6.19	6.19	0.67		
$1^1\mathbf{A_g}$	**5.12**	**-**	**6.39**	**-**	**6.32**	**6.24**	**6.19**	**-**	**6.10**	**6.01**
Triplet states										
1^3B_u							3.28			
1^3A_g							5.02			

Hexatriene

State	ADC(2)-x		SOS-ADC(2)-x		SOS-ADC(2)-x	SOS-ADC(2)-x	SOS-ADC(2)-x		SOS-ADC(2)-x	SOS-ADC(2)-x
$c^{os}_{coupling}$			1.0		1.0	1.0	1.0		1.0	1.0
c^{os}_{x}			0.85		0.87	0.89	0.9		0.92	0.94
	ΔE	f	ΔE	f	ΔE	ΔE	ΔE	f	ΔE	ΔE
Singlet states										
1^1B_u	4.60	1.08	5.34	1.13			5.33	1.12		
$1^1\mathbf{A_g}$	**4.06**	**-**	**5.40**	**-**	**5.31**	**5.21**	**5.16**	**-**	**5.06**	**4.95**
Triplet states										
1^3B_u							2.67			
1^3A_g							4.19			

Octatetraene

State	ADC(2)-x		SOS-ADC(2)-x		SOS-ADC(2)-x	SOS-ADC(2)-x	SOS-ADC(2)-x		SOS-ADC(2)-x	SOS-ADC(2)-x
$c^{os}_{coupling}$			1.0		1.0	1.0	1.0		1.0	1.0
c^{os}_{x}			0.85		0.87	0.89	0.9		0.92	0.94
	ΔE	f	ΔE	f	ΔE	ΔE	ΔE	f	ΔE	ΔE
Singlet states										
1^1B_u	3.96	1.46	4.77	1.56			4.75	1.55		
$1^1\mathbf{A_g}$	**3.36**	**-**	**4.69**	**-**	**4.60**	**4.50**	**4.45**	**-**	**4.35**	**4.23**
Triplet states										
1^3B_u							2.31			
1^3A_g							3.56			

Cyclopropene

State	ADC(2)-x		SOS-ADC(2)-x		SOS-ADC(2)-x	SOS-ADC(2)-x	SOS-ADC(2)-x		SOS-ADC(2)-x	SOS-ADC(2)-x
$c^{os}_{coupling}$			1.0		1.0	1.0	1.0		1.0	1.0
c^{os}_{x}			0.85		0.87	0.89	0.9		0.92	0.94
	ΔE	f	ΔE	f	ΔE	ΔE	ΔE	f	ΔE	ΔE
Singlet states										
1^1B_1	6.00	0.00	6.68	0.00			6.65	0.00		
1^1B_2	6.15	0.07	6.82	0.08			6.80	0.08		
Triplet states										
1^3B_2							6.43			
1^3B_1										

Cyclopentadiene

State	ADC(2)-x		SOS-ADC(2)-x		SOS-ADC(2)-x	SOS-ADC(2)-x	SOS-ADC(2)-x		SOS-ADC(2)-x	SOS-ADC(2)-x
$c^{os}_{coupling}$			1.0		1.0	1.0	1.0		1.0	1.0
c^{os}_{x}			0.85		0.87	0.89	0.9		0.92	0.94
	ΔE	f	ΔE	f	ΔE	ΔE	ΔE	f	ΔE	ΔE
Singlet states										
1^1B_2	4.91	0.10	5.55	0.10			5.54	0.10		
$2^1\mathbf{A_1}$	**5.10**	**0.00**	**6.20**	**0.00**	**6.14**	**6.08**	**6.05**	**0.00**	**5.97**	**5.90**
Triplet states										
1^3B_2							3.21			
1^3A_1							4.92			

Norbornadiene

State	ADC(2)-x		SOS-ADC(2)-x		SOS-ADC(2)-x	SOS-ADC(2)-x	SOS-ADC(2)-x		SOS-ADC(2)-x	SOS-ADC(2)-x
$c^{os}_{coupling}$			1.0		1.0	1.0	1.0		1.0	1.0
c^{os}_{x}			0.85		0.87	0.89	0.9		0.92	0.94
	ΔE	f	ΔE	f	ΔE	ΔE	ΔE	f	ΔE	ΔE
Singlet states										
1^1A_2			5.55	-			5.53	-		
1^1B_2			6.47	0.03			6.44	0.03		
Triplet states										
1^3A_2							3.73			
1^3B_2							4.07			

Benzene

State	ADC(2)-x		SOS-ADC(2)-x		SOS-ADC(2)-x	SOS-ADC(2)-x		SOS-ADC(2)-x	SOS-ADC(2)-x
$c^{os}_{coupling}$			1.0		1.0	1.0		1.0	1.0
c^{os}_{x}			0.85		0.87	0.89	0.9	0.92	0.94
	ΔE	f	ΔE	f	ΔE	ΔE	f	ΔE	ΔE
Singlet states									
1^1B_{2u}	4.21	-	4.60	-		4.57	-		
1^1B_{1u}	5.93	-	6.29	-		6.28	-		
1^1E_{1u}	6.47	0.65	7.07	0.76		7.06	0.76		
$\mathbf{1^1E_{2g}}$	**7.06**	**-**	**7.69**	**-**	**7.67**	**7.64**	**7.63**	**7.62**	**7.59**
Triplet states									
1^3B_{1u}							4.12		
1^3E_{1u}							4.65		
1^3B_{2u}							5.85		
1^3E_{2g}							7.10		

Naphthalene

State	ADC(2)-x		SOS-ADC(2)-x		SOS-ADC(2)-x	SOS-ADC(2)-x	SOS-ADC(2)-x		SOS-ADC(2)-x	SOS-ADC(2)-x
$c^{os}_{coupling}$			1.0		1.0	1.0	1.0		1.0	1.0
c^{os}_{x}			0.85		0.87	0.89	0.9		0.92	0.94
	ΔE	f	ΔE	f	ΔE	ΔE	ΔE	f	ΔE	ΔE
Singlet states										
1^1B_{3u}			3.69	0.00			3.92	0.00		
1^1B_{2u}			4.82	0.07			4.81	0.08		
2^1A_g			5.53	-			5.46	-		
1^1B_{1g}			**5.70**	**-**	**5.69**	**5.67**	**5.66**	**-**	**5.64**	**5.62**
2^1B_{3u}			6.09	1.63			6.07	1.62		
2^1B_{2u}			6.32	0.34			6.29	0.33		
2^1B_{1g}			6.32	-			6.30	-		
2^1B_{3u}			**7.33**	**0.04**	**7.32**	**7.30**	**7.29**	**0.02**	**7.27**	**7.23**
Triplet states										
1^3B_{2u}							3.11			
1^3B_{3u}							3.99			
1^3B_{1g}							4.35			
2^3B_{2u}							4.51			
2^3B_{3u}							5.01			
1^3A_g							5.30			
2^3B_{1g}							6.03			
2^3A_g							6.11			
3^3A_g							6.55			
3^3B_{1g}							6.39			

Furan

State	ADC(2)-x		SOS-ADC(2)-x		SOS-ADC(2)-x	SOS-ADC(2)-x	SOS-ADC(2)-x		SOS-ADC(2)-x	SOS-ADC(2)-x
$c^{os}_{coupling}$			1.0		1.0	1.0	1.0		1.0	1.0
c^{os}_{x}			0.85		0.87	0.89	0.9		0.92	0.94
	ΔE	f	ΔE	f	ΔE	ΔE	ΔE	f	ΔE	ΔE
Singlet states										
1^1B_2	5.81	0.18	6.35	0.18			6.33	0.18		
2^1A_1	5.44	0.00	6.18	0.00			6.11	0.00		
3^1A_1	7.39	0.35	8.12	0.47			8.08	0.46		
Triplet states										
1^3B_2							4.09			
1^3A_1							5.23			

Pyrrole

State	ADC(2)-x		SOS-ADC(2)-x		SOS-ADC(2)-x	SOS-ADC(2)-x	SOS-ADC(2)-x		SOS-ADC(2)-x	SOS-ADC(2)-x
$c^{os}_{coupling}$			1.0		1.0	1.0	1.0		1.0	1.0
c^{os}_{x}			0.85		0.87	0.89	0.9		0.92	0.94
	ΔE	f	ΔE	f	ΔE	ΔE	ΔE	f	ΔE	ΔE
Singlet states										
2^1A_1	5.37	0.00	5.90	0.00			5.87	0.00		
3^1A_1	7.02	0.46	7.62	0.49			7.59	0.50		
Triplet states										
1^3B_2							4.41			
1^3A_1							5.26			

Imidazole

State	ADC(2)-x		SOS-ADC(2)-x		SOS-ADC(2)-x	SOS-ADC(2)-x	SOS-ADC(2)-x		SOS-ADC(2)-x	SOS-ADC(2)-x
$c_{coupling}^{os}$			1.0		1.0	1.0	1.0		1.0	1.0
c_{x}^{os}			0.85		0.87	0.89	0.9		0.92	0.94
	ΔE	f	ΔE	f	ΔE	ΔE	ΔE	f	ΔE	ΔE
Singlet states										
$2^1A'$	5.53	0.07	6.13	0.08			6.09	0.08		
$1^1A''$	5.73	0.00	6.58	0.00			6.54	0.01		
$3^1A'$	6.12	0.11	6.62	0.10			6.59	0.10		
Triplet states										
$1^3A'$							4.63			
$2^3A'$							5.54			
$1^3A''$							5.51			
$3^3A'$							6.42			

Pyridine

State	ADC(2)-x		SOS-ADC(2)-x		SOS-ADC(2)-x	SOS-ADC(2)-x	SOS-ADC(2)-x		SOS-ADC(2)-x	SOS-ADC(2)-x
$c^{os}_{coupling}$			1.0		1.0	1.0	1.0		1.0	1.0
c^{os}_{x}			0.85		0.87	0.89	0.9		0.92	0.94
	ΔE	f	ΔE	f	ΔE	ΔE	ΔE	f	ΔE	ΔE
Singlet states										
1^1B_2	4.26	0.02	4.68	0.02			4.65	0.02		
1^1B_1	4.10	0.00	5.01	0.00			4.97	0.00		
1^1A_2	4.33	-	5.32	-			5.29	-		
2^1A_1	6.05	0.01	6.45	0.01			6.44	0.00		
2^1B_2	6.53	0.48	7.17	0.57			7.15	0.56		
3^1A_1	6.75	0.55	7.34	0.52			7.32	0.50		
3^1B_2	**7.44**	**0.07**					**8.01**	**0.00**		
4^1A_1	**7.26**	**0.01**	**7.96**	**0.01**	**7.94**	**7.91**	**7.89**	**0.02**	**7.86**	**7.83**
Triplet states										
1^3A_1							4.27			
1^3B_1							4.56			
1^3B_2							4.63			
2^3A_1							4.81			
1^3A_2							5.25			
2^3B_2							6.23			

Pyrazine

State	ADC(2)-x		SOS-ADC(2)-x		SOS-ADC(2)-x	SOS-ADC(2)-x	SOS-ADC(2)-x		SOS-ADC(2)-x	SOS-ADC(2)-x
$c^{os}_{coupling}$			1.0		1.0	1.0	1.0		1.0	1.0
c^{os}_{x}			0.85		0.87	0.89	0.9		0.92	0.94
	ΔE	f	ΔE	f	ΔE	ΔE	ΔE	f	ΔE	ΔE
Singlet states										
1^1B_{3u}	3.34	0.00	4.23	0.01			4.20	0.01		
1^1A_u	3.97	-	4.99	-			4.96	-		
1^1B_{2u}	4.09	0.06	4.50	0.06			4.47	0.06		
1^1B_{2g}	4.72	-	5.58	-			5.52	-		
1^1B_{1g}	5.47	-	6.50	-			6.45	-		
1^1B_{1u}	6.34	0.04	6.76	0.06			6.75	0.06		
2^1B_{2u}	7.06	0.43	7.64	0.48			7.62	0.48		
2^1B_{1u}			7.85	0.40			7.83	0.40		
1^1B_{3g}	**7.34**	**-**	**7.99**	**-**	**7.97**	**7.95**	**7.94**	**-**	**7.91**	**7.89**
2^1A_g	**7.13**	**-**	**7.81**	**-**	**7.78**	**7.75**	**7.74**	**-**	**7.71**	**7.67**

Pyrimidine

State	ADC(2)-x		SOS-ADC(2)-x		SOS-ADC(2)-x	SOS-ADC(2)-x	SOS-ADC(2)-x		SOS-ADC(2)-x	SOS-ADC(2)-x
$c^{os}_{coupling}$			1.0		1.0	1.0	1.0		1.0	1.0
c^{os}_{x}			0.85		0.87	0.89	0.9		0.92	0.94
	ΔE	f	ΔE	f	ΔE	ΔE	ΔE	f	ΔE	ΔE
Singlet states										
1^1B_1	3.50	0.00	4.45	0.01			4.42	0.01		
1^1A_2	3.82	-	4.80	-			4.77	-		
1^1B_2	4.46	0.02	4.88	0.02			4.85	0.02		
2^1A_1	6.15	0.03	6.66	0.03			6.64	0.02		

Pyridazine

State	ADC(2)-x		SOS-ADC(2)-x		SOS-ADC(2)-x	SOS-ADC(2)-x	SOS-ADC(2)-x		SOS-ADC(2)-x	SOS-ADC(2)-x
$c^{os}_{coupling}$			1.0		1.0	1.0	1.0		1.0	1.0
c^{os}_{x}			0.85		0.87	0.89	0.9		0.92	0.94
	ΔE	f	ΔE	f	ΔE	ΔE	ΔE	f	ΔE	ΔE
Singlet states										
1^1B_1	2.93	0.00	3.83	0.01			3.81	0.00		
1^1A_2	3.31	-	4.35	-			4.30	-		
2^1A_1	4.25	0.01	4.67	0.01			4.64	0.01		
2^1A_2	4.67	-	5.58	-			5.53	-		

Triazine

State	ADC(2)-x		SOS-ADC(2)-x		SOS-ADC(2)-x	SOS-ADC(2)-x	SOS-ADC(2)-x		SOS-ADC(2)-x	SOS-ADC(2)-x
$c^{os}_{coupling}$			1.0		1.0	1.0	1.0		1.0	1.0
c^{os}_{x}			0.85		0.87	0.89	0.9		0.92	0.94
	ΔE	f	ΔE	f	ΔE	ΔE	ΔE	f	ΔE	ΔE
Singlet states										
$1^1A''_1$	3.64	-	4.55	-			4.53	-		
$1^1A''_2$	3.81	0.01	4.80	0.02			4.78	0.02		
$1^1E''$	3.77	-	4.73	-			4.71	-		
$1^1A'_2$	4.77	-	5.19	-			5.17	-		
2^1E$'$	**8.14**	**0.07**	**8.83**	**0.03**	**8.81**	**8.79**	**8.78**	**0.04**	**8.75**	**8.73**

Tetrazine

State	ADC(2)-x		SOS-ADC(2)-x		SOS-ADC(2)-x	SOS-ADC(2)-x	SOS-ADC(2)-x		SOS-ADC(2)-x	SOS-ADC(2)-x
$c^{os}_{coupling}$			1.0		1.0	1.0	1.0		1.0	1.0
c^{os}_{x}			0.85		0.87	0.89	0.9		0.92	0.94
	ΔE	f	ΔE	f	ΔE	ΔE	ΔE	f	ΔE	ΔE
Singlet states										
1^1B_{3u}	1.57	0.00	2.46	0.01			2.45	0.01		
1^1A_u	2.66	-	3.73	-			3.70	-		
1^1B_{1g}	3.76	-	4.59	-			4.56	-		
1^1B_{2u}	4.08	0.04	4.45	0.04			4.43	0.04		
1^1B_{2g}	4.11	-	4.96	-			4.90	-		
2^1A_u	4.46	-	5.35	-			5.33	-		
$2^1\mathbf{B_{2g}}$	**4.85**	**-**	**5.85**	**-**	**5.82**	**5.79**	**5.78**	**-**	**5.75**	**5.71**
$3^1\mathbf{B_{1g}}$	**5.91**	**-**	**6.80**	**-**	**6.76**	**6.72**	**6.70**	**-**	**6.66**	**6.62**
$2^1\mathbf{B_{3g}}$	**6.71**	**-**	**7.29**	**-**	**7.28**	**7.26**	**7.25**	**-**	**7.23**	**7.19**
Triplet states										
1^3B_{3u}							1.94			
1^3A_u							3.50			
1^3B_{1g}							4.12			
1^3B_{1u}							4.27			
1^3B_{2u}							4.27			
1^3B_{2g}							4.78			
2^3A_u							5.03			
2^3B_{1u}							5.06			

Formaldehyde

State	ADC(2)-x		SOS-ADC(2)-x		SOS-ADC(2)-x	SOS-ADC(2)-x	SOS-ADC(2)-x		SOS-ADC(2)-x	SOS-ADC(2)-x
$c^{os}_{coupling}$			1.0		1.0	1.0	1.0		1.0	1.0
c^{os}_{x}			0.85		0.87	0.89	0.9		0.92	0.94
	ΔE	f	ΔE	f	ΔE	ΔE	ΔE	f	ΔE	ΔE
Singlet states										
1^1A_2	3.03	-	3.76	-			3.74	-		
1^1B_1	8.31	0.00	9.04	0.00			9.01	0.00		
2^1A_1	8.64	0.16	9.26	0.18			9.21	0.18		
Triplet states										
1^3A_2							3.43			
1^3A_1							5.82			

Acetone

State	ADC(2)-x		SOS-ADC(2)-x		SOS-ADC(2)-x	SOS-ADC(2)-x	SOS-ADC(2)-x		SOS-ADC(2)-x	SOS-ADC(2)-x
$c^{os}_{coupling}$			1.0		1.0	1.0	1.0		1.0	1.0
c^{os}_{x}			0.85		0.87	0.89	0.9		0.92	0.94
	ΔE	f	ΔE	f	ΔE	ΔE	ΔE	f	ΔE	ΔE
Singlet states										
1^1A_2	3.48	-	4.27	-			4.23	-		
1^1B_1	8.30	0.00	9.12	0.00			9.09	0.00		
Triplet states										
1^3A_2							3.99			
1^3A_1							6.07			

Benzoquinone

State	ADC(2)-x		SOS-ADC(2)-x		SOS-ADC(2)-x	SOS-ADC(2)-x	SOS-ADC(2)-x		SOS-ADC(2)-x	SOS-ADC(2)-x
$c^{os}_{coupling}$			1.0		1.0	1.0	1.0		1.0	1.0
c^{os}_{x}			0.85		0.87	0.89	0.9		0.92	0.94
	ΔE	f	ΔE	f	ΔE	ΔE	ΔE	f	ΔE	ΔE
Singlet states										
1^1B_{1g}	1.71	-	2.79	-			2.75	-		
1^1A_u	1.79	-	2.86	-			2.83	-		
1^1B_{3g}	3.64	-	4.64	-			4.59	-		
1^1B_{1u}	4.56	0.49	5.56	0.61			5.54	0.61		
1^1B_{3u}	**4.35**	**0.00**	**5.86**	**0.00**	**5.81**	**5.75**	**5.72**	**0.00**	**5.65**	**5.57**
2^1B_{3g}		-	7.14	-	-	-	7.08	-	-	-
2^1B_{1u}	**6.17**	**0.02**	**7.42**	**0.04**	**7.35**	**7.28**	**7.24**	**0.03**	**7.16**	**7.08**
Triplet states										
1^3B_{1g}							2.59			
1^3A_u							2.68			
1^3B_{1u}							3.01			
1^3B_{3g}							3.46			

Formamide

State	ADC(2)-x		SOS-ADC(2)-x		SOS-ADC(2)-x	SOS-ADC(2)-x	SOS-ADC(2)-x		SOS-ADC(2)-x	SOS-ADC(2)-x
$c^{os}_{coupling}$			1.0		1.0	1.0	1.0		1.0	1.0
c^{os}_{x}			0.85		0.87	0.89	0.9		0.92	0.94
	ΔE	f	ΔE	f	ΔE	ΔE	ΔE	f	ΔE	ΔE
Singlet states										
$1^1A''$	4.66	0.00	5.42	0.00			5.40	0.00		
$2^1A'$	6.62	0.29	7.40	0.21			7.37	0.22		
Triplet states										
$1^3A''$							5.19			
$1^3A'$							5.72			

Acetamide

State	ADC(2)-x		SOS-ADC(2)-x		SOS-ADC(2)-x	SOS-ADC(2)-x	SOS-ADC(2)-x		SOS-ADC(2)-x	SOS-ADC(2)-x
$c^{os}_{coupling}$			1.0		1.0	1.0	1.0		1.0	1.0
c^{os}_{x}			0.85		0.87	0.89	0.9		0.92	0.94
	ΔE	f	ΔE	f	ΔE	ΔE	ΔE	f	ΔE	ΔE
Singlet states										
$1^1A''$	4.69	0.00	5.48	0.00			5.45	0.00		
$2^1A'$	6.51	0.16	7.03	0.19			7.00	0.19		
Triplet states										
$1^3A''$							5.27			
$1^3A'$							5.90			

Propanamide

State	ADC(2)-x		SOS-ADC(2)-x		SOS-ADC(2)-x	SOS-ADC(2)-x	SOS-ADC(2)-x		SOS-ADC(2)-x	SOS-ADC(2)-x
$c_{coupling}^{os}$			1.0		1.0	1.0	1.0		1.0	1.0
c_{x}^{os}			0.85		0.87	0.89	0.9		0.92	0.94
	ΔE	f	ΔE	f	ΔE	ΔE	ΔE	f	ΔE	ΔE
Singlet states										
$1^1A''$	4.70	0.00	5.53	0.00			5.49	0.00		
$2^1A'$	6.43	0.17	7.03	0.16			7.00	0.15		
Triplet states										
$1^3A''$							5.31			
$1^3A'$							6.28			

C. Selected character tables

Below, the character tables of those point groups are given that are important to understand the selection rules for spin-orbit coupling elements in Sections 5 and 7. The last column states according to which irrep the three components of translations (T_x, T_y, T_z) and rotations (R_x, R_y, R_z) are transforming.

Table C.1.: Character table for the molecular point group C_1.

C_1	I	
A	1	all T and R

Table C.2.: Character table for the molecular point group C_s.

C_s	I	σ	
A'	1	1	T_x, T_y, R_z
A''	1	-1	T_z, R_x, R_y

Table C.3.: Character table for the molecular point group C_2.

C_2	I	C_2	
A	1	1	T_z, R_z
B	1	-1	T_x, T_y, R_x, R_y

Table C.4.: Character table for the molecular point group C_{2v}.

C_{2v}	I	C_2	$\sigma_v(xz)$	$\sigma'_v(yz)$	
A_1	1	1	1	1	T_z
A_2	1	1	-1	-1	R_z
B_1	1	-1	1	-1	T_x, R_y
B_2	1	-1	-1	1	T_y, R_x

D. Linear Polyenes: Analysis of the ADC Eigenvectors

Below, the important contributions to the eigenvectors, oscillator strengths, and, in relevant cases, the norm of double amplitudes is given for the excited states of the linear polyenes of Chapter 8.

Table D.1.: Excitation energies, important contributions to the eigenvectors and oscillator strengths for the first four excited states with B_u symmetry of octatetraene. The values for the first plasmon of this symmetry are given in red and the ones for the second in blue. Method: ADC(2)-s/cc-pVTZ.

State	Δ E[eV]	important contributions[%]		Osc. Str.
1	4.59	**4** $\rightarrow$ **5**	89	1.69
2	7.04	**2** $\rightarrow$ **5**	43	0.00
		3 $\rightarrow$ **6**	0	
		4 $\rightarrow$ **7**	38	
3	7.99	**2** $\rightarrow$ **5**	37	0.07
		3 $\rightarrow$ **6**	12	
		4 $\rightarrow$ **7**	40	
4	8.71	**2** $\rightarrow$ **5**	6	0.17
		3 $\rightarrow$ **6**	70	
		4 $\rightarrow$ **7**	4	

Table D.2.: Excitation energies, important contributions to the eigenvectors and oscillator strengths for the first four excited states with B_u symmetry of octatetraene. The values for the first plasmon of this symmetry are given in red and the ones for the second in blue. Method: SOS-ADC(2)-s/cc-pVTZ.

State	Δ E[eV]	important contributions[%]		Osc. Str.
1	4.69	**4** → **5**	89	1.50
2	7.14	**2** → **5**	43	0.00
		3 → **6**	0	
		4 → **7**	36	
3	8.01	**2** → **5**	34	0.08
		3 → **6**	16	
		4 → **7**	38	
4	9.01	**2** → **5**	6	0.09
		3 → **6**	64	
		4 → **7**	8	

Table D.3.: Excitation energies, important contributions to the eigenvectors, oscillator strengths, and norms of double amplitudes for the first five excited states with B_u symmetry of octatetraene. The values for the first plasmon of this symmetry are given in red and the ones for the second in blue. Method: SOS-ADC(2)-x/cc-pVTZ.

State	Δ E[eV]	important contributions[%]		Osc. Str.	Norm of doubles
1	4.91	**4** → **5**	86	1.56	0.11
2	5.60	**2** → **5**	23	0.00	0.58
		3 → **6**	1		
		4 → **7**	15		
3	8.00	**1** → **6**	8	0.00	0.76
		2 → **7**	0		
		3 → **8**	14		
4	8.06	**2** → **5**	25	0.05	0.13
		3 → **6**	10		
		4 → **7**	47		
5	8.68	**2** → **5**	2	0.10	0.32
		3 → **6**	59		
		4 → **7**	11		

Table D.4.: Excitation energies, important contributions to the eigenvectors, oscillator strengths, and norms of double amplitudes for the first five excited states with A_g symmetry of octatetraene. The values for the first plasmon of this symmetry are given in red. Method: SOS-ADC(2)-x/cc-pVTZ.

State	Δ E[eV]	important contributions[%]		Osc. Str.	Norm of doubles
1	4.47	**3** → **5**	17	-	0.67
		4 → **6**	12		
2	6.19	**1** → **5**	25	-	0.46
		2 → **6**	1		
		3 → **7**	1		
		4 → **8**	25		
3	6.88	**3** → **5**	40	-	0.11
		4 → **6**	44		
4	7.38	**1** → **5**	0	-	0.81
		2 → **6**	6		
		3 → **7**	7		
		4 → **8**	2		
5	7.73	**3** → **5**	20	-	0.60
		4 → **6**	17		

Table D.5.: Excitation energies, important contributions to the eigenvectors, oscillator strengths, and norm of double amplitudes for the first six excited states with B_u symmetry of $C_{16}H_{18}$. The values for the first plasmon of this symmetry are given in red and the ones for the second in blue. Method: SOS-ADC(2)-x/cc-pVDZ.

State	Δ E[eV]	important contributions[%] (singles part)		Osc. Str.	Norm of doubles
1	3.75	**8** → **9**	81	3.14	0.12
2	3.91	**6** → **9**	15	0.00	0.70
		7 → **10**	10		
		8 → **11**	0		
3	5.23	**4** → **9**	17	0.00	0.60
		5 → **10**	4		
		6 → **11**	0		
		7 → **12**	3		
		8 → **13**	9		
4	5.74	**4** → **9**	0	0.00	0.88
		5 → **10**	4		
		6 → **11**	0		
		7 → **12**	2		
		8 → **13**	0		
5	6.10	**2** → **9**	18	0.00	0.50
		3 → **10**	5		
		4 → **11**	1		
		5 → **12**	1		
		6 → **13**	0		
		7 → **14**	4		
		8 → **15**	13		
6	6.18	**6** → **9**	20	0.31	0.14
		7 → **10**	41		
		8 → **11**	19		

Table D.6.: Excitation energies, important contributions to the eigenvectors, oscillator strengths, and norm of double amplitudes for the first four excited states with A_g symmetry of $C_{16}H_{18}$. The values for the first plasmon of this symmetry are given in red. Method: SOS-ADC(2)-x/cc-pVDZ.

State	Δ E[eV]	important contributions[%] (singles part)		Osc. Str.	Norm of doubles
1	3.32	**7** → **9**	11	-	0.74
		8 → **10**	9		
2	4.76	**5** → **9**	16	-	0.65
		6 → **10**	0		
		7 → **11**	0		
		8 → **12**	10		
3	5.11	**7** → **9**	3	-	0.88
		5 → **9**	0		
		6 → **10**	3		
		7 → **11**	2		
		8 → **12**	0		
4	5.27	**7** → **9**	42	-	0.12
		8 → **10**	41		

Bibliography

[1] N. J. Turro, V. Ramamurthy, and J. C. Scaiano. *Modern molecular photochemistry of organic molecules*. University Science Books, Sausalito, California, 1st ed. (2010).

[2] M. Klessinger and J. Michl. *Excited states and photochemistry of organic molecules*. VCH Publishers, Inc., New York, 1st ed. (1995).

[3] W. Domcke, D. R. Yarkony, and H. Köppel, eds. *Conical Intersections: Electronic Structure, Dynamics & Spectroscopy*, vol. 15 of *Advanced Series in Physical Chemistry*. World Scientific Publishing Co. Pte. Ltd., Singapore (2004).

[4] W. Domcke, D. R. Yarkony, and H. Köppel, eds. *Conical Intersections: Theory, Computation and Experiment*, vol. 17 of *Advanced Series in Physical Chemistry*. World Scientific Publishing Co. Pte. Ltd., Singapore (2011).

[5] M. A. El-Sayed. "The Radiationless Processes Involving Change of Multiplicity in the Diazenes". In: *J. Chem. Phys.* **36**, 573 (1962).

[6] F. C. De Schryver, S. De Feyter, and G. Schweitzer, eds. *Femtochemistry: With the Noble Lecture of A. Zwail*. Wiley-VCH Verlag GmbH, Weinheim, 1st ed. (2001).

[7] R. Schanz, S. A. Kovalenko, V. Kharlanov, and N. P. Ernsting. "Broadband fluorescence upconversion for femtosecond spectroscopy". In: *Appl. Phys. Lett.* **79**, 566 (2001).

[8] A. Cannizzo, O. Bräm, G. Zgrablic, A. Tortschanoff, A. A. Oskouei, F. van Mourik, and M. Chergui. "Femtosecond fluorescence upconversion setup with broadband detection in the ultraviolet". In: *Opt. Lett.* **32**, 3555 (2007).

[9] S. Grimme. "Calculation of the Electronic Spectra of Large Molecules". In: *Rev. Comput. Chem.* **20**, 153 (2004).

[10] A. Dreuw and M. Head-Gordon. "Single-Reference ab Initio Methods for the Calculation of Excited States of Large Molecules". In: *Chem. Rev.* **105**, 4009 (2005).

[11] M. Merchán and L. Serrano-Andrés. "Ab Initio Methods for Excited States". In: M. Olivucci, ed., *Computational Photochemistry*, vol. 16 of *Theoretical and Computational Chemistry*, chap. II. Elsevier, Amsterdam (2005).

[12] A. Dreuw. "Quantum Chemical Methods for the Investigation of Photoinitiated Processes in Biological Systems: Theory and Applications". In: *ChemPhysChem* **7**, 2259 (2006).

[13] L. González, D. Escudero, and L. Serrano-Andrés. "Progress and Challenges in the Calculation of Electronic Excited States". In: *ChemPhysChem* **13**, 28 (2012).

[14] J. Schirmer. "Beyond the random-phase approximation: A new approximation scheme for the polarization propagator". In: *Phys. Rev. A* **26**, 2395 (1982).

[15] J. Schirmer and A. B. Trofimov. "Intermediate state representation approach to physical properties of electronically excited molecules". In: *J. Chem. Phys.* **120**, 11449 (2004).

[16] A. B. Trofimov, G. Stelter, and J. Schirmer. "A consistent third-order propagator method for electronic excitation". In: *J. Chem. Phys.* **111**, 9982 (1999).

[17] A. B. Trofimov and J. Schirmer. "An efficient polarization propagator approach to valence electron excitation spectra". In: *J. Phys. B* **28**, 2299 (1995).

[18] A. B. Trofimov, G. Stelter, and J. Schirmer. "Electron excitation energies using a consistent third-order propagator approach: Comparison with full configuration interaction and coupled cluster results". In: *J. Chem. Phys.* **117**, 6402 (2002).

[19] Y. Shao, L. F. Molnar, Y. Jung, J. Kussmann, C. Ochsenfeld, S. T. Brown, A. T. Gilbert, L. V. Slipchenko, S. V. Levchenko, D. P. O'Neill, R. A. DiStasio Jr, R. C. Lochan, T. Wang, G. J. Beran, N. A. Besley, J. M. Herbert, C. Yeh Lin, T. Van Voorhis, S. Hung Chien, A. Sodt, R. P. Steele, V. A. Rassolov, P. E. Maslen, P. P. Korambath, R. D. Adamson, B. Austin, J. Baker, E. F. C. Byrd, H. Dachsel, R. J. Doerksen, A. Dreuw, B. D. Dunietz, A. D. Dutoi, T. R. Furlani, S. R. Gwaltney, A. Heyden, S. Hirata, C.-P. Hsu, G. Kedziora, R. Z. Khalliulin, P. Klunzinger, A. M. Lee, M. S. Lee, W. Liang, I. Lotan, N. Nair, B. Peters, E. I. Proynov, P. A. Pieniazek, Y. Min Rhee, J. Ritchie, E. Rosta, C. David Sherrill, A. C. Simmonett, J. E. Subotnik, H. Lee Woodcock III, W. Zhang, A. T. Bell, A. K. Chakraborty, D. M. Chipman, F. J. Keil, A. Warshel, W. J. Hehre, H. F. Schaefer III, J. Kong, A. I. Krylov, P. M. W. Gill, and M. Head-Gordon. "Advances in methods and algorithms in a modern quantum chemistry program package". In: *Phys. Chem. Chem. Phys.* **8**, 3172 (2006).

[20] M. Wormit, D. R. Rehn, P. H. P. Harbach, J. Wenzel, C. M. Krauter, E. Epifanovsky, and A. Dreuw. "Investigating Excited Electronic States using the Algebraic Diagrammatic Construction (ADC) Approach of the

Polarisation Propagator". In: *Mol. Phys.* (2014). Accepted for publication.

[21] Y. Jung, R. C. Lochan, A. D. Dutoi, and M. Head-Gordon. "Scaled opposite-spin second order Møller–Plesset correlation energy: An economical electronic structure method". In: *J. Chem. Phys.* **121**, 9793 (2004).

[22] AMFI is an atomic mean-field spin-orbit integral program written by B. Schimmelpfennig, University of Stockholm, 1996.

[23] C. M. Krauter, J. Möhring, T. Buckup, M. Pernpointner, and M. Motzkus. "Ultrafast branching in the excited state of coumarin and umbelliferone". In: *Phys. Chem. Chem. Phys.* **15**, 17846 (2013).

[24] M. Born and R. Oppenheimer. "Zur Quantentheorie der Molekeln". In: *Ann. d. Phys.* **389**, 457 (1927).

[25] I. N. Levine. *Quantum Chemistry.* Pearson Education, Inc., Upper Saddle River, 6th ed. (2009).

[26] C. M. Marian. "Spin-orbit coupling in Molecules". In: *Rev. Comput. Chem.* **17**, 99 (2001).

[27] A. Szabo and N. S. Ostlund. *Modern Quantum Chemistry.* Mc-Graw-Hill, Inc., Mineola, New York, first, rev. ed. (1989).

[28] T. Helgaker, P. Jørgensen, and J. Olsen. *Molecular Electronic-Structure Theory.* John Wiley & Sons, Ltd, Chichester, West Sussex, 1st ed. (2000).

[29] A. L. Fetter and J. D. Walecka. *Quantum Theory of Many-Particle Systems.* Dover Publications, Mineola, New York (2003).

[30] C. Møller and M. S. Plesset. "Note on an Approximation Treatment for Many-Electron Systems". In: *Phys. Rev.* **46**, 618 (1934).

[31] E. Schrödinger. "An Undulatory Theory of the Mechanics of Atoms and Molecules". In: *Phys. Rev.* **28**, 1049 (1926).

[32] W. Koch and M. C. Holthausen. *A Chemist's Guide to Density Functional Theory.* Wiley-VCH, Weinheim, 2nd ed. (2001).

[33] P. Hohenberg and W. Kohn. "Inhomogeneous Electron Gas". In: *Phys. Rev.* **136**, B864 (1964).

[34] W. Kohn and L. J. Sham. "Self-Consistent Equations Including Exchange and Correlation Effects". In: *Phys. Rev.* **140**, A1133 (1965).

[35] A. D. Becke. "Density-functional exchange-energy approximation with correct asymptotic behavior". In: *Phys. Rev. A* **38**, 3098 (1988).

[36] C. Lee, W. Yang, and R. G. Parr. "Development of the Colle-Salvetti correlation-energy formula into a functional of the electron density". In: *Phys. Rev. B* **37**, 785 (1988).

[37] J. P. Perdew. "Density-functional approximation for the correlation energy of the inhomogeneous electron gas". In: *Phys. Rev. B* **33**, 8822 (1986).

[38] A. D. Becke. "Density-functional thermochemistry. III. The role of exact exchange." In: *J. Chem. Phys.* **98**, 5648 (1993).

[39] C. Adamo and V. Barone. "Toward reliable density functional methods without adjustable parameters: The PBE0 model". In: *J. Chem. Phys.* **110**, 6158 (1999).

[40] A. D. Becke. "A new mixing of Hartree-Fock and local density-functional theories." In: *J. Chem. Phys.* **98**, 1372 (1993).

[41] E. Runge and E. K. U. Gross. "Density-Functional Theory for Time-Dependent Systems". In: *Phys. Rev. Lett.* **52**, 997 (1984).

[42] F. Furche and D. Rappoport. "Density functional methods for excited states: equilibrium structure and electronic spectra". In: M. Olivucci, ed., *Computational Photochemistry*, vol. 16 of *Theoretical and Computational Chemistry*, chap. III. Elsevier, Amsterdam (2005).

[43] J. E. del Bene, R. Ditchfield, and J. A. Pople. "Self-Consistent Molecular Orbital Methods. X. Molecular Orbital Studies of Excited States with Minimal and Extended Basis Sets". In: *J. Chem. Phys.* **55**, 2236 (1971).

[44] M. Head-Gordon, R. J. Rico, M. Oumi, and T. J. Lee. "A doubles correction to electronic excited states from configuration interaction in the space of single substitutions". In: *Chem. Phys. Lett.* **219**, 21 (1994).

[45] K. Andersson, P.-Å. Malmqvist, B. O. Roos, A. J. Sadlej, and K. Wolinski. "Second-order perturbation theory with a CASSCF reference function". In: *J. Phys. Chem.* **94**, 5483 (1990).

[46] K. Andersson, P.-Å. Malmqvist, and B. O. Roos. "Second-order perturbation theory with a complete active space self-consistent field reference function". In: *J. Chem. Phys.* **96**, 1218 (1992).

[47] O. Christiansen, H. Koch, and P. Jørgensen. "The second-order approximate coupled cluster singles and doubles model CC2". In: *Chem. Phys. Lett.* **243**, 409 (1995).

[48] C. Hättig and F. Weigend. "CC2 excitation energy calculations on large molecules using the resolution of the identity approximation". In: *J. Chem. Phys.* **113**, 5154 (2000).

[49] S. Grimme and M. Waletzke. "A combination of Kohn–Sham density functional theory and multi-reference configuration interaction methods". In: *J. Chem. Phys.* **111**, 5645 (1999).

[50] M. Head-Gordon, M. Oumi, and D. Maurice. "Quasidegenerate second-order perturbation corrections to single-excitation configuration interaction". In: *Mol. Phys.* **96**, 593 (1999).

[51] C. Hättig. "Structure Optimizations for Excited States with Correlated Second-Order Methods: CC2 and ADC(2)". In: *Adv. Quant. Chem.* **50**, 37 (2005).

[52] F. Mertins and J. Schirmer. "Algebraic propagator approaches and intermediate-state representations. I. The biorthogonal and unitary coupled-cluster methods". In: *Phys. Rev. A* **53**, 2140 (1996).

[53] M. Wormit. *Development and Application of Reliable Methods for the Calculation of Excited States: From Light-Harvesting Complexes to Medium-Sized Molecules*. Ph.D. thesis, Johann Wolfgang Goethe Universität Frankfurt am Main (2009).

[54] J. H. Starcke, M. Wormit, J. Schirmer, and A. Dreuw. "How much double excitation character do the lowest excited states of linear polyenes have?" In: *Chem. Phys.* **329**, 39 (2006).

[55] J. Schirmer and F. Mertins. "Review of biorthogonal coupled cluster representations for electronic excitation." In: *Theor. Chem. Acc.* **125**, 145 (2010).

[56] P. H. Harbach. *Development and Application of Efficient Theoretical Approaches to Molecular Systems in Photochemistry*. Ph.D. thesis, Ruprecht-Karls-Universität Heidelberg (2013).

[57] J. Schirmer. "Reexamination of the Runge-Gross action-integral functional". In: *Phys. Rev. A* **86**, 012514 (2012).

[58] J. Schirmer and A. Dreuw. "Critique of the foundations of time-dependent density-functional theory". In: *Phys. Rev. A* **75** (2007).

[59] J. Plötner and A. Dreuw. "Pigment Yellow 101: A showcase for photo-initiated processes in medium-sized molecules". In: *Chem. Phys.* **347**, 472 (2008).

[60] A. Görling. "New KS Method for Molecules Based on an Exchange Charge Density Generating the Exact Local KS Exchange Potential". In: *Phys. Rev. Lett.* **83**, 5459 (1999).

[61] S. Ivanov, S. Hirata, and R. J. Bartlett. "Exact Exchange Treatment for Molecules in Finite-Basis-Set Kohn-Sham Theory". In: *Phys. Rev. Lett.* **83**, 5455 (1999).

[62] A. Dreuw, J. L. Weisman, and M. Head-Gordon. "Long-range charge-transfer excited states in time-dependent density functional theory require non-local exchange". In: *J. Chem. Phys.* **119**, 2943 (2003).

[63] Y. Tawada, T. Tsuneda, S. Yanagisawa, T. Yanai, and K. Hirao. "A long-range-corrected time-dependent density functional theory". In: *J. Chem. Phys.* **120**, 8425 (2004).

[64] T. Yanai, D. P. Tew, and N. C. Handy. "A new hybrid exchange–correlation functional using the Coulomb-attenuating method (CAM-B3LYP)". In: *Chem. Phys. Lett.* **393**, 51 (2004).

[65] R. Baer and D. Neuhauser. "Density Functional Theory with Correct Long-Range Asymptotic Behavior". In: *Phys. Rev. Lett.* **94**, 043002 (2005).

[66] J.-D. Chai and M. Head-Gordon. "Long-range corrected hybrid density functionals with damped atom-atom dispersion corrections". In: *Phys. Chem. Chem. Phys.* **10**, 6615 (2008).

[67] J.-D. Chai and M. Head-Gordon. "Systematic optimization of long-range corrected hybrid density functionals". In: *J. Chem. Phys.* **128**, 084106 (2008).

[68] H. Iikura, T. Tsuneda, T. Yanai, and K. Hirao. "A long-range correction scheme for generalized-gradient-approximation exchange functionals". In: *J. Chem. Phys.* **115**, 3540 (2001).

[69] O. A. Vydrov, J. Heyd, A. V. Krukau, and G. E. Scuseria. "Importance of short-range versus long-range Hartree-Fock exchange for the performance of hybrid density functionals". In: *J. Chem. Phys.* **125**, 074106 (2006).

[70] O. A. Vydrov and G. E. Scuseria. "Assessment of a long-range corrected hybrid functional". In: *J. Chem. Phys.* **125**, 234109 (2006).

[71] S. Grimme. "Improved second-order Møller–Plesset perturbation theory by separate scaling of parallel- and antiparallel-spin pair correlation energies". In: *J. Chem. Phys.* **118**, 9095 (2003).

[72] R. F. Fink. "Spin-component-scaled Möller–Plesset (SCS-MP) perturbation theory: A generalization of the MP approach with improved properties". In: *J. Chem. Phys.* **133**, 174113 (2010).

[73] S. Grimme, L. Goerigk, and R. F. Fink. "Spin-component-scaled electron correlation methods". In: *WIREs Comput. Mol. Sci.* **2**, 886 (2012).

[74] W. Klopper. "Highly accurate coupled-cluster singlet and triplet pair energies from explicitly correlated calculations in comparison with extrapolation techniques". In: *Mol. Phys.* **99**, 481 (2001).

[75] T. H. Dunning Jr. "Gaussian basis sets for use in correlated molecular calculations. I. The atoms boron through neon and hydrogen". In: *J. Chem. Phys.* **90**, 1007 (1989).

[76] M. Feyereisen, G. Fitzgerald, and A. Komornicki. "Use of approximate integrals in ab initio theory. An application in MP2 energy calculations". In: *Chem. Phys. Lett.* **208**, 359 (1993).

[77] F. Weigend, M. Häser, H. Patzelt, and R. Ahlrichs. "RI-MP2: optimized auxiliary basis sets and demonstration of efficiency". In: *Chem. Phys. Lett.* **294**, 143 (1998).

[78] J. Almlöf. "Elimination of energy denominators in Møller-Plesset perturbation theory by a Laplace transform approach". In: *Chem. Phys. Lett.* **181**, 319 (1991).

[79] S. Grimme and E. I. Izgorodina. "Calculation of 0-0 excitation energies of organic molecules by CIS(D) quantum chemical methods". In: *Chem. Phys.* **305**, 223 (2004).

[80] Y. M. Rhee and M. Head-Gordon. "Scaled Second-Order Perturbation Corrections to Configuration Interaction Singles: Efficient and Reliable Excitation Energy Methods". In: *J. Phys. Chem. A* **111**, 5314 (2007).

[81] D. Casanova, Y. M. Rhee, and M. Head-Gordon. "Quasidegenerate scaled opposite spin second order perturbation corrections to single excitation configuration interaction". In: *J. Chem. Phys.* **128**, 164106 (2008).

[82] Y. M. Rhee, D. Casanova, and M. Head-Gordon. "Quartic-Scaling Analytical Gradient of Quasidegenerate Scaled Opposite Spin Second-Order Perturbation Corrections to Single Excitation Configuration Interaction". In: *J. Chem. Theory Comput.* **5**, 1224 (2009).

[83] Y. M. Rhee, D. Casanova, and M. Head-Gordon. "Performance of Quasi-Degenerate Scaled Opposite Spin Perturbation Corrections to Single Excitation Configuration Interaction for Excited State Structures and Excitation Energies with Application to the Stokes Shift of 9-Methyl-9,10-dihydro-9-silaphenanthrene". In: *J. Phys. Chem. A* **113**, 10564 (2009).

[84] A. Hellweg, S. A. Grün, and C. Hättig. "Benchmarking the performance of spin-component scaled CC2 in ground and electronically excited states". In: *Phys. Chem. Chem. Phys.* **10**, 4119 (2008).

[85] TURBOMOLE, a development of the University of Karlsruhe and ForschungszentrumKarlsruhe GmbH, 1989-2007, TURBOMOLE GmbH since 2007; availabe from http://www.turbomole.com.

[86] N. O. C. Winter and C. Hättig. "Scaled opposite-spin CC2 for ground and excited states with fourth order scaling computational costs". In: *J. Chem. Phys.* **134**, 184101 (2011).

[87] Y. Jung, A. Sodt, P. M. W. Gill, and M. Head-Gordon. "Auxiliary basis expansions for large-scale electronic structure calculations". In: *Proc. Natl. Acad. Sci.* **102**, 6692 (2005).

[88] M. Schreiber, M. R. Silva-Junior, S. P. A. Sauer, and W. Thiel. "Benchmarks for electronically excited states: CASPT2, CC2, CCSD, and CC3". In: *J. Chem. Phys.* **128**, 134110 (2008).

[89] M. R. Silva-Junior, M. Schreiber, S. P. A. Sauer, and W. Thiel. "Benchmarks of electronically excited states: Basis set effects on CASPT2 results". In: *J. Chem. Phys.* **133**, 174318 (2010).

[90] F. Weigend, A. Köhn, and C. Hättig. "Efficient use of the correlation consistent basis sets in resolution of the identity MP2 calculations". In: *J. Chem. Phys.* **116**, 3175 (2002).

[91] M. R. Silva-Junior, M. Schreiber, S. P. A. Sauer, and W. Thiel. "Benchmarks for electronically excited states: Time-dependent density functional theory and density functional theory based multireference configuration interaction". In: *J. Chem. Phys.* **129**, 104103 (2008).

[92] A. Einstein. "Zur Elektrodynamik bewegter Körper". In: *Ann. d. Phys.* **322**, 891 (1905).

[93] P. A. M. Dirac. "The Quantum Theory of the Electron". In: *Proc. R. Soc. Lond. A* **117**, 610 (1928).

[94] P. A. M. Dirac. "The Quantum Theory of the Electron. Part II". In: *Proc. R. Soc. Lond. A* **118**, 351 (1928).

[95] J. M. Hollas. *Modern Spectroscopy.* John Wiley & Sons, Ltd, Chichester, West Sussex, 4th ed. (2004).

[96] M. Reiher and A. Wolf. *Relativistic Quantum Chemistry.* WILEY-VCH Verlag GmbH & Co. KGaA, Weinheim, 1st ed. (2009).

[97] K. G. Dyall and K. Fægri Jr. *Introduction to Relativistic Quantum Chemistry.* OxfJohn Wiley & Sons, Inc., New York, 1st ed. (2007).

[98] G. Breit. "The Effect of Retardation on the Interaction of Two Electrons". In: *Phys. Rev.* **34**, 553 (1929).

[99] C. M. Marian. "Spin-orbit coupling and intersystem crossing in molecules". In: *WIREs Comput. Mol. Sci.* **2**, 187 (2012).

[100] W. J. Thompson. *Angular Momentum.* John Wiley & Sons, Inc., New York, 1st ed. (1994).

[101] B. A. Hess and C. M. Marian. "Relativistic Effects in the Calculation of Electronic Energies". In: P. Jensen and P. R. Bunker, eds., *Computational Molecular Spectroscopy*, chap. VI, p. 169. John Wiley & Sons, Ltd, Chichester, West Sussex, 1st ed. (2000).

[102] W. Pauli Jr. "Zur Quantenmechanik des magnetischen Elektrons". In: *Z. Phys.* **43**, 601 (1927).

[103] B. A. Hess, C. M. Marian, U. Wahlgren, and O. Gropen. "A mean-field spin-orbit method applicable to correlated wavefunctions". In: *Chem. Phys. Lett.* **251**, 365 (1996).

[104] J. Tatchen and C. M. Marian. "On the performance of approximate spin-orbit Hamiltonians in light conjugated molecules: the fine-structure splitting of HC_6H^+, NC_5H^+, and NC_4N^+". In: *Chem. Phys. Lett.* **313**, 351 (1999).

[105] M. Iliaš, V. Kellö, L. Visscher, and B. Schimmelpfennig. "Inclusion of mean-field spin-orbit effects based on all-electron two-component spinors: Pilot calculations on atomic and molecular properties". In: *J. Chem. Phys.* **115**, 9667 (2001).

[106] F. Neese. "Efficient and accurate approximations to the molecular spin-orbit coupling operator and their use in molecular g-tensor calculations". In: *J. Chem. Phys.* **122**, 034107 (2005).

[107] A. de Shalit and I. Talmi. *Nuclear Shell Theory.* Academic Press, Inc., New York, 1st ed. (1963).

[108] J. Tatchen. *Spin-verbotene photophysikalische Prozesse in organischen Molekülen: Entwicklung quantenmechenischer Methoden und Anwendung auf Psoralene.* Ph.D. thesis, Heinrich-Heine Universität Düsseldorf (2005).

[109] F. A. Cotton. *Chemical Application of Group Theory.* John Wiley & Sons, Inc., New York, 3rd ed. (1990).

[110] C. Kittel. *Introduction to Solid State Physics.* John Wiley & Sons, Inc., New York (2005).

[111] M. Faraday. "The Bakerian Lecture: Experimental Relations of Gold (and Other Metals) to Light". In: *Philos. Trans. Roy. Soc. London* **147**, 145 (1857).

[112] K. M. Mayer and J. H. Hafner. "Localized Surface Plasmon Resonance Sensors". In: *Chem. Rev.* **111**, 3828 (2011).

[113] Y. Li, C. Jing, L. Zhang, and Y.-T. Long. "Resonance scattering particles as biological nanosensors in vitro and in vivo". In: *Chem. Soc. Rev.* **41**, 632 (2012).

[114] M. Swierczewska, G. Liu, S. Lee, and X. Chen. "High-sensitivity nanosensors for biomarker detection". In: *Chem. Soc. Rev.* **41**, 2641 (2012).

[115] J. A. Schuller, E. S. Barnard, W. Cai, Y. C. Jun, J. S. White, and M. L. Brongersma. "Plasmonics for extreme light concentration and manipulation". In: *Nat. Mater.* **9**, 193 (2010).

[116] H. A. Atwater and A. Polman. "Plasmonics for improved photovoltaic devices". In: *Nat. Mater.* **9**, 205 (2010).

[117] H. J. Lezec, J. A. Dionne, and H. A. Atwater. "Negative Refraction at Visible Frequencies". In: *Science* **316**, 430 (2007).

[118] T. Ergin, N. Stenger, P. Brenner, J. B. Pendry, and M. Wegener. "Three-Dimensional Invisibility Cloak at Optical Wavelengths". In: *Science* **328**, 337 (2010).

[119] A. Boltasseva and H. A. Atwater. "Low-Loss Plasmonic Metamaterials". In: *Science* **331**, 290 (2011).

[120] C. M. Soukoulis and M. Wegener. "Past achievements and future challenges in the development of three-dimensional photonic metamaterials". In: *Nat. Photon.* **5**, 523 (2011).

[121] W. Cai, J. S. White, and M. L. Brongersma. "Compact, High-Speed and Power-Efficient Electrooptic Plasmonic Modulators". In: *Nano Lett.* **9**, 4403 (2009).

[122] A. Hryciw, Y. C. Jun, and M. L. Brongersma. "Plasmonics: Electrifying plasmonics on silicon". In: *Nat. Mater.* **9**, 3 (2010).

[123] A. V. Akimov, A. Mukherjee, C. L. Yu, D. E. Chang, A. S. Zibrov, P. R. Hemmer, H. Park, and M. D. Lukin. "Generation of single optical plasmons in metallic nanowires coupled to quantum dots". In: *Nature* **450**, 402 (2007).

[124] L. Tang, S. E. Kocabas, S. Latif, A. K. Okyay, D.-S. Ly-Gagnon, K. C. Saraswat, and D. A. B. Miller. "Nanometre-scale germanium photodetector enhanced by a near-infrared dipole antenna". In: *Nat. Photon.* **2**, 226 (2008).

[125] D. Pines. "A Survey, with Emphasis on Physical Considerations". In: D. Pines, ed., *The Many-Body Problem*, Frontiers in Physics: A Lecture Note and Reprint Series, chap. I. W. A. Benjamin, Inc., Reading, Massachusetts (1961).

[126] N. W. Ashcroft and N. D. Mermin. *Solid State Physics*. Holt, Rinehart and Winston (1976).

[127] S. M. Morton, D. W. Silverstein, and L. Jensen. "Theoretical Studies of Plasmonics using Electronic Structure Methods". In: *Chem. Rev.* **111**, 3962 (2011).

[128] W. A. de Heer, K. Selby, V. Kresin, J. Masui, M. Vollmer, A. Châtelain, and W. D. Knight. "Collective dipole oscillations in small sodium clusters". In: *Phys. Rev. Lett.* **59**, 1805 (1987).

[129] V. Bonačić-Koutecký, P. Fantucci, and J. Koutecký. "Quantum chemistry of small clusters of elements of groups Ia, Ib, and IIa: fundamental concepts, predictions, and interpretation of experiments". In: *Chem. Rev.* **91**, 1035 (1991).

[130] V. Bonačić-Koutecký, J. Pittner, C. Scheuch, M. F. Guest, and J. Koutecký. "Quantum molecular interpretation of the absorption spectra of Na_5, Na_6, and Na_7 clusters". In: *J. Chem. Phys.* **96**, 7938 (1992).

[131] M. Koskinen, M. Manninen, and P. Lipas. "Many-body origin of the plasmon resonance in small metal clusters". In: *Z. Phys. D* **31**, 125 (1994).

[132] M. Koskinen, M. Manninen, and P. O. Lipas. "Configuration-interaction calculations of jellium clusters by the nuclear shell model". In: *Phys. Rev. B* **49**, 8418 (1994).

[133] M. Koskinen and M. Manninen. "Photoionization of metal clusters". In: *Phys. Rev. B* **54**, 14796 (1996).

[134] S. Kümmel and M. Brack. "Quantum fluid dynamics from density-functional theory". In: *Phys. Rev. A* **64**, 022506 (2001).

[135] S. Kümmel, K. Andrae, and P.-G. Reinhard. "Collectivity in the optical response. of small metal clusters". In: *Appl. Phys. B* **73**, 293 (2001).

[136] J.-P. Connerade and A. V. Solov'yov. "Formalism for multiphoton plasmon excitation in jellium clusters". In: *Phys. Rev. A* **66**, 013207 (2002).

[137] J. Yan, Z. Yuan, and S. Gao. "End and Central Plasmon Resonances in Linear Atomic Chains". In: *Phys. Rev. Lett.* **98**, 216602 (2007).

[138] C. M. Aikens, S. Li, and G. C. Schatz. "From Discrete Electronic States to Plasmons: TDDFT Optical Absorption Properties of Ag_n (n = 10, 20, 35, 56, 84, 120) Tetrahedral Clusters". In: *J. Phys. Chem. C* **112**, 11272 (2008).

[139] J. Yan and S. Gao. "Plasmon resonances in linear atomic chains: Free-electron behavior and anisotropic screening of d electrons". In: *Phys. Rev. B* **78**, 235413 (2008).

[140] D. Gambacurta and F. Catara. "Collective excitations in metallic clusters within the second random phase approximation". In: *J. Phys.: Conference Series* **168**, 012012 (2009).

[141] A. E. DePrince III, M. Pelton, J. R. Guest, and S. K. Gray. "Emergence of Excited-State Plasmon Modes in Linear Hydrogen Chains from Time-Dependent Quantum Mechanical Methods". In: *Phys. Rev. Lett.* **107**, 196806 (2011).

[142] T. Yasuike, K. Nobusada, and M. Hayashi. "Collectivity of plasmonic excitations in small sodium clusters with ring and linear structures". In: *Phys. Rev. A* **83**, 013201 (2011).

[143] N. Nayyar, V. Turkowski, and T. S. Rahman. "Optical Generation of Collective Plasmon Modes in Small Gold Chains Induced by Doping Transition-Metal Impurities". In: *Phys. Rev. Lett.* **109**, 157404 (2012).

[144] J. A. Scholl, A. L. Koh, and J. A. Dionne. "Quantum plasmon resonances of individual metallic nanoparticles". In: *Nature* **483**, 421 (2012).

[145] A. V. Luzanov and V. É. Umanskii. "On the determination of the degree of collectivity of electronic excitations in molecules". In: *Theor. Exp. Chem.* **13**, 162 (1977).

[146] A. V. Luzanov and O. A. Zhikol. "Electron invariants and excited state structural analysis for electronic transitions within CIS, RPA, and TDDFT models". In: *Int. J. Quantum Chem.* **110**, 902 (2010).

[147] G. F. Bertsch, A. Bulgac, D. Tománek, and Y. Wang. "Collective plasmon excitations in C_{60} clusters". In: *Phys. Rev. Lett.* **67**, 2690 (1991).

[148] I. V. Hertel, H. Steger, J. de Vries, B. Weisser, C. Menzel, B. Kamke, and W. Kamke. "Giant plasmon excitation in free C_{60} and C_{70} molecules studied by photoionization". In: *Phys. Rev. Lett.* **68**, 784 (1992).

[149] G. Gensterblum, J. J. Pireaux, P. A. Thiry, R. Caudano, J. P. Vigneron, P. Lambin, A. A. Lucas, and W. Krätschmer. "High-resolution electron-energy-loss spectroscopy of thin films of C_{60} on Si(100)". In: *Phys. Rev. Lett.* **67**, 2171 (1991).

[150] A. Lucas, G. Gensterblum, J. J. Pireaux, P. A. Thiry, R. Caudano, J. P. Vigneron, P. Lambin, and W. Krätschmer. "Elementary excitations of C_{60} from the far infrared to the far vacuum ultraviolet studied by high-resolution electron-energy-loss spectroscopy". In: *Phys. Rev. B* **45**, 13694 (1992).

[151] E. Sohmen, J. Fink, and W. Krätschmer. "Electron energy-loss spectroscopy studies on C_{60} and C_{70} fullerite". In: *Z. Phys. B* **86**, 87 (1992).

[152] J. W. Keller and M. A. Coplan. "Electron energy loss spectroscopy of C_{60}". In: *Chem. Phys. Lett.* **193**, 89 (1992).

[153] A. Bulgac and N. Ju. "Collective electronic excitations in C_{60}clusters". In: *Phys. Rev. B* **46**, 4297 (1992).

[154] N. Ju, A. Bulgac, and J. W. Keller. "Excitation of collective plasmon states in fullerenes". In: *Phys. Rev. B* **48**, 9071 (1993).

[155] H. Ajie, M. M. Alvarez, S. J. Anz, R. D. Beck, F. Diederich, K. Fostiropoulos, D. R. Huffman, W. Krätschmer, Y. Rubin, K. E. Schriver,

D. Sensharma, and R. L. Whetten. "Characterization of the soluble all-carbon molecules C_{60} and C_{70}". In: *J. Phys. Chem.* **94**, 8630 (1990).

[156] H. Weiss, R. Ahlrichs, and M. Häser. "A direct algorithm for self-consistent-field linear response theory and application to C_{60}: Excitation energies, oscillator strengths, and frequency-dependent polarizabilities". In: *J. Chem. Phys.* **99**, 1262 (1993).

[157] J. F. Armbruster, M. Roth, H. A. Romberg, M. Sing, M. Schmidt, P. Schweiss, P. Adelmann, M. S. Golden, J. Fink, R. H. Michel, J. Rockenberger, F. Hennrich, and M. M. Kappes. "Electron energy-loss and photoemission studies of solid C_{84}". In: *Phys. Rev. B* **50**, 4933 (1994).

[158] C. Yannouleas, E. N. Bogachek, and U. Landman. "Collective excitations of multishell carbon microstructures: Multishell fullerenes and coaxial nanotubes". In: *Phys. Rev. B* **53**, 10225 (1996).

[159] R. Bauernschmitt, R. Ahlrichs, F. H. Hennrich, and M. M. Kappes. "Experiment versus Time Dependent Density Functional Theory Prediction of Fullerene Electronic Absorption". In: *J. Am. Chem. Soc.* **120**, 5052 (1998).

[160] S. V. Rotkin and R. A. Suris. "Plasmon-Frenkel-exciton in a clustered solid". In: *Phys. Lett. A* **245**, 292 (1998).

[161] R.-H. Xie, G. W. Bryant, G. Sun, M. C. Nicklaus, D. Heringer, T. Frauenheim, M. R. Manaa, J. Vedene H. Smith, Y. Araki, and O. Ito. "Excitations, optical absorption spectra, and optical excitonic gaps of heterofullerenes. I. C_{60}, $C_{59}N^+$, and $C_{48}N_{12}$: Theory and experiment". In: *J. Chem. Phys.* **120**, 5133 (2004).

[162] T. L. J. Toivonen and T. I. Hukka. "A Density Functional Theory (DFT) and Time-Dependent Density Functional Theory (TDDFT) Study on Optical Transitions in Oligo(p-phenylenevinylene)-Fullerene Dyads and the Applicability to Resonant Energy Transfer". In: *J. Phys. Chem. A* **111**, 4821 (2007). PMID: 17477511.

[163] A. Schlachter. "Collective electron motion in a C_{60} molecule: bridging the gap between atoms and bulk matter". In: *Rev. Mex. Fís. S* **56**, 30 (2010).

[164] M. Ruggenthaler, S. V. Popruzhenko, and D. Bauer. "Recollision-induced plasmon excitation in strong laser fields". In: *Phys. Rev. A* **78**, 033413 (2008).

[165] P. Bolognesi, L. Avaldi, A. Ruocco, A. Verkhovtsev, A. Korol, and A. Solov'yov. "Collective excitations in the electron energy loss spectra of C_{60}". In: *Eur. Phys. J. D* **66**, 1 (2012).

[166] A. Verkhovtsev, A. Korol, and A. Solov'yov. "Formalism of collective electron excitations in fullerenes". In: *Europ. Phys. J. D* **66**, 1 (2012).

[167] S. Bernadotte, F. Evers, and C. R. Jacob. "Plasmons in Molecules". In: *J. Phys. Chem. C* **117**, 1863 (2013).

[168] D. Pines and D. Bohm. "A Collective Description of Electron Interactions: II. Collective vs. Individual Particle Aspects of the Interactions". In: *Phys. Rev.* **85**, 338 (1952).

[169] D. Pines. "A Collective Description of Electron Interactions: IV. Electron Interaction in Metals". In: *Phys. Rev.* **92**, 626 (1953).

[170] D. Bohm and D. Pines. "A Collective Description of Electron Interactions. I. Magnetic Interactions". In: *Phys. Rev.* **82**, 625 (1951).

[171] D. Bohm and D. Pines. "A Collective Description of Electron Interactions: III. Coulomb Interactions in a Degenerate Electron Gas". In: *Phys. Rev.* **92**, 609 (1953).

[172] P. Ring and P. Schuck. *The nuclear many-body problem.* Springer, New York (1980).

[173] M. Pabst. *Übergangsmomente zwischen angeregten Zuständen mit der RI-CC2-Methode: Implementierung und Anwendung auf Triplet-Excimere.* Ph.D. thesis, Johannes Gutenberg-Universität Mainz (2011).

[174] F. Neese. "The ORCA program system". In: *WIREs Comput. Mol. Sci.* **2**, 73 (2012).

[175] M. Kleinschmidt, J. Tatchen, and C. M. Marian. "Spin-orbit coupling of DFT/MRCI wavefunctions: Method, test calculations, and application to thiophene". In: *J. Comput. Chem.* **23**, 824 (2002).

[176] G. Karlström, R. Lindh, P.-Å. Malmqvist, B. O. Roos, U. Ryde, V. Veryazov, P.-O. Widmark, M. Cossi, B. Schimmelpfennig, P. Neogrady, and L. Seijo. In: *Comput. Mater. Sci.* **28**, 222 (2003).

[177] B. Bak, D. Christensen, L. Hansen-Nygaard, and J. Rastrup-Andersen. "The structure of thiophene". In: *J. Mol. Spectrosc.* **7**, 58 (1961).

[178] S. Salzmann, M. Kleinschmidt, J. Tatchen, R. Weinkauf, and C. M. Marian. "Excited states of thiophene: ring opening as deactivation mechanism". In: *Phys. Chem. Chem. Phys.* **10**, 380 (2008).

[179] F. Weigend and R. Ahlrichs. "Balanced basis sets of split valence, triple zeta valence and quadruple zeta valence quality for H to Rn: Design and assessment of accuracy". In: *Phys. Chem. Chem. Phys.* **7**, 3297 (2005).

[180] B. O. Roos. "The Complete Active Space Self-Consistent Field Method and its Applications in Electronic Structure Calculations". In: K. P. Lawley, ed., *Ab Initio Methods in Quantum Chemistry - II*, vol. 69 of *Advances in Chemical Physics*, chap. 399. John Wiley & Sons, Ltd (1987).

[181] B. O. Roos, K. Andersson, and M. P. Fülscher. "Towards an accurate molecular orbital theory for excited states: the benzene molecule". In: *Chem. Phys. Lett.* **192**, 5 (1992).

[182] E. K. U. Gross and E. Runge. *Vielteilchentheorie*. Teubner Studienbücher Physik, Stuttgart (1986).

[183] I. Kostova, S. Raleva, P. Genova, and R. Argirova. "Structure-activity relationships of synthetic coumarins as HIV-1 inhibitors". In: *Bioinorg. Chem. Appl.* **2006**, 68274 (2006).

[184] M. V. Kulkarni, G. M. Kulkarni, C. H. Lin, and C. M. Sun. "Recent advances in coumarins and 1-azacoumarins as versatile biodynamic agents". In: *Curr. Med. Chem.* **13**, 2795 (2006).

[185] H.-C. Kim, S. Härtner, M. Behe, T. M. Behr, and N. A. Hampp. "Two-photon absorption-controlled multidose drug release: A novel approach for secondary cataract treatment". In: *J. Biomed. Opt.* **11**, 034024 (2006).

[186] J. Träger, H.-C. Kim, and N. Hampp. "Ophthalmology - Two-photon treatment". In: *Nat. Photon.* **1**, 509 (2007).

[187] T. Buckup, A. Southan, H.-C. Kim, N. Hampp, and M. Motzkus. "Optimisation of two-photon induced cleavage of molecular linker systems for drug delivery". In: *J. Photochem. Photobiol. A: Chem.* **210**, 188 (2010).

[188] J. S. Seixas de Melo, R. S. Becker, and A. L. Maçanita. "Photophysical Behavior of Coumarins as a Function of Substitution and Solvent: Experimental Evidence for the Existence of a Lowest Lying $^1(n\pi^*)$ State". In: *J. Phys. Chem.* **98**, 6054 (1994).

[189] J. R. Heldt, J. Heldt, M. Stoń, and H. A. Diehl. "Photophysical properties of 4-alkylcoumarin and 7-alkoxycoumarin derivatives - Absorption and emission spectra, fluorescence quantum yield and decay time". In: *Spectrochim. Acta, Part A* **51**, 1549 (1995).

[190] J. S. Seixas de Melo, R. S. Becker, F. Elisei, and A. L. Maçanita. "The photophysical behavior of 3-chloro-7-methoxy-4-methylcoumarin related to the energy separation of the two lowest-lying singlet excited states". In: *J. Chem. Phys.* **107**, 6062 (1997).

[191] W. A. Wassam Jr. and E. C. Lim. ""Proximity effect" and radiationless transitions in aromatic molecules with non-bonding electrons". In: *J. Mol. Struct.* **47**, 129 (1978).

[192] E. C. Lim. "Proximity effect in molecular photophysics: dynamical consequences of pseudo-Jahn-Teller interaction". In: *J. Phys. Chem.* **90**, 6770 (1986).

[193] T.-I. Lai, B. T. Lim, and E. C. Lim. "Photophysical properties of biologically important molecules related to proximity effects: psoralens". In: *J. Am. Chem. Soc.* **104**, 7631 (1982).

[194] A. Kobayashi, K. Takehira, T. Yoshihara, S. Uchiyama, and S. Tobita. "Remarkable fluorescence enhancement of benzo[g]chromen-2-ones induced by hydrogen-bonding interactions with protic solvents". In: *Photochem. Photobiol. Sci.* **11**, 1368 (2012).

[195] T. Wolff and H. Görner. "Photodimerization of coumarin revisited: Effects of solvent polarity on the triplet reactivity and product pattern". In: *Phys. Chem. Chem. Phys.* **6**, 368 (2004).

[196] I. Georgieva, N. Trendafilova, A. J. A. Aquino, and H. Lischka. "Excited State Properties of 7-Hydroxy-4-methylcoumarin in the Gas Phase and in Solution. A Theoretical Study". In: *J. Phys. Chem. A* **109**, 11860 (2005).

[197] D. Jacquemin, E. A. Perpète, X. Assfeld, G. Scalmani, M. J. Frisch, and C. Adamo. "The geometries, absorption and fluorescence wavelengths of solvated fluorescent coumarins: A CIS and TD-DFT comparative study". In: *Chem. Phys. Lett.* **438**, 208 (2007).

[198] D. Jacquemin, E. A. Perpète, G. Scalmani, M. J. Frisch, X. Assfeld, I. Ciofini, and C. Adamo. "Time-dependent density functional theory investigation of the absorption, fluorescence, and phosphorescence spectra of solvated coumarins". In: *J. Chem. Phys.* **125**, 164324 (2006).

[199] J. Preat, D. Jacquemin, V. Wathelet, J.-M. André, and E. A. Perpète. "TD-DFT Investigation of the UV Spectra of Pyranone Derivatives". In: *J. Phys. Chem. A* **110**, 8144 (2006).

[200] H. Nakai, Y. Yamauchi, A. Nakata, T. Baba, and H. Takahashi. "Ab initio molecular dynamics study on the excitation dynamics of psoralen compounds". In: *J. Chem. Phys.* **119**, 4223 (2003).

[201] S. Ionescu and M. Hillebrand. "Theoretical study of the excited states of 3-phenyl- and 3-thiophenyl-coumarins". In: *Chem. Phys.* **293**, 53 (2003).

[202] A. J. A. Aquino, H. Lischka, and C. Hättig. "Excited-State Intramolecular Proton Transfer: A Survey of TDDFT and RI-CC2 Excited-State Potential Energy Surfaces". In: *J. Phys. Chem. A* **109**, 3201 (2005).

[203] J. Tatchen and C. M. Marian. "Vibronic absorption, fluorescence, and phosphorescence spectra of psoralen: a quantum chemical investigation". In: *Phys. Chem. Chem. Phys.* **8**, 2133 (2006).

[204] I. Georgieva, N. Trendafilova, A. J. A. Aquino, and H. Lischka. "Excited-State Proton Transfer in 7-Hydroxy-4-methylcoumarin along a Hydrogen-Bonded Water Wire". In: *J. Phys. Chem. A* **111**, 127 (2007).

[205] C. A. Franca, A. C. González Baró, and R. Pis Diez. "Theoretical study and vibrational spectroscopy of two 5,6,7-trioxygenated coumarins". In: *J. Mol. Struct.* **843**, 57 (2007).

[206] T. Sakata, Y. Kawashima, and H. Nakano. "Low-lying excited states of 7-aminocoumarin derivatives: A theoretical study". In: *Int. J. Quantum Chem.* **109**, 1940 (2009).

[207] I. D. Petsalakis, N. N. Lathiotakis, and G. Theodorakopoulos. "Theoretical study on tertiary amine-fluorophore photoinduced electron transfer (PET) systems". In: *J. Mol. Struct. (Theochem)* **867**, 64 (2008).

[208] W. Zhao and W. Bian. "Investigation of the structures and electronic spectra for coumarin 6 through TD-DFT calculations including PCM solvation". In: *J. Mol. Struct. (Theochem)* **818**, 43 (2007).

[209] V. F. Traven, L. I. Vorobjeva, T. A. Chibisova, E. A. Carberry, and N. J. Beyer. "Electronic absorption spectra and structure of hydroxycoumarin derivatives and their ionized forms". In: *Can. J. Chem.* **75**, 365 (1997).

[210] R. J. Cave, K. Burke, and E. W. Castner Jr. "Theoretical Investigation of the Ground and Excited States of Coumarin 151 and Coumarin 120". In: *J. Phys. Chem. A* **106**, 9294 (2002).

[211] M. Sulpizi, U. F. Röhrig, J. Hutter, and U. Rothlisberger. "Optical properties of molecules in solution via hybrid TDDFT/MM simulations". In: *Int. J. Quantum Chem.* **101**, 671 (2005).

[212] Y. Kurashige, T. Nakajima, S. Kurashige, K. Hirao, and Y. Nishikitani. "Theoretical Investigation of the Excited States of Coumarin Dyes for Dye-Sensitized Solar Cells". In: *J. Phys. Chem. A* **111**, 5544 (2007).

[213] W. Zhao and W. Bian. "Investigation of the structures and electronic spectra of two coumarins with heterocyclic substituents through TD-DFT calculations". In: *J. Mol. Struct. (Theochem)* **859**, 73 (2008).

[214] P. K. McCarthy and G. J. Blanchard. "AM1 study of the electronic structure of coumarins". In: *J. Phys. Chem.* **97**, 12205 (1993).

[215] N. Kuş, S. Breda, I. Reva, E. Tasal, C. Ogretir, and R. Fausto. "FTIR Spectroscopic and Theoretical Study of the Photochemistry of Matrix-isolated Coumarin". In: *Photochem. Photobiol.* **83**, 1237 (2007).

[216] K. Rechthaler and G. Köhler. "Excited state properties and deactivation pathways of 7-aminocoumarins". In: *Chem. Phys.* **189**, 99 (1994).

[217] T. Sakata, Y. Kawashima, and H. Nakano. "Low-Lying Excited States of C120 and C151: A Multireference Perturbation Theory Study". In: *J. Phys. Chem. A* **114**, 12363 (2010).

[218] J. Preat, D. Jacquemin, and E. A. Perpète. "Theoretical investigations of the UV spectra of coumarin derivatives". In: *Chem. Phys. Lett.* **415**, 20 (2005).

[219] T. Moriya. "Excited-state Reactions of Coumarins in Aqueous Solutions. I. The Phototautomerization of 7-Hydroxycoumarin and Its Derivative". In: *Bull. Chem. Soc. Jpn.* **56**, 6 (1983).

[220] T. Moriya. "Excited-State Reactions of Coumarins. VII. The Solvent-Dependent Fluorescence of 7-Hydroxycoumarins". In: *Bull. Chem. Soc. Jpn.* **61**, 1873 (1988).

[221] E. Bardez, P. Boutin, and B. Valeur. "Photoinduced biprotonic transfer in 4-methylumbelliferone". In: *Chem. Phys. Lett.* **191**, 142 (1992).

[222] C. Hättig, A. Hellweg, and A. Köhn. "Distributed memory parallel implementation of energies and gradients for second-order Møller-Plesset perturbation theory with the resolution-of-the-identity approximation". In: *Phys. Chem. Chem. Phys.* **8**, 1159 (2006).

[223] C. Hättig and A. Köhn. "Transition moments and excited-state first-order properties in the coupled-cluster model CC2 using the resolution-of-the-identity approximation". In: *J. Chem. Phys.* **117**, 6939 (2002).

[224] A. Klamt and G. Schüürmann. "COSMO: a new approach to dielectric screening in solvents with explicit expressions for the screening energy and its gradient". In: *J. Chem. Soc., Perkin Trans. 2* **1993**, 799 (1993).

[225] T.-J. Hsieh, C.-C. Su, C.-Y. Chen, C.-H. Liou, and L.-H. Lu. "Using experimental studies and theoretical calculations to analyze the molecular mechanism of coumarin, p-hydroxybenzoic acid, and cinnamic acid". In: *J. Mol. Struct.* **741**, 193 (2005).

[226] P. Celani, F. Bernardi, M. Olivucci, and M. A. Robb. "Conical Intersection Mechanism for Photochemical Ring Opening in Benzospiropyran Compounds". In: *J. Am. Chem. Soc.* **119**, 10815 (1997).

[227] A. Nenov, W. J. Schreier, F. O. Koller, M. Braun, R. de Vivie-Riedle, W. Zinth, and I. Pugliesi. "Molecular Model of the Ring-Opening and Ring-Closure Reaction of a Fluorinated Indolylfulgide". In: *J. Phys. Chem. A* **116**, 10518 (2012).

[228] J. S. Seixas de Melo, C. Cabral, J. C. Lima, and A. L. Maçanita. "Characterization of the Singlet and Triplet Excited States of 3-Chloro-4-methylumbelliferone". In: *J. Phys. Chem. A* **115**, 8392 (2011).

[229] B. N. Mattoo. "Absorption and fluorescence spectra of coumarins". In: *Trans. Faraday Soc.* **52**, 1184 (1956).

[230] J. S. Seixas de Melo and P. F. Fernandes. "Spectroscopy and photophysics of 4- and 7-hydroxycoumarins and their thione analogs". In: *J. Mol. Struct.* **565-566**, 69 (2001).

List of Acronyms

ADC algebraic diagrammatic construction

ADC(2) second-order ADC

ADC(2)-s strict ADC(2)

ADC(2)-x extended ADC(2)

ADC(3) third-order ADC

BO Born-Oppenheimer approximation

CASSCF complete active space self-consistent field

CASPT2 complete active space second-order perturbation theory

CI configuration interaction

CIS CI singles

CIS(D) CIS with a perturbative doubles correction

CIS(D_∞) CIS with quasidegenerate second-order perturbation corrections

CC coupled-cluster

CCS CC singles

CCSD CC singles and doubles

CC2 approximate coupled-cluster singles and doubles model

DFT density functional theory

ESA excited state absorption

FC Franck-Condon

FCI full-CI

GTA global target analysis

HF Hartree-Fock theory

ISC inter-system crossing

ISR intermediate state representation

irrep irreducible representation

MP2 Møller-Plesset perturbation theory in second order

ON occupation number

PES potential energy surface

PT perturbation theory

RPA random-phase approximation

ri resolution of the identity

SAS species associated spectrum

SCF self-consistent field

SCS spin-component scaled

SD Slater determinant

SE stimulated emission

SOC spin-orbit coupling

SOS scaled opposite-spin

TDDFT time-dependent density functional theory

List of Figures

List of Tables

Danksagung

An erster Stelle danke ich Herrn PD Dr. Markus Pernpointner für die sehr gute Betreuung und die vielen Ratschläge während meiner Doktorandenzeit sowie die Möglichkeit sehr selbstständig zu forschen. Ebenso möchte ich mich bei Herrn Prof. Dr. Andreas Dreuw herzlich dafür bedanken, dass ich an der Entwicklung des ADC Moduls in Q-Chem mitwirken und den theoretischen Teil meiner Promotion in Kooperationsprojekten mit ihm erarbeiten konnte. Die vielen wissenschaftlichen Diskussionen mit ihnen beiden haben mir immer sehr geholfen.

Außerdem hat es mich gefreut mit zwei weiteren Arbeitsgruppen zusammenarbeiten zu können: In der Gruppe von Prof. Dr. Marcus Motzkus wurden die Messungen an den Cumarinderivaten durchgeführt. Daran waren insbesondere Dr. Tiago Buckup und Dr. Jens Möhring beteiligt. Zum anderen bin ich Dr. Stefan Bernadotte und PD Dr. Christoph Jacob dankbar für den Vorschlag ihren Skalierungsansatz zur Identifizierung von Plasmonen auf ADC Methoden zu übertragen und für die daraus resultierende Zusammenarbeit.

Bei Herrn Prof. Dr. Jochen Schirmer möchte ich mich für die gastfreundliche Aufnahme in seinem Büro und die angenehme Arbeitsatmosphäre bedanken. In den vielen (nicht nur fachlichen) Gesprächen habe ich sehr viel gelernt, sei es bezüglich der theoretischen Beschreibung von Plasmonen, ADC oder des Sinns und Unsinns von TDDFT. Auch für viele hilfreiche Anmerkungen zu den Abschnitten meiner Arbeit, die sich mit Plasmonen beschäftigen, bin ich ihm sehr dankbar.

Ein besonderer Dank gilt auch Markus Rössler, Steffen Mader, J. Patrick Zobel, David F. Schrempp sowie Jan Gotthardt, die ich während ihrer Forschungspraktika oder Bachelorarbeiten betreuen konnte und die damit auch meine Arbeit unterstützt haben.

Bei der gesamten TC-Gruppe unter der Leitung von Prof. Dr. Lorenz S. Cederbaum möchte ich mich für die freundliche Aufnahme und die stets angenehme Arbeitsatmosphäre bedanken. Insbesondere danke ich den Systemadministratoren für die hervorragende Verwaltung der Rechner und des Netzwerkes, die dadurch ein problemloses und angenehmes Arbeiten ermöglichten. Auch die Arbeitsgruppe von Prof. Dr. Andreas Dreuw hat mich sehr gastfreundlich aufgenommen. Vor allem konnte ich bei den Programmierarbeiten jederzeit auf die Hilfe von Dr. Michael Wormit zählen.

Der Heidelberg Graduate School for Mathematical and Computational Sciences (HGSMathComp) danke ich für das Bereitstellen eines Doktorandenstipendiums. Im Rahmen der zahlreichen Veranstaltungen habe ich an vielen interes-

santen Kursen und Seminaren teilnehmen können, die die wissenschaftlichen Arbeit hervorragend ergänzt haben.

Ein besonderer Dank gilt all meinen Freunden, die mich während meines Studiums begleitet haben. Insbesondere sind hier Sabine Kopec sowie mein Freund Matthias Kümmerer zu nennen, denen ich für das Korrekturlesen meiner Arbeit sehr dankbar bin.

Zu guter Letzt danke ich meiner Familie und insbesondere meinen Eltern für die stete und liebevolle Unterstützung.

Eidesstattliche Versicherung gemäß § 8 der Promotionsordnung der Naturwissenschaftlich-Mathematischen Gesamtfakultät der Universität Heidelberg

1. Bei der eingereichten Dissertation zu dem Thema

Development, Benchmarking, and Applications of Efficient Theoretical Approaches
for the Calculation of Excited States in Organic Systems

handelt es sich um meine eigenständig erbrachte Leistung.

2. Ich habe nur die angegebenen Quellen und Hilfsmittel benutzt und mich keiner unzulässigen Hilfe Dritter bedient. Insbesondere habe ich wörtlich oder sinngemäß aus anderen Werken übernommene Inhalte als solche kenntlich gemacht.

3. Die Arbeit oder Teile davon habe ich ~~wie folgt/~~bislang nicht[1)] an einer Hochschule des In- oder Auslands als Bestandteil einer Prüfungs- oder Qualifikationsleistung vorgelegt.

Titel der Arbeit:_____

_____

Hochschule und Jahr:_____

Art der Prüfungs- oder Qualifikationsleistung:_____

4. Die Richtigkeit der vorstehenden Erklärungen bestätige ich.

5. Die Bedeutung der eidesstattlichen Versicherung und die strafrechtlichen Folgen einer unrichtigen oder unvollständigen eidesstattlichen Versicherung sind mir bekannt.

Ich versichere an Eides statt, dass ich nach bestem Wissen die reine Wahrheit erklärt und nichts verschwiegen habe.

_____ _____
Ort und Datum Unterschrift

[1)] Nicht Zutreffendes streichen. Bei Bejahung sind anzugeben: der Titel der andernorts vorgelegten Arbeit, die Hochschule, das Jahr der Vorlage und die Art der Prüfungs- oder Qualifikationsleistung.